NASA SP-375

THE USE OF LASERS FOR HYDROGRAPHIC STUDIES

A symposium held at

WALLOPS FLIGHT CENTER

Wallops Island, Virginia

September 12, 1973

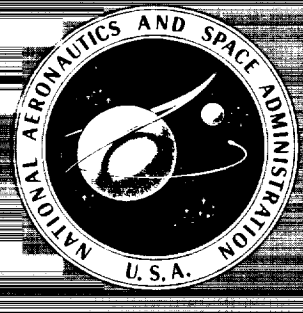

NATIONAL AERONAUTICS AND SPACE ADMINISTRATION

NASA SP-375

THE USE OF LASERS FOR HYDROGRAPHIC STUDIES

Edited by
HONGSUK H. KIM AND PHILIP T. RYAN

Proceedings of a symposium held at
Wallops Flight Center, Wallops Island, Virginia,
September 12, 1973

Scientific and Technical Information Office 1975
NATIONAL AERONAUTICS AND SPACE ADMINISTRATION
Washington, D.C.

For sale by the National Technical Information Service
Springfield, Virginia 22151 $7.25

FOREWORD

Recent progress in laser technology has opened new and important possibilities for applications in hydrospheric measurements. These applications have yet to be studied and developed. Yet, a hastily called conference on the theme of "The Use of Lasers for Hydrographic Studies" at NASA-Wallops Station, September 12, 1973, drew more than one hundred experts from all over the United States and Canada. During the one-day meeting, twenty-one papers were presented on topics ranging from surface wavelet study to underwater Raman spectroscopy. The interest and expertise shared by all participants ensured a most worthwhile symposium.

The meeting was divided into two sessions; the morning sessions was chaired by me, Hongsuk H. Kim of NASA-Wallops Station, Virginia. Dr. George D. Hickman of Sparcom Incorporated, Alexandria, Virginia chaired the afternoon session. The advisory panel for the conference included Dr. Theodore Chamberlain, Chesapeake Research Consortium; Dr. Murray Felsher, Environmental Protection Agency; Dr. Charles Yentsch, University of Massachusetts; and Dr. V. Klemas, University of Delaware.

I particularly would like to thank Mr. Maurice Ringenbach, National Ocean Survey, and Dr. James Bailey, Office of Naval Research, who encouraged us to pursue the idea of the meeting.

Some of the papers herein have been derived primarily from oral presentations made during the symposium. Because of this, and in order to achieve a uniform format, a considerable amount of editing was performed. Although contributors were afforded an opportunity to revise their oral transcripts, the time alloted them for this purpose was short in order to expedite the timely publication of this document. Therefore, while care was exercised not to alter a contributor's context, this may have happened inadvertently; in which case, the editors assume full responsibility.

A goal of the meeting was to bring laser and oceanographic technology together. I hope this report will further contribute to this goal.

Hongsuk H. Kim
Morning Session Chairman

TABLE OF CONTENTS

WELCOMING REMARKS

Abraham D. Spinak, Associate Director
NASA, Wallops Station

Wallops has, during recent years, participated in NASA's efforts to find practical applications for its capabilities. We have a small SR&T program which is centered on finding ways that remote sensing can be used to help solve some of the problems of the Chesapeake Bay Region. Additionally, there are activities with interests in oceanography and the atmosphere. We have an aircraft, helicopter and some laboratories which support these activities and give us the capability of carrying out experiments and demonstrations.

Mr. Kim's work in developing and finding uses for laser technology has been very exciting to all of us here at Wallops. We feel that it holds much promise and we encourage it very much. Obviously, the turnout today and the interesting agenda for this conference shows that there are many with similar interests who have been doing much work in this field and are now ready to share the results. Your achievements complement each other and will contribute to the application of aeronautics and space technology to earthly problems.

It is a pleasure for Wallops to host this meeting. I hope that it is very productive.

NOAA'S LIDAR PROGRAM

Maurice E. Ringenbach
National Oceanic and Atmospheric Administration

I would like to acquaint you with the National Oceanic and Atmospheric Administration's (NOAA) Lidar program, the reason we're in this program, and why we feel this program is important to increasing the effectiveness of our work in near-shore nautical charting.

Anyone who has conducted near-shore depth soundings is familiar with the reduced effectiveness of the operation due to surf conditions and the safety hazards occasioned by land outcroppings.

Therefore, it is our opinion that increased survey effectiveness can be realized in these areas with a remote sensing technique operated from a non-displacement platform, such as surface effect ship or helicopter.

In a meeting with personnel of the Navy we learned of experimental laser depth soundings conducted from a helicopter. As a result of the apparent success of these experiments, a contract with Sparcom, Inc., was jointly funded by the Office of Naval Research (ONR) and ourselves. The purpose of this contract was to establish quantitatively, the propagation characteristics of a laser beam and determine if through physical measurement of water and bottom samples of an area the feasibility of conducting bathymetry in that area could be established.

Dr. Dan Hickman will discuss the results of this work later.

In addition to lasers, we are also investigating the possibility of using air-coupled acoustic transducers. Preliminary analysis, on paper, shows that while attenuation due to the air-water interface is high, the signal-to-noise level of the returned signal is adequate.

There may be corollary benefits if LIDAR is used. Based on experimental work it appears reasonable to measure water quality parameters such as hydrocarbons and algae, as well as physical parameters such as turbidity, salinity, and water currents.

In short, we are not committed to the use of lasers. Within the next two years, when the overall capability of the laser and air-coupled acoustic transducers are known, a systems engineering analysis will be conducted to determine the most effective approach.

ONR'S LIDAR PROGRAM

Dr. James S. Bailey
Office of Naval Research

This talk is restricted in general to ONR Code 414 activity; however, other research projects are in effect in our Physical Sciences Division. Projects concerned with xtals, designators, range finders, and high powered and dye lasers constitute the bulk of this research--much of which is directed toward improving the efficiency of the laser. Other Navy interests in laser applications, particularly to hydrographic studies, will be covered in part by Mr. Avery who follows me and later by Mr. Ott.

The ONR coastal remote sensing program recognizes the unique attributes of both aircraft and spacecraft for the applications of remote sensing to the total environment in which the Navy operates. The total coastal environment encompasses nearshore, deltaic, and estuarine zones. Nearshore, coastal, and estuarine environmental analyses are essentially studies of the behavior, variability, and mechanisms of change of conditions in this dynamic zone. A need arises, from the military problems inherent in this zone, for a capability to reconstruct the conditions and follow the sequential changes in the environment, determine the mechanisms of these changes (the driving forces) and, in some cases, determine complex cause and effect chains to determine how certain conditions are developed and what will happen if certain characteristics are changed. The availability of combinations of remote sensors and platforms now provides the capability to obtain synoptic and repetitive data from any prospective survey area. The synoptic, time series attributes of remote sensing are the critical factors since the extreme areal and temporal variability of the coastal environmental characteristics successfully defy adequate coverage by conventional survey methods and analyses techniques.

Present electromagnetic sensing technology and the ability to operate from platforms above the earth has permitted the development of systems having a greatly increased ability to sense the meaningful characteristics of the earth and its environment. Increased information can be obtained through the use of combinations of sensors, with each individual sensor exploiting a different portion of the electromagnetic spectrum. Laser infrared, active and passive radar, and other radio frequency sensor systems show great promise in providing surface and subsurface information. Much of this information is also needed in target-background, and signature-characterization efforts. Regardless of the application, when used in aircraft or spacecraft vehicles, these devices provide a means of acquiring repetitive synoptic data on coastal zones otherwise inaccessible because of physical limitations or political restraint. In some instances, remote sensors may be the only means of acquiring certain data; in others, they may be the most economical means, but certainly they are the only means of acquiring data from space.

The purpose of this research program is to provide the Navy and Marine Corps with an added and needed capability for obtaining timely environmental data. By environment is meant the complex and intricately related ocean-nearshore, deltaic and estuarine environments. The data referred to are measurements of dimensions, temperatures, concentrations, emissivities, reflectances, times-rates, and velocities, etc. They are measurements of parameters that are peculiar to specific environments and that will inform us of the actions within these environments.

The primary objective of the program is to define and demonstrate the ways in which remote sensors can be applied to Navy problem areas such as arctic and coastal environmental predictions, amphibious and other inshore warfare planning, and certain aspects of ASW.

The most difficult problem in establishing the laser as a practical reconnaissance/surveillance tool is in developing the capability to extract particular information from the total data recorded by the sensor. Two basic approaches are open to solving this type of problem. The first is to study the data output from remote sensors and determine those characteristics that are immediately obvious such as observing that water appears hot in the 8-14 micron region of the electromagnetic spectrum and cold to a microwave radiometer when the measurements are made at night. Using this approach, little attempt is made to understand why this is true but only that it is. This is the empirical technique of the application scientist.

The ONR program has continually been dedicated to conducting rigorous scientific studies into the basic physics producing and affecting the energy field measured by the sensor and to deriving the analytical formulations which describe the various elements of this natural field. This is the analytical approach of the basic research scientist.

ONR Code 414 laser research efforts have been to define the critical parameters of the coastal environment imposing limitations on the laser capabilities.

Additionally, the temporal and spatial aspects of the measured parameters have been considered so that data sampling rates and resolution capabilities could be accurately engineered into the sensor and recording system.

The effectiveness of military planning is frequently measured by the ability of forces to successfully move across a coastal zone in obtaining an assigned objective. The coastal environment imposes constraints and can largely influence system composition and function; i.e., the choice of weapons and vehicles, the deployment of forces and selection of methods of operation. Similarly, present state of the art in amphibious technology limits the range of candidate landing sites. Knowledge of the coastal environment and ability to predict its variations are necessary to the selection processes.

Amphibious operations may employ any of a wide variety of methods and techniques but the purpose is basically the transportation of men and material from ocean-going ships offshore to secure positions onshore.

Decision making and model selection are today largely based on intelligence gained from maps, charts, photographs, tabulations and texts which describe separately certain aspects of the environment as they existed at a point in time, or in the case of highly variable elements, statistically.

Amphibious and inshore warfare are perhaps the most complicated and sophisticated forms of warfare, combining mobility and flexibility with the element of surprise. It is quite probable that no other military operation is as concerned with and as vulnerable to its complex and rapidly changing environment.

The principal parameters of beaches and the nearshore zone--length of usable beach, beach width, beach gradient, beach approach, surf and tidal range, beach material, nearshore current, waves, offshore bars, etc., are subject to changes of wind, water, and land interactions. The result is that beaches and the nearshore zone are the most dynamically complex of all land forms.

Mobility and flexibility of operation are critically impaired unless adequate and timely data collection is conducted. Surprise is lost if data collection is too apparent. Perhaps the most complicating factor is the political turmoil of the mid-twentieth century that demands U.S. military forces be prepared to operate on and over a variety of widely dispersed beaches within a very narrow time frame.

The requirements, therefore, exist for properly maintaining current general coastal and estuarine data and having the capability to rapidly update and incorporate data of specific parameters that are subject to rapid change and to acquire these data over coastal areas that may be inaccessible because of physical limitations or political restraint.

An area of concern to Navy-Marine Corps planning and operations is coastal bathymetry. Naval inshore warfare requirements include a need for relatively detailed knowledge of the sea floor topography of the world's coastal environment including beaches, wetlands, and other fringing land forms.

Bathymetric data are also an indispensible input to all coastal environmental predictive models and in most instances must be obtained on a recurring basis to validate the model output.

Clearly, then, means of obtaining this information synoptically, rapidly, and under varying environmental conditions are required. The laser is one instrument that can be applied to this task. The feasibility of applying the laser to coastal bathymetry/topography has been proved by the research of Dr. Hickman while at the University of Syracuse, the Electro-Science Laboratory of Ohio State University, and later work by the Naval Air Development Center and NAVOCEANO conclusively determined the utility of the laser for this work.

The laser research program in Code 414 has been directed toward obtaining definitive, qualitative data (measurements) on the coastal ocean parameters affecting the laser energy field. By defining the significant parameters and subjecting the laser beam to variations of these parameters, a set of criteria have been developed from which an optimally efficient and portable coastal laser bathymetry system can now be built.

This work and some of the salient results presumably will be discussed later by Dr. Hickman.

NAVOCEANO'S LIDAR PROGRAM

Duane Bright
U. S. Naval Oceanographic Office

NAVOCEANO (U.S. Naval Oceanographic Office) has a continuous requirement to conduct hydrographic surveys along coastlines throughout the world. These surveys are now, of course, conducted using sound boats equipped with acoustic transponders (echo sounders). Problems such as flow noise and cavitation limit the speed of these boats to 20 or 30 knots at best, even if the sound boats could go that fast in near shore waters. The development of the laser has provided a new medium-light- for depth sounding to perhaps five fathoms in most coastal areas. Light pulses can be transmitted through the air-sea interface, reflected from the bottom, and detected by the airborne receiver to provide both the water depth and the height of the aircraft. With such an airborne system, there is no speed limitation, either in sounding or obstacle avoidance.

During the early part of 1966, the need for more and better charts of the rivers and shallow coastal waters in and around South Vietnam required surveying hundreds of miles of survey lines using sound boats that were within range of enemy controlled territory. The danger involved, plus the slow rate of data collection in these high priority areas, caused NAVOCEANO to take a new look at the equipment being used. As a result, a decision was made to investigate the practicability of using the laser as an airborne depth sounder.

Our program was called the PLADS, an acronym for Pulsed Light Airborne Depth Sounder. The objective of PLADS was to develop enough test data to write a procurement specification for operational equipment. An R&D contract was made with the Raytheon Company for a prototype system with the objectives listed in the first column of TABLE 1. The system characteristics that we deemed necessary to meet the objectives of the first column are listed in column two and three.

TABLE 1. - PULSED LIGHT AIRBORNE DEPTH SOUNDER OBJECTIVES AND CHARACTERISTICS

SYSTEM		TRANSMITTER		RECEIVER	
Altitude	62-310m	PK Power	2-3Mw	Aperture	6 cm
Alt. Accuracy	.3048m	Pulse Width	4-7ns	F/#	f/8
Depth Penetration	30m	Pulse Fall	2-3ns	F.O.V.	5° MAX
Depth Accuracy	.465m	Wavelength	0.58	Bandwidth	50Å
Atten. Length	1-10m	Divergence	1/2=14mr	Video B.W.	400 MHz
Target Reflect.	0%	PRF	1-30pps	P./C.	S-20
Vertical Stability	±1 1/2°			Spatial Filters.	A/R
					4ns AT S/N=1
				Sensitivity	400nw AT S/N=10

The PLADS is composed of four main components as show in Figure 1. The electronic control console, the transceiver, which is the transmitter and receiver of the laser, water cooler for the laser head, and the laser power supply. The rest of the equipment is for readout and recording.

A beam divergency system was included to control the area illuminated by the laser on the sea surface. The spot size, on the surface of the water, has to be sufficiently large to illuminate a large number of small wind wavelets. The laser that we used transmitted about 500 kilowatts per pulse. Of this amount of power, the water surface was expected to reflect from 2.5 to 90 watts. About 10^{-6} watts, one microwatt was expected to be the smallest detectable return. This detection range of 90 watts to one microwatt placed a very stringent requirement on the dynamic range capability of the receiver. Spatial filters and linear polerizers were used in the receiver to allow this wide range.

The PLADS was tested at the Naval Air Test Center on the Patuxent River in Maryland, at the Naval Ship R&D Lab. in Panama City, Flordia, and from the Chesapeake Bay Bridge. Two preliminary test reports were written. The system was delivered by the contractor in September of 1969, and required less than three hours to install in a helicopter. The flight test at Patuxent showed the system feasibility. Accurate depths to about 5½ meters (18 feet) were measured in the muddy Potomac River.

The Panama City tests in 1970 included both flight tests and static tests from a Texas tower type platform. The flight tests measured water depths up to 30.48m in the relevantly clear waters off of Panama City. For both the platform and flight tests, the change in the number of small capillary wavelets on the water surface, due to wind conditions, had a very marked effect on the signal returns. When the wind was less than five knots, the water surface was relatively smooth and the return signals were very erratic. Good returns were obtained when the winds were above five knots. The Bay Bridge tests helped to further validate our working design concept; however, little data was collected due to hardware failures.

To conclude, although the hardware was unreliable, the PLADS system did demonstrate the feasibility of sounding in this manner. It appears that all design and equipment deficiencies can be corrected, at least to the extent necessary to produce a good operational mode. The polarizer and the spatial filters did indeed enable a single photomultiplier tube to handle both the very strong surface return and the very weak bottom return. Our office has also been deeply involved in the use of color-aerial photography for near-shore hydrographic survey work. Because of the relative success we have had with both the color photography program and the PLADS program, we have begun an effort, under DMA (Defense Mapping Agency) sponsorship, to develop a Coastal Aerial Photo Laser Survey System, called "CAPS", which will marry a laser system with a color photo system. This will provide a total system capability for nearshore hydrographic survey, amphibious reconnaissance, beach gradients, and a number of other things. CAPS will use the laser to control the photographic system without the need for expensive control surveys. Our first step will be to develop a new and reliable depth sounder. We are pursuing this at present with NASA. Later, the integration with the photogrammetric system will be made.

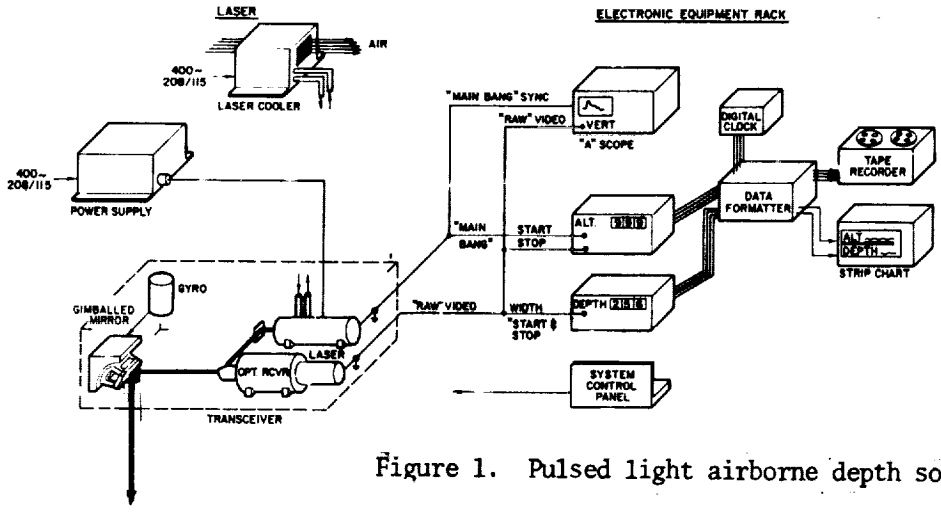

Figure 1. Pulsed light airborne depth sounder

NASA'S LIDAR PROGRAM

Bernard Rubin
NASA Headquarters

Let me extend to all of you a hearty welcome on behalf of NASA Headquarters, the Office of Aeronautics and Space Technology, and particularly Mr. Frank J. Sullivan, the Director of the Guidance, Control and Information Systems Division, which sponsors most of the NASA effort that you will hear about today. It is gratifying to me to be here to participate in this cooperative program in which representatives from different U.S. and Canadian government agencies, universities and industrial organizations convene and exchange information. The subject of this Conference is a relatively new one, but one which you will hear more about with time because LIDAR Systems represent an extensively applicable technology for environmental studies. They provide a rapid, highly sensitive, broad-coverage, multimode, high-resolution method for studying not only the planet on which we live, but other planets as well.

NASA has always had both of these interests...it has sent up such spacecraft as the Mariner to probe the planet Mars; and on July 23, 1972, it launched ERTS-1, the first Earth Resources Technology Satellite. On that occasion, Dr. Fletcher, the NASA Administrator wrote: "...it demonstrates how we have begun to turn the space program of the U.S. around, how we are returning to the home seas of space after 12 years of strenuous and highly successful effort to explore the moon. It symbolizes our determination to concentrate in this decade on winning more practical benefits from spacecraft in earth orbit at much less cost."

LIDAR will enhance NASA's ability to obtain more accurate information about this planet and to respond to society's interest and concern about its ecology. In 1969, NASA developed its first successful LIDAR system consisting of a pulsed ruby laser, a collecting 30.5 cm (12 in.) telescope for day use and a detector for the purpose of looking at latitudinal variation of aerosols in the atmosphere. This system which was designed and fabricated at the Langley Research Center, was used successfully in the Barbados Oceanographic and Meteorological Experiment in the summer of that year. Figure 1 shows the working system as a shipboard instrument.

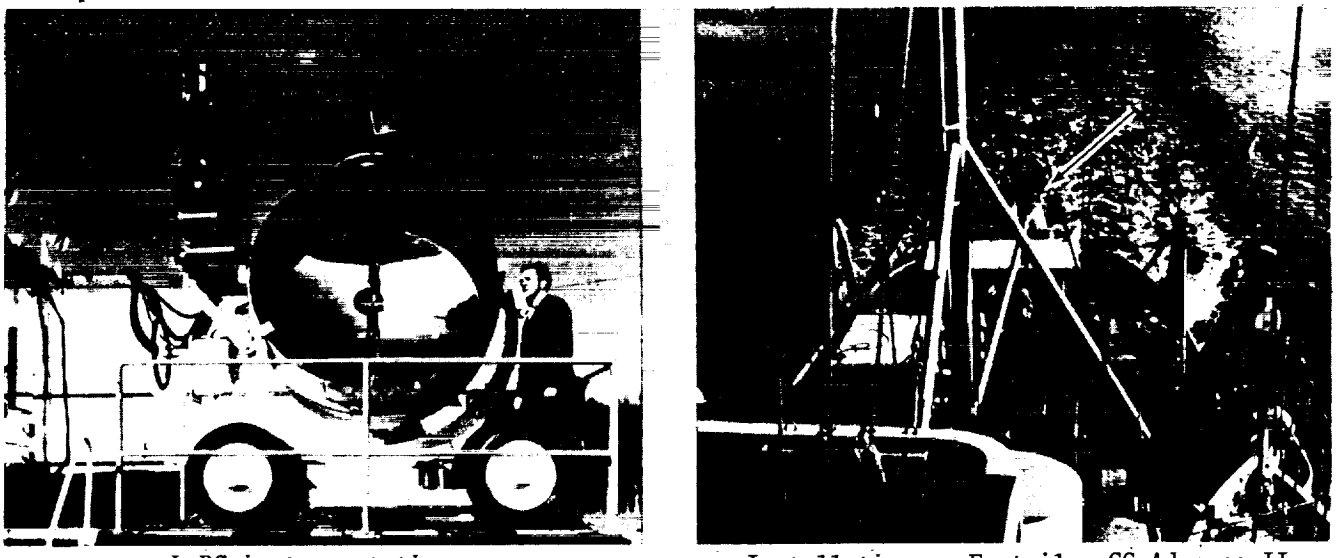

LaRC instrumentation Installation on Fantail - SS Advance II

Figure 1. Laser system for atmospheric measurement used in Bomex.

In the following year, the LIDAR System was placed on board a van, and sent to the Willamette Valley in Oregon, and in conjunction with the University of Oregon, assisted the farmers in deciding when to burn their fields. This practice takes place annually after the harvest, and was carried out haphazardly, often to the dismay of the farmers. If an inversion layer settled over a valley and its altitude was below the height of the surrounding mountain tops, then the smoke from the burning would rise to the height of the inversion layer and would become entrapped. In Figure 2, such a phenomenon is observed. Note the horizontal flow of the smoke and its failure to rise and become dissipated at higher altitudes. The NASA system was used to probe the area above the valley for the presence or absence of inversion layers. That year, the farmers were grateful to the NASA/University of Oregon team for its assistance in deciding the proper time to burn the fields.

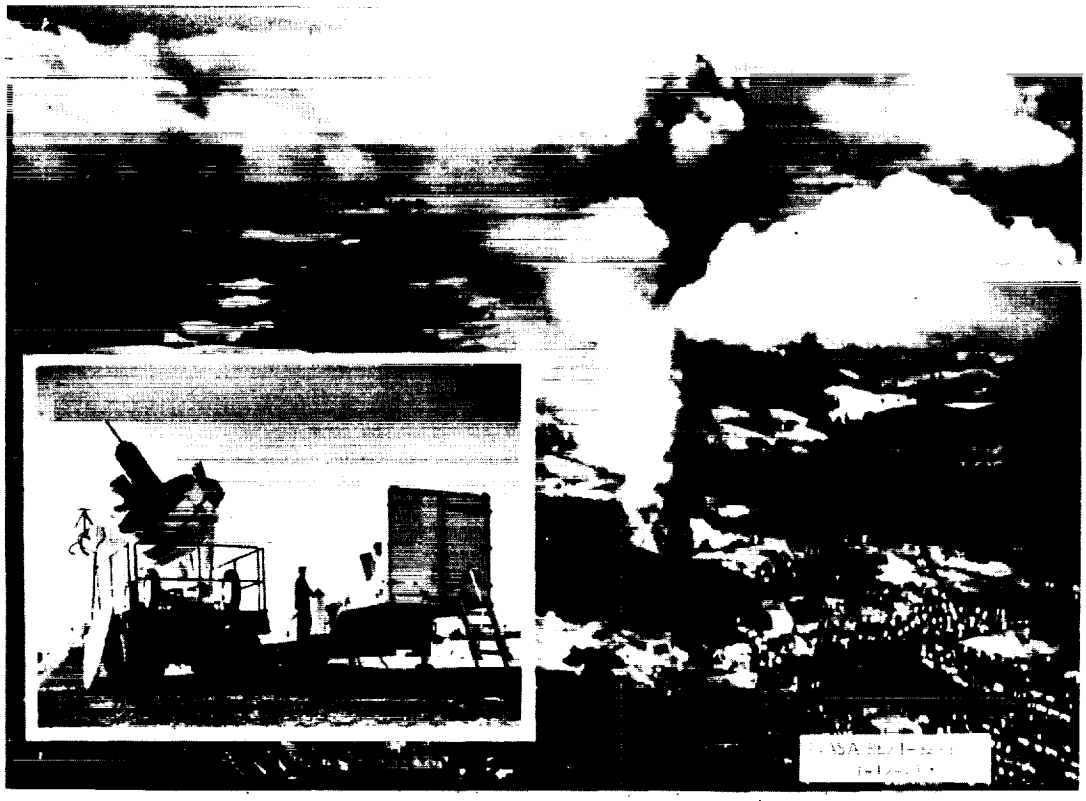

Figure 2. Atmospheric pollution measurements

The next generation of this LIDAR was completed in 1972 and is shown in Figure 3. This is a 60.96 cm (24 in.) system, and has been recently used in smokestack effluent investigations. Figure 4 shows the same system in position for measurement. This LIDAR was also used in a Raman backscattering mode to detect SO_2 and, in Figure 5, results of the experiment are shown for sulfur dioxide. Similar results are given in Figure 6 for nitric oxide.

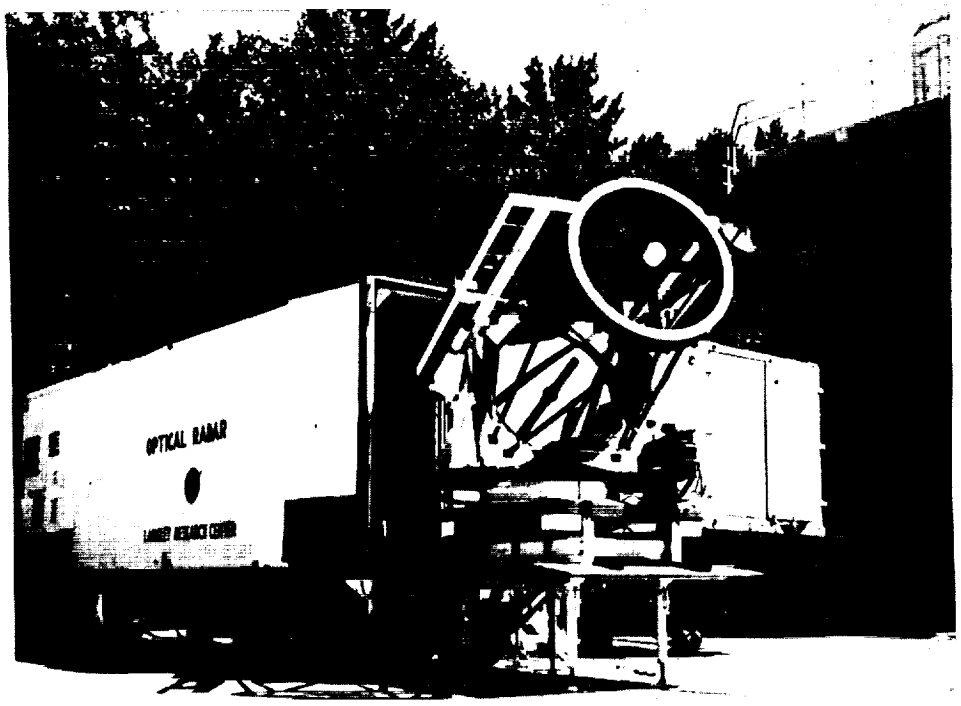

Figure 3. 1972 LIDAR with 60.96 cm laser radar system

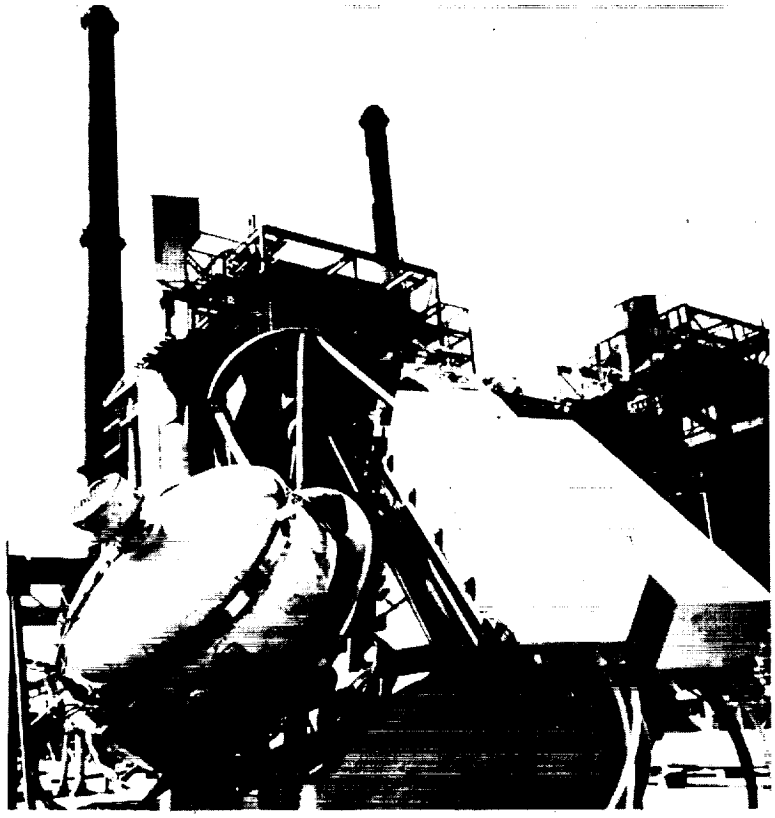

Figure 4. 60.96 cm laser radar system for stack plume measurements

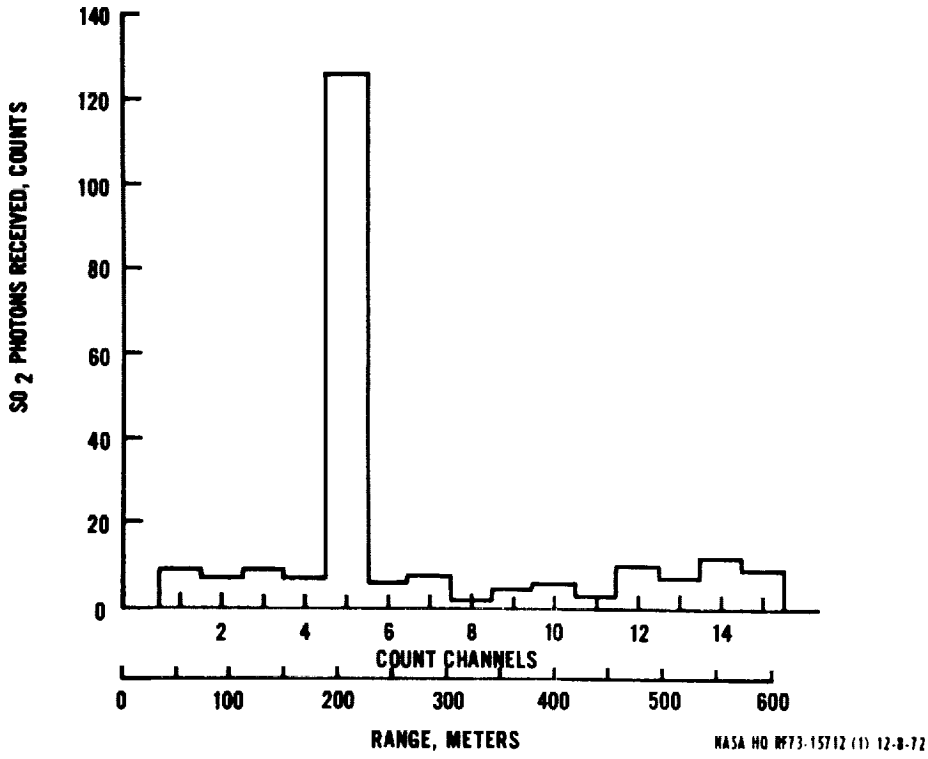

Figure 5. Sulfur dioxide measurement (October 1972)

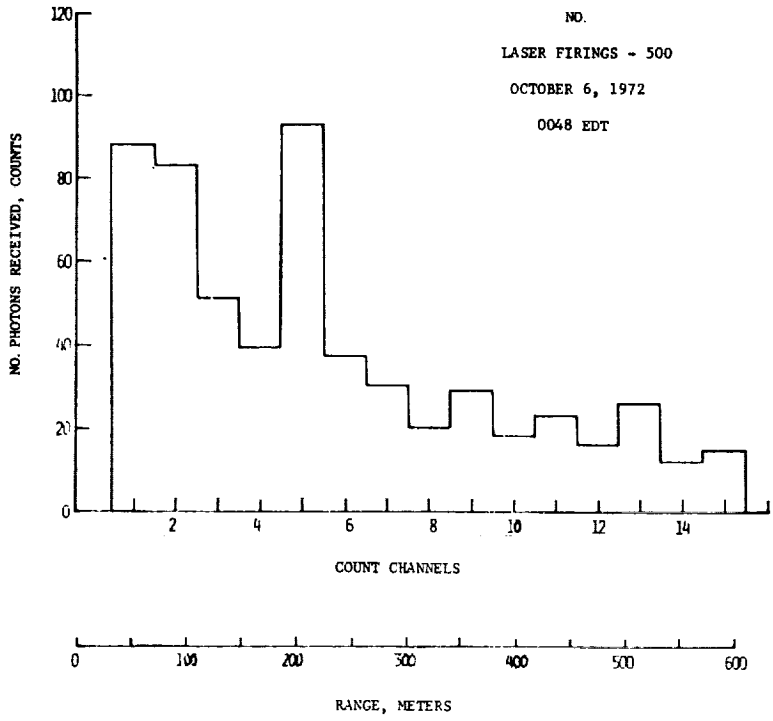

Figure 6. Nitric oxide measurement

The success of the application of NASA's LIDAR System with particulates prompted the initiation of a new LIDAR program, aimed at investigating some of the properties of the oceans. In 1970, contact was made with Mr. Kim of Wallops Station and was the beginning of a joint Wallops/Langley program in LIDAR hydrography. Langley's strength in designing and fabricating tuned lasers was coupled with Wallops background in the receiver end of the LIDAR System. The program was an ambitious one and its many applications are shown in Figure 7. Our plan was to approach the detection and measurement of each of the variables, depth, turbidity, oil pollution, and phytoplankton in the laser mode that was optimum for each.

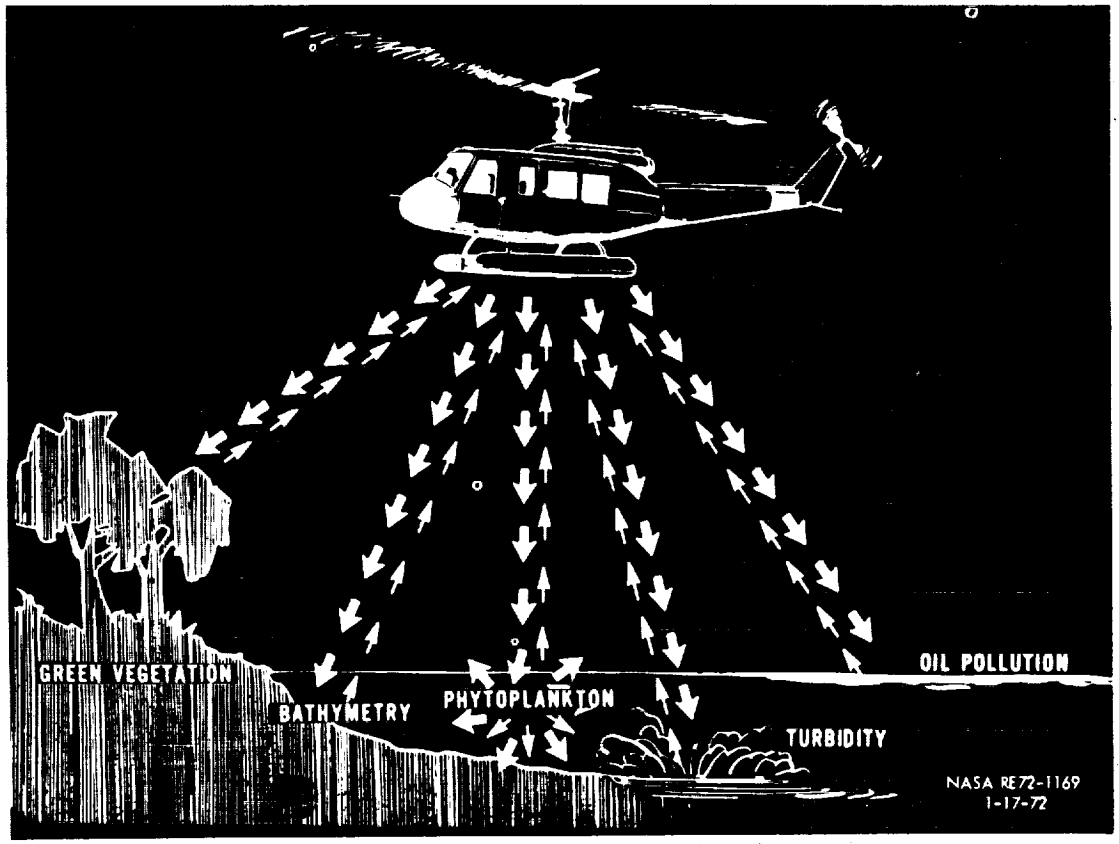

Figure 7. Laser radar sensing technology

The first choice was phytoplankton and, in particular, the chlorophyll a that was a major constituent. The fluorescence mode was chosen because it was specific to chlorophyll a, a relatively strong return signal could be expected, and a dye laser could be fabricated for the excitation. The specificity of the system is shown in Figure 8. Notice the differentiation that could be made from plant foliage that might be in the surrounding area if an excitation wave length of 590 nanometers were used. Figure 9 shows how the system works, both for oil spills and phytoplankton. In the case of oil, an excitation of 430 nanometers would yield a return signal at 530 nanometers. The plankton is also shown with a Rhodamine - 6G dye laser as the radiation source.

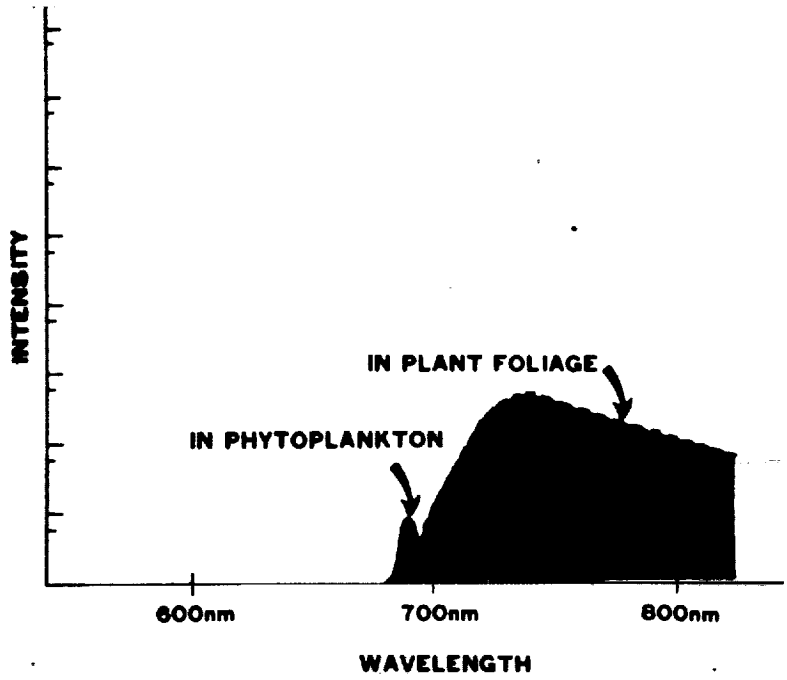

Figure 8. Fluorescence spectra of chlorophyll a

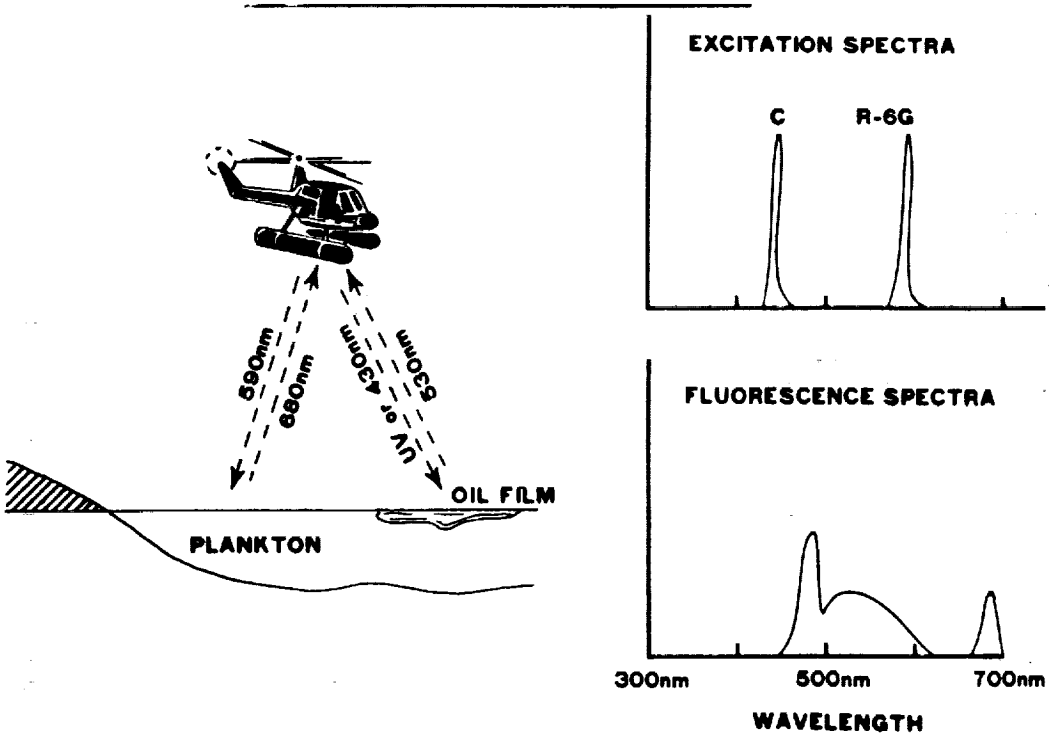

Figure 9. Laser radar technology

Once the system was designed and built, it was tested for practicality and calibrated. Figure 10 shows the calibration of NASA's first laser fluorescence LIDAR. The system was mounted on a pier, 8 meters above the water's surface, and a sufficiently strong return signal at the proper wave length indicated that the system did respond to phytoplankton.

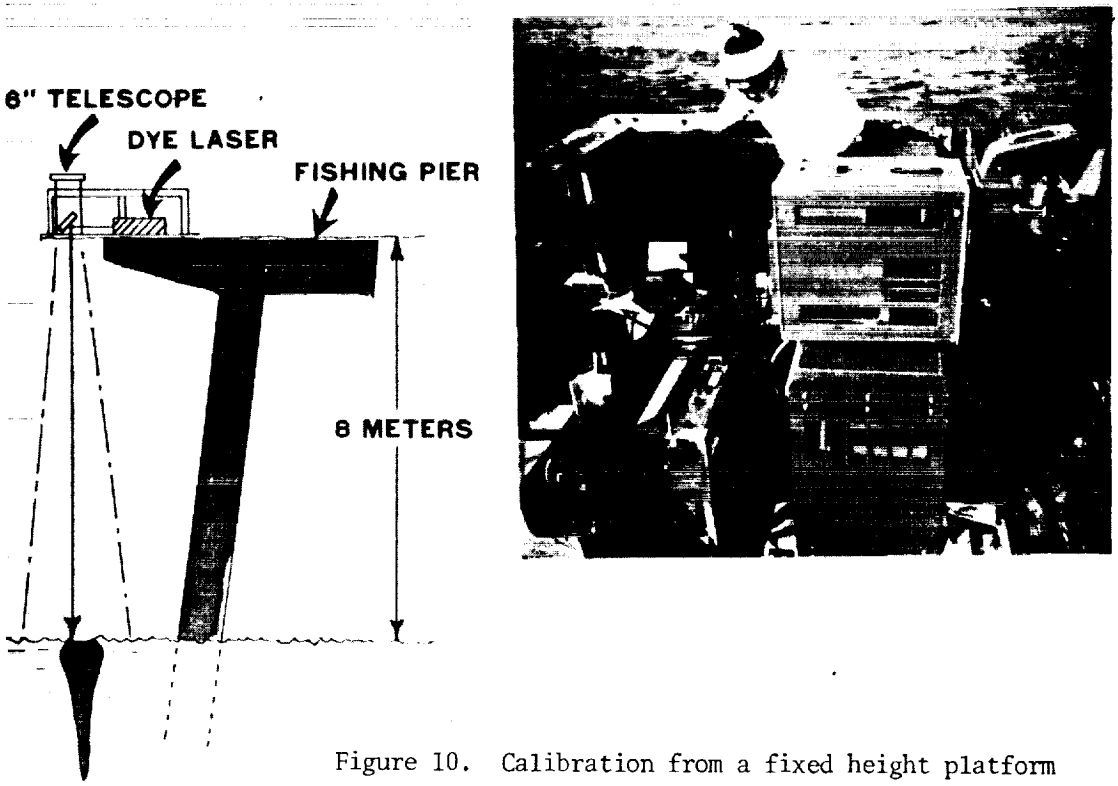

Figure 10. Calibration from a fixed height platform

The next step was to package the LIDAR for flight use. The finished flightworthy system is shown in Figure 11. Here may be seen the dye laser, the receiver telescope, and the power supply and controls as they were positioned in the helicopter.

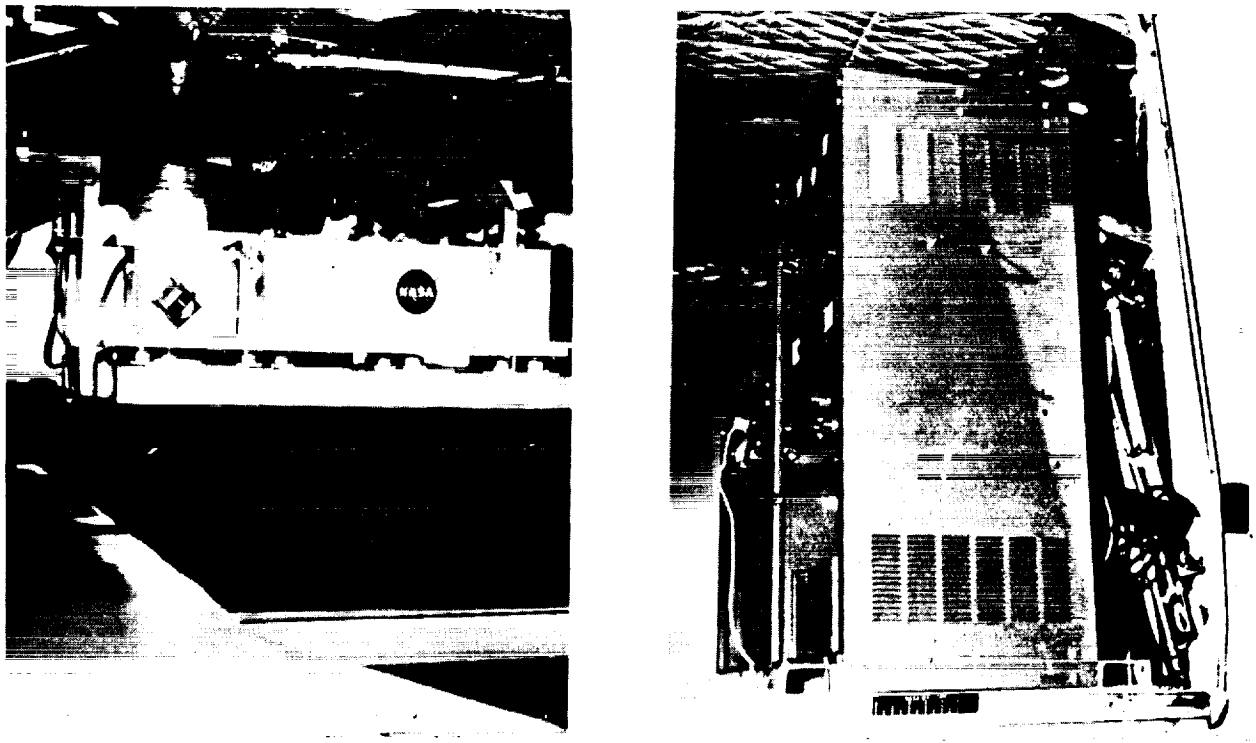

Figure 11. LIDAR prepared for flight use
LIDAR system platform (left), control cabinet (right)

The results of the first airborne experiment are shown in Figure 12, carried out about six months after the program was given the go-ahead. This shows the concentration of phytoplankton in the Chesapeake Bay over a 24-hour period. NASA's results are given by the upper broken line in units of millivolts response of the detector. EPA carried out simultaneous measurements by taking bottled water samples from a boat in the same area as the helicopter fly-by and carrying the samples back to the Annapolis laboratory for analysis. The agreement in the diurnal variation is striking and, at levels of milligrams per cubic meters, the difference in the results is good. It should be mentioned that NASA's results were not calibrated at that time so that good agreement was still possible.

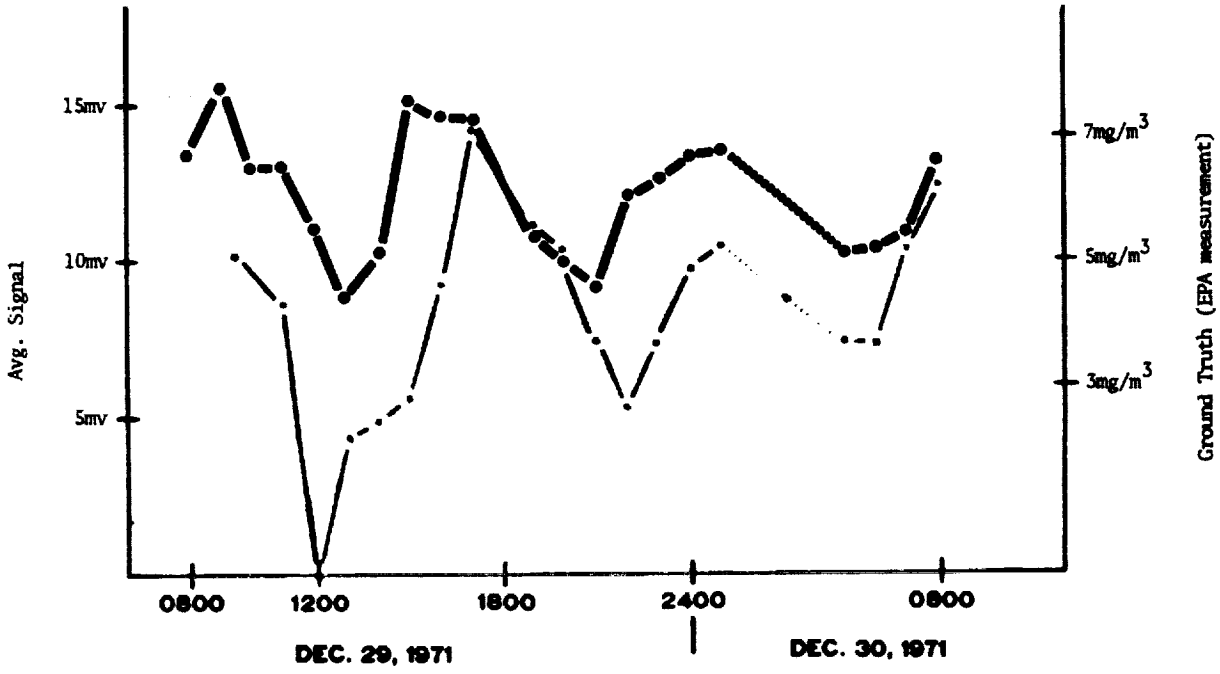

Figure 12. Concentration of phytoplankton in the Chesapeake Bay

The dissemination of these results to the scientific community evoked considerable interest in the method. Amongst them was an invitation by the Canadian government to participate in the International Year of the Great Lakes. Mr. Kim took his airborne system to the Rochester, New York area of Lake Ontario to make measurements. Results are shown in Figure 13. Ten-mile long transects, one-half miles apart were flown and phytoplankton concentrations were plotted as shown. Variations in concentrations are apparent, and what is significant, although not shown, is that the United States side of the Lake is more polluted than the Canadian.

Continued interest in phytoplankton prompted Dr. Mumola of the Langley Research Center this past year to extend the previous fluorescence work to the various types of algae. He has built a four dye laser system, concentrically placed around an excitation flash lamp shown in Figure 14. The working system and its application to the four different colored algae are shown in Figure 15. The upper right corner shows the multicolor laser and the upper left shows the complete package of telescope, laser and detector.

NASA's other activities at the Langley Research Center include a Raman absorption LIDAR System development for the study of soluble constituents of the oceans. The first anion of interest is sulfate, and the flight system for its detection is shown in Figure 16. This system is excited by a 5300 A°1 joule 10 nanosecond pulsed laser and the return signal is received by a 30.5 cm(12 in.) diameter telescope. Initial results from laboratory studies on

sea water indicate the feasibility of sulfate ion detection as shown in Figure 17. Our plan of operation is shown in Figure 18, and it is expected that flight tests using this technique will be completed in Fiscal Year 1977.

Another hydrographic application of LIDAR in a backscattering mode is the measurement of depths of bays and estuaries. Figure 19* is a representation of this application of LIDAR hydrography. In Figures 20, a and b*, an oscilloscope trace shows the surface and bottom return signals from a LIDAR, indicating the feasibility of the approach.

Many other applications of LIDAR suggest themselves. Current flow, rescue of downed pilots, the presence of schools of fish, and oil spills are all possibilities, some of which are currently under NASA consideration and investigation.

NASA is also looking upward in an attempt to measure the background constituents in the atmosphere, as well as airplane emission exhausts and pollutants . Figure 21 shows the first breadboard model of an infrared LIDAR system that can operate in the absorption mode using tunable diode lasers. We have already detected in the laboratory, using a lead selenide laser, the presence of ammonia and sulfur dioxide. We are planning to cover the 2 to 12 micrometer region of the spectrum with several lasers to detect at least six major constituents of interest to our program.

It is obvious from what I have said that NASA has a major stake in LIDAR technology; from the need to provide information as a back-up to our Earth observations, to monitor the exhaust emissions from aircraft, to study our seas and oceans, and to provide sensors for future planetary missions. NASA is prepared to cooperate with interested agencies, universities, and industry in this area to provide more and better information for all mankind.

*Figures 19 and 20 a and b were provided by courtesy of Sparcom Inc.

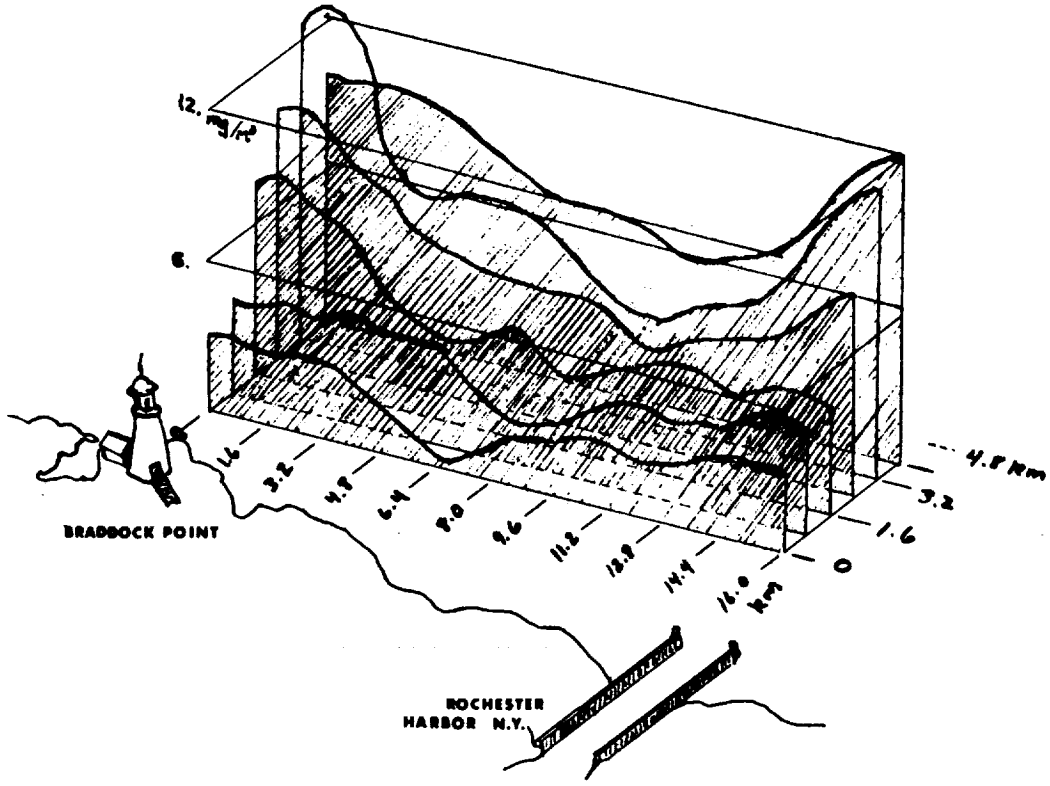

Figure 13. Measurements of phytoplankton levels in Lake Ontario

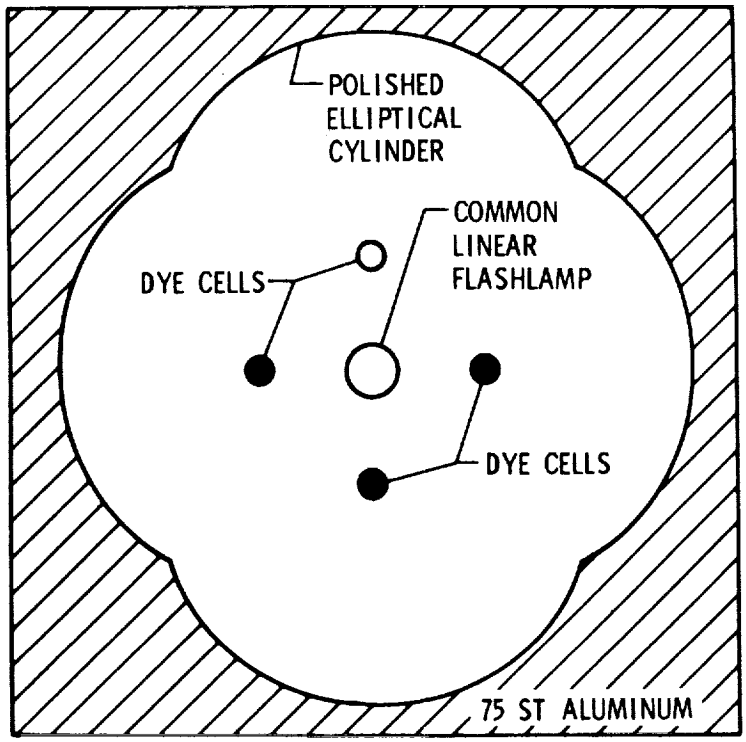

Figure 14. Multicolor dye laser

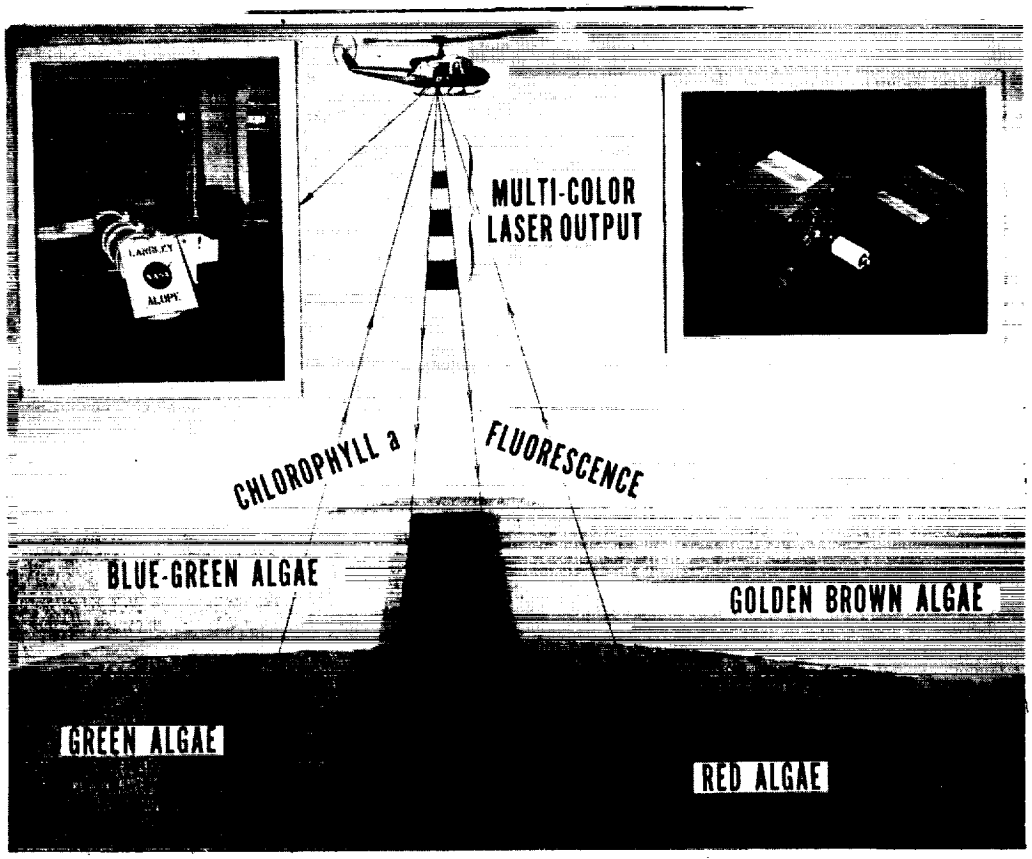

Figure 15. Fluorescence laser techniques applied to algae.

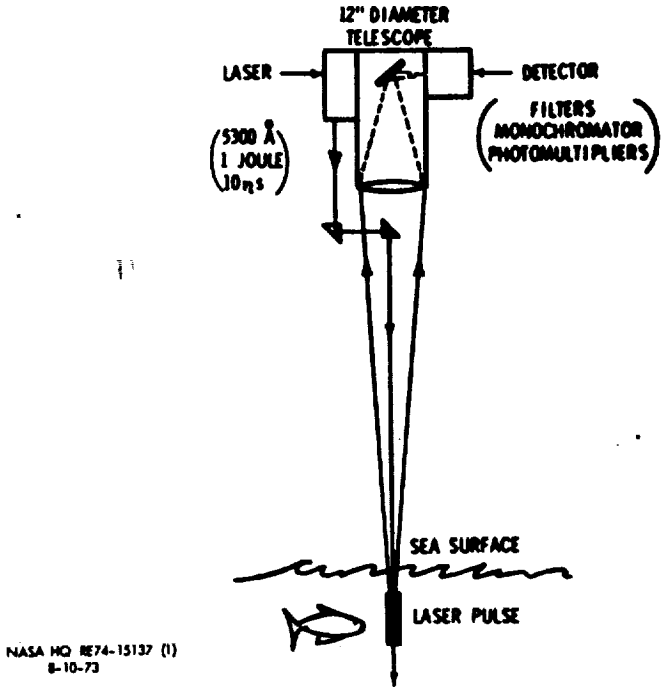

Figure 16. Flight system for remote sensing of salinity by laser Raman spectroscopy of the SO_4=ion

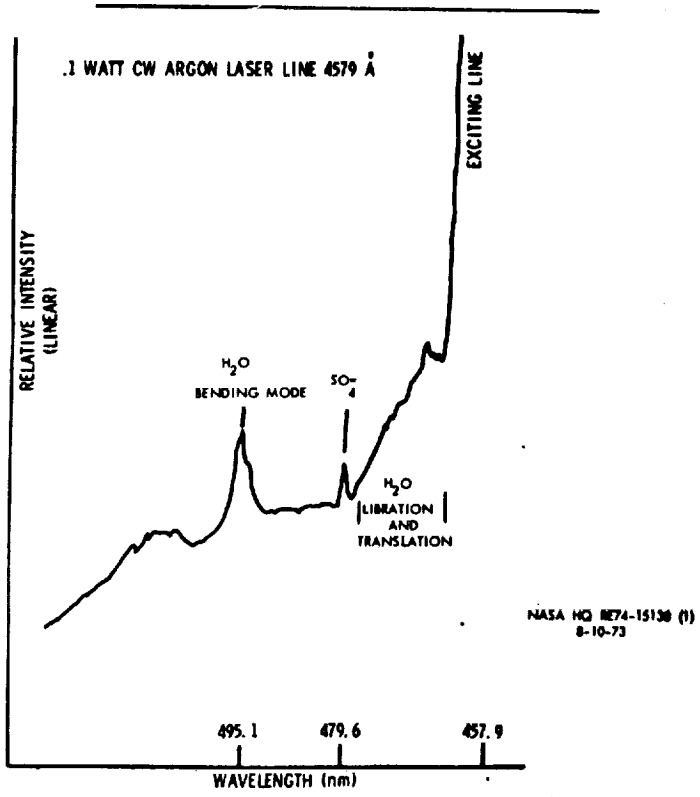

Figure 17. Raman spectrum-water sample from Hampton Roads area

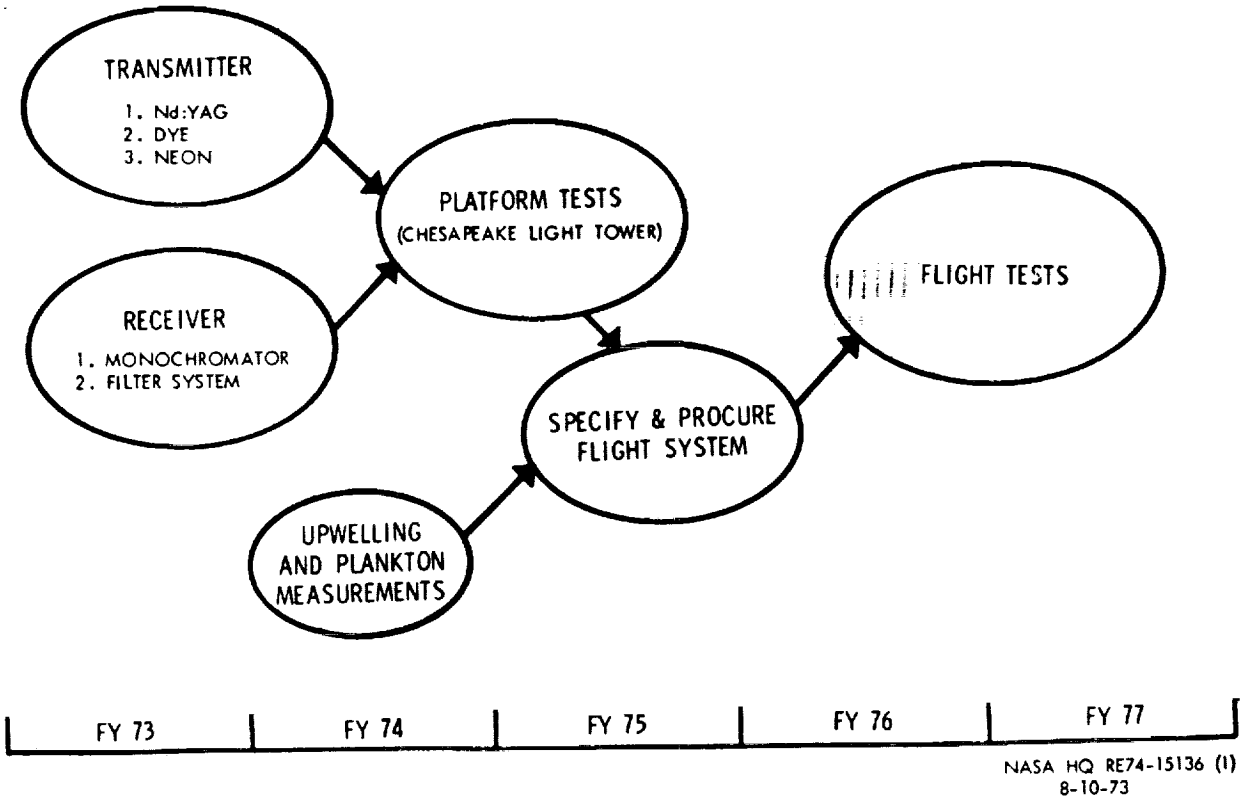

Figure 18. Remote measurement of salinity by laser Raman scattering from $SO_4^=$

Figure 19. Airborne laser bathymetry

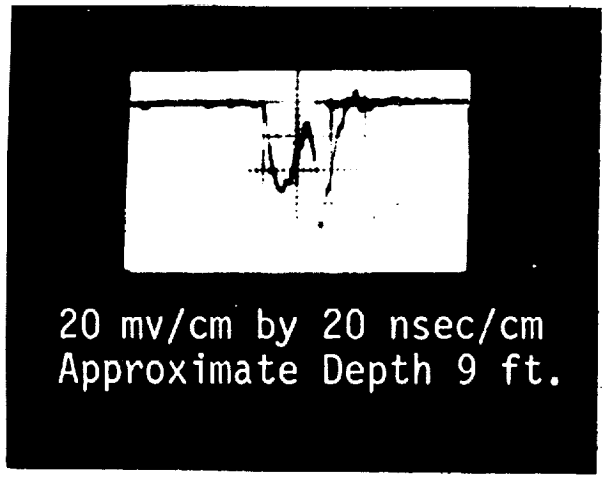

Figure 20a. Oscilloscope trace showing surface and bottom returns

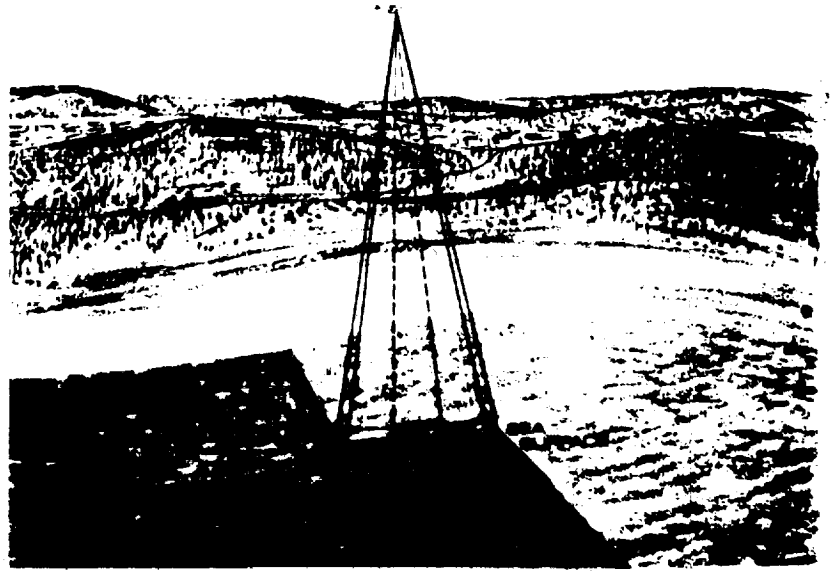

Figure 20b. Cut away view showing laser illumination (dotted) and receiver field of view (solid)

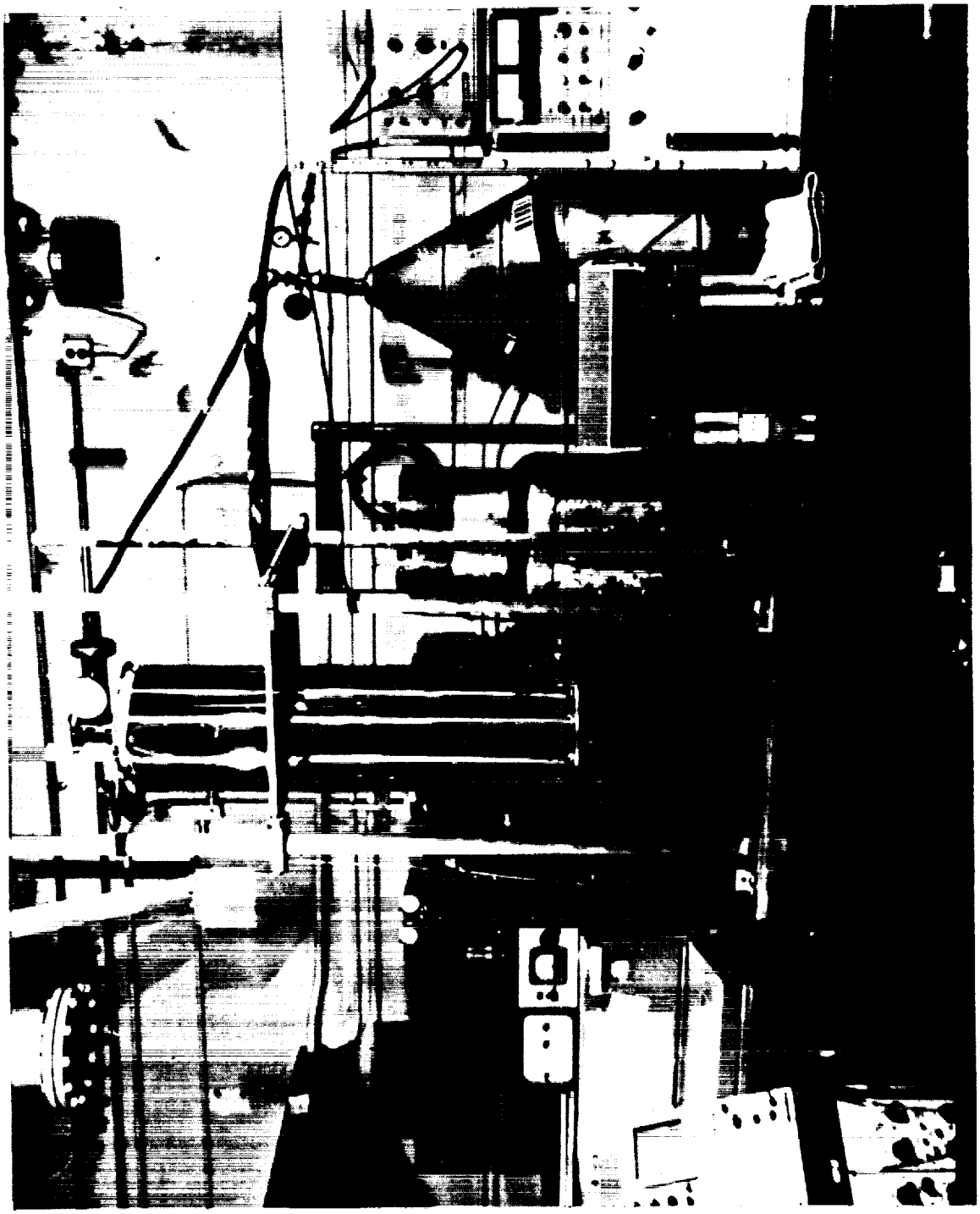

Figure 21. Infrared LIDAR system

EPA'S LIDAR PROGRAM

John D. Koutsandreas
Environmental Protection Agency

(Paper not available at time of publication)

LIDAR PROGRAMS IN CANADA

Dr. Raymond M. Measures
University of Toronto

Canada is a vast country and within her borders lies the largest supply of fresh water in the world. It is therefore natural for airborne hydrographic probing to be regarded as a vital part of her resource surveillance program. Indeed, some three years ago, the Canada Centre for Remote Sensing was created to coordinate the data collection from both aircraft and satellite sensors. Even before the Canada Centre for Remote Sensing was created, Dr. L.W. Morely, the first Director of the Centre, initiated an exploratory program to stimulate new sensor development. This farsighted approach has been reasonably successful; for within this short space of time, three hydrographic LIDAR groups have emerged within Canada.

I shall attempt to present a survey of the hydrographic LIDAR programs in Canada, but will make this a rather brief review as each of the groups are present and we will be discussing their results in detail this afternoon. Figure 1 attempts to illustrate the various ways lasers can be used in environmental sensing to monitor both the atmosphere and the ground. Indeed, a laser may be used to study the atmosphere itself, or probe its contaminants. Lasers may also be used in sampling techniques or they may be mounted on airborne of shipborne platforms.

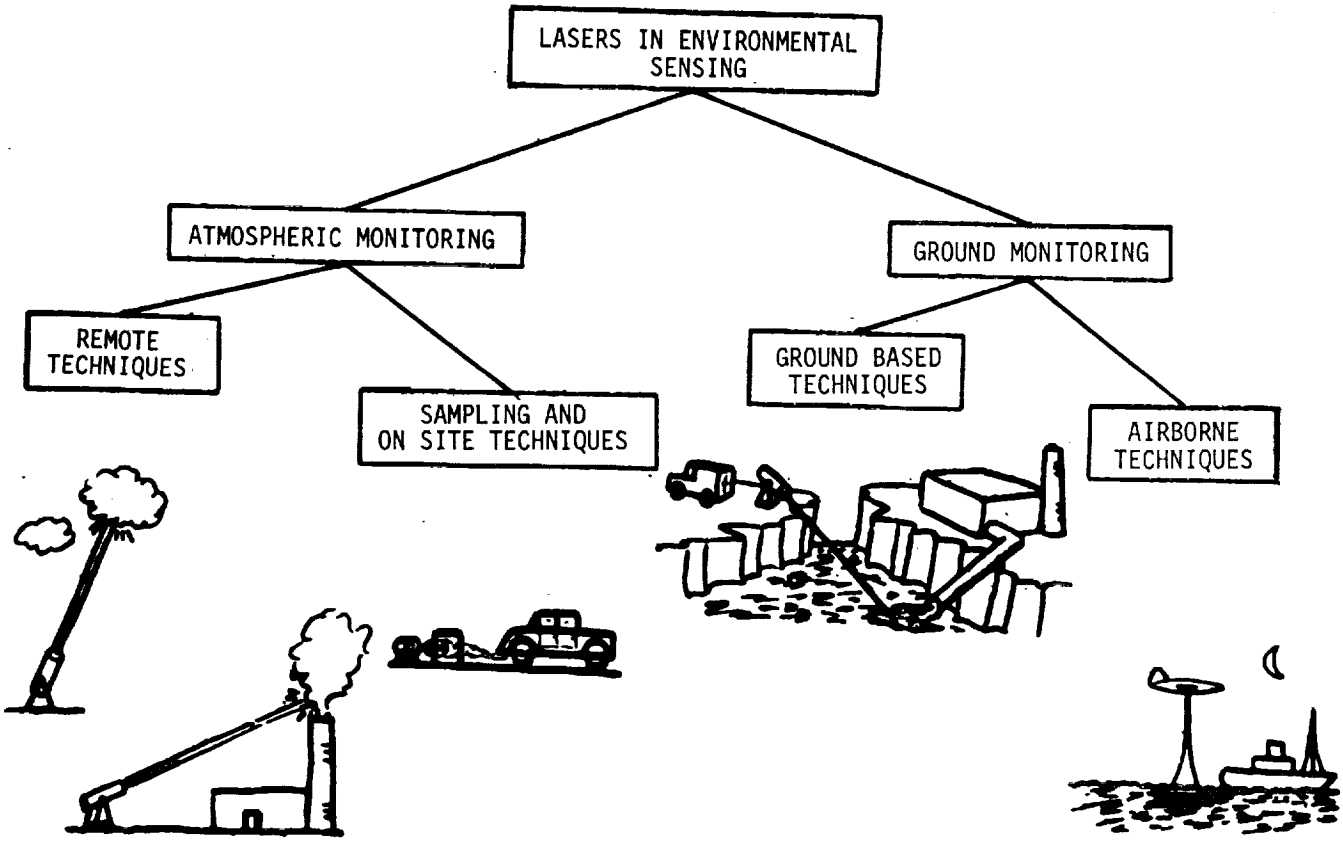

Figure 1. Lasers and environmental sensing

A schematic block diagram for a typical LIDAR system is illustrated in Figure 2. We have, of course, a laser to illuminate the target, some form of output optics, and normally some form of output sampler to maintain a check on the laser output and to provide a zero time reference pulse. The target may then scatter and/or reflect some fraction of the laser beam, or it may be induced to fluoresce. The returned radiation is focused by a telescope onto some form of spectrum analyzer and then detected by a photomultiplier tube arrangement. Both laser induced fluorescence and Raman scattering are techniques that are capable of extracting a great deal of information relating to the target under investigation. In Canada, we have programs which include both of these approaches to remote sensing.

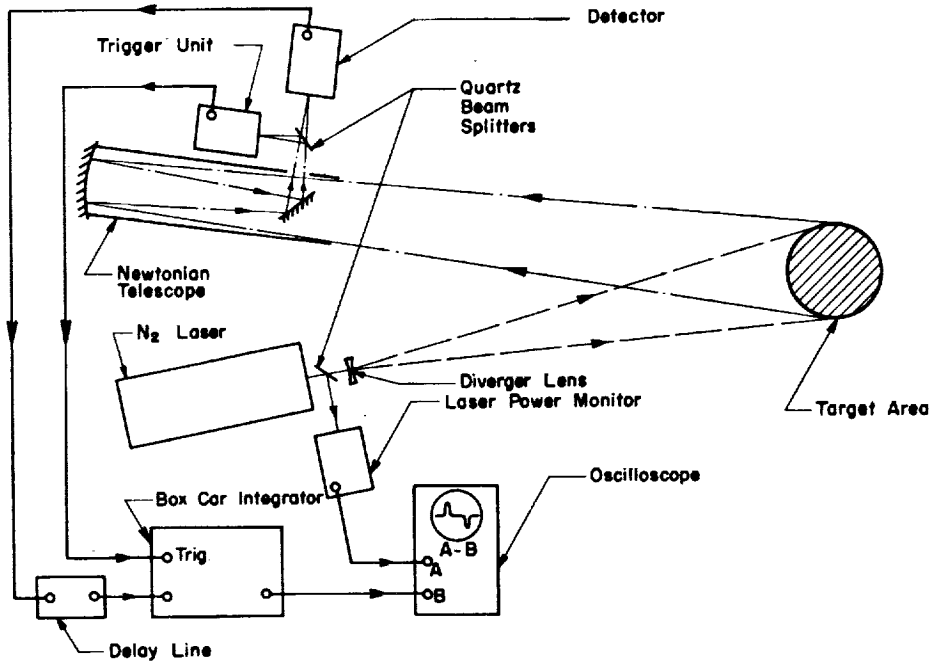

Figure 2. Schematic of typical LIDAR system

Before I go any further, I would like to ensure that the rather diverse audience that we have at this meeting is familiar with these two terms. In both laser induced fluorescence and laser Raman scattering, the radiation field interacts with a specific molecule in such a way that an emission is observed at a frequency that is different from the exciting beam. Here, however, the similarity ends. In the case of fluorescence, the molecule absorbs a quantum of radiation and is raised to an excited state from which it may decay by one of several mechanisms. The decay process of interest arises from the emission of radiation and this we term, fluorescence. In the case of Raman scattering, the laser radiation can be thought to suffer inelastic scattering from the molecules in question. This scattering process changes both the frequency and the direction of the incident radiation. In the case of laser induced fluorescence, the cross-section may be large but due to a number of alternative decay modes, the net emission can sometimes be small and spread over a large spectral interval. On the other hand, in the case of Raman scattering, the cross-section is normally very small (many orders of magnitude smaller than that corresponding to the absorption process) but the radiation is confined to a very narrow spectral interval. This spectral difference between the two techniques leads to a significant difference in the kind of monitoring technique employed. In general, laser induced fluorescence will yield a much larger signal than obtained with Raman scattering, although the difference will not simply reflect the difference in the effective cross-section if the fluorescing molecule is strongly quenched. Moreover, the Raman cross-section may be greatly enhanced if the frequency of the laser is tuned to closely coincide with an allowed transition within the scattering molecules.

In Figure 3, I have attempted to indicate some of the potential applications that are conceived for the laser induced fluorescence approach. I should, however, mention that bathymetry, although listed, does not involve laser induced fluorescence, but can be undertaken with the same system with but minor modification. The facilities and phase of the respective program of the three major hydrographic LIDAR groups in Canada, is represented in Table 1.

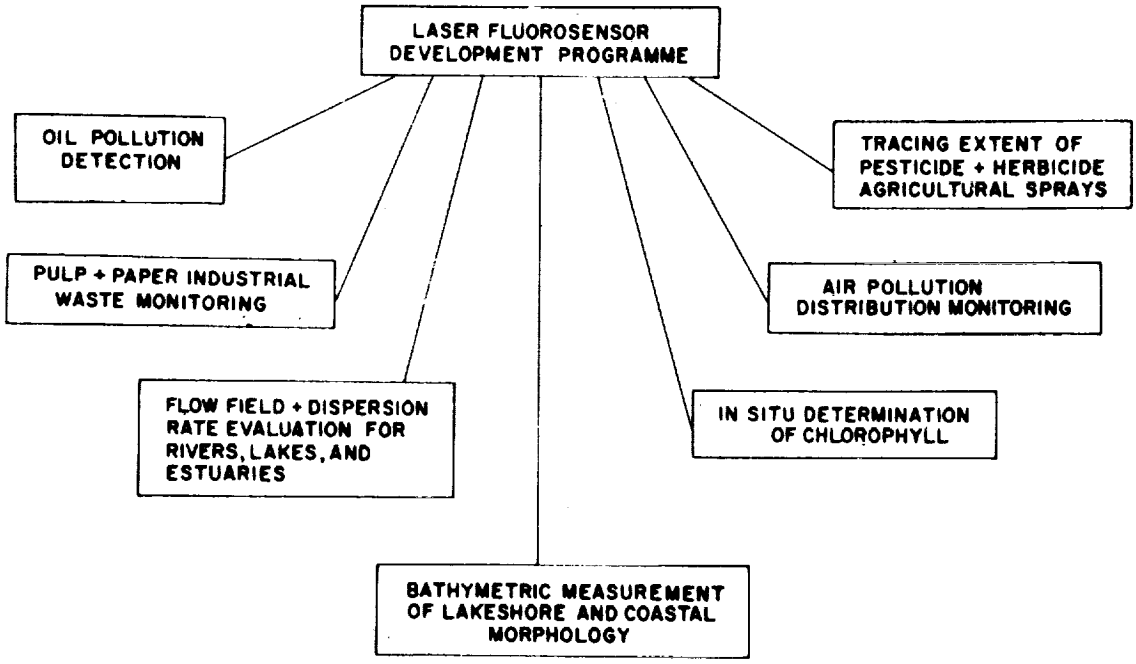

Figure 3. Potential applications for laser fluorosensor

TABLE 1.-CANADIAN HYDROGRAPHIC LIDAR PROGRAMS

	LABORATORY TESTS	PRELIMINARY FIELD TESTS	AIRBORNE TESTS	ADVANCED TECHNOLOGY DEVELOPMENT
UTIAS and CCRS (LIF PROGRAM)	UTIAS Q-switched ruby laser with second harmonic generator (3472Å, 300kW, 17ns, 1ppm)	UTIAS Large nitrogen laser and 8 inch telescope Range = 304.8 m (3371Å, 100kW, 10ns, 100pps)	CCRS UTIAS laser fluorosensor, modified & mounted in DC-3	UTIAS Tunable Dye Laser (4400-4800 Å, 10kW, 15ns, 1ppm) and Small Nitrogen Laser (1kW, 4ns, 20pps)
ENVIRONMENT CANADA (LIF PROGRAM)	Helium-Cadmium Laser & Telescope	Helium-Cadmium Laser & Telescope (4416Å, 15mW cw, 500Hz)	Helium-Cadmium Laser & Telescope Range = 152.4 m	
YORK UNIVERSITY (RAMAN PROGRAM)	Argon Laser 1/2 W av.power cw (single line)	Cavity Dumped Argon Laser 100 W p.power DC-5MHz 1/2 W av.power cw-10ns		

The University of Toronto Institute for Aerospace Studies (UTIAS) has been working in collaboration with the Canada Centre for Remote Sensing (CCRS). The initial UTIAS laboratory work involved a ruby laser with a second harmonic generator; the characteristics of this system are shown in TABLE 1. The preliminary laboratory work using this system was sufficiently encouraging that we developed a prototype version of this instrument, named a "Laser Fluorosensor", to be used initially in field work and eventually in flight trials. This prototype laser fluorosensor uses a nitrogen laser with a 20.3cm Newtonian telescope and was operated during the field trials at a range of close to 304.8 meters (1000 ft). The wavelength of the nitrogen laser was in the near ultraviolet part of the spectrum (3371°A) and the output was 100 kw in a pulse of 10 nsec's duration. The repetition rate could be adjusted to a maximum of 100 pulses per second.

This system has now been taken to the Canada Centre for Remote Sensing where it is being installed in a DC-3 for flight testing. The current UTIAS activity is centered on what we call "advanced technology development" and involves two advances that could lead to a wider range of application for the laser fluorosensor. In the first place, we have demonstrated that the use of an exciting source that can operate at several wavelengths (for example, a dye laser) can improve the specificity of the approach over and above that obtained by studying only the emission profile. Second, we are using a miniature laser fluorosensor of short response that we developed explicitly to study the fluorescent lifetimes of a variety of materials. This system employs a small nitrogen laser which has an output of close to one kw and a duration of about four nsecs. With this facility we have discovered that spectral variations in the temporal profiles of fluorescence represents another parameter, in many ways superior to that of the normal emission and excitation profiles, that one might use for the identification of various target species.

At Environment Canada some initial work has been done with a CW helium-cadmium laser posessing the characteristics indicated in TABLE 1 and shown in Figure 4. In preliminary studies using this system, night observation of the fluorescence of a number of materials, such as crude oils and fish oils, has been demonstrated. Recent low-level aircraft tests have confirmed these results and we will hear more about them this afternoon.

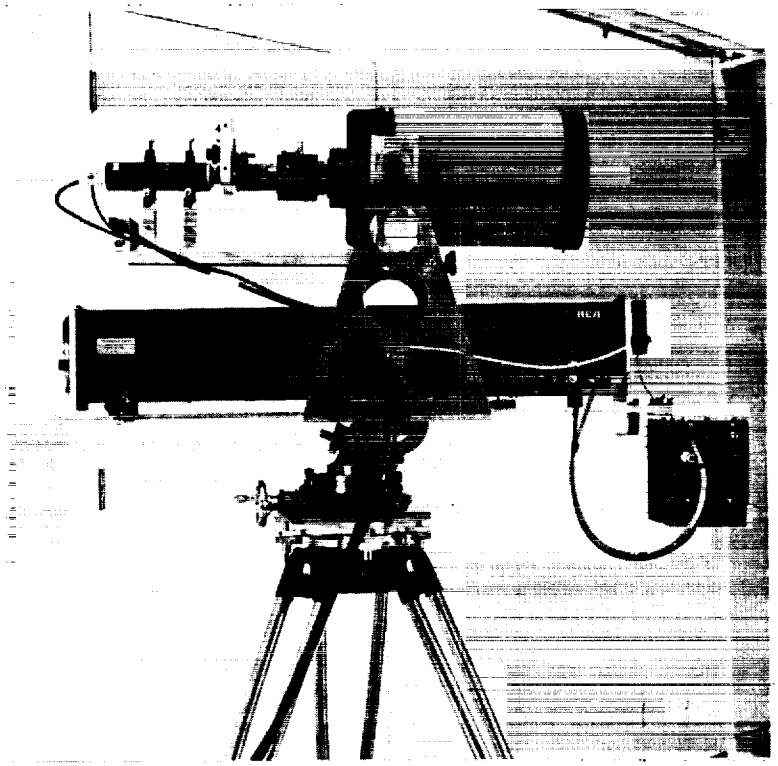

Figure 4. Department of Environment's C.W. Laser fluorosensor

At York University, Dr. Carswell and his group have used lasers to study both the atmosphere and the aquatic environment. The characteristics of his argon laser used for the hydrographic work is presented in TABLE 1. The initial laboratory work was directed at studying the laser beam extinction properties for various samples of water and was undertaken in collaboration with the Canada Centre of Inland Waters. These water scattering measurements have now been extended with the introduction of a cavity dumped argon laser which can produce a high repetition rate output with pulses of 10 nsec duration. This technique also increases the power to about 100 watts which then makes possible ranging measurements. Presently, this system in undergoing field work from a ship on Lake Ontario.

The next figure represents a matrix of measured parameters and targets under study. I have attempted, in TABLE 2, to present an overview of the field and indicate the area of endeavor that each group has undertaken and the stage reached. As you can see, the program can be divided into laser induced fluorescence and Raman scattering. I should, however, reiterate that Dr. Carswell at York is also engaged in work concerning turbidity measurements but this has not been specifically included in this table. For laser induced fluorescence, the major parameters under consideration are: fluorescence intensity against emission wavelength, fluorescence emission as a function of excitation wavelength, fluorescence lifetime and polarization effects. In the case of Raman scattering, the Raman shift may be used for identification, while the relative intensity of a Raman line of a substance of interest to that of, say, water, might be capable of giving directly the concentration of the specific contaminant. Each approach is seen to have a different application and I have selected here three obvious ones: "oil pollution", which includes crude oils and refined petroleum products; "natural resources", which includes fish oils, algae and dye tracing; lastly, I have chosen the heading of "water pollution", which is taken to include both general water quality measurements and identification of specific contaminants of the water.

Measurements of fluorescence intensity as a function of wavelength of emission, for excitation at a fixed laser frequency, have been undertaken at UTIAS, CCRS and DOE. The relative phase of the respective programs is indicated in TABLE 2. The asterisk is intended to represent the advanced technology development that is currently underway at UTIAS and involves the use of a tunable dye laser to excite fluorescence at more than one frequency and also a careful study of the fluorescent lifetimes of a number of materials of interest. This laboratory study at UTIAS has been able to show that a combination of two wavelength excitation and lifetime observation should increase considerably the identification potential of laser induced fluorescence.

TABLE 2.-MATRIX OF MEASURED PARAMETERS VS. TARGETS STUDIED

		OIL POLLUTION		NATURAL RESOURCES			WATER POLLUTION	
		CRUDE OILS	PETROL. PRODUCTS	FISH OILS	ALGAE	DYE TRACING	WATER QUALITY	SPECIFIC CONTAM.
LASER INDUCED FLUORESCENCE	EMISSION WAVE-LENGTH	UTIAS * CCRS C DOE C	UTIAS * DOE A	UTIAS * DOE A	UTIAS B DOE C	UTIAS A DOE C	UTIAS B CCRS C	UTIAS A CCRS C DOE C
	EXCITN. WAVE-LENGTH	UTIAS *						
	FLUOR. LIFETIME	UTIAS *	UTIAS *	UTIAS *				
	FLUOR. POLARIZ-ATION	UTIAS A	UTIAS A					
LASER RAMAN	RAMAN SHIFT						YORK B DOE A	YORK B DOE A
	RAMAN INTENSITY (ratio)						YORK B DOE A	YORK B DOE A

KEY: Development phase attained
A Laboratory Testing
B Field Testing
C Flight Testing
* Advanced Technology Development

The initial laser fluorosensor developed at UTIAS and used for the field work is shown in Figure 5 and is now at CCRS where it will be flight tested shortly. The preliminary field observations of crude oil fluorescence was made from a site on the cliffs overlooking Lake Ontario and were conducted from a range of close to 304.8 meters (1000 ft.). An overview of the mobile facility is shown in Figure 6. The laboratory work at UTIAS has so far indicated that polarization effects are unlikely to be useful in environment studies of oil pollution.

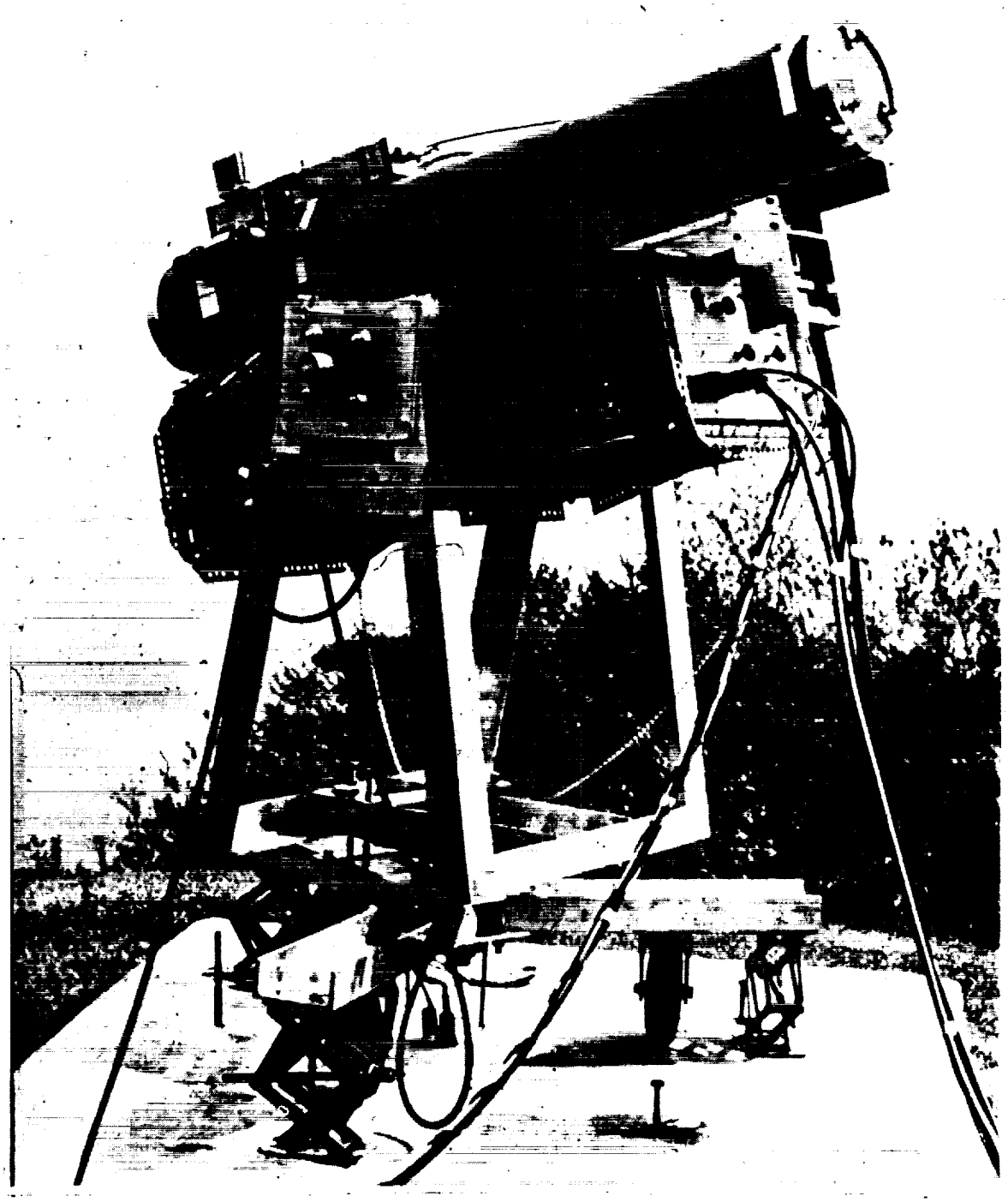

Figure 5. UTIAS - laser fluorosensor

Figure 6. UTIAS - laser fluorosensor field site facility

The Department of Environment is shown here to have conducted some preliminary airborne flight trials for crude oil, pulp and paper waste products, dye tracers and algae, and they have also undertaken some laboratory work in connection with petroleum products and fish oils. However, the work at DOE has so far been restricted to relatively straightforward emission profile evaluation. The Raman work is relatively new with the group at York University having only recently undertaken field tests for both water quality and specific contaminants, while Dr. A. R. Davis at the Department of Environment is concentrating on laboratory Raman studies. However, both groups seem well aware of the possibility of making contaminant concentration determinations by the direct comparison of the relative magnitude of Raman signals due to the OH stretch band of water and that of any given contaminant.

Figure 7 shows the York University hydrographic LIDAR system being used at the Canada Centre for Inland Waters to make observations of extinction and turbidity in a large water tank.

To summarize then, in Canada there are three hydrographic LIDAR groups and their current activities can be classified along three main lines of attack; laser induced fluorescence, Raman scattering, and laser extinction measurements. In several areas, both field and flight trials are either underway or currently planned and the results so far obtained have been encouraging and are likely to stimulate further work in the future, depending on user requirements.

Figure 7. York University hydrographic LIDAR at a Canada Centre for inland waters test tank

REQUIREMENTS FOR AIRBORNE LASER SYSTEMS USED IN COASTAL STUDIES

V. Klemas
University of Delaware

Introduction

One of our investigations in the Delaware Bay region, sponsored by the Office of Naval Research Geography Programs, requires the use of airborne lasers for wave profiling. Several other studies could definitely be enhanced by introduction of active remote sensors, such as lasers. In this paper, I intend to review the requirements for airborne laser systems to be used for the following applications:

a. Photo-optical determination of shallow water wave spectra.

b. Bathymetry in highly turbid waters.

c. Chlorophyll concentration monitoring.

d. Oil dispersion mapping.

As will be shown in the following sections, each of these applications would provide solutions to environmental and ecological problems eagerly sought by national and regional agencies.

Photo-Optical Determination of Directional Shallow Water Wave Spectra

The single most important parameter in Coastal Dynamics is the shallow water wave characteristics concisely described in terms of a directional spectrum for which there is no simple forecasting method. The information about the near-shore wave field can therefore be obtained either through direct measurements of a long term nature, or indirectly through a spatial transformation from the deep water wave field. The latter has more practical potential and is simpler, since there exist some convenient wind-wave forecasting techniques for a deep water wave field, such as the Pierson-Moskowitz (ref. 1) method, and a wealth of wind records already available which are the only required input data for such an analysis. The deep water wave characteristics can subsequently be transformed to the near-shore conditions using a spatial transformation (ref. 2) that is, in general, a function of directional characteristics, depth profile and bottom characteristics. For a given geographical location such as the Delaware Coast, a spatial transformation of deep water characteristics to the shallow water can be obtained via the particular features of the location. High altitude photography can be used as a major tool in correlating and checking the particular transformation as follows: a sequence of aerial photographs taken within a short time period from deep water to one near-shore provides the information on the directional spectrum of the waves, and its spatial change as the waves progress into the shallow water. This is directly used to check the spatial transformation based on the local characteristics in terms of depth profile, bottom characteristics and boundaries.

A similar but limited type of information can be obtained by studying a profile of the sea surface with an airborne laser (ref. 3). A profile taken along the direction from deep to shallow water provides the surface characteristics and their spatial modifications in that

particular direction. The inhomogeneous wave characteristics in that direction are analyzed in a fashion analogous to that of the non-stationary wave spectrum of wave records collected as a function of time at a fixed reference (ref. 4 and 5). The concepts are exactly the same if the time variable is replaced with the spatial variable.

One additional significance of a laser profile is that it may provide additional information as to how to choose the optimal size of the area to be photographed from high altitude. This can be explained as follows: the directional spectral estimates from aerial photographs involve statistical errors due to three principle sources; i.e., statistical variability, resolution in wave number, and bias due to spatial inhomogeneity. An optimal choice of the area size must be uniquely determined by minimizing the error due to all three of these sources of error. An inhomogeneous wave field is also characterized by measures of bandwidth in wave number and space domains. These respectively measure how the directional spectrum changes as a function of wave numbers and space. For instance, a small bandwidth in space implies a highly inhomogeneous sea surface with respect to space.

A test on Delaware's Atlantic coastline, 3.2 kilometers north of Indian River Inlet, was selected for reasons of convenient access and suitable bottom profile. Two wave towers were erected in 5.49 meters (18-feet) depth, well outside the surf zone. Cables from 1.82 meters capacitive wave probes, mounted on the tower, carried calibration and wave signals to tape and strip chart recorders located in a trailer in an enclosed state compound.

Tri-X acetate-base film was selected for its speed, resolution and optical processing properties. Since the image of the sea bottom shows up as background noise in the wave transforms, a Kodak Wratten 25A filter was used to eliminate the water penetration of the blue and green bands. Also the sun angle was selected so as to minimize shadowing.

The Fourier transforms of wave patterns in aerial photographs were produced by illuminating the photograph with a laser beam and focusing the transmitted beam with a spherical lens (Figure 1). The transform pattern shows the dominant wave pattern as a circular dot of finite size at the appropriate wave length and angles (Figures 2 and 3). The distance of the dot from the center of the pattern is inversely proportional to the wave length (ref. 6, 7, and 8). The finite size and irregular elongation of the spot is used to identify higher and lower frequency components in the wave spectrum. Microdensitometer scans across photographs of the optical Fourier transform in Figure 3 are shown in Figure 4. Since the image of the sea bottom shows up as background noise in the wave transforms, spectral bands such as the red and near infrared were used to minimize water penetration. Also sun-camera angles were selected so as to decrease the relative visibility of underwater features.

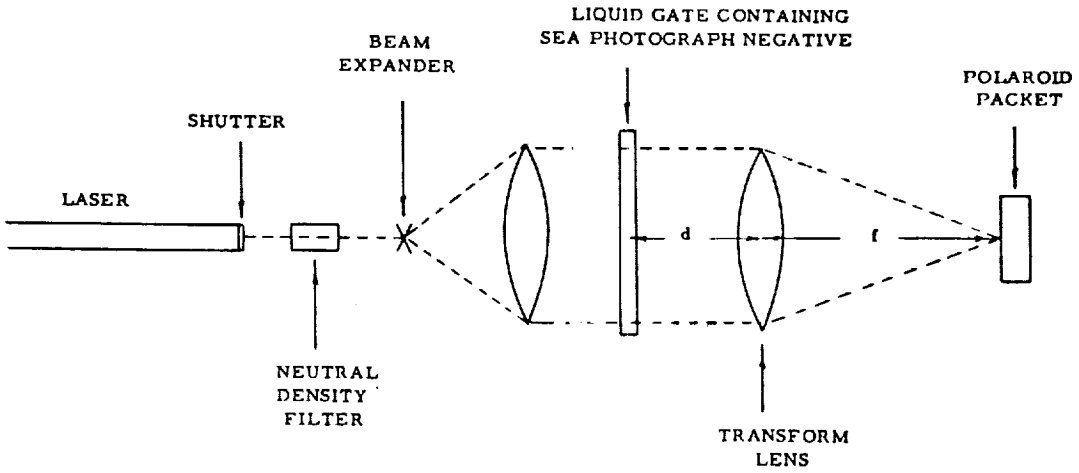

Figure 1. Schematic of optical bench for processing of sea photographs

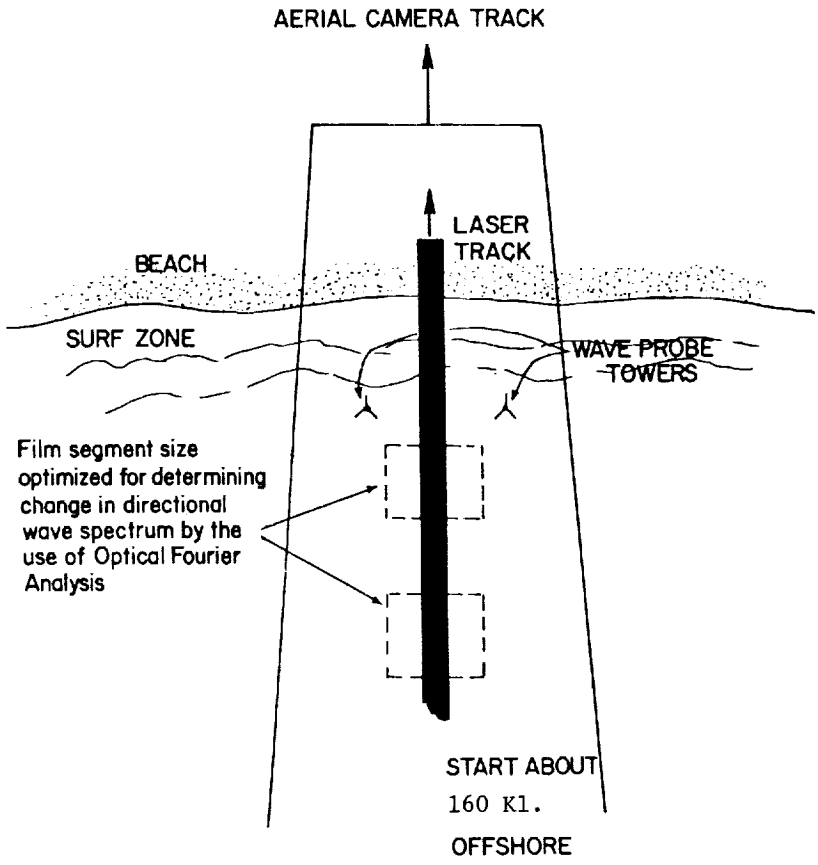

Figure 2. Aircraft camera and laser profiler ground tracks

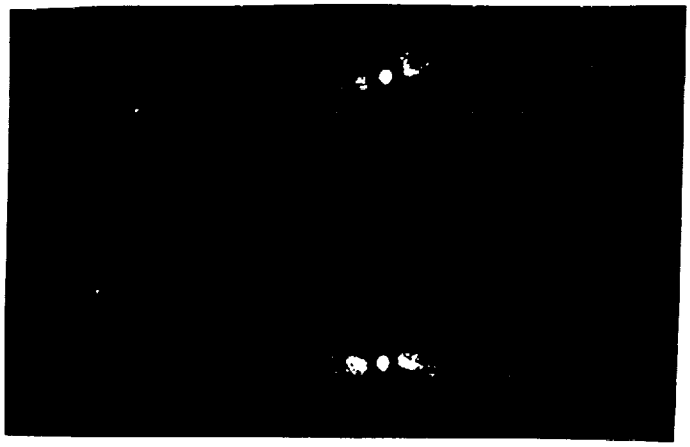

Figure 3. Optical fourier transform of wave patterns

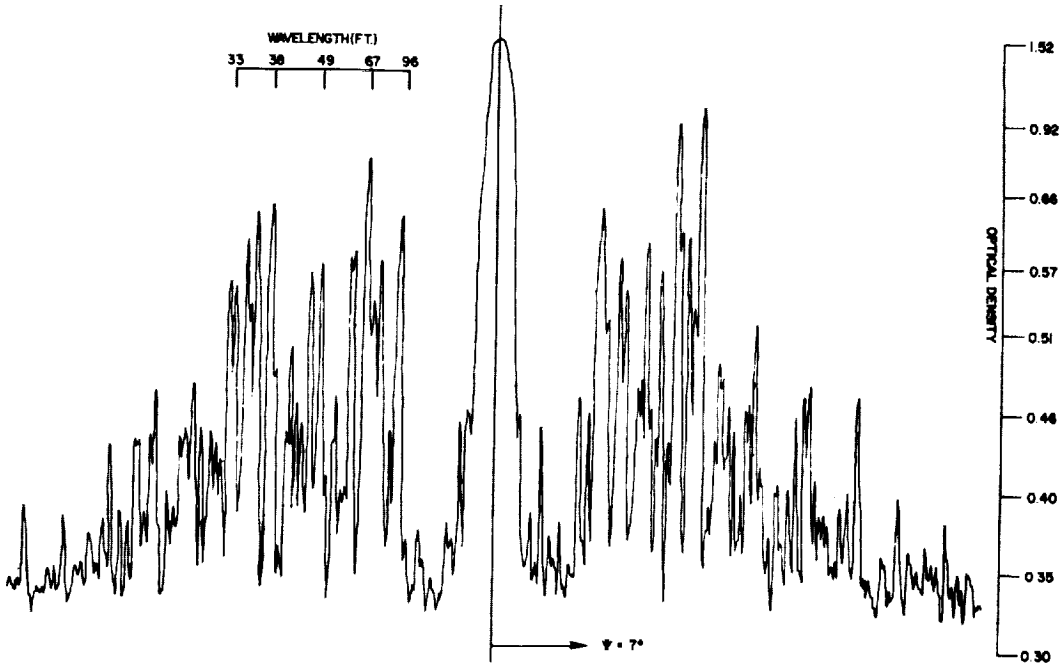

Figure 4. One-dimensional density tracing of fourier transform

During the summer and fall of 1973, flights of aircraft equipped with cameras and a laser profiler were flown along a 161 kilometer long transects into shore, monitoring waves going from deep water to near-shore conditions. The laser profiler was provided by the Naval Oceanographic Office and is mounted on a NASA aircraft stationed at Wallops Island, Virginia. The ranging technique utilized consisted of amplitude modulation of a continuous wave helium-neon laser of red light at 0.6328 microns. The laser beam can be 100% amplitude modulated at frequencies of 1, 5 and 25 MHz with a maximum altitude resolution of $\pm$ .061 meters (0.2) ft. The resolution and accuracy of the laser system appears sufficient for this study, but the biggest problem seems to be unfavorable weather conditions and availability of aircraft.

Bathymetry in Highly Turbid Waters

In Figure 5a is shown an MSS band 5 image of Delaware Bay obtained from NASA's ERTS-1 satellite on January 26, 1973. (I.D. No. 1187-15140). The cross-section monitored in the upper portion of the bay shown in Figure 6 exhibits a Secchi depth variation from 19 to 51 centimeters only. Such studies of turbidy, circulation and water boundaries from aircraft, satellites and boats (ref. 9) have shown that Secchi depths in Delaware Bay vary from about 2.5 to 0.1 meters with corresponding sediment concentrations from 2 to 40 mg/liter. The equivalent attenuation coefficients (oC) for these conditions are 1.3 and 30, respectively. A 30 Kw pulsed neon laser system operating at 0.5401 microns as described by Hickman, Hogg and Ghavanlon (ref. 10) would from 500 meters altitude be able to penetrate to depths from about 12.5 to 0.5 meters, respectively. The deeper penetration depth will occur over the less turbid central portion of the bay, where the water depth in many places exceeds 12.5 meters. As a result bathymetry of turbid coastal waters will be difficult indeed.

Figure 5a. ERTS-1 image of Delaware Bay obtained in MSS Band 5 on January 26, 1973 (I.D. No. 1187-15140).

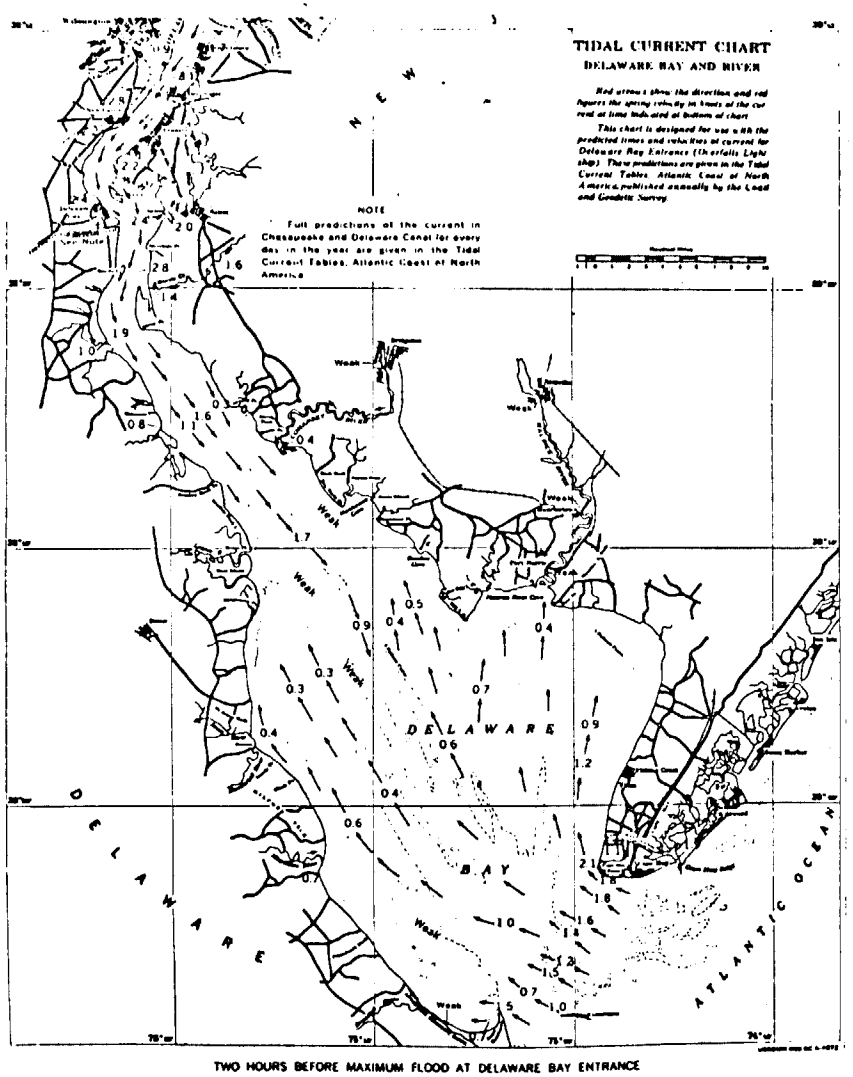

Figure 5b. Predicted tidal currents in Delaware Bay during ERTS-1 overpass on January 26, 1973

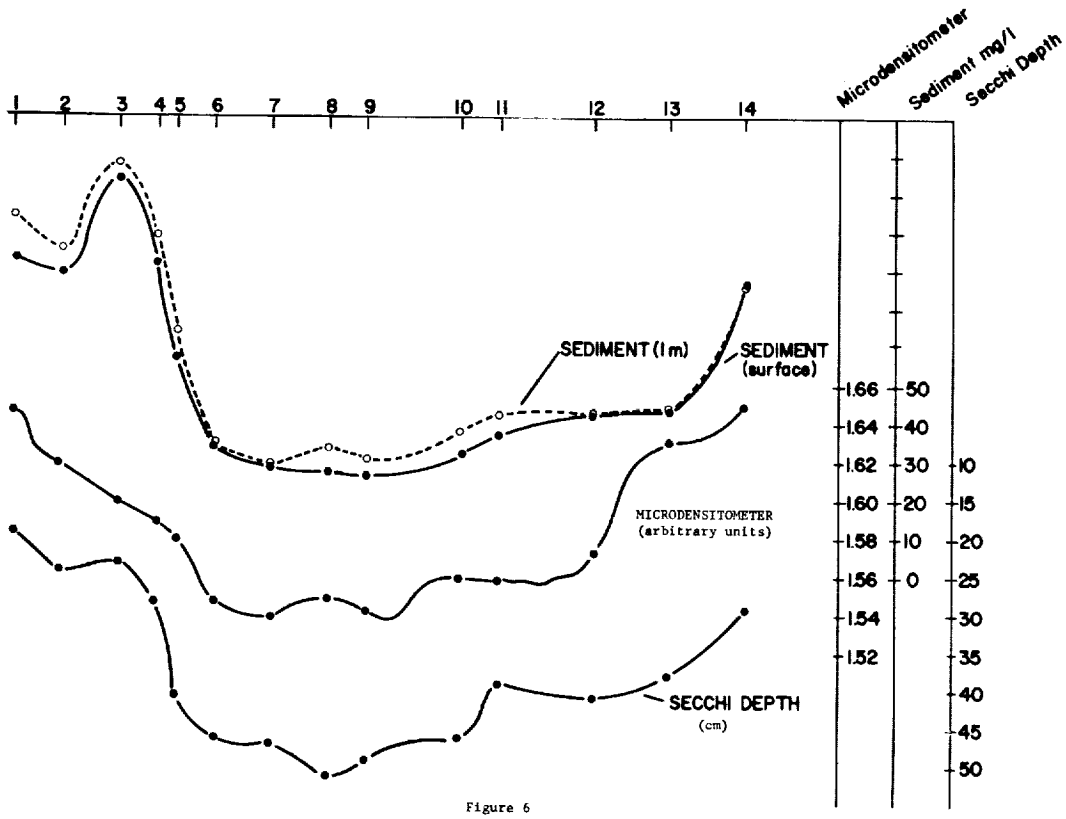

Figure 6

Figure 6. Secchi depth variations in Delaware Bay

Mapping Oil Dispersion and Predicting Oil Slick Movement

Approximately 70 percent of all the oil that is delivered to the east coast of the United States moves by water up the Delaware Bay and River. Much of this oil is transferred several miles off the coast or inside the Bay mouth from large deep draft tankers to barges (lighters) or to small tankers to reduce the draft of the large tankers and allow navigation up the Bay and River for unloading at docks. In 1971, over 45 million short-tons of crude petroleum was transported through the Bay. Over 200 tankers and 330 barges used the Big Stone Beach Anchorage Area within the Bay that year (ref. 11). In over ten years of lightering operations in the lower Bay, no major oil spills attributable to this transfer operation have occurred. However, the heavy shipping traffic within the Bay and large transfer operations in the lower Bay indicate a finite probability for the occurrence of either collision and grounding of tankers or lighter barges or spills due to transfer operations.

Due in part to the nation's energy shortage, studies (ref. 11) indicate that oil transport through Delaware Bay and transfer activities in the Bay will increase markedly in the future. The accelerated growth of these activities is inevitable whether a superport is developed in the Bay or adjacent waters or whether oil is extracted from the Continental Shelf. The national and regional concerns over such development focus in large measure on the environmental vulnerability due to oil spills. Regional concern over the potential hazard of present transfer operations has increased recently. Central to all facility development, oil transfer operations, and clean-up operations is information regarding the physical movement and distribution of an oil spill. Site selection, environmental impact assessments and prevention and clean-up strategies for the Bay region all require information about potential oil spills. Moreover, planning and management agencies require a model of oil slick movement in Delaware Bay which has predictive or forecasting ability.

The model being developed is expected to perform two functions at two different levels. The first function is to provide technical information for tracing oil spills as they occurred; whereas, the second function is to furnish strategic information about oil spill potential at various regions in the lower Delaware Bay. The former is aimed at assisting users engaged in operation and control such as oil transshipment companies, U.S. Coast Guard and the like. The latter, in addition to aid operation and control agencies, is expected to provide information for planning and management agencies in the Delaware Bay area including Delaware State Planning Office and Delaware River Basin Commission, etc.

As a result, there is a need to map oil dispersion and movement in Delaware Bay in several different ways. First, ultraviolet and infrared photography are being employed to track oil slicks to determine their movement as a function of tide, current, wind and location with the intent to calibrate and verify the models. Second, biologists need to know the average concentration of oil and related products down to about 10 ppm throughout the Bay in order to assess its effect on bay ecology. The airborne laser fluorosensor for the detection of oil derivatives on water successfully tested by NASA (Kim and Hickman, ref. 12) seems capable of meeting most oil monitoring requirements. The system transmits 337 nm U.V. radiations at the rate of 100 pulses per second and monitors flourescent emission at 540 nm. Daylight flight tests were made over the areas of controlled oil spills and additional reconnaissance flights were made over a 50 km stretch of the Delaware River to establish ambient oil baseline in the river. The results show that the the system is capable of monitoring low concentrations of oil which cannot be identified by ordinary photographic flights while water samples are taken from boats along the same transsect. The correlation of actual oil content in the water samples with the laser detector output trace would produce a calibration of the system and give an indication of its accuracy.

Marsh Productivity and Chlorophyll Concentration Monitoring

The tidal marsh is considered to be one of the most dynamic natural units. It is an ecosystem where there is a continual interaction between the various biotic and abiotic components. We can see some of the obvious results of these interactions, plant and animal distributions, sediment accumulation and erosion, feeding, resting and breeding of various animals, the ebb and flood of the tide. The tidal marsh can also be considered to be an ecotone, the boundary area between two major ecosystems, yet has its own unique features. The tidal marsh has plants and animals found in the adjoining uplands and in the sea. These marsh acres receive water from upland drainage and from the sea. The results of these interactions produce something unique - a tidal marsh.

It is most important to evaluate the potential contribution of a salt marsh ecosystem to the marine environment and how man's activity can alter this contribution. The salt marsh, one of the most productive regions of the temperature zone, has received only moderate attention in terms of quantitative evaluation of its importance as a natural resource. The biogeochemical cycles of salt marsh are intimately associated with the estuarine environment in terms of conservation, fisheries, industrial developments, and aesthetics. Quantitative evaluation of Delaware salt marshes, would delimit the parameters to allow more effective utilization of this valuable natural source. This study would provide the knowledge needed to properly assess the value of the wetlands to the estuary and coastal waters.

Remote sensing techniques, including color infrared photography, thermal infrared photography and airborne laser techniques can be employed in conjunction with ground measurements to map the primary productivity of tidal marshes (ref. 13). Initial steps towards mapping marsh productivity and relative value have already been taken. Overlay maps of Delaware's wetlands have been prepared, showing the dominant species or group of species of vegetation present (ref. 14 and 15).

Five such categories of vegetation were used indicating marshes dominated by (1) salt marsh cord grass (Spartina alterniflora), (2) salt marsh hay and spike grass (Spartina patens and Distichilis spicata), (3) reed grass (Phragmites communis), (4) high tide bush and sea myrtle (Iva species and Baccharus halimifolia), and (5) a group of fresh water species found in impounded areas built to attract waterfowl. In addition, major secondary species were indicated where appropriate. As shown in the two sample maps of the Bombay Hook and Taylor's Bridge marshes small representative areas of each of the major marsh regions were analyzed and enhanced to show detailed growth patterns not shown on the large scale maps. Photo-interpretation of NASA RB-57 and other aerial photographs were checked out by field teams and low altitude aircraft. As shown in Figures 7 and 8, the overlay maps have a scale of 1:24,000 and can be superimposed on USGS Topographic or Soil maps. Fifteen such maps cover Delaware's wetlands from the Pennsylvania to Maryland borders.

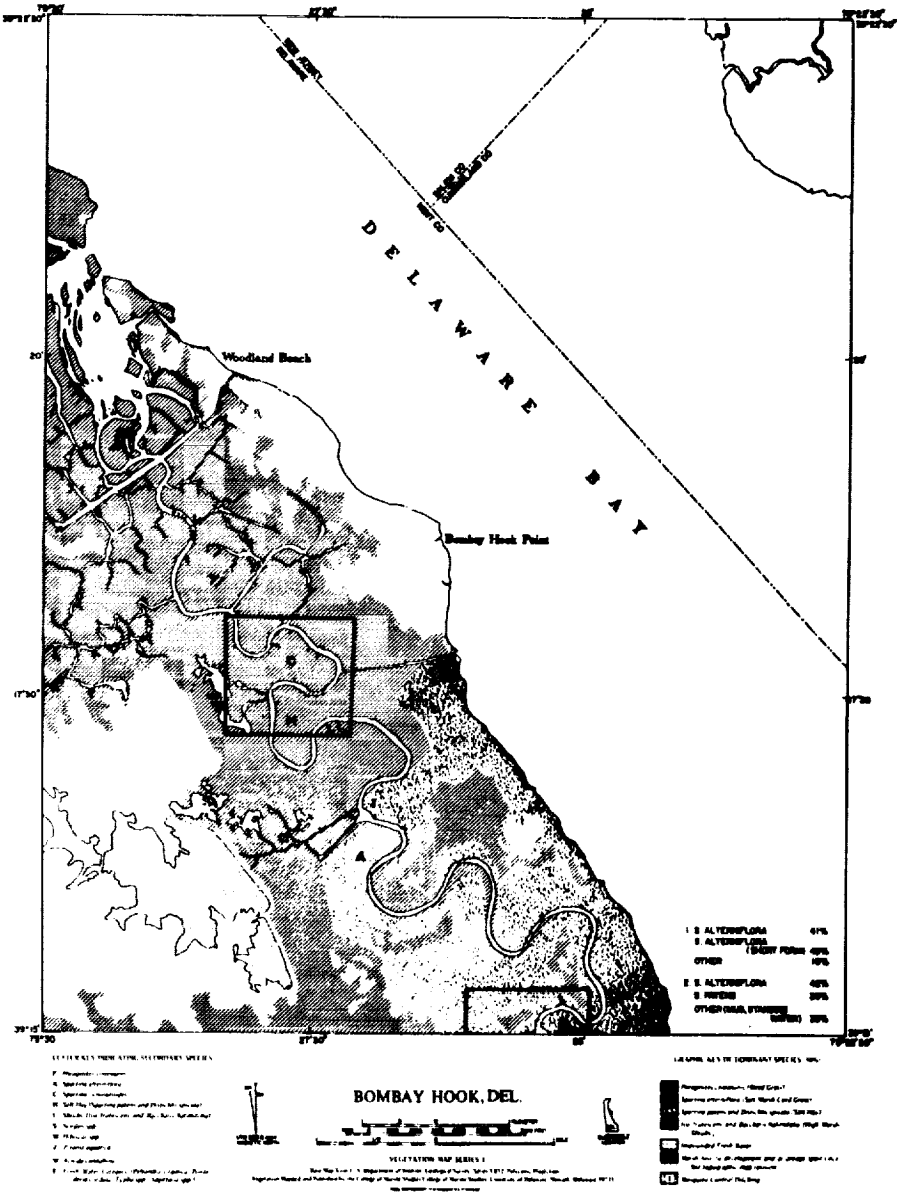

Figure 7. Wetlands map of Bombay Hook, Delaware

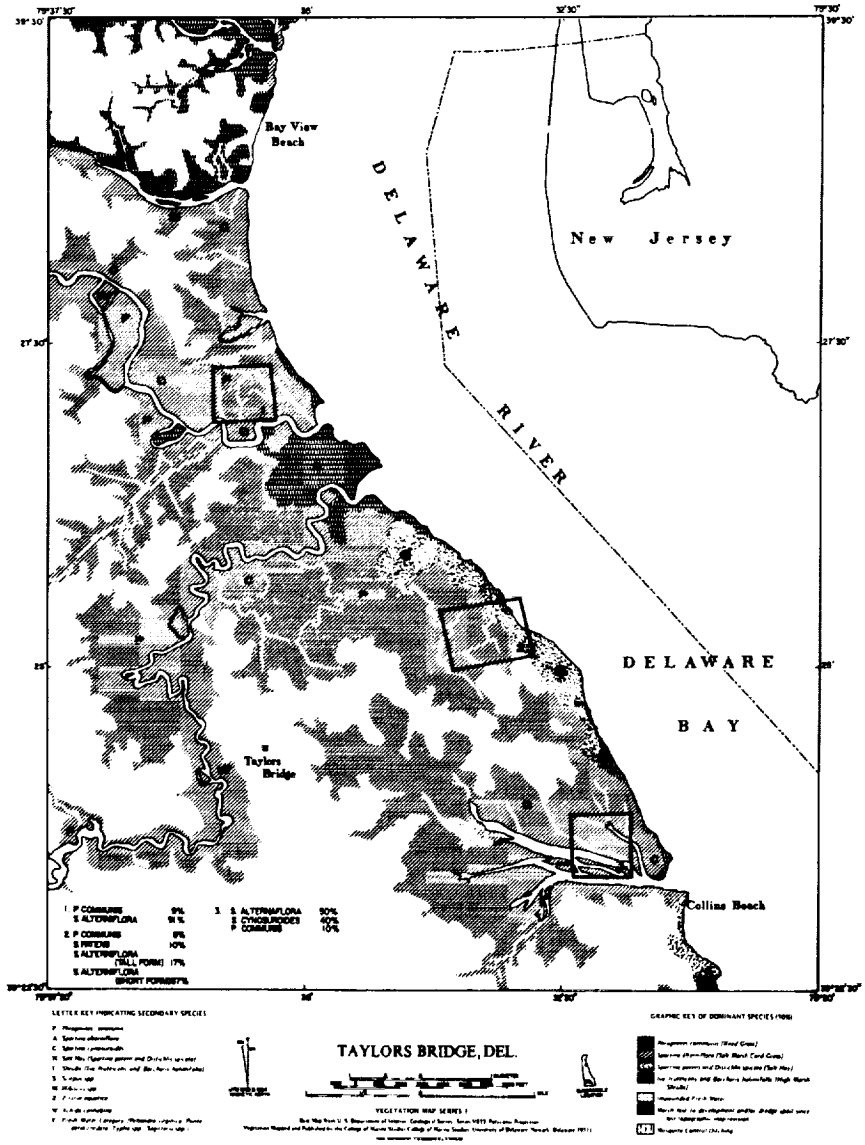

Figure 8. Wetlands map of Taylor's Bridge, Delaware

The mapping technique employed utilizes the General Electric Multi-spectral Data Processing System (GEMSDPS). The GEMSDPS is a hybrid analogue-digital system designed as an analysis tool to be used by an operator whose own judgment and knowledge of ground truth can be incorporated at any time into the analyzing process. The operator can combine his knowledge of the scene gained in the field and by visual interpretation of the aerial photographs with electronic analysis: (1) measure the spectral characteristics of any chosen region of any size in the scene; (2) search the scene for regions with similar characteristics and once they are identified, enhance and store them; (3) modify the stored image if necessary to make it compatible with his knowledge of the area; and (4) read out the percentage of the total scene occupied by regions with the specified spectral signature. By repeating the procedure for other regions in the scene, the operator can quickly produce a composite photo map, enhancing all of the spectrally classified objects or regions of interest. The result is a high speed, cost-effective method for producing enhanced photo maps showing a number of spectral classes -- each enhanced spectral class being representative of a vegetative species or group of species.

A laser fluorosensor can be used to map the chlorophyll concentration in the water and quantify it in terms of plankton and detritus. This approach may enable us to assess the amount of detritus and plankton transferred from the marshes into the bay. The chlorophyll concentration determined with the laser fluorosensor could be used to extend on-boat fluorometer readings to large areas. The final concentration maps can be compared to predictions derived from a dynamic model of the bay.

The airborne laser fluorosensor for the remote measurement of algae (phytoplankton) and chlorophyll in the sea has been successfully operated over the test areas of Lake Ontario where the U.S. Chemical and Biological Programs for the International Field Year for the Great Lakes (IFYGL) were conducted during the summer and fall of 1972 (ref. 16).

The NASA prototype unit works on the principle of monitoring laser induced fluorescence from chlorophyll a pigment bearing algae. An organic dye laser and a 18 cm diameter Newtonian telescopic receiver mounted on a helicopter are salient features. Laser pulses at 590 nm (Rhodamine 6G) were transmitted downward and the induced fluorescence due to the presence of algae was monitored at 685 nm. Previous laboratory measurements indicate that the conversion efficiency for fluorescent signal is in the order of 1.0×10^{-9}. A combination of 5 nm bandwidth optical filter, and fast measurement time of the detector enables us to discern the faint signal from other background noises. The system is capable of measuring the chlorophyll a concentration from 0.5 mgs/m^3 to 30 mgs/m^3 in 256 scales from aircraft altitudes of about 100 meters (ref. 17).

The state of the art of laser development is such that it now seems possible to measure chlorophyll concentrations near the surface of the water. This is important since chlorophyll is a major factor in the ability of plants to utilize light for energy by photosynthesis. But we would like to go a step further. First of all, we would like to excite not only the chlorophyll line but we would like to obtain ratios of chlorophyll a to other pigments. The multiwavelength LIDAR described by Mumola, Jarett and Brown (ref. 18) at this conference, would be ideally suited for this task. Such ratios could provide an indication of the actual nutritional status of the material. For instance, as the carotenoid to chlorophyll a ratio increases, the culture is getting older and its nutritional capability is being depleted. Also it would be ideal if the laser monitoring system would integrate optically over the entire euphotic zone.

References

1. Pierson, W.J. and Moskowitz, L., 1964. A proposed spectral form for fully developed wind seas based on the similarity theory of S. A. Kitaigordoskii, J. Geophysical Res., Vol. 69, No. 24, p. 5181-5190.

2. Collins, I. J., 1972. Prediction of shallow water spectra, J. Geophysical Res., Vol. 77, No. 15, May.

3. Schule, J. J.; Simpson, L. S.; and Deleonibus, P.S., 1971. A study of fetch-limited wave spectra with an airborne laser, J. Geophysical Res., 76, 4160-4171.

4. Tayfun, M. A.; Yang, C. Y.; and Hsiao, G., 1973. Non-stationary spectrum analysis of ocean waves, accepted for publication, Proc. of the Thirteenth Int. Conf. on Coastal Engr., ASCE.

5. Tayfun, M. A.; Yang, C. Y.; and Hsiao, G., 1971. On non-stationary random wave spectra, Proc. First Int. Symposium on Stochastic Hydraulics, Univ. Pittsburgh Publ.

6. Barber, N. F., 1949. A diffraction analysis of photographs of the sea. Nature, 164, p. 485.

7. Stilwell, D., 1969. Directional energy spectra of the sea from photographs. J. of Geophysical Research, Vol. 74, No. 8, p. 1974-1968.

8. Kasevish, R.S.; Tang, C.H.; and Henriksen, S.W., 1971. Energy spectra of sea waves from photographic interpretation. 7th Int. Symp. on Remote Sensing, University of Michigan.

9. Klemas, V.; Borchardt, J.F.; and Treasure, W.M., Suspended Sediment Observations from ERTS-1, Remote Sensing of Environment, 2, 205-221, 1973.

10. Hickman, G.D.; Hogg, J.E.; and Ghovanlou, A.H., Pulsed Neon Laser Bathymetric Studies Using Simulated Delaware Bay Waters, Sparcom, Inc., Tech. Report No. 1, September 1972.

11. Gaither, W.S., 1973, "Energy, Oil, and the State of Delaware," A report of Delaware Bay Oil Transport Committee of the State of Delaware.

12. Kim, H.H. and Hickman, G.D., Recent Overflight Results from an Airborne Oil Fluorosensor, Conf. on the Use of Lasers for Hydrographic Studies, Wallops Island, VA., September 1973.

13. Reimold, R.J.; Gallagher, J.L.; and Thompson, D.E., Remote Sensing of Tidal Marsh, Photogrammetric Engineering, 1973.

14. Klemas, V.; Daiber, F.; Bartlett, D; Crichton, O; and Fornes, A., Application of Automated Multispectral Analysis to Delaware's Coastal Vegetation Mapping, American Society of Photogrammetry Annual Meeting, Washington, D.C., March 11-16, 1972.

15. Klemas, V.; Bartlett, D; and Daiber, F., Mapping Delaware's Coastal Vegetation and Land Use from Aircraft and Satellites, A.S.P., Symposium on Remote Sensing in Oceanography, Orlando, Fla., October 2-5, 1973.

16. Friedman, E.J., and Hickman, G.D., Laser Induced Fluorescence in Algae: A New Technique for Remote Detection.

17. Kim, H.H., Personal Communication, 1973.

18. Mumola, P.B.; Jarett, O.; and Brown, G.A., Multiwavelength LIDAR for Remote Sensing of Algae and Phytoplankton, Conf. on the Use of Lasers for Hydrographic Studies, Wallops Island, Va., September 12, 1973.

USE OF LIDAR SYSTEMS IN MEASURING CERTAIN PHYSICAL OCEANOGRAPHIC PARAMETERS

Davidson T. Chen
NASA, Wallops Station

ABSTRACT

Remote sensing techniques, such as LIDAR, are the only observation methods which are capable of fast scanning over a vast area to produce synoptic views which are necessary for time and space study of the ocean. However, due to the very nature of the way data are collected, all the information thus obtained is confined, to or in the immediate neighborhood of, the surface. Nevertheless, all the physical processes in the ocean are controlled mainly by both surface and subsurface parameters; they act and interact among themselves and produce the phenomena we actually observe in time and space. Remote sensing techniques are very effective for those phenomena controlled by surface parameters which account for most of the crucial problems in physical oceanography.

INTRODUCTION

Oceanography is an old science. Until recently, the methods of study were limited to the standard shipbound tools. By comparing the area that can be covered by a ship in a reasonable amount of time to the total ocean, it is obvious that trying to understand the whole ocean by using the standard method is a big undertaking in both manpower and time. This does not say that the traditional methods are useless, rather they are actually indispensable in some particular aspects of our understanding of the ocean. However, as far as the global ocean model or large scale phenomenon is concerned, the traditional methods are not effective enough to produce a synoptic view. This shortcoming can be compensated to a large extent by the newly developed remote sensing techniques of which LIDAR is a part.

Remote sensing techniques are the only observation methods that are capable of fast scanning over a large area. With this unique capability, they will become the most important tools in large scale physical oceanographic research. However, due to the very nature of the way data are collected, all the information thus obtained is confined to or in the immediate neighborhood of the surface. But the ocean's environment is a complicate one; all the physical processes in the ocean are controlled mainly by both surface and subsurface parameters. These parameters act and interact and finally produce the phenomena we actually observe. Remote sensing techniques are only effective for those phenomena controlled by surface parameters - fortunately such phenomena include most, if not all, of the crucial problems in physical oceanography.

What I am going to cover today does not aim at the present capabilities of LIDAR techniques. Instead, I am going to point out several important physical parameters that are important to the community of physical oceanographers. In this way I hope that I will have left ample room for the experts in the field of LIDAR to decide for themselves what is best for them to do at present and in the future.

PHYSICAL PARAMETERS

Since remote sensing techniques are capable of rapidly scanning large areas, they can be used to obtain continuous data on a large scale. Such data are essential to the predictive models for weather and sea state. Nevertheless, it is to our advantage to classify the physical parameters into several groups.

Air-Sea Interactions:

Surface Temperature Field.-The earth is actually a big heat engine; the energy source is primarily the heat of the sun. The energy from the sun reaches the earth by radiation and then it is transported by large scale convection motions (the oceanic and the atmospheric circulations), evaporation and reflection. In order to improve our understanding of the ocean, a global heat budget is indispensible. For this kind of large scale problem the remote sensing technique is the only solution. In addition, a surface temperature reading can help to delineate the boundary of large scale motions such as the Gulf Stream or river effluents because water from different sources usually have different temperatures.

Ocean Surface Wind Fields.-Most currents and ocean waves are generated by ocean surface wind. Since wind itself is random in both direction and magnitude the presentation in the form of wind spectrum will be desirable. Presently, the measurement of wind in the field has been standardized to be located at 10 meters above the sea surface and the data are further reduced to wind stresses through some empirical formula. The percentage of white cap area of the ocean surface has been proposed as a way to measure wind magnitude by virtue of remote sensing techniques. It is also possible to get wind field information from the statistical measures of the wave field, but since the basic problem of wind-wave relation is still undetermined, the result will be empirical and crude at best.

Sea State.-Since most ocean waves are generated by wind, the sea state is closely related to weather conditions. Unfortunately, a definite knowledge of the relationship between a given wind and the resulting sea state is still wanting, and the progress is hampered both by difficulties in theoretical analysis and the lack of reliable field data.

Available data collected by traditional methods up to now are limited to shallow water or calm sea cases. But the central problem here is how to relate sea state with severe weather conditions in the open ocean; it will supply a boundary condition to the problem of predicting storm surge at a given coastal area. Since the sea surface is always random, the meaningful specification of the sea state is always the various statistical measures.

Empirically, there are data showing that: the mean energy density of the waves is proportional to wind speed squared; the mean surface slope of the surface is proportional to the local wind speed under low wind condition; the skewness of the probability distribution of the surface slope is also related to wind field. Theoretically, we can show that: for a given wind condition, the sea state will change if there are local current changes; the sea state will change if the depth becomes shallow and changes appreciably.

Sea state date contains a lot of information, but in order to interpret them correctly, data are required to be as detailed as possible.

Radiation Input.-This parameter indicates the energy received from the sun. Due to different values of reflection and refraction at different location, this parameter, again, is actively measured.

Density Distribution:

The density of sea water depends on the temperature and salinity of the sea water and also, as a result of the slight compressibility of water, on the sea pressure. The horizontal and vertical density distributions are as essential to the circulation field as temperature fields are to the circulation field.

The Mean Sea Level:

The mean sea level is controlled by many parameters; the principal ones are gravity anomalies surface pressure changes, density structure of the water column, surface wind field, current, and astronomical forces. A single reading of sea level can hardly mean anything. However, since most of the parameters are acting on different time scales, a proper averaging can lead to meaningful interpretations. If we average our data over a long time, we can filter out the influences of the transient events except the quasi-permanent features along the major ocean current systems. Thus, we get a reference state. In most cases, currents and the ocean density structure can be related by the geostrophic assumption. This, of course, requires in situ measurement to determine it uniquely. But if we further assume barostropic motion, then the current can be related directly to the mean sea level slope. Once the reference state is established, the instantaneous reading can be used to deduce tidal waves and other transient phenomena as tsunami, storm surges, etc.

Tides:

Tides on the earth are caused by the gravitation attraction between the sun and the earth and the moon and the earth. The effects of tides are important for the coastal and estuary regions.

Currents:

Currents in the ocean are generated primarily by wind stress, temperature and density differences and pressure gradient. The motions are modified by the rotation of the earth, friction forces and astronomical forces. The heat transported by the currents has a tre-

mendous effect on our global weather. The nutrients carried by the currents have sustained the biological life in the ocean. All of these and the problems of pollution and navigation require us to study the currents intensively. NASA Wallops has pursued continuously the recognition of currents using remote sensing devices. At a region of high velocity gradient, such as at the boundary of the Gulf Stream, the depth of the water is still large and the ratio of wind speed to phase speed of the wave will not change appreciably over the length scale, then the current can be determined by the changes in wave characteristics.

Sea-Earth Interactions:

Storm Surges.-The piling up of water against coasts under the action of wind becomes very dangerous if wind is in the magnitude of hurricane. The change in sea level and such parameters as air pressure distribution, wind speed, fetch, duration of wind action and bottom topography are all involved.

Wave Refraction.-Wave refraction is caused by the change in bottom topography as wave propagates into the coast. Wave refraction can cause the change in shore lines by eroding the beach away and depositing the material somewhere else.

Shallow Water Charting and Topography.-It has been proposed that, from long waves observation, we can deduce some information on bottom topography; since the waves propagate from the open ocean to the coastal region, the sea state will be controlled by the parameter which is the result of the multiplication of wave number and water depth.

Sediment Transport.-The wave and longshore current can erode and deposit materials along the coastline. This problem becomes acute at the inlets.

Eddy Diffusion Coefficients, Eddy Heat Conductivity Coefficient and Eddy Viscosity Coefficient:

These are the exchange coefficients for salt content or any other property, for heat and momentum, respectively. They are, generally, functions of space and time, and they depend on the scale of the turbulent eddy motion.

CONCLUSION

The ocean is a large complicated environment controlled mostly by surface parameters; therefore, it is well suited to remote sensing observation. Only by remote sensing can we get global information without worrying about time scale. Only by these techniques can we establish a global reference without going through the painful pace of in situ measurements. By careful processing and interpretation of the data, and coupled with well planned in situ checks, remote sensing techniques will become the single most important tool in physical oceanography.

REFERENCES

1. Defant, A., Physical Oceanography, Vol. II, Pergamon Press, N.Y., 1960.
2. Fomin, L. M., The Dynamic Method in Oceanography, Elsevier Publishing Co., N.Y., 1964.
3. Hill, M. N. (General Editor), The Sea, Vol. I, Interscience Publishers, N.Y., 1962.
4. Ippen, A. T. (Editor), Estuary and Coastline Hydrodynamics, McGraw-Hill, N.Y., 1966.
5. Kraus, E. B., Atmosphere-Ocean Interaction, Clarendon Press, Oxford, 1972.
6. Neumann, G., and Pierson, W. J., Jr., Principles of Physical Oceanography, Prentice-Hall, Englewood Cliffs, N.J., 1966.
7. Phillips, O. M., The Dynamics of the Upper Ocean, Cambridge University Press, 1969.
8. Stommel, H., The Gulf Stream, University of California Press, 1966.

EXPERIMENTAL RESULTS OF A CONTINUOUS WAVE LASER RADAR SYSTEM

Kenneth J. Petri and Robert F. Starry
Department of the Navy
Naval Air Development Center

ABSTRACT

A 1.06 micron CW laser radar system was used to establish the feasibility of remotely measuring sea surface wind magnitude and direction. Experiments were conducted from the NRL (Naval Research Laboratory) Chesapeake Bay Bridge Facility, Annapolis, Maryland. Simultaneous correlation of the collected laser data with the environment was established using meteorological instruments. The experimental system and methods of analysis are summarized. Results of the experiments including wind magnitude and direction correlation are reported. Results are compared with theoretical predictions.

INTRODUCTION

Various controlled environmental studies[1,2] and theoretical research[3,4] have suggested that ocean surface wind magnitude and direction could be remotely measured from an airborne platform by utilizing a laser radar system. These studies and the present cumbersome methods of measuring winds at sea served to initiate the first real environment feasibility experiments. The experiments were conducted by the Naval Air Development Center* from the NRL Chesapeake Bay Bridge Facility. This paper describes the equipment used, the tests conducted, the results obtained, and compares the results with theoretical predictions.

MEASUREMENT CONCEPT

The establishment of the feasibility of remotely measuring sea surface wind velocity required the line scanning of an area of the water surface with a continuous wave laser and optical receiver. The reflected intensity was recorded as a function of angle of observation with respect to the normal to the water surface. The process was repeated for 18 equally spaced azimuth positions, creating a three-dimensional model of the reflected intensity pattern. The shape of the recorded intensity pattern had characteristic features for various imposed wind fields. By processing and examining these patterns, inference to the wind magnitude and direction were made by comparison with ground truth.

EQUIPMENT DESCRIPTION

The experimental system used was a continuous wave laser radar (Figure 1). The transmitter was a cw Neodymium-YAG laser operating at 1.06 microns. The output radiation was modulated by an electro-optic modulator at a frequency of 45 kHz. A dichroic beam splitter directed 1% of the exit energy through a fiber optic bundle which directed the energy to a photodiode detector. The output of the photodiode provided continuous power measurements available for real time display and magnetic tape recording. The main laser beam was directed onto an octagonal scanning mirror, which served to vertically scan the laser beam $\pm 37.5°$. The return energy from the water surface was collected via the same octagonal scanning mirror. Two surfaces of the octagon were used when receiving. The return energy was then directed by fixed mirrors to a cassegrain optical receiver which focused the energy on a photodiode detector. Field of view was selectable and neutral density filters could be inserted in the return beam path. Major transmitter/receiver parameters are listed in TABLE 1. The output of the photodiode detector was passed through a tuned preamplifier (45 kHz). This allowed the receiver to discriminate against background noise. The return signal and monitor signal were both rectified by ideal rectifiers before being recorded on an Ampex (FR-1300) 14-channel instrumentation recorder. The resolution bandwidth of the system was limited by the recorder to 2.5 kHz at a tape speed of 7.5 ips.

Laboratory equipment used to prepare data for processing by the Naval Air Development Center CDC 6600 computer facility included a Varian 620/i minicomputer/analog-to-digital converter and a PEC 6860 digital tape recorder. The Varian 620/i was used to convert the return signal and other parameters to a digital format compatible with the CDC 6600. The PEC 6860 was used to record the digital information on magnetic tape.

*This work is sponsored by the Naval Air Systems Command, Mr. M. Schefer, Code 370C.

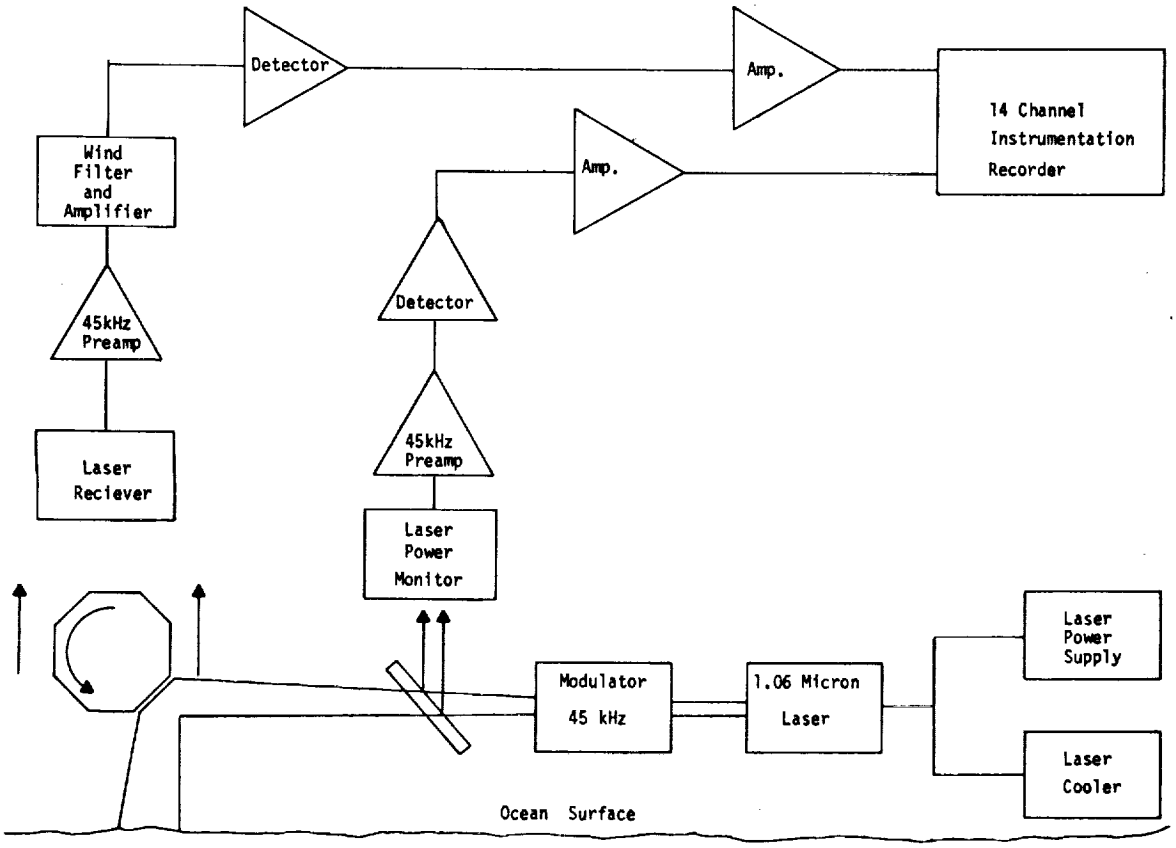

Figure 1. Block diagram of experimental laser remote wind measuring system

TABLE 1.-TRANSMITTER AND RECEIVER PARAMETERS

Transmitter	
Laser Type:	CW ND;YAG
Wavelength:	1.06 micron
Modulation:	Sine wave (45 KHz)
Modulated Output Power:	0.2 to 1 watt
Output Beam Divergence:	9 milliradians
Spot Size at 18.3 meters (60 ft.):	15.2 cm (6 in.)
Laser Scan Angle:	$\pm 37.5^{o}$
Scanner Speed:	8, 16, 32, 64, or 128 scans/sec
Receiver	
Collector:	Reflective Cassegrain
Clear Aperture	30.5 sq. cm (12 in.)
Effective Focal Length:	50.8 cm (20 in.)
Detector:	Pin 10 silicon photodiode
Field of View:	4-24 milliradians
Neutral Density Filters:	Selectable 0, 1, 2 and 3
Sensitivity:	10^{-9} watts
Receiver Scan Angle:	$\pm 37.5^{o}$

EXPERIMENTAL TEST FACILITY

The NRL Chesapeake Bay Bridge Facility was selected as a test site because of its suitability as a water environment test platform. It is physically a 15 x 3.7 meter (50 x 12 foot) gondola (Figure 2) located 18.3 meters (60 feet) above the water underneath the eastern end of the William Preston Lane, Jr. Memorial Bridge near Annapolis, Maryland. The water area directly under the gondola is clear of obstructions (necessary for scanning the laser beam $\pm 37.5°$ from the normal to the water surface), and is 1.6-.8 km (1-1/2 miles) from the nearest shoreline.

Figure 2. NRL Chesapeake Bay Bridge Facility

EXPERIMENTAL TEST PROCEDURE

In a normal data run, an area of water surface was line scanned, $\pm 37.5°$ with respect to the normal to the water surface, with the cw laser and optical receiver at a preset system azimuth position. After a selected number of scans, the system azimuth position was automatically moved 10°. Once locked in position, the data were collected during the identical number of selected scans before moving another 10° in azimuth position. The process was repeated for a total of 18 azimuth positions. Thus, a full 360° was covered (Figure 3).

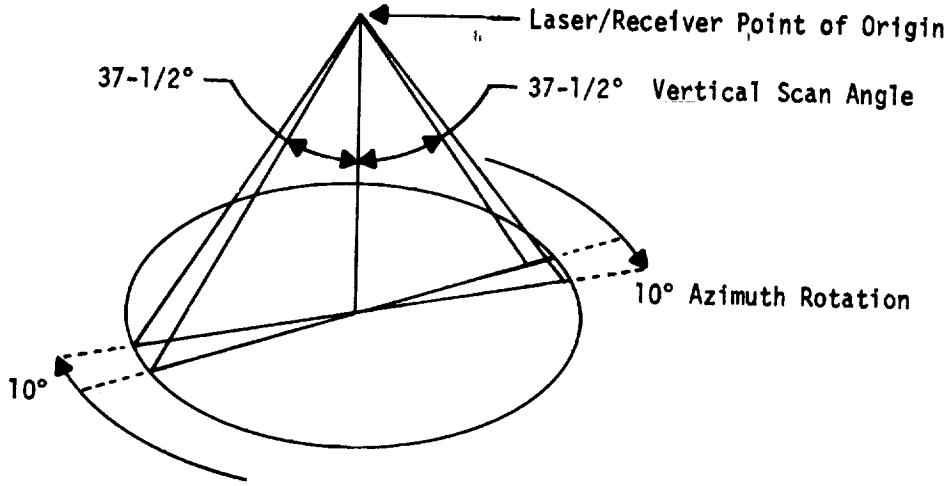

Figure 3. Laser system scanning geometry

The collected data recorded on the Ampex instrumentation recorder included the return signal power, laser monitor power, necessary synchronizing pulses from the optical scanner and the azimuth positioner, voice comments, and various system check signals.

Additional data recorded on data sheets included the date of recording, assigned data run number, time of day, initial system orientation with respect to true north, receiver field of view, system gain, number of scans per azimuth position, laser/receiver scanning rate, neutral density filters used and general environmental conditions (including photographs).

SUPPORT DATA

To provide simultaneous correlation of the experimental system data with actual environmental conditions, ground truth support data was collected and submitted[5] to the Naval Air Development Center by C.W. Thornthwaite Associates, Laboratory of Climatology. The measurements included vertical profiles of mean wind speed at 2.1, 4.3, 8.5, and 12.8 meters (7, 14, 28, and 42-foot) elevations; air temperature at a 4.3 meter (14-foot) elevation; wind direction at a 4.3 meter (14-foot) elevation; water temperature at .464 m below mean sea level; and air temperature difference between the 2.1 and 8.5 meter (7 and 28-foot) levels (Figure 4).

DATA PROCESSING

Processing was accomplished on the CDC 6600. For each laser/receiver scan ($\pm 37.5^0$), 356 evenly spaced samples of return power were taken. Approximately 486 scans were processed for each azimuth position. An average value of return power was then calculated for each azimuth position at each of the 356 sample points. Using a Calcom plotter, the averaged return power was plotted as a function of laser/receiver scan angle for each azimuth position. Both the individual data points and the plotted curves were then compared with the collected support data for individual azimuth positions. Most of the wind magnitude support data collected, however, were the average wind magnitude for an entire run of all azimuth positions. Therefore, the average return power for all azimuth positions at each of the 356 sample points was also calculated and plotted as a function of laser/receiver scan angle.

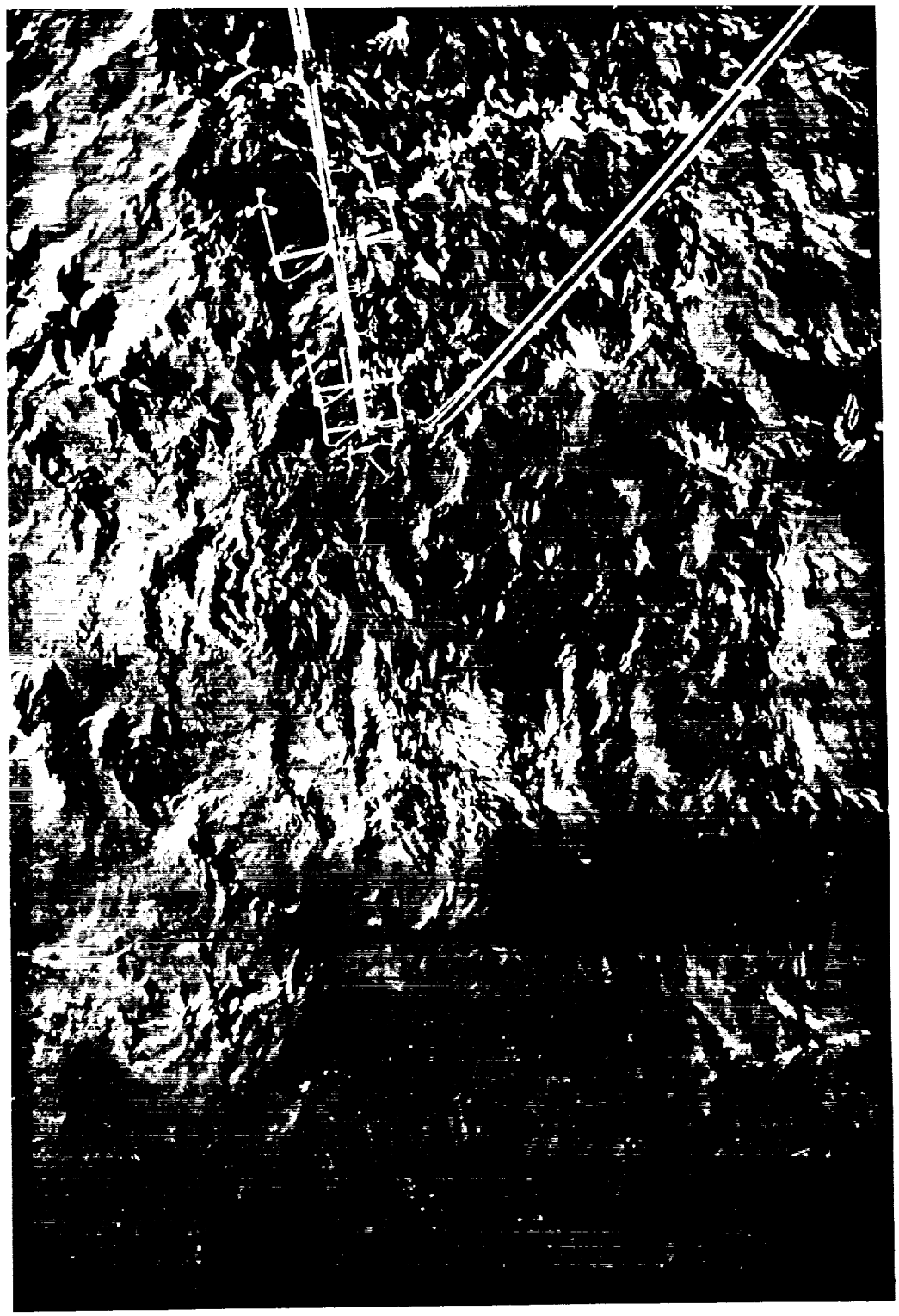

Figure 4. Meteorological measuring equipment

EXPERIMENTAL RESULTS

The experimental equipment, installed in the NRL Bridge Facility on 30 May 1972 yielded experimental data on nine days over the period 31 May through 5 October 1972. The most definitive results were obtained in relating wind magnitude to averaged return power at normal incidence. Over the range of surface wind speeds from 3 to 17 mph, the averaged return power (normal incidence) decreased with increasing wind speed (TABLE 2). The averaged power return at 3 mph was six times as great as that at 17 mph. TABLE 2 indicates the average return power can be used to predict the actual wind magnitude to within ±1 mph. The same results are repeated in Figure 5, which plots the averaged return power over the entire ±37.5° scan for all azimuth positions. In addition, it can be observed that averaged return power falls off sharply from normal incidence at the lowest wind magnitude. The results presented in TABLE 2 and Figure 5 are normalized and represent the average of 486 scans per azimuth position for all 18 azimuth positions. Corresponding wind speeds and air/water temperature differences were averaged at 1-minute intervals over the same time interval. Reducing the averaging time by a factor of 18 also gives reliable results (TABLE 3). TABLE 3 represents the averaged return power (normal incidence) collected in just one azimuth position (28 seconds). The corresponding wind speed represents a 1-minute average. Limited fetch was encountered on many data runs but did not appear to have any effect. Results of this nature support the suggestions of Pierson and Stacy[6] that high frequency waves (i.e., capillaries) are the indicators of the local wind velocity because they are independent of fetch (greater than five meters) and are almost in instantaneous equilibrium with the wind.

TABLE 2.-COMPARISON OF NORMALIZED AVERAGED RETURN SIGNAL (ALL 18 AZIMUTH POSITIONS) AT NORMAL INCIDENCE WITH SUPPORT DATA

Date	Run No.	Wind Speed (mph)	$T_{Air} - T_{Water}$ (Deg)	Relative Averaged Return Power
27 Jun.	1	3 (Estimated)	-	700
28 Jun.	5	6.4	4.6	490
28 Jun.	1	7.4	7.2	480
29 Jun.	3	8.8	3.7	325
4 Oct.	1	9.6	1.3	282
29 Jun.	2	9.6	3.8	320
4 Oct.	2	10.3	0.4	274
29 Jun.	1	10.4	3.5	275
4 Oct.	5	10.8	-1.5	244
29 Jun.	4	10.8	3.7	245
5 Oct.	3	13.7	0.3	162
5 Oct.	1	15.0	0.7	134
5 Oct.	2	16.9	0.9	116

TABLE 3.-COMPARISON OF NORMALIZED AVERAGED RETURN SIGNAL (ONE AZIMUTH POSITION) AT INCIDENCE WITH SUPPORT DATA

Date	Run No.	Wind Speed	Relative Averaged*
4 Oct.	5	7.7	429
4 Oct.	2	10.0	378
5 Oct.	3	12.9	301
5 Oct.	2	16.7	215
5 Oct.	1	16.8	179

* All data collected with a scanner speed of 16 scans/sec and a field view of 24 milliradians.

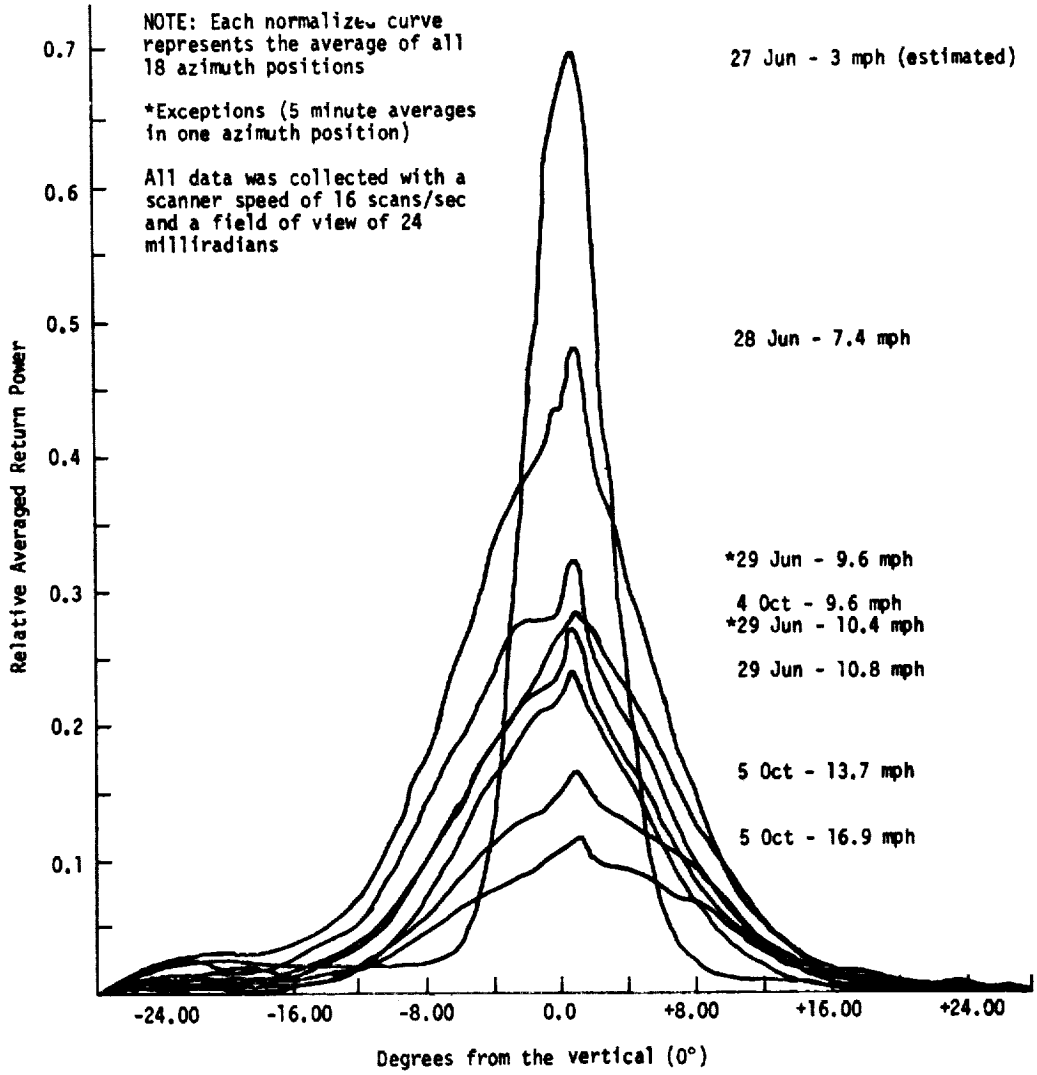

Figure 5. Normalized average return signal vs. laser/receiver scan angle

In addition to magnitude, it seems clear that wind direction can be inferred by examining the averaged return power versus scan angle curves for the various azimuth positions. Figures 6a, 6b, 7, and 8 are presented as examples. The averaged curves shown represent a total collection time of 28 seconds. The wind direction support data used for comparison were simply the averaged wind direction at a height of 4.3 meters (14 feet) above mean sea level for all azimuth positions. Thus, the average wind direction for the entire run, for any given azimuth position, would therefore not be correlatable. In general, it was noted that the width of the crosswind curve was the narrowest while that of the upwind/downwind curve was the widest. On a few occasions due to apparent wind direction changes, the averaging time interval (28 seconds) was too short to establish the phenomenon. Special arrangements that were made on 29 June 1972 allowed the laser system to stay in the crosswind and upwind/downwind azimuth positions for a period of 5 minutes in each position immediately after a normal azimuth sequence. The wind direction support data was also measured for 5 minutes. Figure 9 shows the normal azimuth sequence (28 seconds average time per azimuth position) where it is difficult to establish the phenomenon, and Figure 10 shows the special 5-minute average run where the phenomenon is clearly visible. It seems reasonable to state, from this kind of data, that high accuracies in determining upwind/downwind direction will require a greater time to acquire sufficient samples of laser return power.

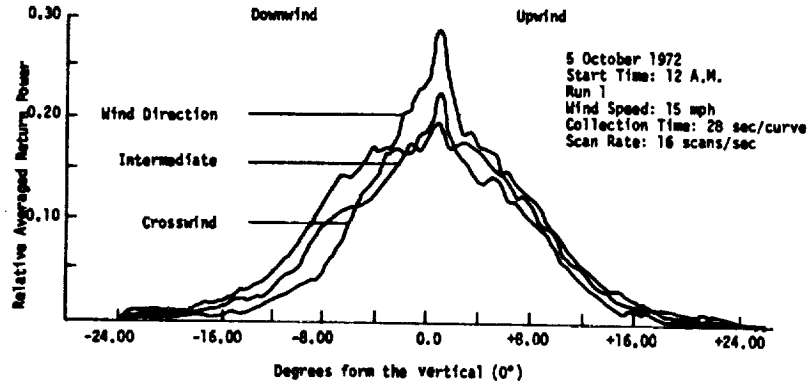

Figure 6a. Averaged return signal vs. laser/receiver scan angle for three individual azimuth positions at 12 a.m. on 5 Oct. 1972

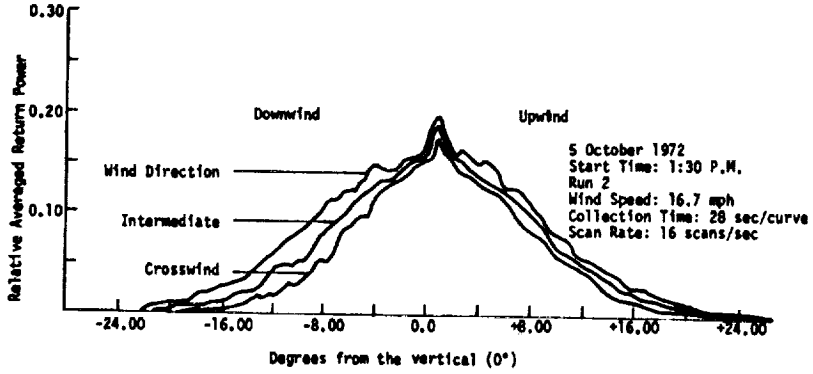

Figure 6b. Averaged return signal vs. laser/receiver scan angle for three individual azimuth positions at 12 a.m. on 5 Oct. 1972

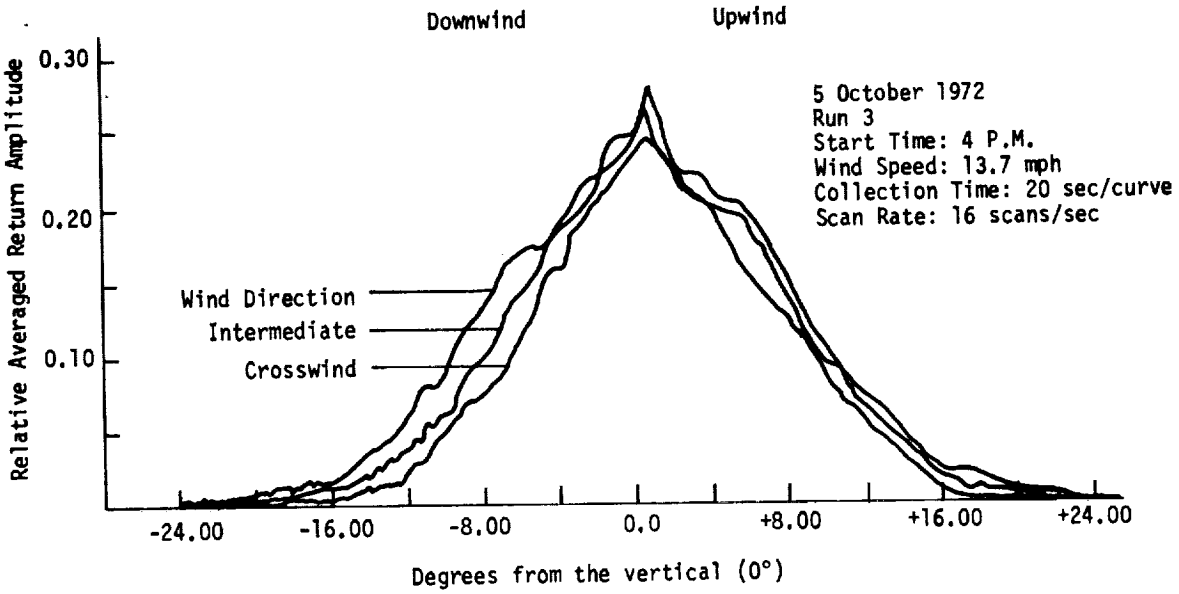

Figure 7. Averaged return signal vs. laser/receiver scan angle for three individual azimuth positions at 4 p.m. on 5 Oct. 1972

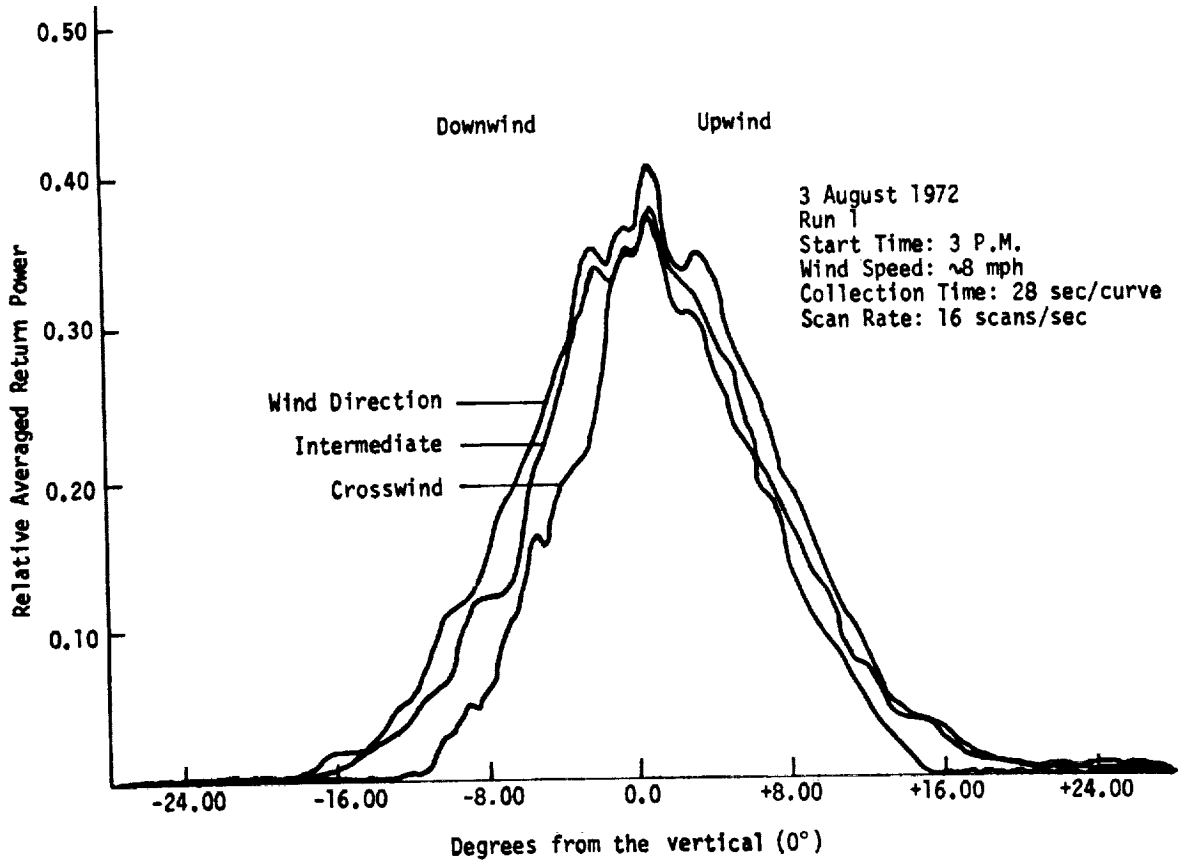

Figure 8. Averaged return signal vs. laser/receiver scan angle for three individual azimuth positions at 3 p.m. on 3 Aug. 1972

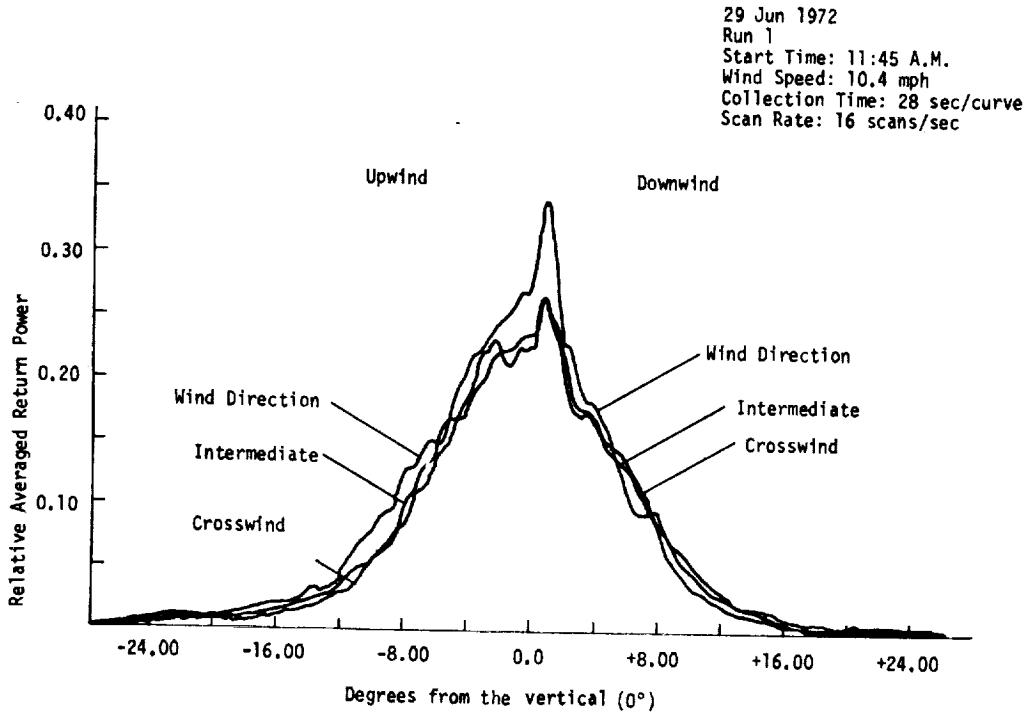

Figure 9. Averaged return signal vs. laser/receiver scan angle for three individual azimuth positions at 11:45 a.m. on 29 Jun. 1972

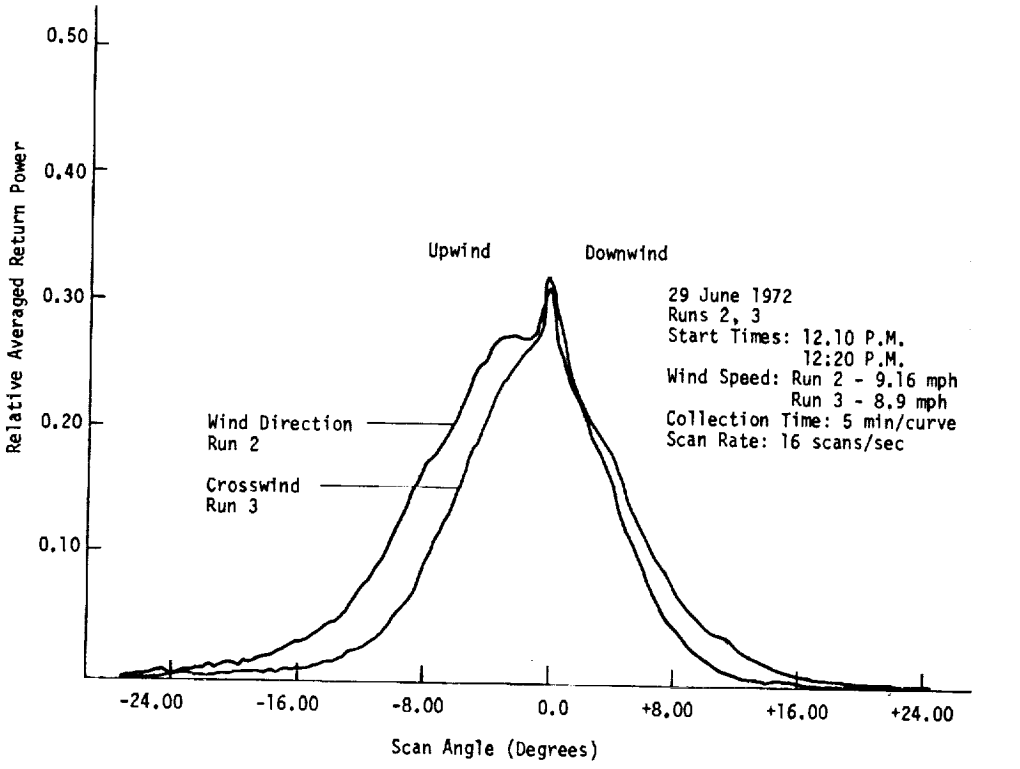

Figure 10. Averaged return signal vs. laser/receiver scan angle for two individual azimuth positions at 12:10 and 12:20 p.m. on 29 Jun. 1972

On 3 August 1972, with relatively constant winds, the curve width relationship between crosswind and upwind/downwind azimuth positions existed for the normal run (28 seconds/curve). In addition, by filtering and smoothing the actual data, it was revealed that additional information existed on the downwind side of the curve. The averaged return power over the scan angle of approximately 4-8° increased in value, in perfect order, as the azimuth position was rotated from the crosswind position to the wind direction position. The same effect was not nearly as well defined, for the same sampling interval, on the upwind side of the curve. Figure 11 shows the effect on the downwind side of the curve. On some other days (more variable wind conditions), the effect was still detectable but not as obviously as the case presented. Once the upwind/downwind azimuth position is located via the curve width phenomenon, this effect can be used to determine wind direction. Observation of the slope of the curve from its peak to approximately 8° on both the upwind and downwind side revealed a sharper slope always existed on the downward side. Figures 7, 8, 9, 10, and 11 all indicate this result. Thus another way of establishing the wind direction exists.

Considering all the results presented, it is estimated that wind direction should be measurable within $\pm 10°$.

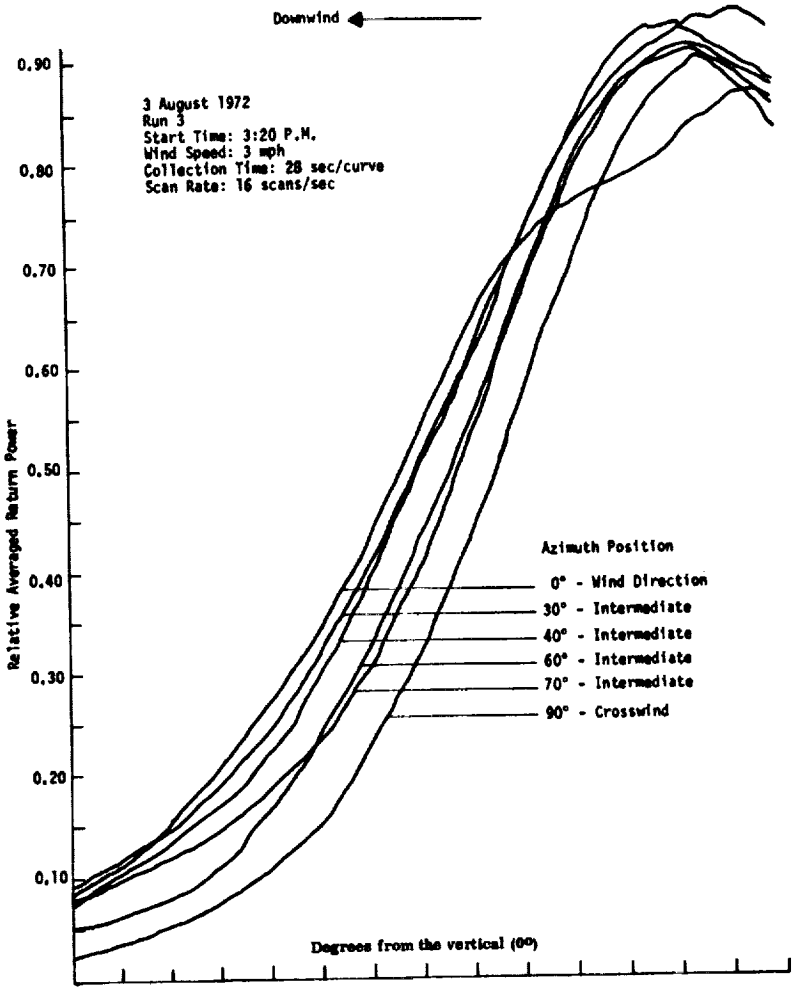

Figure 11. Filtered averaged return power vs. laser/receiver scan angle for six individual azimuth positions at 3:20 p.m. on 3 Aug. 1972

THEORETICAL PREDICTION COMPARISON

The Poseidon Scientific Corporation under contract to the Naval Air Development Center performed a literature search[7] to determine what existing theories were available that could be used as wind predictors. Two theories, limited by the basic assumption that the sea surface is a linear, stationary, Gaussian process, were extracted and modified; (1) Jackson[4] and (2) Swennen[3].

The Jackson theory was limited to upwind/downwind traverses but could be and was modified to all azimuth positions. The modification of Jackson's theory required the expansion of his geometric optics term. The mathematical assumptions used were (1) the co-variance function of the surface can be represented by a Taylor series truncated at second degree; (2) the surface is a stationary Gaussian random process of zero mean; and (3) the horizontal illumination area is large compared to the roughness scale of the surface. The incorporation of the spectrum of Pierson and Stacy[6] into the Jackson theory yielded the NILCS (Normalized Isotropic Laser Cross Section) $\sigma_{11}{}^0$, which could be evaluated as a function of scan angle for all azimuth positions. The NILCS varies linearly with received laser power and can be considered equivalent to it in this paper. In addition, the slope statistics of Cox and Munk[8] were used as empirical inputs into the modified Jackson theory. This allowed the prediction of the NILCS $\sigma_{22}{}^0$, which could be evaluated at a function of scan angle for the upwind/downwind azimuth position only.

The modified Swennen theory, limited to predicted power return at vertical incidence, was not used because of geometric incompatibility with the experimental system.

A range of real environment wind magnitudes and their corresponding air/sea temperature difference were used as inputs to the Jackson predictors. $\sigma_{11}{}^0$ and $\sigma_{22}{}^0$ were then calculated using the CDC 6600 computer. $\sigma_{11}{}^0$ is plotted in Figure 12 as a function of scan angle for the crosswind, upwind/downwind direction, and two intermediate azimuth positions. The results indicate clear general agreement with actual collected data. The magnitude of the curves reduce with increasing wind speeds and the width of the curves increase as the azimuth position is varied from crosswind to upwind/downwind direction. A relative comparison of theoretical predictions ($\sigma_{11}{}^0$) with experimental average laser received power data for the highest wind speed encounters is plotted in Figure 13. Correlation is good over the scan angle range 0 to ±12°. A considerably larger spread between azimuth positions than was experimentally observed is predicted at scan angles >10°. A relative comparison of $\sigma_{11}{}^0$ and $\sigma_{22}{}^0$ with the actual laser power received at normal incidence to the sea surface is listed in Table 4. Better correlation was obtained between the experimental data and $\sigma_{22}{}^0$ than $\sigma_{11}{}^0$. Over the wind speed range used, $\sigma_{11}{}^0$ increased by a factor of 2.16, $\sigma_{22}{}^0$ by a factor of 2.58, and the experimental data by a factor of 4.14.

TABLE 4.-COMPARISON OF THEORETICAL RETURN SIGNALS VS. EXPERIMENTAL RETURN AT NORMAL INCIDENCE TO THE SEA SURFACE

Date	Run	Wind Speed	$\sigma_{11}{}^0$	$\sigma_{22}{}^0$	Avg. Laser Power Reed	Scan Angle	T Air -T Water (deg)
5 Oct	2	16.9	.106	.211	.166	0	.9
5 Oct	3	13.7	.195	.254	.162	0	.3
4 Oct	4	10.5	.169	.310	.244	0	-.9
4 Oct	2	10.3	.160	.334	.274	0	.4
29 Jun	3	8.8	.134	.414	.325	0	3.7
28 Jun	1	7.4	.229	.545	.480	0	7.2

$\sigma_{11}{}^0$ - NILCS (Using theoretical statistics of Pierson and Stacy)

$\sigma_{11}{}^0$ - NILCS (Using empirical statistics of Cox and Munk)

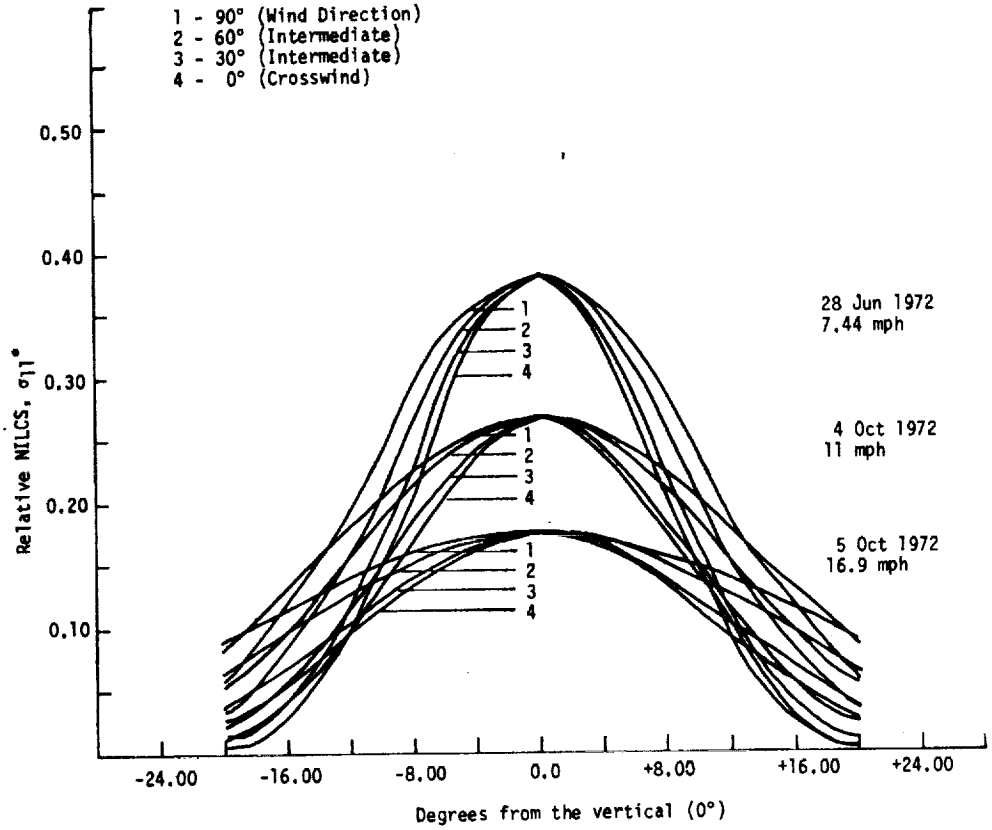

Figure 12. Predicted normalized isotropic cross section (σ_{11}^{0}) vs. scan angle for three environmental conditions.

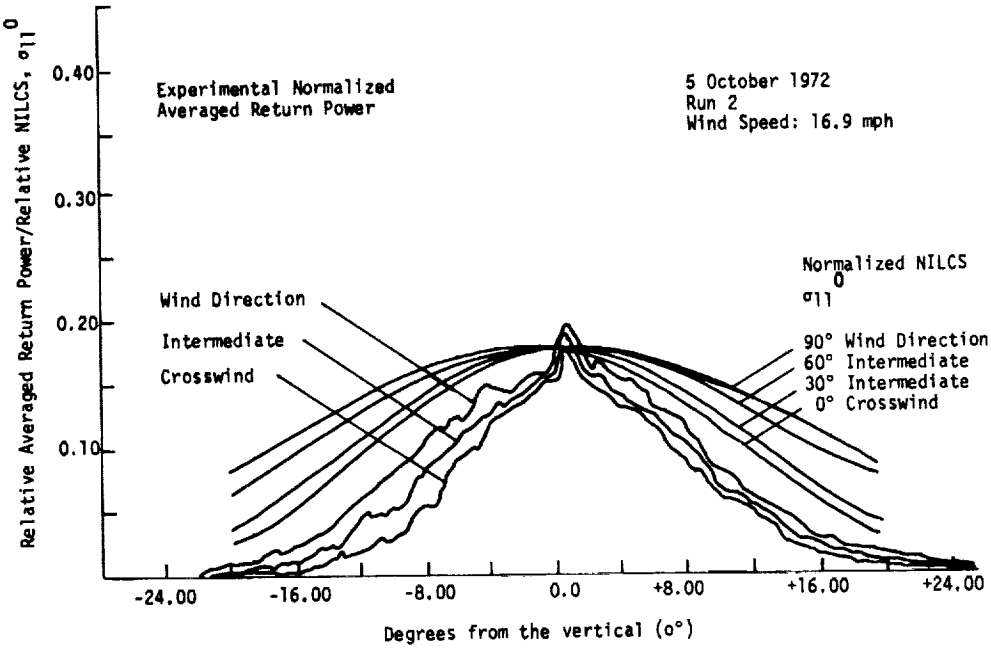

Figure 13. Comparison of predicted normalized isotropic laser cross section, σ_{11}^{0} with the experimental averaged return power.

CONCLUSIONS

The completed experimental and analytical efforts described have established the feasibility of remotely measuring wind magnitude and direction in a real environment.

For the surface wind conditions encountered during these tests, 3-17 mph, the wind magnitude was measured to within ±1 mph accuracy. In addition, the experimental results predict that ±10° accuracies in wind direction can be obtained.

The experimental results obtained support the suggestion of Pierson and Stacy[6] that high frequency waves are the indicators of the local wind velocity because they are independent of each fetch and are almost in instantaneous equilibrium with the wind.

A comparison of experimental data with two wind predictors developed from theoretical work by Jackson[4] shows very good correlation considering the theory assumes that the sea surface is a linear, stationary Gaussian process.

ACKNOWLEDGEMENT

The authors wish to thank P. J. Santi for his aid in the construction and testing of the system; A. W. Kelch for converting and preparing the data for analysis; C. E. Peterson for valuable bridge assistance and the Lane Memorial Bridge Authority for their cooperation and support.

REFERENCES

1. Kirk, R. L., Surface Evaluation and Definition (SUEDE) Program, EOS Report 7067-Final, 13 Dec. 1966.

2. Wu, Jin, Surface Curvature of Wind WAves Observed from Different Angles, Apr. 1971.

3. Swennen, J. P. J. W., Surface Reflected Energy Received from a Normally Incident Collimated Beam of Optical Radiation, Ohio University Antenna Laboratory, Report 1675-8, 1965.

4. Jackson, F. C., A Curvature Corrected Kirchoff Formulation for Radar-Sea-Return from the Near Vertical, New York University, Department of Meteorology and Oceanography, GSL, TR-72-1, 1972.

5. C. W. Thornthwaite Associates, Data Summary Chesapeake Bay Bridge Site, Oct. 1972.

6. Pierson, W. J., Jr., and Stach, R. A., The Elevation, Slope and Curvature Spectra of a Wind Roughened Sea. Contribution No. 132, Geophysical Science Laboratory, New York University, Dept. of Meteorological and Oceanography, 1972.

7. Marks, W.; Stacy, R. A.; and Ponamgi, S. R., Correlation of Laser Sea Return with the Wind Profile - Assessment of Prediction Models, Report No. 1015-TR-1(72), Sept. 1972.

8. Cox, C. S. and Munk, W. H., Statistics of the Sea Surface Derived from Sun Glitter, Journ. Optic. Soc. Am., Vol. 44, 1954.

AN OPTICAL RADAR FOR AIRBORNE USE OVER NATURAL WATERS*

C. A. Levis, W. G. Swarner, C. Prettyman**, and G. W. Reinhardt***
The Ohio State University-Electro Science Laboratory

ABSTRACT

An optical radar for detecting targets in natural waters was built and tested in the Gulf of Mexico. The transmitter consists of a Q-switched neodymium-glass laser, with output amplified and doubled in KDP to 0.53 micrometer wavelength. The receiver incorporates a noval optical spatial filter to reduce the dynamic range required of the photodetector to a reasonable value.

Detection of targets to a depth of 26 meters (84 feet) was achieved with a considerable sensitivity margin. The sensitivity of the radar is highly dependent on the optical attenuation coefficient. In general, measured returns fell between the values predicted on the basis of monopath and multipath attenuation.

By means of simple physical arguments, a radar equation for the system was derived. To validate this theoretical model, measurements of optical attenuation and of water surface behavior were also instrumented, and some of these results are given.

Volumetric backscatter was measurable over the entire depth range; such radars should therefore be useful for monitoring natural water quality. Airborne bottom-profiling is another application.

*This work was supported by the Air Force Avionics Laboratory, Wright-Patterson Air Force Base, Ohio under Contracts AF 33(657)-11198 and AF 33(615)-3667.

**Now with the Firestone Tire and Rubber Company, Akron, Ohio.

***Now with Air Force Avionics Laboratory,Wright-Patterson Air Force Base, Ohio.

INTRODUCTION

Water is highly absorbent of electromagnetic energy except at very-low-frequency (VLF) and in the blue-green region of the optical spectrum. VLF has found communications uses, but the large wavelength does not allow the resolution needed for a radar. Optical wavelengths do not have this limitation, and the advent of lasers has made the use of radars below the ocean surface quite practicable. This paper discusses experiments designed to demonstrate this feasibility in the field. A system model was developed, verified with the field measurements, and used to show under what conditions such a system can operate, by calculating the maximum range for various water conditions. Certain water parameters, especially extinction coefficient and surface slope distribution, were also measured in order to estimate their effect on radar performance.

SYSTEM MODEL

A model of the radar system is shown pictorially in Figure 1, and a system equation derived from this picture is given in Equation (1), which can best be understood by reference to the figure and noting the processes by which the transmitted power P_t causes a power P_r to be detected in the receiver.

$$P_r = \frac{P_t T_1 e^{-\alpha_1 R_w} \rho e^{-\alpha_2 R_w} T_2}{2\pi\left(R_a + \frac{R_w}{n}\right)^2 n^2} A_r \qquad (1)$$

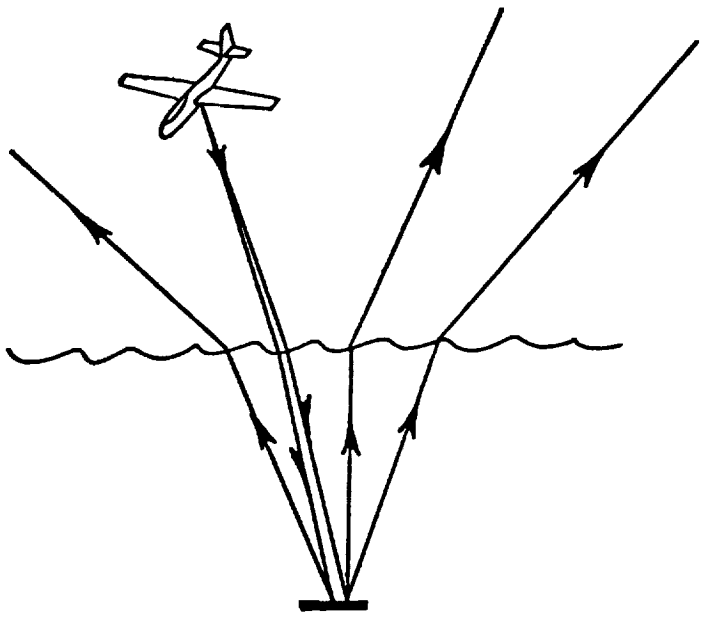

Figure 1. Airborne subsurface radar.

The laser beam first must be transmitted through the surface. The transmission coefficient T_1 represents the fraction of the incident energy which is transmitted in the direction of the target. The energy is attenuated on its way to the target; this attenuation follows a well-known exponential law (ref. 1) with extinction coefficient α_1. We assume the transmitted beam to be sufficiently narrow so that the target intercepts essentially all the energy transmitted to its depth, and that it scatters this energy back toward the receiver with the same intensity as an isotropic upward scatterer of reflectivity ρ. The energy now again is attenuated on its way toward the surface, resulting in another exponential; the reason for using a different coefficient α_2 is discussed below. At the surface another transmission coefficient T_2 is used to account for loss of energy due to reflection and a change in power density due to change in beam direction. Above the surface, the beam appears to come from an apparent source at 0' (Figure 2) instead of the target at 0. By geometry the distance 0'P is given by

$$0'P = R_w \sin\theta_1 / \sin\theta_2, \tag{2}$$

and Snell's law gives

$$0'P = R_w/n, \qquad \text{where n is the index of refraction.} \tag{3}$$

The power density in the air is therefore given in terms of an apparent source of strength S' at 0' as

$$P = \frac{S'}{2\pi\left(R_a + \frac{R_w}{n}\right)^2} \tag{4}$$

The apparent source strength S' can be evaluated from the fact that at the surface, $R_a = 0$, it must produce the same intensity as the true target-scattered return,

$$\frac{S'}{2\pi\left(\frac{R_w}{n}\right)^2} = \frac{P_T T_1 e^{-\alpha_1 R_w} \rho e^{-\alpha_2 R_w} T_2}{2\pi R_w^2} \tag{5}$$

Solving for S', substituting in Equation (4), and multiplying by the receiving aperture A_r yields Equation (1).

Several approximations were made in deriving this model. First, the extinction coefficient was assumed constant along the downward and upward paths. In practice, optical opacity varies as a function of depth; depending on locality, the variations can be very significant and quite complex. The extinction coefficient also is a function of the beam collimation, which changes along the path due to scattering by particles as the beam progresses. Thus, to be precise, the exponentials should be replaced with attenuation functions A_1, A_2 of the form

$$A_i = \exp\left[-\int_0^{R_w} \alpha_i(\ell)\, d\ell\right], \tag{6}$$

where the α_i are functions of the water at the location specified by ℓ and also of the beam collimation at that point of the path. Since this collimation is not easy to predict or measure and complete profiles of water properties are seldom available, calculations were based on the simplified model of Equation (1).

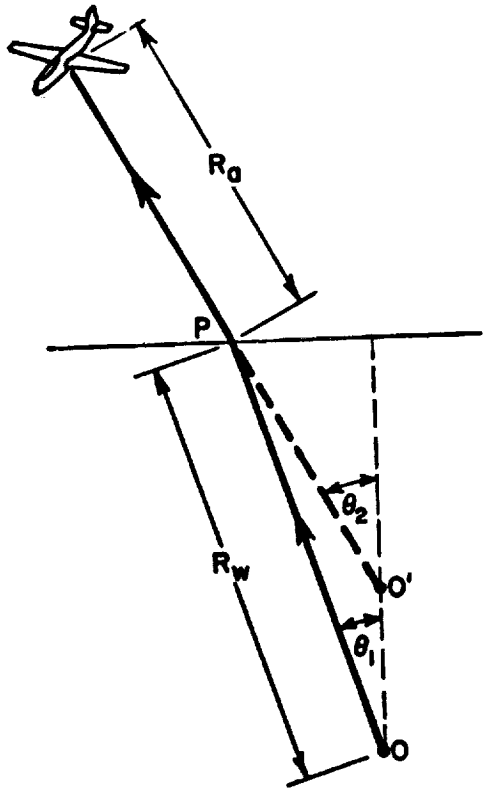

Figure 2. Upward path geometry.

The collimation enters into the extinction because it determines what portion of the energy scattered from the beam is permanently lost. On one extreme, one may have a very tightly collimated beam pointed toward a detector with very small acceptance angle. In this case, essentially all energy scattered from the beam is lost and the resulting attenuation is relatively high--this is termed monopath attenuation. On the other extreme, we may have a plane wave directed toward a detector with hemispherical acceptance. In this case, all forward-scattered energy is still available--this is termed multipath attenuation. A relation between the extinction coefficient for these two cases has been derived by Battelle, Gillette and Honey (ref. 2) for typical ocean waters. Two parameters, α_1 and α_2, are retained in Equation (1) in order to allow use of monopath on the downward path and the multipath coefficient on the upward path.

The transmission coefficients T_1 and T_2 must take into account the roughness of the sea surface. Depending on the diameter of the beam at the surface, an integration over a few or many facets may be needed. This is the reason for two coefficients since the beam diameter is much larger on the upward than on the downward path. Calculations pertaining to the time-averaged transmission on the downward path were performed by Swennen as part of this project (ref. 3), and those for the upward path by Upp (ref. 4), both based on the sea-slope probability data of Cox and Munk (ref. 5). The effect of surface roughness is to lower the transmission by a few decibels in the direction in which it is maximum (the angle corresponding to Snell's law) and to allow transmission for a narrow range of angles about this maximum. A rough sea would thus be expected to give some reduction in range and loss of angular resolution.

The maximum range predicted on the basis of Equation (1) for various transmitted power levels and extinction coefficients are given for black and white targets in Figures 3a and 3b. respectively. The values of attenuation length (reciprocal of extinction coefficient)

given in these figures corresponds to the monopath value. The dashed curves use these monopath values directly on both down and upward paths. The solid curves use the monopath value for downward and multipath for upward, the latter value being obtained from the monopath coefficient by the curve of Battelle et al (ref. 2). Vertical incidence and smooth seas are assumed in these calculations.

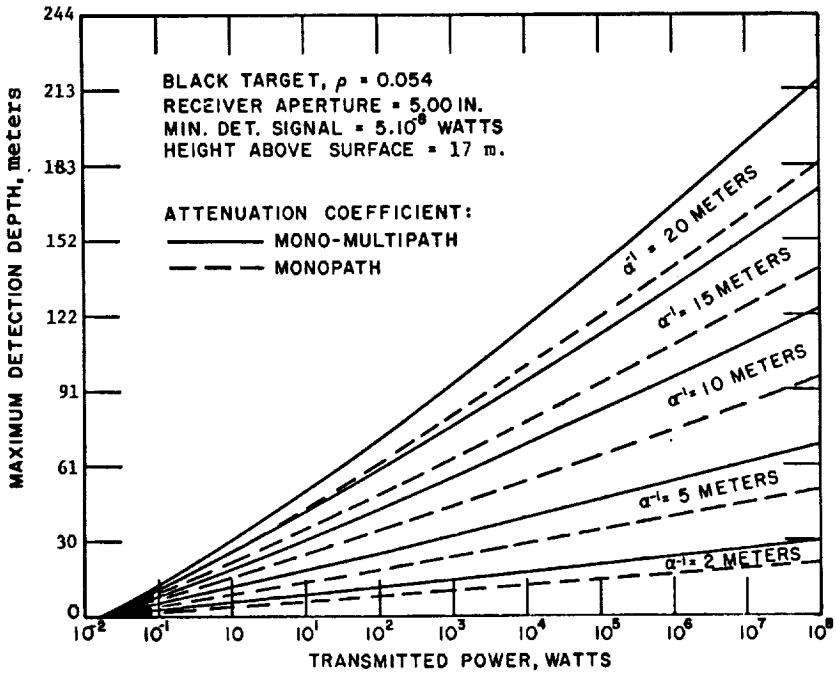

Figure 3a. Predicted maximum range - black target.

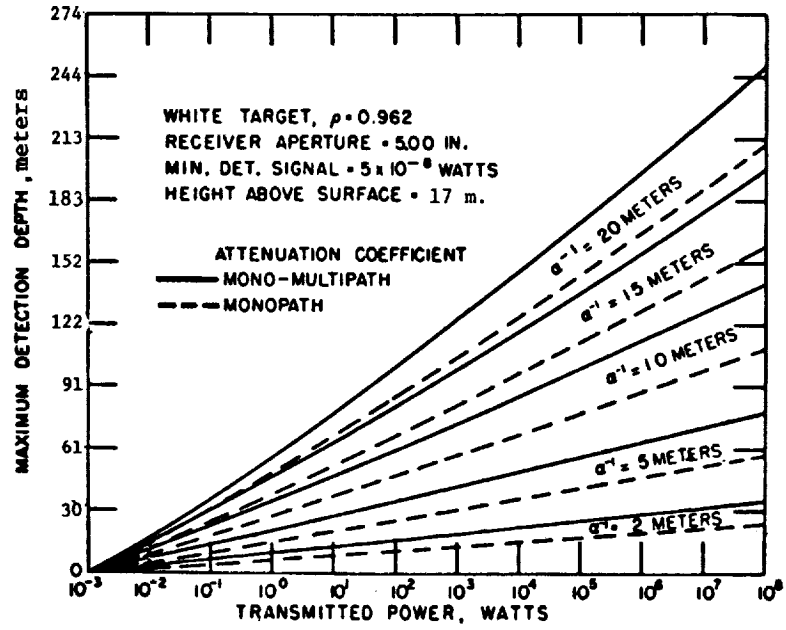

Figure 3B. Predicted maximum range - white target.

THE RADAR

A block diagram of the optical radar is shown in Figure 4. The transmitter consists of a Nd^{3+} laser oscillator and amplifier, frequency-doubled to the desired wavelength. The oscillator is a rotating-prism, Q-switched laser which uses a .95 cm (3/8-inch) diameter, 15.2 cm (6-inch) long glass laser rod with a 2% doping of Nd^{3+}, three linear flash lamps, and a cylindrical cavity. The oscillator output drives a laser amplifier which uses a 1.27 cm (1/2-inch) diameter, 30.5 cm (12-inch) long glass laser rod with a 3% doping of Nd^{3+}, one linear flash lamp and cylindrical cavity. The second harmonic of the infrared laser amplifier output is generated by means of a phase-matched KDP crystal, protected from moisture in mineral oil. If a steep trailing edge on the outgoing radar pulse is required, a gas breakdown cell is added to the system. A photodetector and a photodiode are used to trigger the oscilloscope and to provide a time and magnitude reference pulse for the transmitted signal.

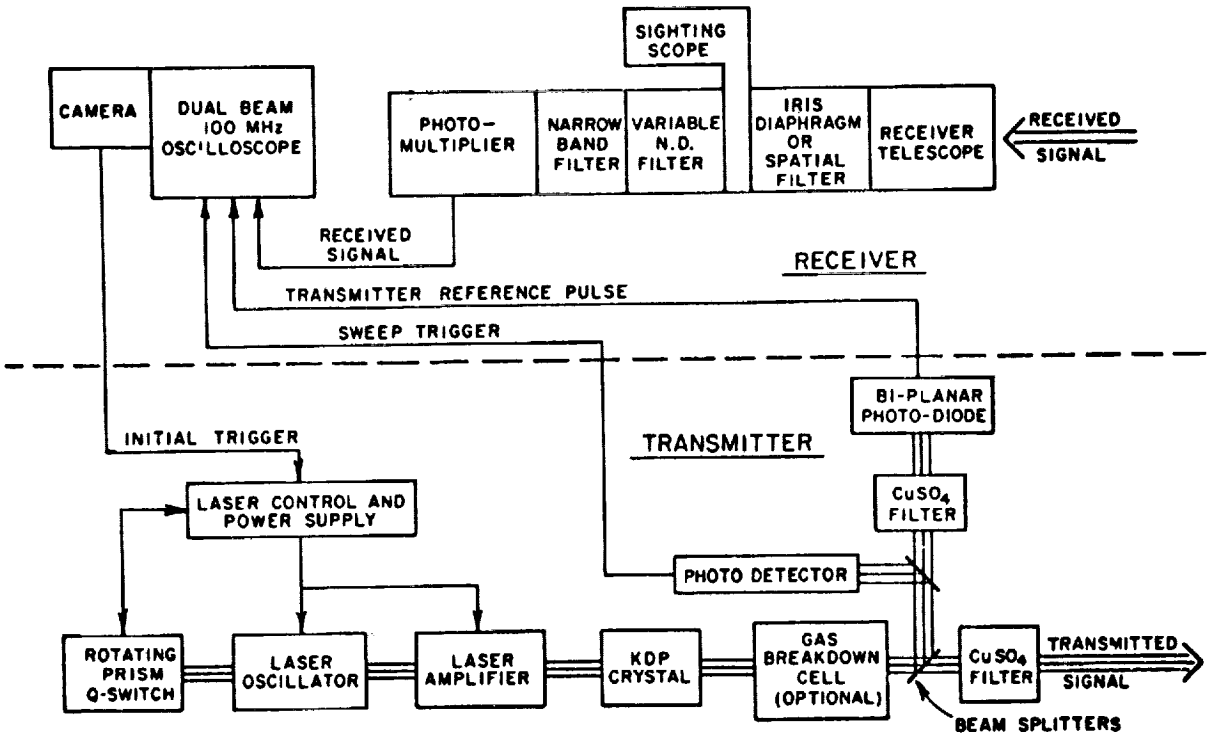

Figure 4. Optical radar block diagram

The receiver consists mainly of a receiving telescope and photomultiplier. An iris diaphragm or spatial filter may be added at the focal plane of the objective lens. Variable neutral density filters and a narrow-band filter centered on the wavelength of the transmitted radar signal are incorporated in the receiver. A sighting scope is provided to facilitate aiming the radar. The output of the photomultiplier is displayed on a dual-beam 100 MHz oscilloscope, which also displays the transmitter reference signal. Characteristics of the final optical radar system are given in TABLE 1. A photograph of an earlier version, which did not employ the laser amplifier, is shown in Figure 5. In this picture, the radar is equipped with periscopes (shown with extension tubes removed) for transmitting the beam horizontally for preliminary testing in a swimming pool. Dry-nitrogen pressurization prevents water condensation on optical components. For field testing, the periscopes were removed and the radar transmitter and receiver were mounted on an electrically-controlled gun mount which provided a means for aiming the radar at any desired location.

TABLE 1.-CHARACTERISTICS OF OPTICAL RADAR SYSTEM

Output wavelength	530.8nm
Peak pulse power	variable over 30 kw to 2 mw range
Pulse rate	1 per min
Pulse width	25 ns
Minimum detectable signal	5×10^{-8} W
Frequency response	100 MHz
Receiver aperture	12.7 cm
Field of view	variable 0.5° to 4.5°
Range resolution	< 3 meters
Narrow band filter	
Center wavelength	530.8 nm
Bandwidth (3 dB)	1.25 nm
Transmission	70%

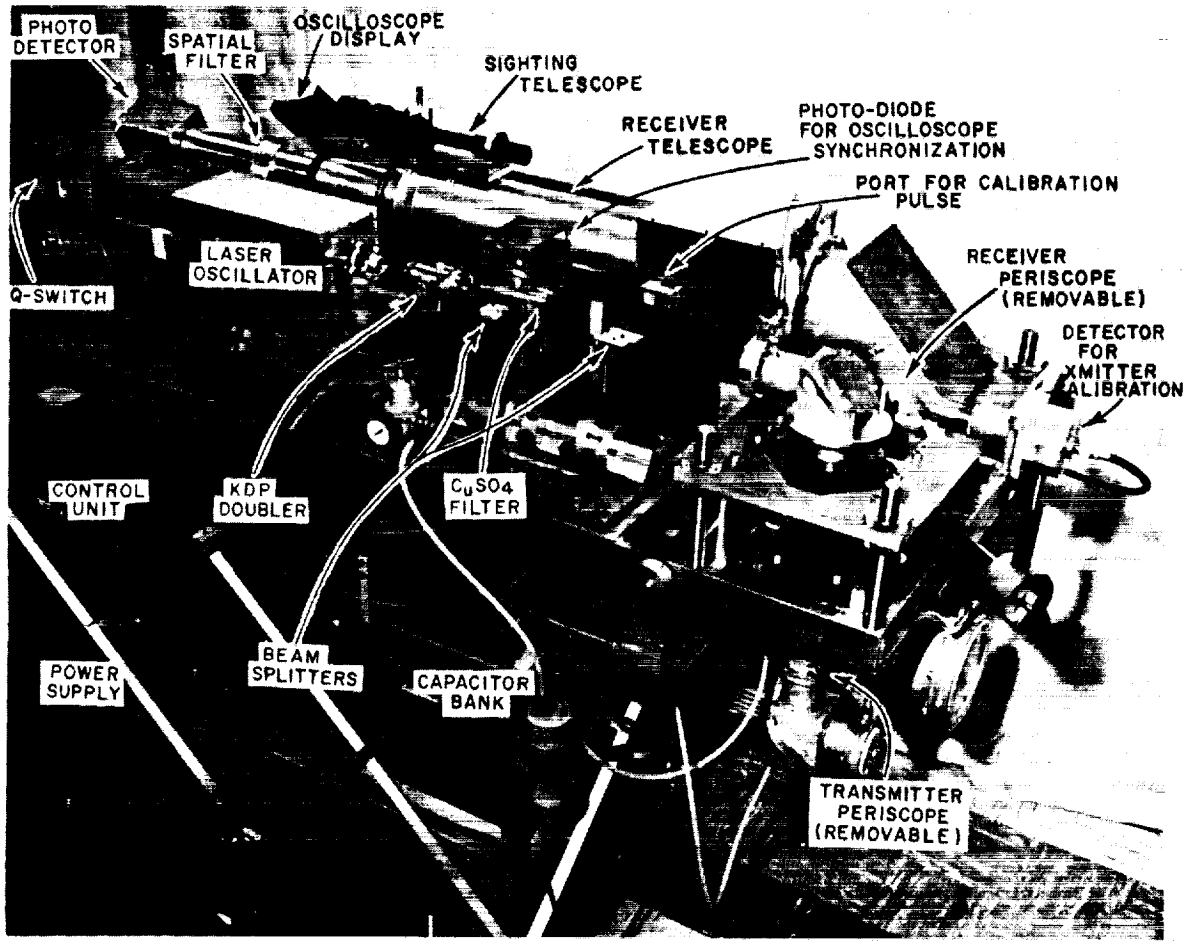

Figure 5. Optical radar.

The optional focal-plane spatial filter (ref. 6) effectively varies the system gain as a function of the depth from which the signal is received. It takes advantage of the fact that, for a rough sea, the signal from a deep target is capable of being refracted to the receiver over a much larger surface area than the signal from a shallow target. By using a focal-plane filter with low transmittance in the center, the returns from shallow targets are deemphasized. Figure 6a shows the A-scope traces without the filter for a white target at 25.6 cm (84 feet). The sweep speed is 100 ns/division and the incidence angle was 18°. Note that the system is saturated for shorter ranges. Figure 6b shows the trace for identical condition, but with the filter in use and the receiver gain increased by approximately 3 dB; there is no saturation at any range although the target return is the same as before.

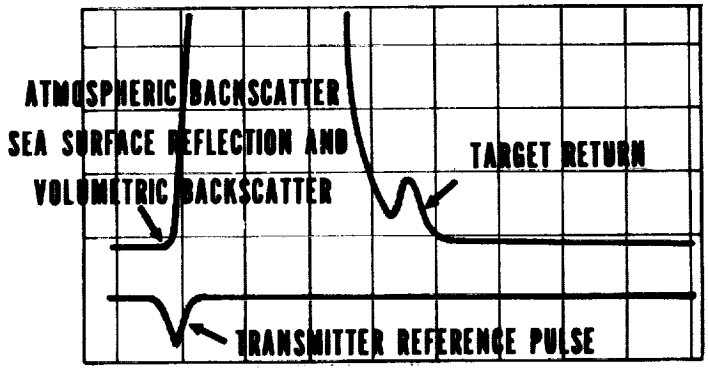

Figure 6a. A-scope presentation: white target at 26-meter depth, incidence angle 18° from vertical - spatial filter not used.

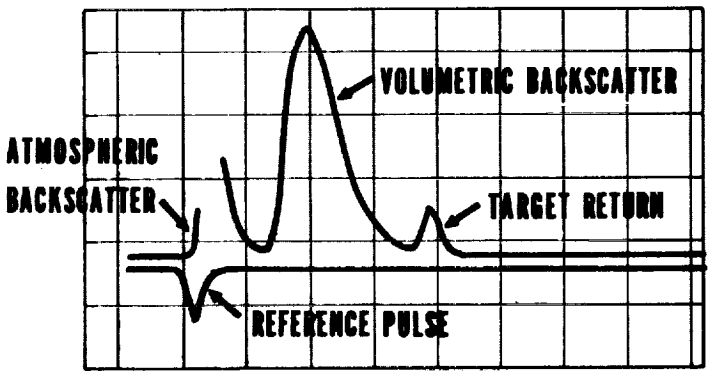

Figure 6b. A-scope presentation: white target at 26-meter depth, incidence angle 18° from vertical - with spatial filter

Since the purpose of the experiment was only to determine feasibility and limitations, no attempt was made to make the equipment flyable; all tests were conducted from fixed platforms above the water. Nor would the repetition rate have been adequate for a flying radar--almost one minute was required to charge the flash-tube capacitor bank. A system based in part on our design, but capable of being flown and having the required higher repetition rate, has since been developed (ref. 7).

PERFORMANCE TESTS

After preliminary horizontal radar ranging tests in a swimming pool and at Wakulla Springs, Florida, the system was evaluated at the Stage I tower of the U.S. Navy Mine Defense Laboratory . The tower is located in the Gulf of Mexico approximately 16 Km (10 miles) offshore, near Panama City, Florida. The water depth is approximately 32 meters (105 feet) and the system was located 14 meters (55 feet) above the surface.

The targets were flat, square aluminum sheets, 158 square-decimeters in area, coated with paints having reflectivities (measured submerged) ranging from approximately 1% to 96%. The targets were attached, one at a time, to a positively buoyant frame which was lowered by means of a winch along guide cables toward lead-weighted sea anchors. Radar ranging was performed at depths of 0 to 25.6 meters (0 to 84 feet) at incidence angles from 5° to 60° with respect to the sea surface normal. For near-vertical incidence, all targets were detected in each case. Ambient light presented no problem; even with the radar aimed directly into the specular reflection of the sun from the ocean surface on a slightly hazy day, no deterioration of radar performance was evident. Figures 7 through 9 show the ratios of received to transmitted power from a white, gray, and black target, respectively. In Figure 7 the ranging is horizontal; in Figures 8 and 9, the beam has an incidence angle of 5° from the vertical. The calculated curves (for monopath attenuation in both directions, monopath down and multipath up, and multipath in both directions) show that the very rough approximation of constant extinction coefficient is useful for estimating approximate signal returns, but that the integrated form of the attenuation function is likely to be needed for more precise estimates. The value of α_1 used in these calculations was measured (see next paragraph); the corresponding α_2 comes from Battelle, Gillette, and Honey (see ref. 2); the values of T_1 and T_2 are calculated for a smooth surface. The scatter of experimental points for a given depth is due to surface roughness.

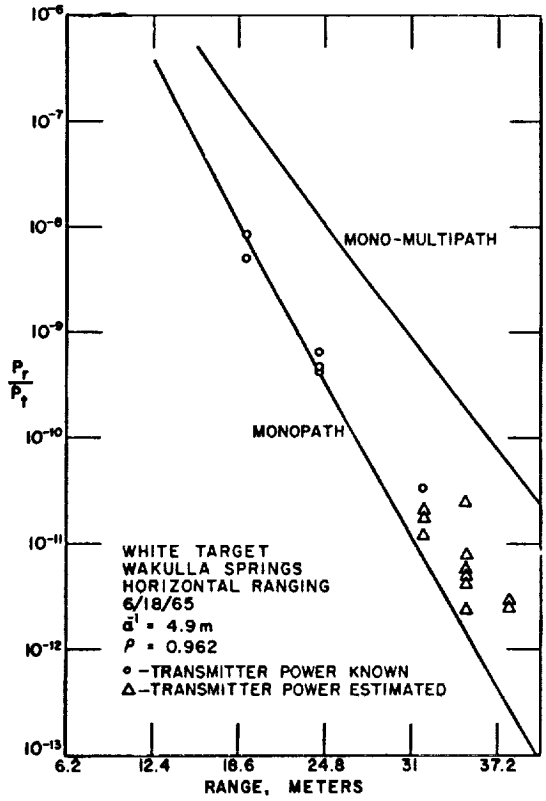

Figure 7. Received-to-transmitted power ratio, Wakulla Springs, white target.

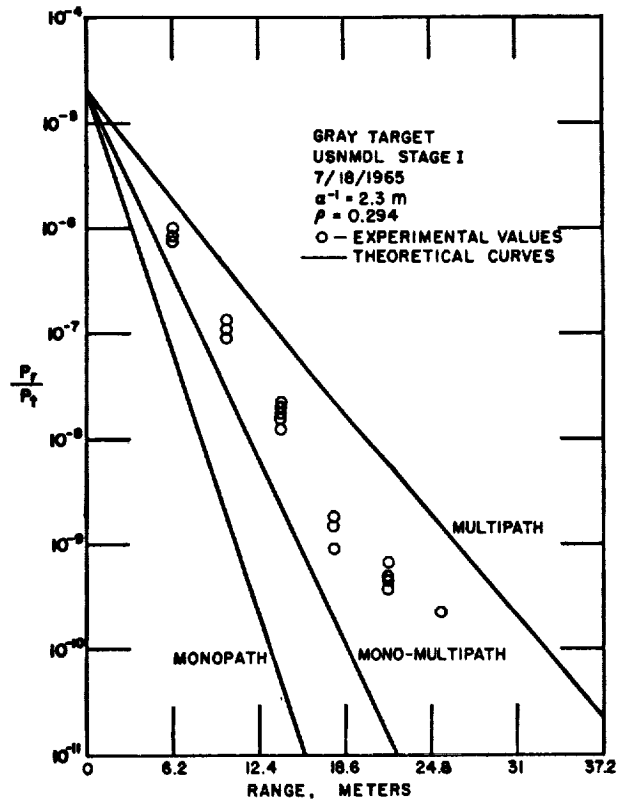

Figure 8. Received-to-transmitted power ratio, U.S. Mine Defense Laboratory, gray target.

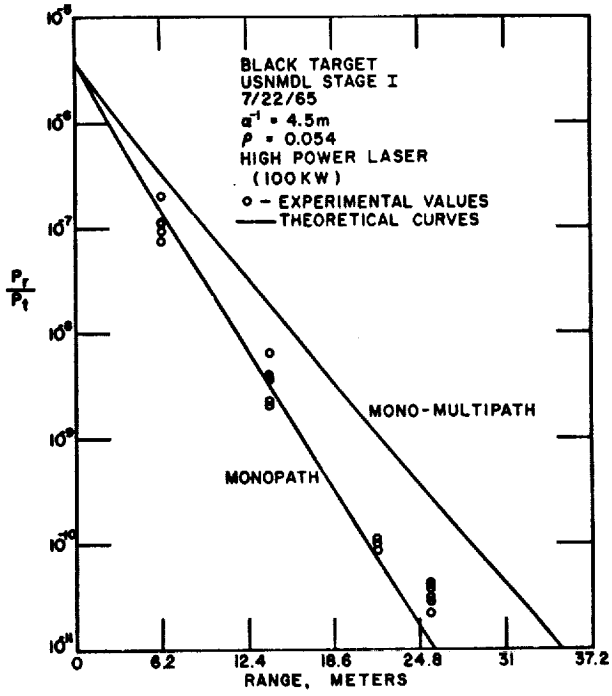

Figure 9. Received-to-transmitted power ratio, U.S. Mine Defense Laboratory, black target.

MEASUREMENTS OF EXTINCTION, SCATTERING, AND SURFACE STRUCTURE

In support of the systems measurements, extinction, scattering, and surface structure measurements were also instrumented. Extinction measurements were made over the wavelength range 400-700 nm by means of absorption cells taken to the site and filled with water from the depth to be sampled, and also in the blue-green spectral region (538 nm with 60 nm bandwidth at 10 dB) with an in-situ transmissometer which could be lowered to the desired depth. Typical measurements at the Mine Defense Laboratory tower often show, as a function of time, considerable correlation with tides, but also considerable randomness (Figure 10). As a function of depth, extinction was relatively constant near the surface and generally increased rather abruptly by a factor of two near the bottom (Figure 11).

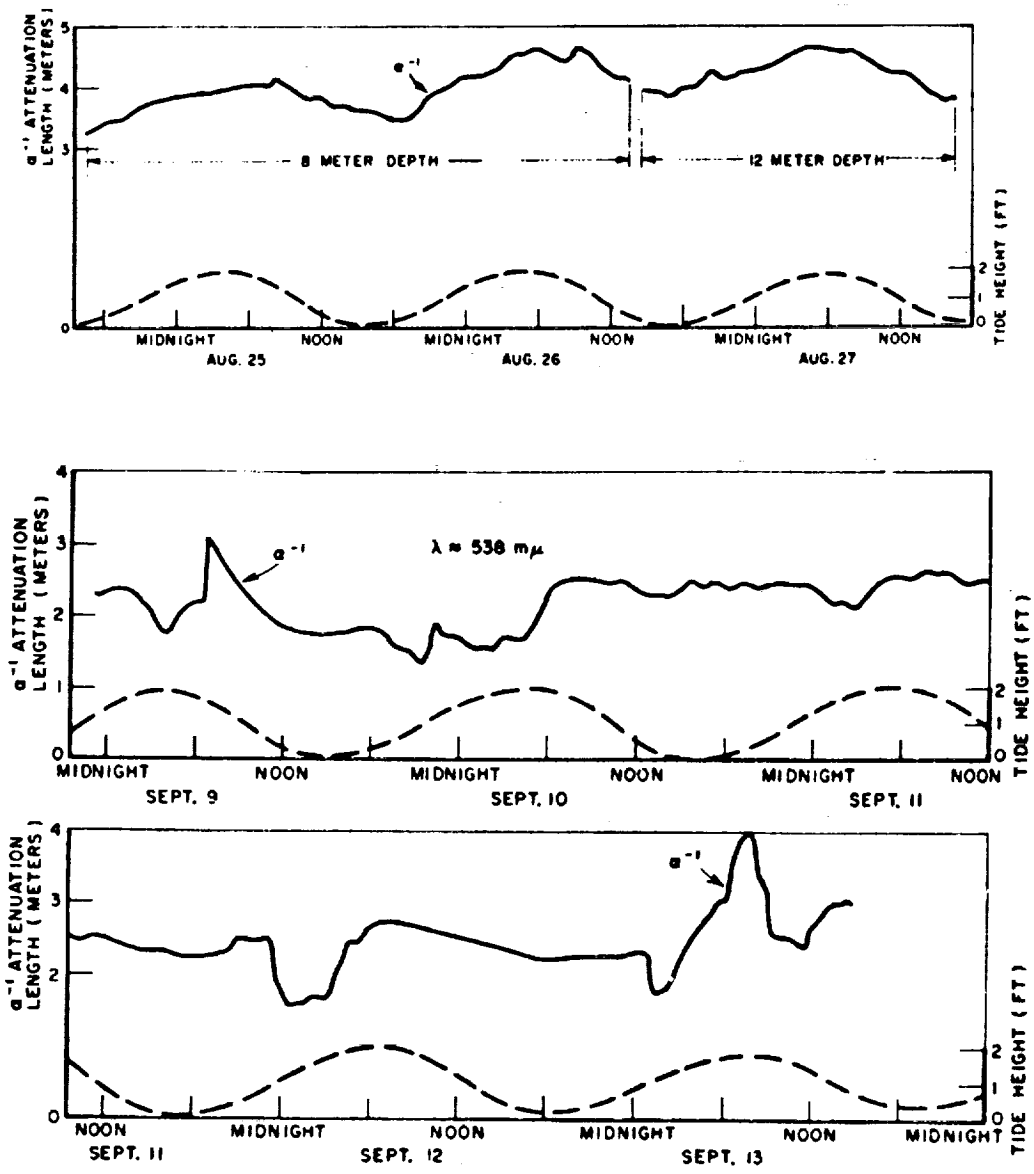

Figure 10. Attenuation length (solid) and relative tide height (dashed) at USNMDL stage I tower.

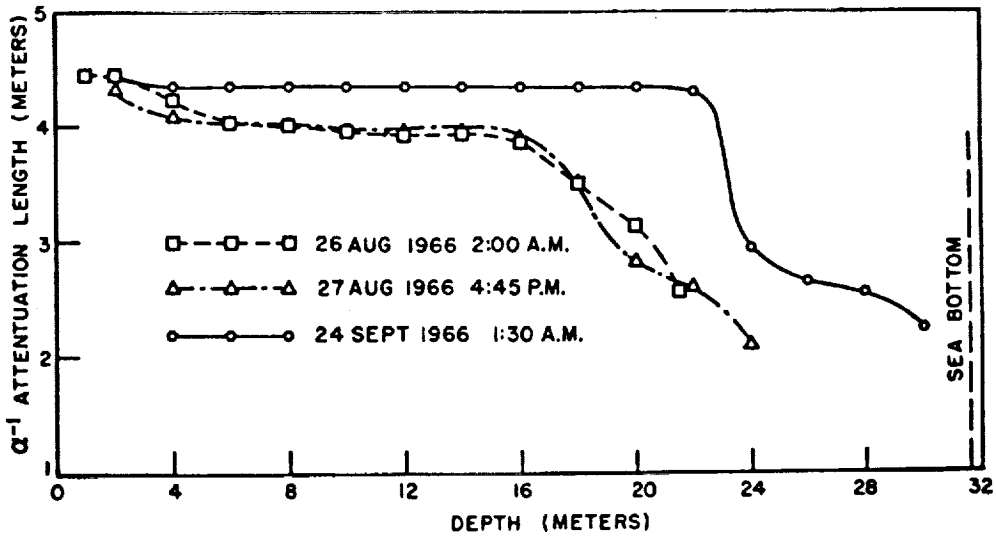

Figure 11. Attenuation length vs. depth at UNMDL stage I tower.

The extinction coefficient is the sum of an absorption coefficient and a scattering coefficient; only the latter has an effect on beam collimation. The scattering coefficient is the integral with respect to scatter angle of the volume scattering function (ref. 8). Instruments were built for measuring this function both by means of a laboratory cell filled with sampled water and by means of an in-situ scatter meter utilizing a fixed argon laser source and movable detector (Figure 12). Typical data are shown in Figure 13. Integration of the volume scattering function showed that the scattering coefficient under relatively clear conditions (α = 0.226 meters^{-1}) at the Mine Defense Laboratory might contribute 1/4 to 1/3 of the total extinction, with absorption accounting for the rest.

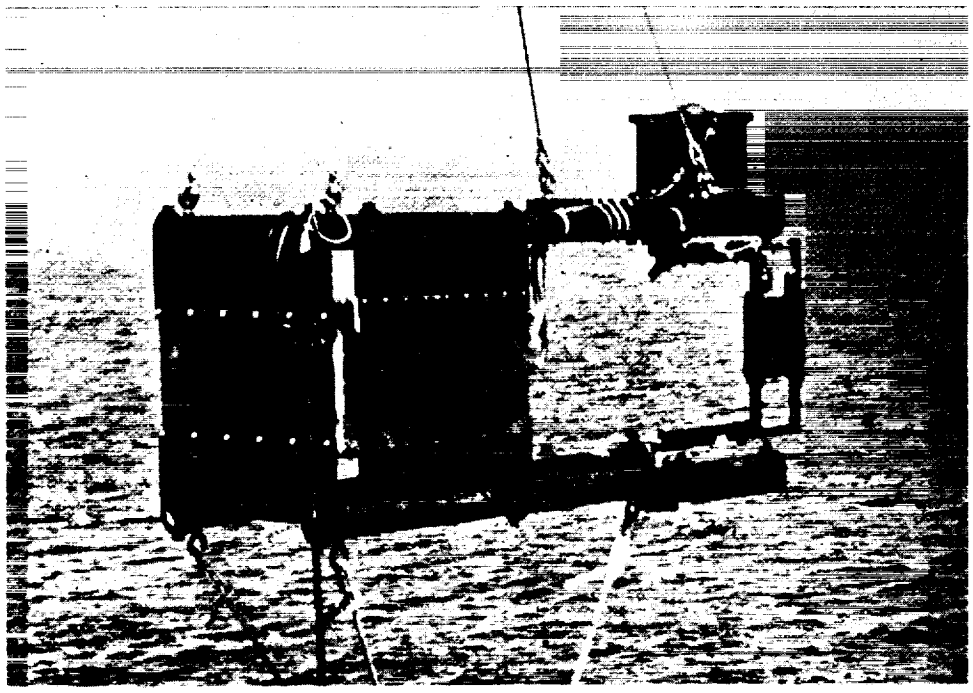

Figure 12. In-situ scatter meter.

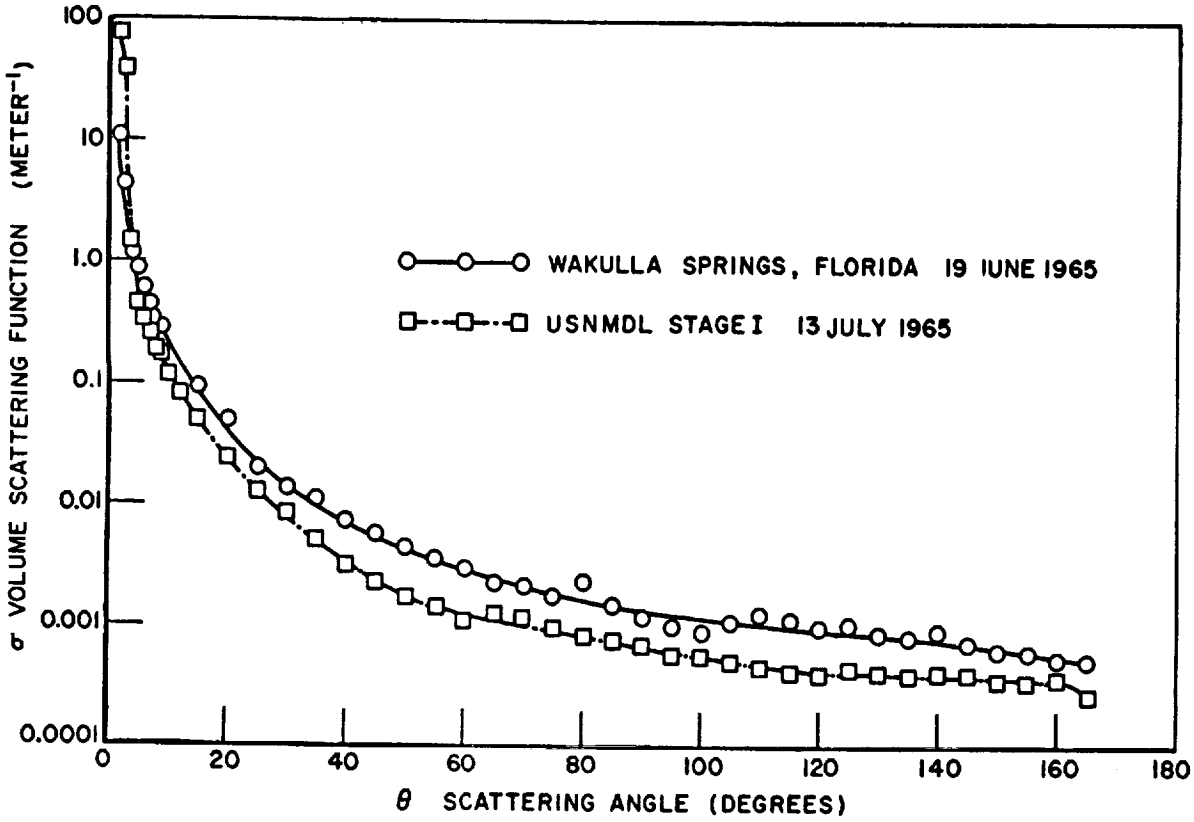

Figure 13. Measured volume scattering functions.

The calculations of upward and downward transmission through the sea surface mentioned above were based on time-averaged sea-slope probabilities measured by Cox and Munk (ref. 5); while useful for predicting average beam intensities, they do not allow calculation of the expected temporal behavior of the beam. An experiment to explore this temporal behavior was instrumented; since it is reported elsewhere (ref. 9), the results are not given here. Unfortunately available time did not allow as much data to be taken or processed as would be desirable for the prediction of such time-related radar parameters as optimum scan rate.

CONCLUSIONS

The detection of targets in coastal waters was demonstrated experimentally up to a depth of 25.6 meters (84 feet), this limit corresponding to the depth at which targets could be conveniently anchored, not the sensitivity limit of the system. The measurements have been used to validate a theoretical model on the basis of which performance of the radar under various water conditions can be estimated. Curves of expected maximum range are given as function of water clarity and transmitter power. These ranges would be decreased somewhat for rough surface conditions, but the principal effect of surface roughness is on angular resolution, not range. A spatial optical filter can be used to vary the system gain as a function of target depth, greatly reducing the dynamic range requirement of the receiver. In moderately clear coastal water, volumetric backscatter returns were observed at all depths; this suggests that such radars might be useful for estimating water quality and observing changes over a considerable range of depths synoptically from the air.

REFERENCES

1. Jenkins, F.A. and White, H.E., Fundamentals of Optics, McGraw-Hill, 1957.

2. Battelle, R.B.; Gillette, P.R.; Honey, R.C., "An Analysis of the Feasibility of Laser Systems for Naval Applications", Stanford Research Institute, Final Report on Project 2167-80. Also see Pressley, R.J. (Ed.) Handbook of Lasers with Selected Data on Optical Technology, The Chemical Rubber Co., Cleveland, Ohio 1971, p. 154.

3. Swennen, J.P.J.W., "Time Average Power Density Probability Distribution Below the Ocean Surface of a Beam of Collimated Optical Radiation Incident on the Surface," Jour. Opt. Soc. Am. 56, February 1966, pp. 224-229.

4. Upp, D.C., "Optical Energy Received Above the Ocean Surface from a Subsurface Scatterer," Thesis and Report 2170-2, 21 March 1967, The Ohio State University Electro-Science Laboratory, Department of Electrical Engineering; prepared under Contract AF33(615)-3667 for Air Force Avionics Laboratory. (AD 809 419)

5. Cox, C. and Munk, W., "Measurements of the Roughness of the Sea Surface from Photographs of the Sun's Glitter," Jour. Opt.Soc. Am. 44, November 1954, pp. 838-850.

6. Swarner, W.G. and Prettyman, C.E."Optical Spatial Filter for Modification of Received Energy vs. Range", U.S. Pat. No. 3,712,985 January 23, 1973.

7. Battman, W. and Smith, T., "Laser Applications to Oceanography", Electronic Progress 13, Spring 1971, pp. 8-10.

8. Jerlov, N.G., Optical Oceanography, Elsevier, 1968, Chapter 2.

9. Prettyman, C.E. and Cermak, M.D., "Time Variation of the Rough Ocean Surface and its Effect on an Incident Laser Beam", IEEE Trans. GE-7, October 1969, pp. 235-243.

RECENT ADVANCES IN THE APPLICATIONS OF PULSED LASERS IN THE HYDROSPHERE

George D. Hickman
Sparcom, Inc.

ABSTRACT

Laboratory and field measurements have been performed on the transmission/scattering characteristics of a pulsed neon laser as a function of water turbidity. These results have been used to establish the criteria for an airborne laser bathymetry system. Extensive measurements have been made of laser induced fluorescence using a pulsed tunable dye laser. Feasibility has been demonstrated for remote detection and possible identification of various types of algae and oils. Similar measurements made on a wide variety of organic dyes have shown this technique to have applications in remote measurements of subsurface currents, temperature and salinity.

LASER BATHYMETRY

During the past two years, Sparcom, Inc. has been investigating through a series of laboratory measurements the transmission of a blue-green laser as a function of water turbidity. The results of these measurements have been used to estimate the capability and limitations of an airborne laser bathymetry system (ref. 3).

The laser used for these measurements was a pulsed neon gas laser at 540 nm. Tunability in wavelength (400-700 nm) is obtained with this laser using nitrogen in the laser cavity to pump various organic dyes. This tunability in wavelength was used in various laser induced fluorescence measurements.

The short pulse width (3-10 nsec) of the laser combined with its high pulse repetition rate (100-1000 pps), make this laser the best transmitter for a high resolution, shallow water and reconnaissance system.

The strength of the signal received by an airborne laser/detector system depends on two different categories of parameters:

a. Environmental parameters; such as depth of water (h), the attenuation (α) and absorption (a) coefficients of the water, bottom reflectivity and the distribution of power at the water/sediment interface.

b. Controllable parameters; such as aircraft altitude, input power of the laser, field of view of detector, etc.

The laboratory measurements were designed to determine the effect of each of the environmental parameters on the detected laser signal. The results have been used to set the criteria for the controllable parameters.

In the laboratory, the turbidity of the water was changed in small increments by addition of various marine sediments to the water in Sparcom's environmental water tank facility. These sediments were collected from selected shallow water sites along the east coast of the United States. Comparison was made between these simulated waters and actual water samples which were obtained at each site.

The following measurements were made for all samples:

a. attenuation coefficient and sediment loading for each water sample,

b. attenuation and absorption coefficients and sediment loading for simulated turbid water,

c. sediment reflectivity, and

d. beam spreading in the water at a given distance (h) as a function of turbidity.

In addition to the natural sediment measurements, quartz (SiO_2) and marl CaO_3) were also used to change the turbidity conditions in the tank.

Optical Properties of Turbid Waters

The measured quantity describing the optical properties of light transmission in turbid water is the normalized integrated power distribution $N_{ga}(h,\Theta)$. This distribution expresses the total power which is contained in a cone angle (half angle Θ) at a distance h in water as shown in Figure 1.

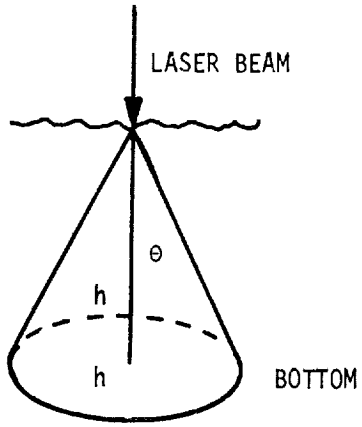

Figure 1. Schematic diagram showing the geometry used for obtaining the integrated power distribution.

To construct the integrated power distributions, one of the bottom sediments was mixed in the environmental simulation tank. The amount of sediment was adjusted in each case to generate turbidities corresponding to α values in the range 0.07 - 2.0 m^{-1} in steps, $\Delta\alpha$, of approximately 0.5 m^{-1}. For each turbidity, the angular power distribution was measured for water paths of 4, 6 and 8 meters by scanning the laser beam (from 0-200 mrad) past an underwater photomultiplier tube (PMT). The PMT was aligned with the original direction of the incident beam (zero angle). The resulting angular power distribution was plotted as a function of the spherical polar angle (Θ). The integrated power distribution was derived by numerically integrating the angular power distribution over the appropriate solid angle. For each distance, the integrated power distribution was normalized to the total power available at that distance in clear water.

The data for the integrated power distributions [$N_{\alpha a}(h,\Theta)$] (refs. 1 & 2) at various distances, for each sediment, have been used to construct composite distribution curves as a function of attenuation length (αh). Figure 2 is a typical curve that was constructed for quartz. Curves similar to those shown in Figure 2 have been obtained for the various simulated waters. The distribution curves generated in this way have been used to analyze the optical properties of turbid water and to predict the limitations of an airborne laser bathymetry system.

System Considerations

A number of the salient parameters have been determined either measured or calculated, which define the capability and system requirements for an airborne laser/receiver bathymetry system in turbid waters. The following is a list of these critical items:

The optimum wavelength for the bathymetry of turbid waters is between 540 and 580 nm. The maximum depth measuring capability $(\alpha h)_{max}$ of such a system is approximately 15 for waters characterized by an a/s ratio of between 0.1 and 0.2 and a sediment reflectivity of $\geq$ 10%. This was determined for a laser having a peak pulse power of 30 kw operating from an altitude of 500 m.

While the effective value of the attenuation coefficient of the water (α_{eff}) for an airborne laser/receiver system is $a \leq \alpha_{eff} \leq \alpha$, it is closer to the value of a than α.

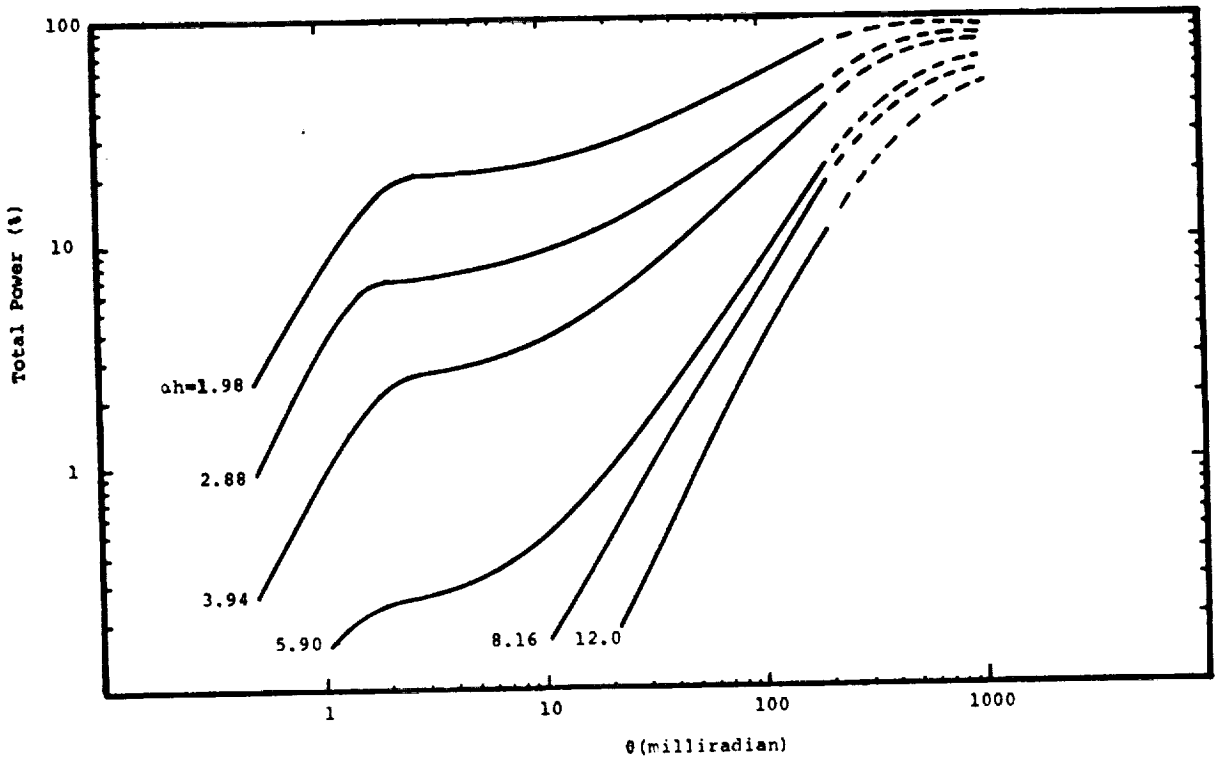

Figure 2. Total power contained in a given cone angle as a function of h for quarts. (a/s = 0.06)

Polarization techniques are essential in depressing the backscattering from the water.

A factor of 10 increase in laser power increases $(\alpha h)_{max}$ by 2.5.

A factor of 10 increase in aircraft altitude decreases $(\alpha h)_{max}$ by 2.5.

The optical scanner should be restricted to scanning angles of approximately 20°.

For maximum laser pulse rate of 100 pps, a scanner period of approximately 1 second is optimum in terms of area coverage and spatial resolution.

LASER STIMULATED FLUORESCENCE

A number of programs have been initiated in the laboratory concerning laser stimulated fluorescence. Fluorescence is the phenomenon whereby radiation is absorbed at one wavelength and re-emitted at a shifted (normally longer) wavelength. The uniqueness of the fluorescent spectrum for a particular molecular structure can be used to identify a substance. The fluorescent technique can be used to measure quantitatively small concentrations since in this region the fluorescent intensity is proportional to the concentration. Extensive fluorescent measurements have been made on algae, organic dyes and oils.

Algae

Each of the specific pigments in algae has a different excitation and fluorescence spectrum. In the case of Chlorophyll a, maximum fluorescence is obtained when excitation is made at either of the absorption peaks; i.e., 400 or 670 nm. From other considerations, (ref. 4) it has been shown that for remote detection of the Chlorophyll a, the optimum wavelength for excitation is at 670 nm. However, since the absorption and fluorescence peaks are relatively close in wavelength, receiver consideration dictate that the excitation should be made at a wavelength shorter than the maximum absorption wavelength. Calculations and laboratory results show that a 100 kw laser/receiver system operating at a wavelength of 600 nm and an altitude of 500 meters should be able to detect Chlorophyll a concentrations as low as 5 mg/m^3.

Identification of various species of algae is a much more difficult problem. One possible technique for detecting and identifying algae is to excite the algae at multiple wavelengths and analyze the ratio of the fluorescent signals at several discrete wavelengths. A prototype based on this principle is currently being investigated (ref. 5).

Dyes

Several organic dyes were investigated that exhibit fluorescence in the 480 to 600 nm region of the spectrum. The absolute value of the fluorescent intensity of the dyes depends on such parameters as temperature, pH, salinity and exposure to ambient light. The effects of the various parameters on fluorescence have been made in Sparcom's laboratory. In addition, the optical density and quantum efficiency of the dyes were determined since these parameters quantify the conversion of absorbed energy into fluorescence. The quantum efficiencies were measured in a spectro-fluorometer on a relative basis similar to that of Parker and Rees (ref. 6). The optical densities were determined as a function of wavelength on a dual beam spectrometer using water as the solvent. The product of the quantum efficiency and the optical density (QEOD) is a good relative parameter for comparing the absorption/fluorescence conversion factor. TABLE 1 lists the measured values of optical density at 540 nm and the measured quantum efficiency for some of the dyes.

TABLE 1.-OPTICAL DENSITY AT 540 NM, QUANTUM EFFICIENCY AND THE RELATIVE PARAMETER QEOD FOR SEVEN ORGANIC DYES THAT EXHIBIT FLUORESCENCE

DYE	Optical Density @ 540 nm	Quantum Efficiency	QEOD
Acridine Red	0.190±0.005	0.71	135
3,6 Dichlorofluorescein	0.015±0.002	0.98	15
Disodium Fluorescein	0.004±0.001	0.54	2
Eosin Y	0.015±0.003	0.32	5
Magdala Red	0.094±0.006	0.22	20
Rhodamine B	0.135±0.004	0.90	122
Rhodamine 6G	0.082±0.006	0.50	42

The two dyes exhibiting the largest values for QEOD are Acridine Red and Rhodamine B. One application where these dyes could be used is in detecting the boundary of a dye cloud, either surface or subsurface. For applications where it is desired to derive information from within the dye cloud, it might prove advantageous to deploy dyes other than those with high QEOD values.

Another application involving the use of these dyes is that of measuring surface or subsurface temperatures. The possibility exists that this could be accomplished by dispensing a dye cloud composed of two dyes which have widely different fluorescent temperature coefficients. The ratio of the two fluorescent signals which is proportional to the temperature would than be monitored. A detector system, based on this technique, could be calibrated to yield absolute temperature. One pair of dyes which might be used for this application is Rhodamine B and Eosin Y. The dependence of the fluorescent signal on temperature for these dyes is shown in Figure 3. It has been determined that the temperature of the water can be determined to $\pm$0.5°C if the ratio of the two fluorescent signals is measured to within 2%.

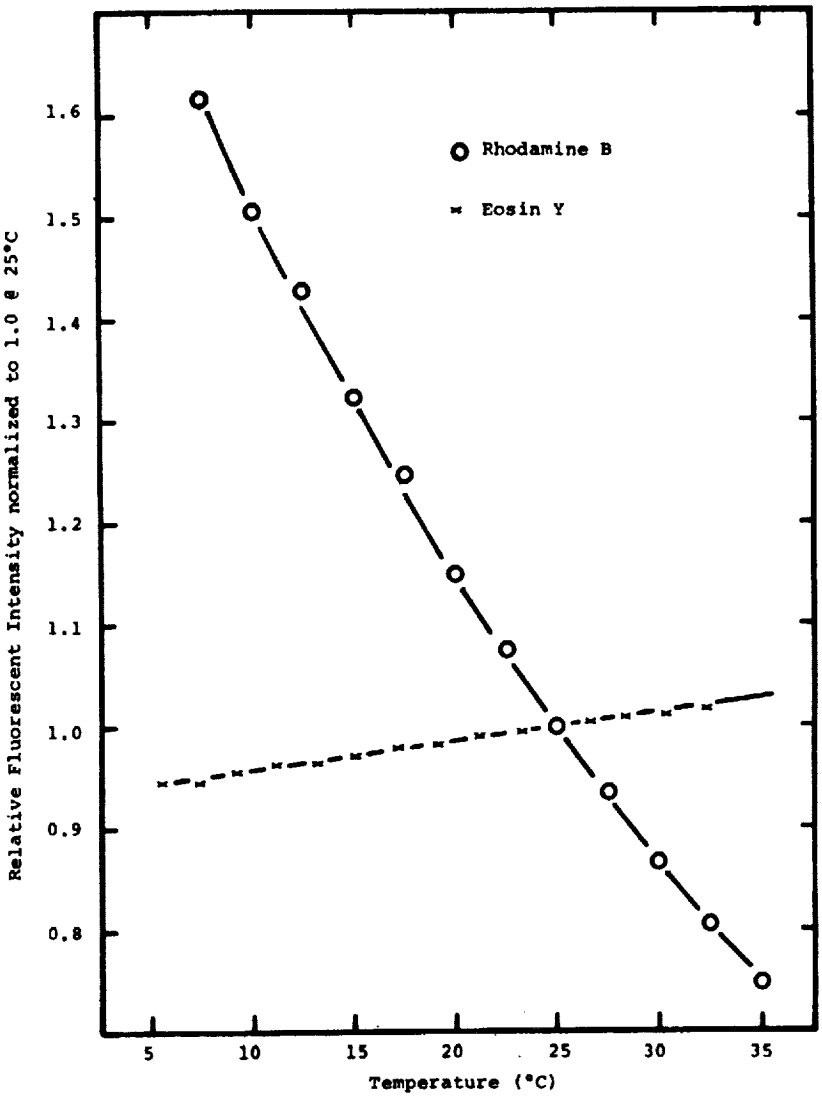

Figure 3. The relative fluorescent intensity of Rhodamine B and Eosin Y as a function of temperature. The relative fluorescent intensity has been normalized to 1.0 at 25°C.

Oils

A variety of fuel and lubrication oils have been investigated for their fluorescence characteristics. The excitation and emission spectra are relatively broad when compared to either the algae or the dyes while the maximum wavelength for excitation occurs below 400 nm. The quantum efficiencies for these oils ranged from 1 to 10%.

In June 1973, airborne laser detection of an oil spill was made by Sparcom in conjunction with NASA (Wallops Island, Virginia) (ref. 1). The pulsed nitrogen laser, which has its emission at 337 nm, was used in this experiment to excite the oil fluorescence. Although the results of the tests are considered preliminary, they represent the first results that have been obtained by an airborne laser fluorometer for detection of surface oils.

LASER TURBIDITY METER

The turbidity of the water is characterized by an attenuation coefficient (α) that quantizes the amount of absorption and scattering a light beam undergoes as it is transmitted through the water. The present method for measuring the attenuation coefficient uses a transmissometer which must be lowered into the water. This procedure is slow and severely limits the quantity of data that can be obtained in a reasonable time frame.

A technique is currently under investigation at Sparcom that uses the amplitude and shape of the laser backscattered signal from the water as a direct measurement of the water turbidity. The backscattered laser signal was measured in a series of water tank experiments as a function of both the water turbidity and laser wavelength. The tunable dye laser was used to obtain the desired wavelengths in the range of 420 to 640 nm. The turbidity of the water in the environmental test tank was changed by the addition of quartz and Chesapeake Bay sediment. The turbidity of the water ranged from equal to 0.5 to 6.0^{-1}. While the magnitude of the laser backscatter increased, at all wavelengths,as the turbidity increased, the percentage increase was greatest at 440 nm. A laser operating at this wavelength would be most sensitive to changes in α, thereby making it the best α detector. The results of these preliminary measurements therefore indicate that it may be feasible to use the backscatter from an airborne laser transmitter/receiver system as a direct reading of α. The sensitivity of this technique for measuring α, at 440 nm has been estimated from our results to be approximately 5-10%. A laser operating at still a lower wavelength may yield better sensitivity.

CONCLUSIONS

Many of the salient parameters have been determined which define the capability and system requirements for an airborne laser/receiver shallow water bathymetric system for surveillance of turbid waters. The maximum depth measuring capability $[(\alpha h)_{max}]$ of such a system has been determined to be approximately 15 attenuation lengths for waters examined in this study. These waters were characterized by an a/s ratio and bottom sediment reflectivity of approximately 0.2 and 0.1, respectively.

It has also been concluded that in situ measurements of α and a are sufficient to predict the transmission properties of a laser beam in water and therefore the performance of a laser bathymetry system in a specific body of water.

The oil flight measurement was a joint effort of Mr. H. H. Kim of NASA Wallops Island and Sparcom.

The fluorescent studies have shown that it is feasible to develop an airborne laser/receiver system for the detection and possible classification of a variety of algae and oils. It has been determined that Chlorophyll a should be detectable in concentrations as low as 5 mg/m^3 using a 100 kw laser/receiver system operating at 600 nm from an altitude of 500 meters.

Preliminary measurements have shown that it may be feasible to use a laser/receiver system operating from a remote platform to determine a number of other parameters of the water environment. These include the measurement of surface/subsurface current, temperature, salinity and turbidity.

REFERENCES

1. Hickman, G. D.; Hogg, J. E.; and Ghovanlou, A. H., "Pulsed Neon Laser Bathymetric Studies Using Simulated Delaware Bay Waters," Technical Report No. 1, Sparcom Inc., Alexandria, Virginia (Sept. 1972).

2. Ghovanlou, A. H.; Hickman, G. D.; and Hogg, J. E., "Laser Transmission Studies of East Coast Waters," Technical Report No. 2, Sparcom, Inc., Alexandria, Virginia (March 1973)

3. Hickman, G. D. and Ghovanlou, A. H., "Preliminary Design Criteria, Performance and Limitations of an Airborne Laser Bathymetric System," Technical Report No. 3, Sparcom Inc., Alexandria, Virginia (Aug. 1973).

4. Friedman, E. J. and Hickman, G. D., "Laser Induced Fluorescence in Algae: A New Technique for Remote Detection," Final Report, Sparcom Inc., Alexandria, Virginia (Oct. 1972)

5. Jarrett, O.; Mumola, P. and Brown, C., "Four Wavelength LIDAR Applied to Determination of Chlorophyll a Concentration and Algae Color Group," Remote Sensing of Water Resources International Symposium, Burlington Ontario, Canada (June 1973).

6. Parker, C. A. and Rees, W. T., Analyst, 85, 587 (1960).

UNDERWATER PROBING WITH LASER RADAR

A. I. Carswell and Sebastian Sizgoric
York University, Toronto, Canada

ABSTRACT

Recent advances in laser and electro-optics technology have greatly enhanced the feasibility of active optical probing techniques aimed at the remote sensing of water parameters. This paper describes a LIDAR (laser radar) that has been designed and constructed for underwater probing. The influence of the optical properties of water on the general design parameters of a LIDAR system is considered. Discussion of the specific details in the choice of the constructed LIDAR is given. This system utilizes a cavity-dumped argon-ion laser transmitter capable of 50-watt peak powers, 10 nanosecond pulses and megahertz pulse repetition rates at 10 different wavelengths in the blue-green (450-520 nm) region of the spectrum. The performance of the system, in proving various types of water, is demonstrated by summarizing the results of initial laboratory and field experiments.

INTRODUCTION

In recent years there has been an increasing interest in the use of LIDAR (laser radar) as an active optical remote sensor. Improved lasers with high powers, short pulses and ever-increasing range of wavelength selection and tunability provide suitable transmitter sources for LIDAR systems. However, to date, the LIDAR work has been almost exclusively concerned with investigations of atmospheric phenomena such as aerosol scattering, cloud studies, and smoke plume tracking (refs. 1, 2, 3).

LIDAR probing underwater is also quite feasible but so far only a few such studies have been reported in the literature (refs. 4, 5, 6, 7) and the true potential of underwater LIDAR systems is not yet clearly established. This paper reports on a newly developed marine LIDAR unit that has been designed and constructed to undertake an evaluation of LIDAR systems for underwater remote sensing purposes (ref. 8).

Although an underwater LIDAR involves the same basic design principles employed in the atmospheric LIDAR, there are a number of very important additional considerations. It is well known that because of the optical absorption properties of water (ref. 9), the available wavelength region for operation of an underwater LIDAR system is limited to the blue-green portion of the spectrum. Even within this relatively clear optical window the absorption is such that LIDAR operation would almost always be at ranges less than about 100 meters. This fact necessitates the use of very short transmitter pulses and rather wide-band electronic detection systems since the total time of useful LIDAR return will only be a few hundred nanoseconds. In addition, the very rapid decrease in signal intensity with depth requires a very wide dynamic range for both the optical and electronic components of the LIDAR receiver.

The water, because of the very large amount of scattering, also degrades the well collimated beam, spreading the illumination and decreasing the light flux per unit area very rapidly with increasing penetration depth (ref. 10). Thus, two of the best features of atmospheric LIDAR operation, i.e., high intensity compared to background (solar) light and good space and time resolution, are very severely restricted in the underwater application. In addition to the beam degradation caused by the volumetric scattering in natural water systems, the surface wave structure will further broaden the beam and decrease the obtainable signal (ref. 11). Thus there is a need for more experimental data to obtain information on the practical utilization of LIDAR systems for measuring underwater parameters of interest.

LIDAR DESIGN CONSIDERATIONS

In designing a LIDAR system, there are two basic configurations of interest. These are schematically illustrated in Figure 1. The first is the monostatic or backscatter LIDAR sketched in Figure 1a in which the transmitter and receiver are located at the same position and are collinearly directed along a single line of sight. The second is the so-called bistatic LIDAR , Figure 1b, in which the source and receiver are spatially separated. With the monostatic configuration, the transmitter must be pulsed to provide spatial information using the time of flight of the backscattered signal. With the bistatic configuration the transmitter can be either pulsed or continuous since the spatial location of the scattering volume is determined by the intersection of the transmitter and receiver beams as illustrated. In atmospheric work, the monostatic LIDAR is most commonly used because of its convenience and relative ease of alignment, although bistatic systems have been used on several occasions (ref. 12).

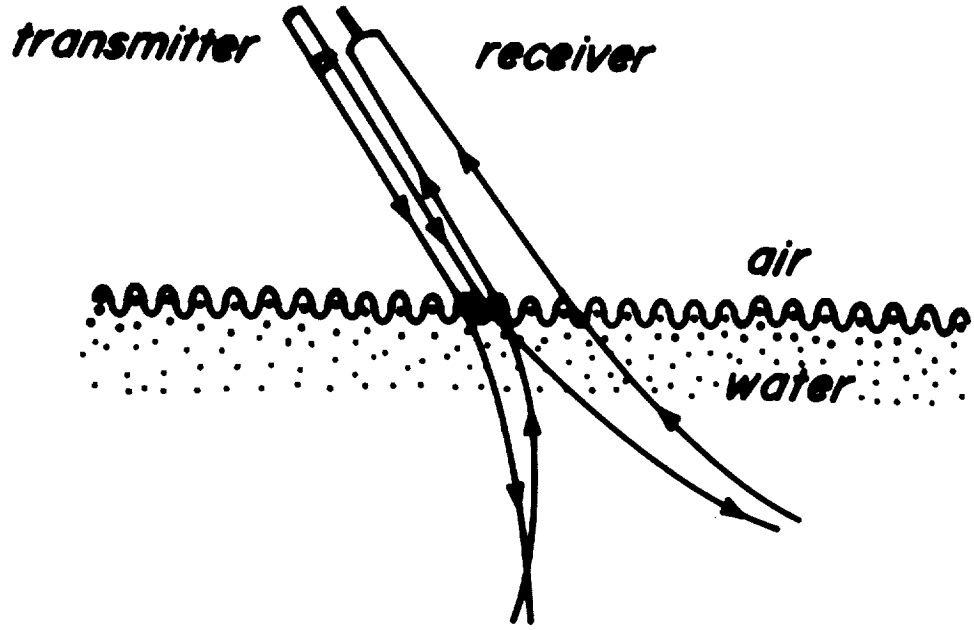

Figure 1a. Possible backscatter LIDAR configuration for underwater studies.

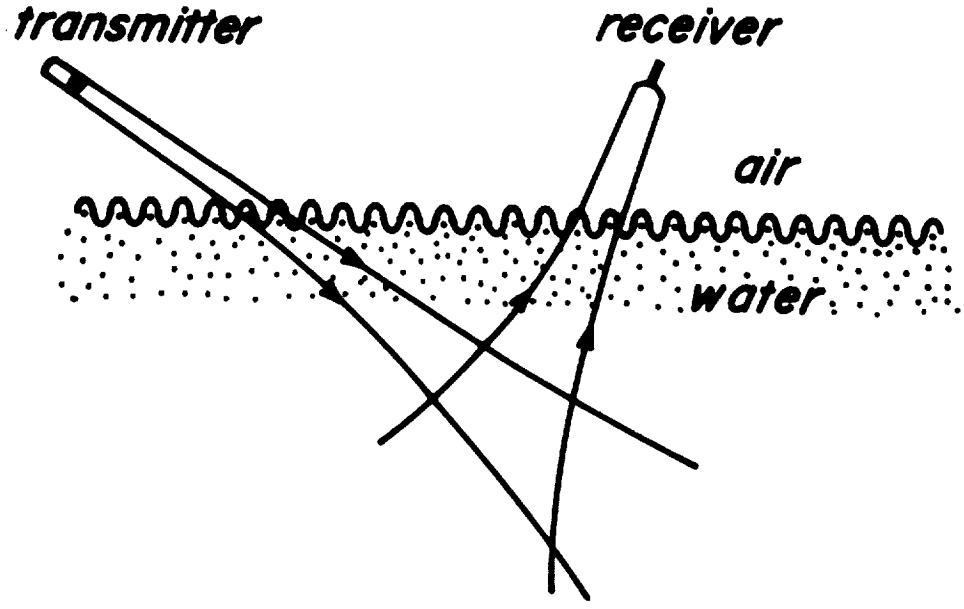

Figure 1b. Possible bistatic LIDAR configuration for underwater studies.

For underwater applications the substantial amount of beam spreading and the very large near field return may make the bistatic system a more attractive configuration than the backscatter system although for any airborne LIDAR instrument the bistatic configuration would be ruled out. For ship based systems, either configuration would be suitable and, in fact, the recent work of Ivanov et al (ref. 6) utilized a bistatic configuration in which the entire laser assembly was lowered to a depth of 5 meters below the sea surface. The backscatter arrangement of Figure 1a is still the most convenient and the most readily analyzed and is the one initially being employed in the present program. In this configuration the received power, P_r, can be expressed approximately as:

$$P_r = \frac{P_t\, C\, A\, T_1 e^{-\alpha_1 R}\, \beta\, e^{-\alpha_2 R}\, T_2}{\left(R^1 + \frac{R}{n}\right)^2} \qquad (1)$$

where P_t is the transmitted power, A the area of the receiver and C a constant including numerical factors and the optical efficiency of the system. R^1 is the distance (in air) from the transmitter to the water surface and R is the distance from the surface to the subsurface scattering location of interest. T_1 is the transmission coefficient of the water surface for the incident beam and α_1 is the average extinction coefficient of the downward traveling beam. For volumetric scattering is the volume backscattering coefficient averaged over a scattering volume of length $\frac{c\tau}{2n}$ in the direction of beam travel where c is the velocity of light, τ is the pulse length and n is the index of refraction of water. For scattering from a submerged surface (e.g. the lake bottom), β would represent the average surface reflectivity assuming that the surface fully intercepted the transmitted beam. α_2 and T_2 are the attenuation and transmission coefficients for the upward traveling beam.

The values for the downward and upward attenuation coefficients, α_1 and α_2, will in general be different because of the effects of beam spreading. The downward traveling beam will initially be rather well collimated and the value to be used is the so-called "monopath" attenuation coefficient (refs. 10, 13). However, as the beam spreads and diffuses, the forward scattering tends to replenish the beam and reduce the rate of attenuation. In this case the "multipath" attenuation coefficient is appropriate. In addition, it is also obvious that in any real situation the attenuations (up and down) would not ever be constant and in reality we would have to write the attenuation as:

$$\exp\left[-\int_0^R \alpha(r)\, dr\right] \qquad (2)$$

where the integrals are over the total two-way path distance and the point values of $\alpha(r)$ would include beam spread effects and any spatial variations of the water properties.

The transmission coefficients, T_1 and T_2, would include the ordinary reflective losses at the airwater interface and the loss of intensity because of surface roughness arising from wave structure. These surface effects would be values averaged over the diameter of the beam and would thus depend on the beam size and water roughness, and would in general differ for the downward and upward paths. As well as altering the values of the transmission coefficients, the surface roughness would also add to the broadening of the beam as it passes through this interface (ref. 11). For some applications, however, such as with shipborne equipment, it is possible to optically couple the transmitter and receiver to the water using emersion optics and in this way these surface complications can be greatly minimized.

From equation (1) it is apparent that the scattered laser signal contains information on the attenuation coefficient and the volume scattering coefficient of the water albeit in a rather complicated form. Thus, this signal should be utilizable to derive measurements of these quantities and their variation with distance along the propagation path as is done with atmospheric LIDAR systems.

It should also be pointed out that in the simple form of equation (1) we are considering only the intensity of the backscattered signal. The signal will also contain a considerable amount of polarization information which can also be used to measure the water properties (ref. 14). Such measurements of the polarization are already demonstrating their usefulness with atmospheric LIDAR measurements (refs. 15, 16).

It should also be noted that β includes both elastic and inelastic scattering processes. For Raman scattering the appropriate Raman scattering cross section would be employed and, by measuring at the appropriate wavelength shift from the incident radiation, this scattering can be used to identify selectively and monitor specific Raman active chemical species in the water in a fashion similar to that already demonstrated with atmospheric LIDARS (refs. 17, 18). The practical problem here, of course, is that the Raman signals are several orders of magnitude below those for the Mie and Rayleigh scattering.

When considering subsurface Raman measurements, it is also necessary to include in equation (1) the wavelength dependence of the water absorption since the transmitted and scattered beams will be at different wavelengths. Figure 2 is a sketch of the absorption coefficient as the function of wavelength in the optical "window" of several water samples. As already noted above, distilled water has minimum absorption in the blue-green, centered at about 500 nm. In natural waters, the overall absorption increases and the center of the window moves towards the yellow portion of the spectrum (ref. 9). Included in Figure 2 are solid lines representing the two strongest emissions of the Argon laser at 488 nm and 514.5 nm. The dotted lines represent the approximate central positions of the Raman shifted Stokes bands of the OH stretch (3450 cm^{-1}) in liquid water arising from these two laser frequencies. These Raman shifts are quite substantial and show that it is necessary to have the primary transmitted wavelength well towards the blue end of the window to ensure that the Raman lines are not too heavily attenuated.

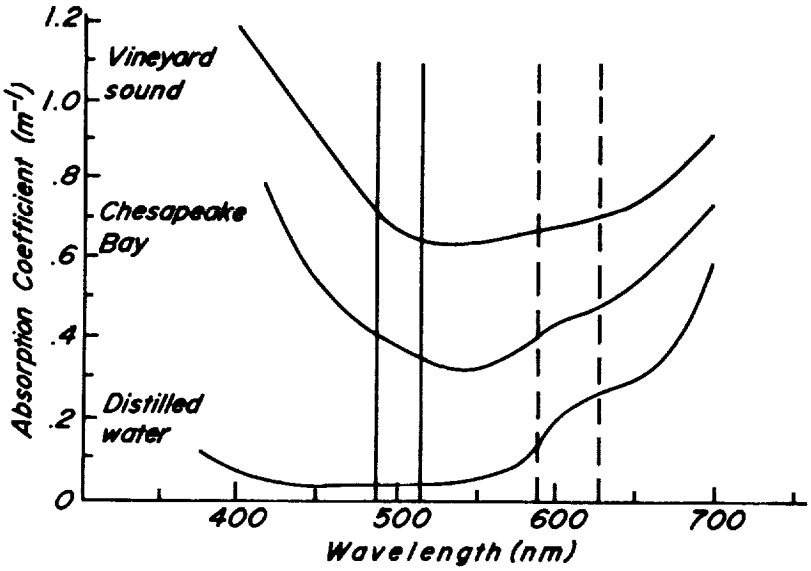

Figure 2. Absorption in the visible "window" for several water samples. The solid lines indicate the major Argon laser emissions at 488 nm and 514.5 nm. The dashed lines indicate the approximate positions of the band centres for the 3450 cm^{-1} H_2O Raman scattering obtained using the Argon lines.

There are, at present, relatively few commercially available lasers which will meet the necessary requirements for subsurface probing. The three best systems are the frequency doubled neodymium laser operating at 530 nm (refs. 6, 7), the neon laser at 540.1 nm (ref. 4), and the Argon ion laser which operates at a number of wavelengths between about 460 nm and 515 nm with its two most intense emissions at 488 nm and 514.5 nm as shown in Figure 2.

The typical operating parameters of these lasers are summarized in TABLE 1. The neodymium laser is flash lamp pumped and operated in the Q-switched mode. The neon laser is excited by electrically pulsing the low pressure gas inside a discharge tube, and the Argon laser is a continuous gas discharge with the laser output pulse being controlled by means of an intra-cavity acousto-optic diffraction cell (ref. 19) to operate in the so-called "cavity dumped" mode.

TABLE 1. Typical Operating Parameters of Lasers Suitable for Underwater LIDAR Systems

Laser	λ nm	τ n sec	PRF Hz	Peak Power Watts	Avg. Power Watts
Neodymium (doubled)	530	15	.1-100	10^6-10^7	0.05-0.2
Ne	540	5	100	10^4	.005
Aaron-Iron	460-515	0.2 10-1000	0-10^7	10^2	0.5

THE MARINE LIDAR SYSTEM

Our system design has been based on the use of the Argon laser operating in this cavity dumped mode. This unit, although it has lower peak powers than either the neodymium or neon lasers, has high average power and was chosen because of its greater all round versatility for underwater studies. The laser employed for the transmitter is a Spectra Physics Model 164 Argon laser with a Model 365 acousto-optic output coupler. This unit at 488 nm delivers peak powers of up to 75 watts, pulse repetition frequencies variable from cw to 10^7 Hz and pulse widths variable from about 10^{-8} to 10^{-6} seconds. Average power in the cavity dumped mode of up to 0.4 watts at these wavelengths is available. The unit will operate on seven other Argon lines in the blue-green spectral range at lower power outputs.

Figure 3 shows a schematic diagram of the overall system and Figure 4 shows a photograph of the apparatus as mounted on its mobile carriage. The laser transmitter is mounted horizontally and the output beam (approximately 1.5 mm diameter) is expanded to a diameter of about 2 cm by an adjustable collimator. The LIDAR can be operated in either a parallel-beam configuration (labelled (1) in Figure 3) or a coaxial-beam configuration (labelled (2) in Figure 3) for the transmitter-receiver geometry. The choice of the geometry is dictated by the specific requirements of the experiment. The parallel geometry provides a very strong suppression of the near field backscattering when the water surface is close to the LIDAR unit. This is achieved by adjusting the alignment so that the receiver does not see the laser beam impingement spot on the surface nor the first few meters of subsurface scattering.

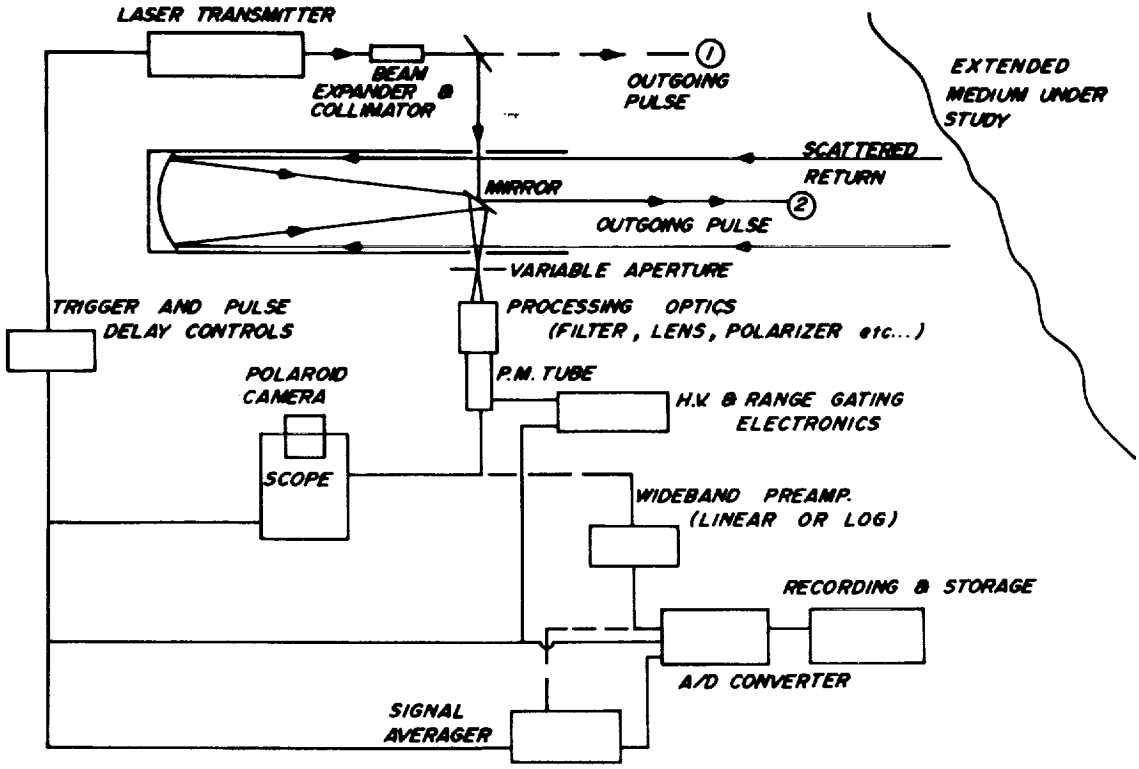

Figure 3. LIDAR system arrangement. (1) and (2) indicate alternative arrangements for the transmitter beam geometry.

The receiver is a 20 cm diameter Newtonian telescope with variable field stop and processing optics which include a 1.0 nm bandpass filter and a quarter wave plate and linear polarizer for analysis of the scattered signal. A very high-speed 5 stage photomultiplier (RCA type C31024) is used as the detector. The output is fed through a preamplifier to either a 250 MHz oscilloscope or to a "boxcar" signal averager. Triggering signals and pulse delays are provided by the associated electronics with the primary synchronization being from the output laser pulse itself which is detected by a fast silicon photodiode mounted in the transmitter section.

The major limitation in the present system is in the frequency response of the boxcar averager which cannot clearly resolve pulses which are shorter than about 30 nsec. This limits the range resolution of the present system to about 4 or 5 meters in water. A new signal averager to be installed shortly will have subnanosecond time resolution and will provide LIDAR operation limited only by the resolution of the optical pulse (1 to 2 meters).

As shown in Figure 4, the LIDAR is mounted on a mobile carriage complete with its electronics and beam steering optics. Seen in this photograph (left foreground) are the 45-degree mounted mirrors for downward direction of the transmitter and receiver beams. These are mounted on an extendable mount which protrudes over the side of the tank (for lab use) or the vessel (for shipborne measurements). The vertical bars shown in this assembly are to support a subsurface mirror-periscope assembly to permit horizontal propagation of the LIDAR beam at depths ranging from zero to about 2 meters when working in the tanks of the Canada Centre for Inland Waters (CCIW) at Burlington where the depth is only about 3 meters.

Figure 4. Mobile LIDAR system.

MEASUREMENTS

Some initial measurements with this LIDAR system have been conducted at the large indoor CCIW tanks. In addition, in August 1973 the system was taken aboard the CCIW research vessel Limnos and measurements were made over a four-day period in Lake Erie at a position about 10 miles south of Port Stanley, Ontario.

In the indoor tank trails, the main aim was to investigate LIDAR signals from the volumetric backscattering of relatively stable and homogeneous water samples and from diffusely scattering surfaces positioned at known underwater distances to ascertain the useful operating range of the LIDAR system. The targets used were 1.22 meters (4 ft.) square plywood sheets painted either black or white.

Figure 5 shows a schematic trace of a typical signal return from a submerged target. As shown in this figure, the return contains an initial broad peak from the volumetric scattering of water itself followed by a narrow pulse from the target. The volumetric return initially increases with range as the receiver field of view encompasses the transmitted beam. After full overlap of the beams at point P, the volumetric signal falls off according to equation (1). The target return will have a range dependent amplitude, h, as also calculated from equation(1) using the reflectivity of the surface in place of the volume backscattering coefficient. The width, w, of the target return is dependent upon the time resolution of the system and is a direct indication of the spatial resolution capability of the system.

If one assumes in equation (1) that $\alpha_1 = \alpha_2 =$ a constant, then a plot of

$$\ln[\,(R^1+R/n)^2\, P_r] \text{ vs } R \qquad (3)$$

should produce a straight line whose slope is twice the attenuation coefficient. This plot can be obtained in two ways: once from the volumetric scattering itself and again from the target pulse amplitude, h, as a function of depth.

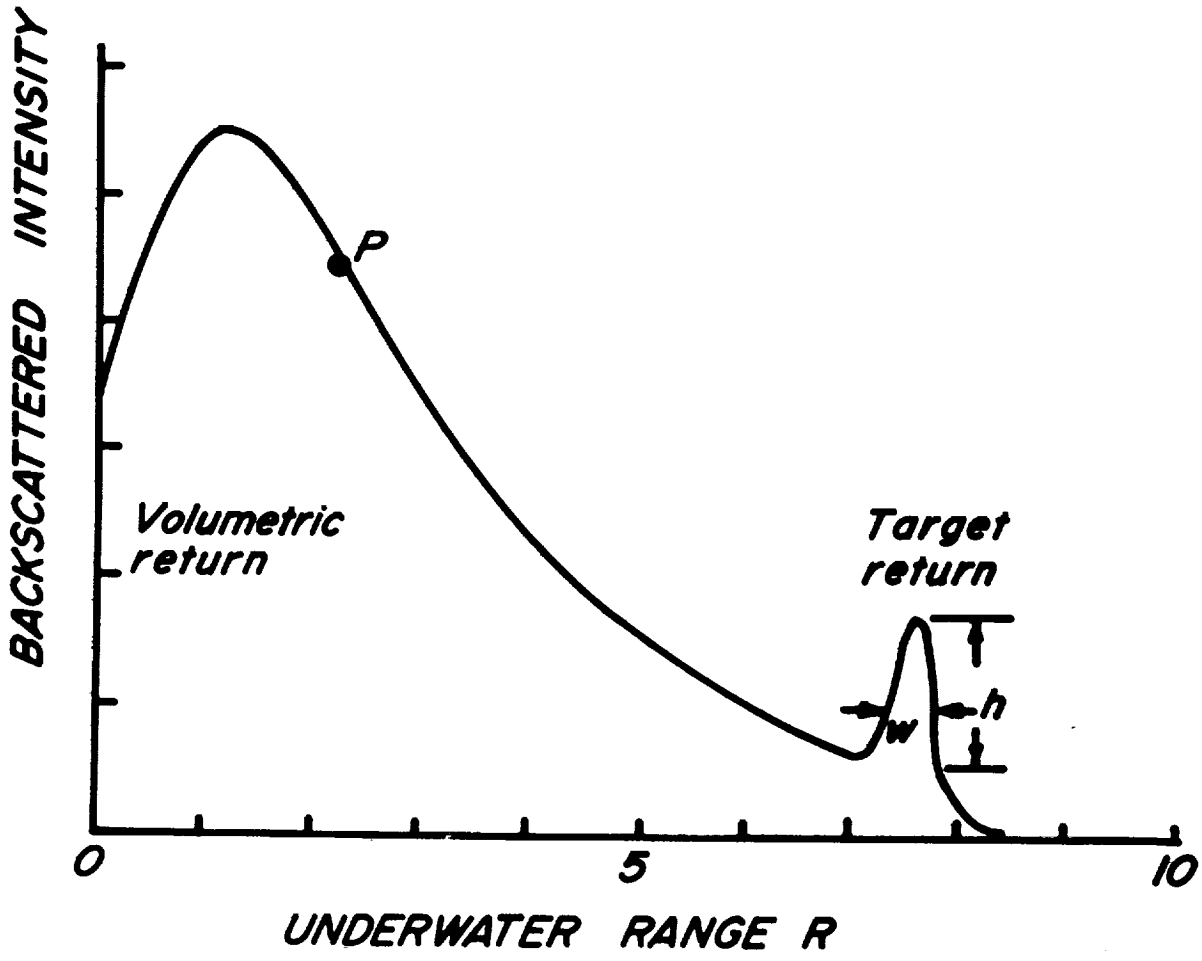

Figure 5. Schematic diagram of a typical LIDAR return from a submerged surface. P is the point at which the receiver beam fully overlaps the transmitter beam. W and h are the measured width and height of the target return.

Figure 6 shows sample results obtained with the LIDAR operating at 514 nm for ranges up to about 17 meters with the white target. The curves shown are a superposition of the scattered signals obtained from the water itself with no target (lowest trace), and from the target when located at several different ranges. These traces are averaged outputs over approximately a one-second averaging time when using a pulse rate of 10^5 Hz. In all cases, the initial pulse of the volumetric scattering is seen to be identical. (The top two traces have gain reductions of 10 and 20 to keep the target return on scale and in these the volumetric return thus appears greatly reduced.)

The target return is seen to drop off very rapidly with increasing range, with the maximum detectable range being about 20 meters. It is apparent from the figure that the width of the target return pulses corresponds to a range of about 4 meters, and, as already mentioned, this width is at present limited by the resolving time of the boxcar averager. Since the target return is, in fact, considerably narrower than this, this electronic limitation is reducing the measured penetration range considerably; i.e., narrow, small signals at greater ranges would not be detectable. Although the width of the target returns corresponds to about 4 meters, it is possible to locate the position of the target to a better accuracy as can be seen from the shapes of the target return peaks.

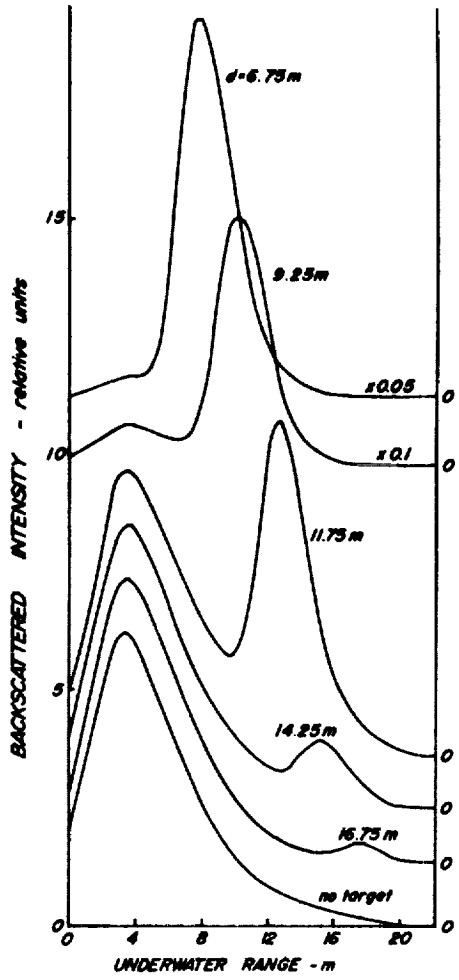

Figure 6. Sample backscattered signal plots as a function of range for white targets at different underwater distances. Note that the top two traces have ordinate scales compressed by the factors shown.

The data shown in Figure 6 were obtained for the receiver without any polarization optics. If a polarizer is inserted in the receiver and aligned either parallel or perpendicular to the polarization direction of the linearly polarized transmitter signal, a considerable variation in the volumetric scattering intensity is observed. Figure 7 shows sample results with a target located at a range of about 7 meters. The perpendicular to parallel ratio (I_2/I_1) for the volumetric scattering is found to be about 0.2 indicating that this scattering strongly retains the polarization of the incident beam. The corresponding ratio (I_4/I_3) for the target, however, is about 0.9 indicating an almost complete depolarization of the signal scattered by the target surface. Such measurements are qualitatively in agreement with polarization studies made by transmission measurements underwater.

The possibility of employing polarization to suppress the volumetric return as already utilized for some underwater photographic application is apparent from such results. The polarization measurements also appear to indicate an increase of depolarization with penetration depth, an effect consistent with the multiple scattering process and recently observed in atmospheric cloud studies (ref. 16). However, the exact magnitude of this increase cannot be obtained until the higher resolution electronic system is available.

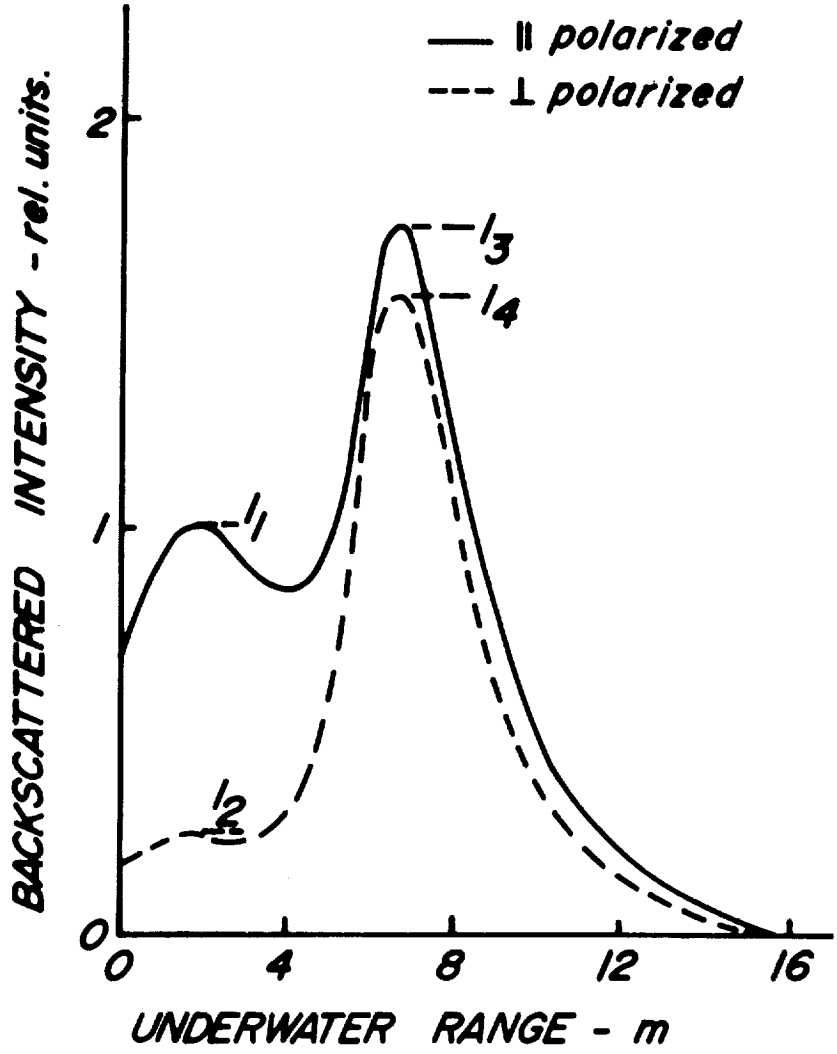

Figure 7. Returns from a target at seven meters as observed with receiver containing a linear polarizing element.

Taking the data shown in Figure 6 and range correcting it as described above, it is possible to evaluate the attenuation coefficient. This has been done in Figure 8 for both the target echoes and the volumetric scattering. For the targets, it is seen that a fairly good straight line is obtained and from this a value of $\alpha = 0.25\ m^{-1}$ is derived. Simultaneous transmissometer measurements over a one meter path length using a wavelength of 490 nm gave values in reasonable agreement with the LIDAR measurement. The volumetric returns in Figure 8 show a nonlinear plot which appears to approach the slope of the target returns with increasing penetration depth. It is believed that this effect is caused by the relatively poor spatial resolution of the system which would tend to reduce the intensity of the near field returns of the volumetric scattering. This feature will be examined more closely with the improved detection system.

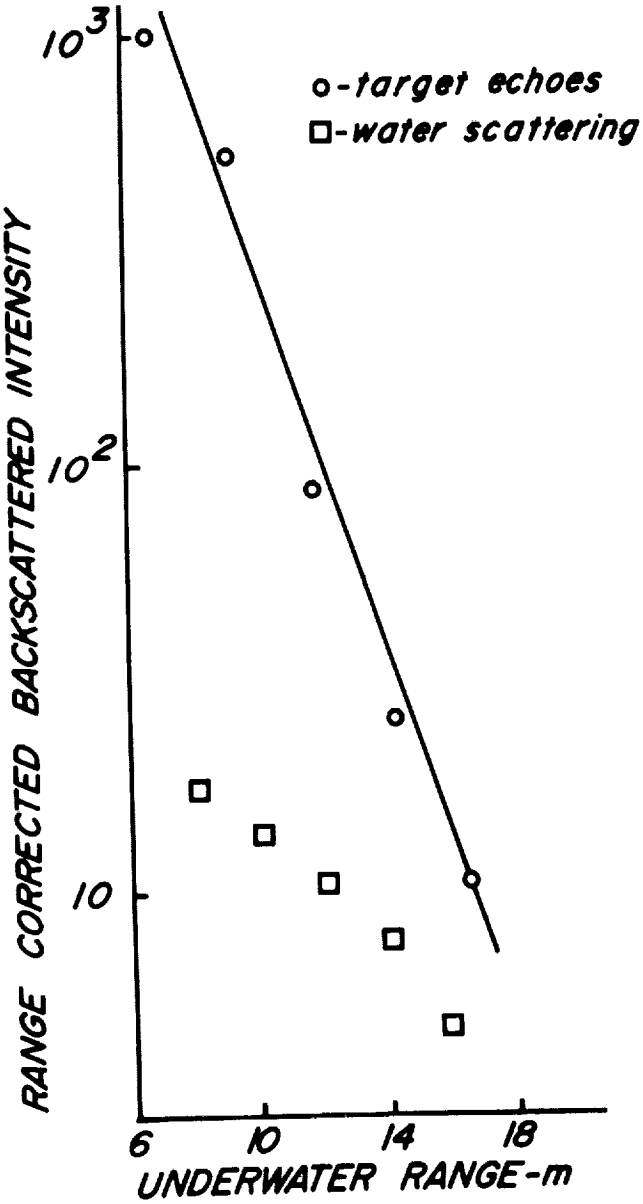

Figure 8. Semilog. plot of the range corrected intensity of returns from both the targets and the volumetric water scattering.

The trials on Lake Erie were conducted to test the system under real field conditions. Measurements were made at 488 and 514 nm and for both receiver polarizations; i.e., parallel and perpendicular to the transmitted polarization. Targets of the same geometry were lowered from the ship and returns were recorded for various depths. As yet, the data have not been fully analyzed but in general the results reflect those found in the tank measurements. Maximum penetration depths obtained in Lake Erie were only about 10 meters. This was caused by the greater turbidity of the lake water (the value of α was generally measured by transmissometer to lie between about 0.5 and 1.0 m^{-1}) and by the signal degradation caused by surface wave structure.

During the trials the lake surface was quite choppy with swells reaching several feet. This introduced additional variability into the signal and degraded the signal-to-noise ratio as anticipated. However, the degradation was not as large as originally feared even considering the rather small beam sizes used in this experiment which would aggravate the beam distortion problem. The LIDAR was directed into the water at an angle of 15 or 20 degrees from the vertical to ensure that the specular surface returns did not enter the receiver. If this was not done, the noise in the return was unacceptably high.

The system performed well for both day and night operation in spite of the rigors of the trip. A large number of profiles similar to those of Figures 6 and 7 were obtained at both wavelengths. Again the data was limited by the bandwidth of the receiving electronics. It had been hoped when planning the trip, that the LIDAR would be able to observe the thermocline in the lake where a substantial discontinuity in the turbidity occurs. However, during the measurement period, the thermocline was at depths of the order of 15 to 16 meters which were beyond the present detection capabilities of the LIDAR.

One other preliminary series of tests has been undertaken with this system as well. In the laboratory, a simple monocromator has been used on the receiver and the Raman backscattered signals from several water samples have been observed. It has been found that, using the 488 nm wavelength, rather good signals from the 3450 cm^{-1} H_2O band are observable at ranges of several meters in these initial tests. One difficulty already encountered, however, is the stray light arising at the Raman frequency from fluorescence in the water. This fluorescence signal is virtually negligible in distilled water but is observable in tap water and is very large in some natural water samples such that the Raman return is markedly obscured. This work is continuing and an effort will be made to ascertain the potential of subsurface diagnostics of natural waters by Raman LIDAR scattering.

CONCLUSION

Although our experience with the marine LIDAR unit is still rather limited, the system has already demonstrated a useful potential. The present system is capable of providing measurable signal returns at depths up to 25 or 30 meters depending on the attenuation. The most direct application of this capability would be for depth sounding and bottom profiling, and accuracies to within a fraction of a meter should be obtainable.

Some spatial "structure" on the volumetric return has already been detected in the Lake Erie data and such variations should provide information on the scattering and attenuation as a function of depth. Also, since the magnitude of the volumetric scattering depends on the optical quality of the water, the relative intensity of this signal may serve as a useful indication of water quality which could be obtained remotely and rapidly.

The polarization of the backscattered signal is also of considerable importance. There is already evidence that the depolarization arises from multiple scattering processes and depends strongly on the turbidity of the water (ref. 14). Since polarization is a readily measurable quantity, it should prove to be another very useful monitor of water conditions. So far, only two components (parallel and perpendicular) of the polarization have been monitored. The complete polarization information of the signal is contained in the four components of the Stokes vector and measurements of these should be even more informative. Such measurements are already being made with our atmospheric LIDAR and should present no difficulty for the marine system.

Finally, the potential usefulness of the Raman return is obvious. The signal is not large but it is definitely quite measurable, particularly near the water surface. This signal, as already indicated by other workers (refs. 17, 18, 20, 21), could be potentially useful for a variety of measurements including pollutant identification and temperature measurement. Such measurements will not be easy in view of the many problems associated with the weak Raman signals and the perturbing effects of fluorescence and the stray background light. It may be that they will only become viable by using tuned lasers to obtain the enhancement of resonant scattering. However, at this stage pertinent experimental field data is still lacking and the need for further measurements of this type is clear.

REFERENCES

1. Collis, R. T. H, Appl. Optics 9, 1782-1788 (1970).

2. Derr, V. W.; Little, C. G., Appl. Optics 9, 1976-1992, (1970).

3. Kildal, H.; Byer, R. L., Proc. IEEE 59, 1644-1663 (1971)

4. Hickman, G. D.p Hogg, J. E., Remote Sensing of the Envir. 1, 47-58 (1969).

5. Ivanov, A. P.; Kalinin, I. I.; Kozlov, V. D.; Skrelin, A. L.; Sherbaf, I. D., Izv. Atmos. & Ocean Phys.5, 212-215 (1969).

6. Ivanov, A. P.; Kalinin, I. I.; Skrelin, A. L.; Sherbaf, I. D., Izv. Atmos. & Ocean Phys. 8, 884-890 (1972).

7. Levis, C. A.; Swarner, W. G.; Prettyman, C.; Reinhardt, G. W., Proc. NASA Wallops Conf. on Hydrographic LIDAR, Sept. 1973.

8. Sizgoric, S.; Carswell, A. I., Cdn. Aeronautics & Space Jour. (to be published Dec. 1973).

9. Fujisawa, A.; Nakao, S., Electronics & Comm. in Japan, 54-B, 77-83 (1971).

10. Duntley, S. Q., J. Opt. Soc. Amer. 53, 214-233 (1963).

11. Prettyman, C. E.; Cermak, M. D., IEEE Trans. GE-7, 235-243 (1969).

12. Ward, G.; Cushing, K. M.; McPeters, R. D.; Green, A. E. S., Appl. Optics 12, 2585 (1973).

13. Tyler, J. E.; Smith, R. C.; Wilson, W. H., J. Opt. Soc. Amer. 62, 83-91 (1972).

14. Granatstein, V. L.; Rhinewine, M.; Levine, A. M., Appl. Optics 11, 1870-1 (1972).

15. Carswell, A. I.; Houston, J. D.; McNeil, W. R.; Pal, S. R.; Sizgoric, S., Cdn. Aero. & Space J. 18, 335 (1972).

16. Pal, S. R.; Carswell, A. I., Appl. Optics 12, 1530-35 (1973).

17. Melfi, S. H., Appl. Phys. Lett. 22, 402-3 (1973).

18. Inaba, H.; Kobayasi, T., Nature, 224, 170-173 (1969).

19. Maydan, D., J. Appl. Phys. 41, 1552-1559 (1970).

20. Bradley, E. B.; Frenzel, C. A., Water Research 4, 125-128 (1970).

21. Schwiesow, R. L., Proc. Conf. on Sensing of Environmental Pollutants AIAA Paper No. 71-1086 (Nov. 1971).

The authors wish to acknowledge the assistance of Dr. W. R. McNeil and the financial support of the Canada Centre for Inland Waters and the Canada Centre for Remote Sensing.

REMOTE MEASUREMENT OF OCEAN TEMPERATURE FROM DEPOLARIZATION IN RAMAN SCATTERING

Chin H. Chang and Lee A. Young
Avco Everett Research Laboratory, Inc.

ABSTRACT

Ocean temperatures may be mapped in three dimensions from an aircraft down to depths of 2 to 4 attenuation lengths by monitoring Raman radiation backscattered from a laser beam. This paper describes laboratory experiments on the temperature dependence of Raman spectra of saline solutions and calculations of the expected performance of a field system.

The Raman spectrum of liquid water shifts toward the red with increasing temperature. Consequently temperature could be measured by a radiometer having two spectral channels which cover two halves of the Raman band. Such a two-color scheme is impractical for ocean sensing, however, because of variability of the relative transmission of seawater at the two wavelengths. Instead, we propose to polarize the laser emission and use a radiometer with two channels which sense two different modes of polarization of the Raman radiation. Laboratory experiments show that the ratio of the two signals changes by about one per cent for each degree centigrade of temperature change. Circular polarization appears preferable to linear polarization because the former affords higher statistical accuracy in the cross-polarized channel.

The Raman technique is of greatest potential utility in coastal and estuarine waters where gradients are relatively high. We estimate that seawater temperature may be measured to a statistical precision of 0.5°C at depths to four attenuation lengths in two-meter water, using one joule of transmitted laser energy.

INTRODUCTION

Remote sensing methods from aircraft allow the possibility of obtaining a synoptic view of the oceanographic properties of estuarine or coastal waters during a given phase of a tidal or meteorological cycle which would be impossible with conventional boat-based measurement methods. In this paper we describe the possibility of using an airborne laser and a two-channel radiometer to measure the temperature and transparency of seawater by monitoring backscattered Raman radiation. Laboratory results will be presented along with calculations of expected field performance.

The Raman spectrum of liquid water is shown schematically in Figure 1. The Raman radiation appears at a longer wavelength than the exciting laser radiation; the energy difference corresponds to one quantum of the stretching modes of vibration of H_2O. If a laser beam is directed downwind into seawater as in Figure 2, the backscattered Raman radiation from a given depth may be detected by a gated receiver.

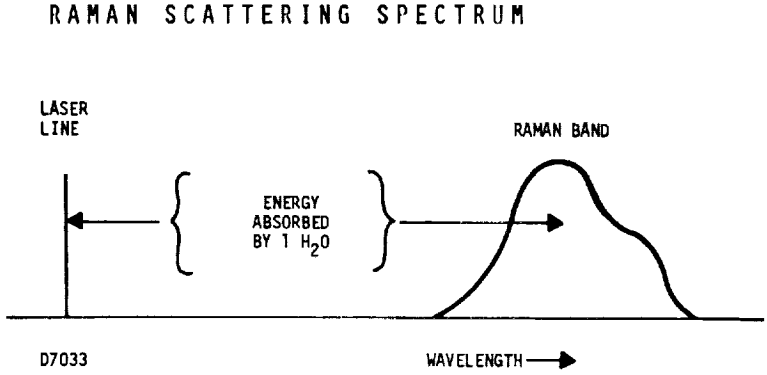

Figure 1. Raman spectrum of water-schematic

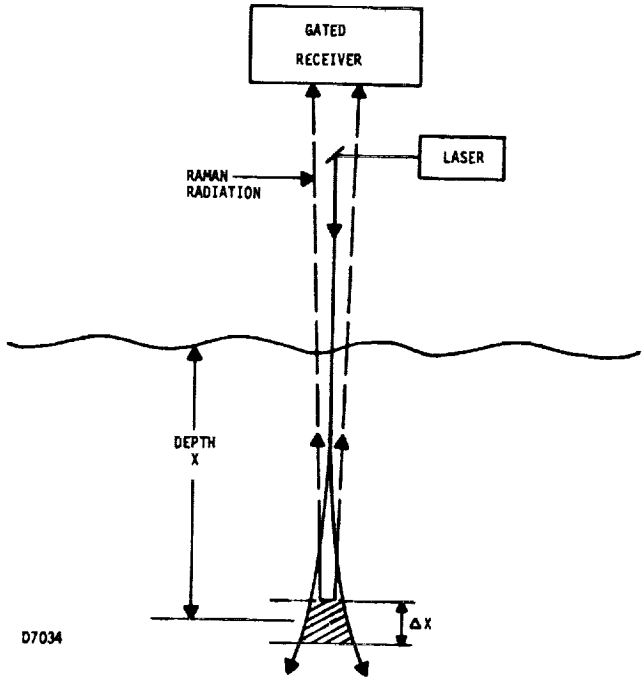

Figure 2. Remote sensing of the ocean using a laser

TWO-COLOR VS CROSS-POLARIZED MEASUREMENTS

Changes in temperature of liquid water affect its structure, which, in turn, modifies its Raman spectrum. The total spectrum is shifted towards longer wavelengths with increasing temperature. Also, if the exciting light is polarized, the two polarization components of the Raman radiation are affected differently by changes in temperature.

The temperature of water could be measured by a two-color radiometer if the spectral transmission of the medium is precisely controlled. The ratio of Raman intensities at two wavelengths, λ_1 and λ_2, is (apart from geometrical factors)

$$R = \frac{I(\lambda_1)}{I(\lambda_2)} = f(T, S)\, e^{-[K(\lambda_1) - K(\lambda_2)]\, x}$$

where $f(T,S)$ is a function of the temperature and salinity of the water at depth x, and $K(\lambda)$ is the spectral transmission of the water. To minimize the effect of differential attenuation in the water, we choose λ_1 and λ_2 such that $K(\lambda_1) \approx K(\lambda_2)$, so the exponential may be expanded as

$$R = f(T,S)\ \{1 - [K(\lambda_1) - K(\lambda_2)]\, x + \ldots\}$$

The sensitivity of the ratio R to temperature (ref. 1) is about one percent per degree centigrade, i.e., $\Delta R/R = \Delta T/100$. The temperature error due to mistuning (i.e., to the inequality of $K(\lambda_1)$ and $K(\lambda_2)$) is then

$$\Delta T = 100\ \Delta R/R$$

$$= 100[K(\lambda_1) - K(\lambda_2)]\, x.$$

If we wish to measure temperature to an accuracy of 0.3°C at a depth of 3 meters, for example, then $K(\lambda_1)$ and $K(\lambda_2)$ must be equal within 10^{-3} m^{-1}. But $K(\lambda)$ has typical values in the coastal water of the order 0.1 - 0.3 m^{-1}, and shows considerable spatial and temporal variation. Thus, the two-color Raman technique would be impractical in natural seawater. To overcome spectral transmission variations, we employ a radiometer in which both channels monitor the same wavelength interval but different modes of polarization of the Raman radiation. Laboratory tests show that the relative transmission of these two modes is about equal (ref. 2).

CIRCULARLY POLARIZED RAMAN SPECTRA

The temperature of liquid water may be measured via the depolarization ratio ($I_\perp/I_\parallel$) for either linearly or circularly polarized exciting light. In the linear case the depolarization ratio is small (~.1-.2). This means that the Raman component whose polarization is perpendicular to that of the laser beam is of weak intensity (ref. 2) and the statistical accuracy of its measurement would be low. The depolarization ratio is larger (~.2-.6) for circularly polarized excitation, so that the weaker component may be measured with greater precision. Also, the depolarization ratio is more temperature-sensitive for circularly than linearly polarized light (ref. 2).

Figures 3 and 4 show the left- and right-handed components of the Raman spectrum backscattered from liquid water. Figure 5 shows a schematic diagram of the laboratory apparatus. The excitation source is a right-handed circularly polarized laser beam at a wavelength of 4600 Å. The stronger (left-handed) component of the spectrum is not depolarized;

like the laser beam, it represents clock-wise rotation as viewed from the source. The depolarization ratio, $\rho = I_L/I_R$, is shown in Figure 6. It can be seen that the depolarization ratio decreases with temperature over the spectral interval from 5400 to 5500 Å. In a field system, this range would be selected by an interference filter. The effective depolarization ratio over this interval $\rho_{eff} = \int I_L(\lambda)d\lambda / \int I_R(\lambda)d\lambda$, is plotted against temperature in Figure 7. It can be seen that the temperature sensitivity of the depolarization ratio is about one percent per degree centigrade. To measure temperature to a precision of one degree centigrade or better using a Raman system, one must achieve the necessary photoelectron statistical accuracy and maintain the relative stability and calibration of the two radiometer channels.

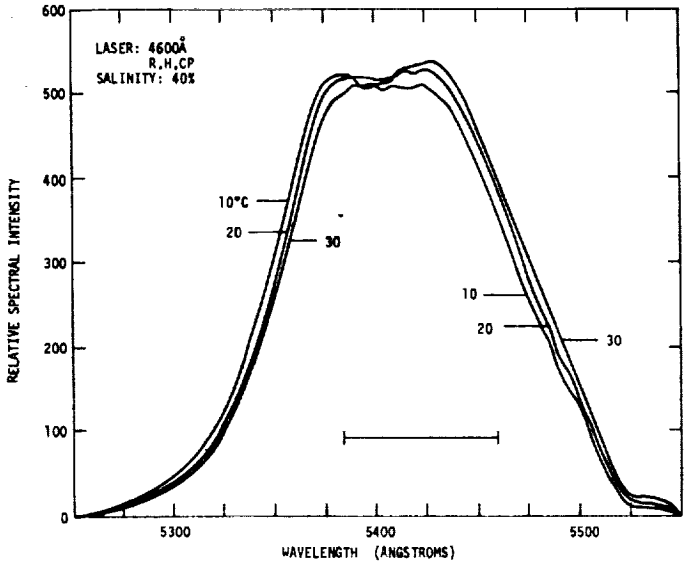

Figure 3. Raman spectrum of 40°/oo aqueous solution of NaCl lefthand circularly polarized component

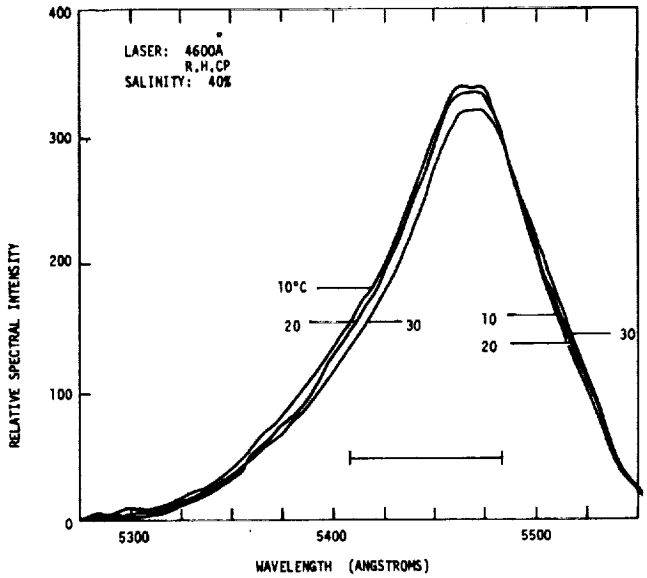

Figure 4. Raman spectrum of 40°/oo aqueous solution of NaCl righthand circularly polarized component

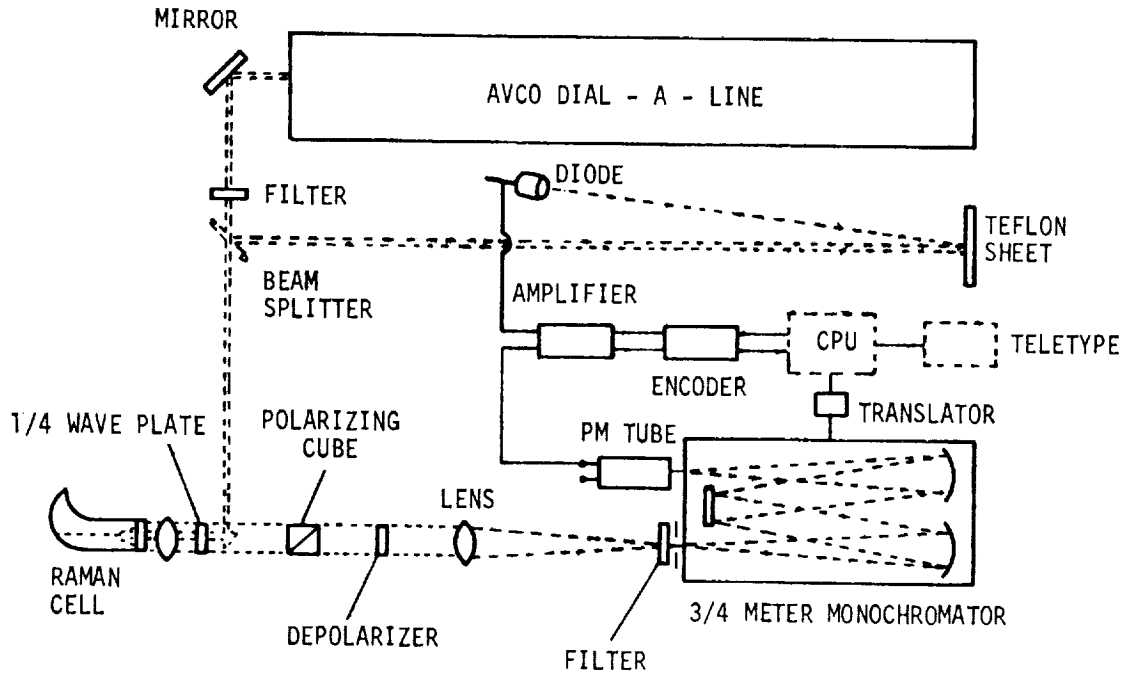

D4652

Figure 5. Laboratory apparatus for measurement of Raman spectra

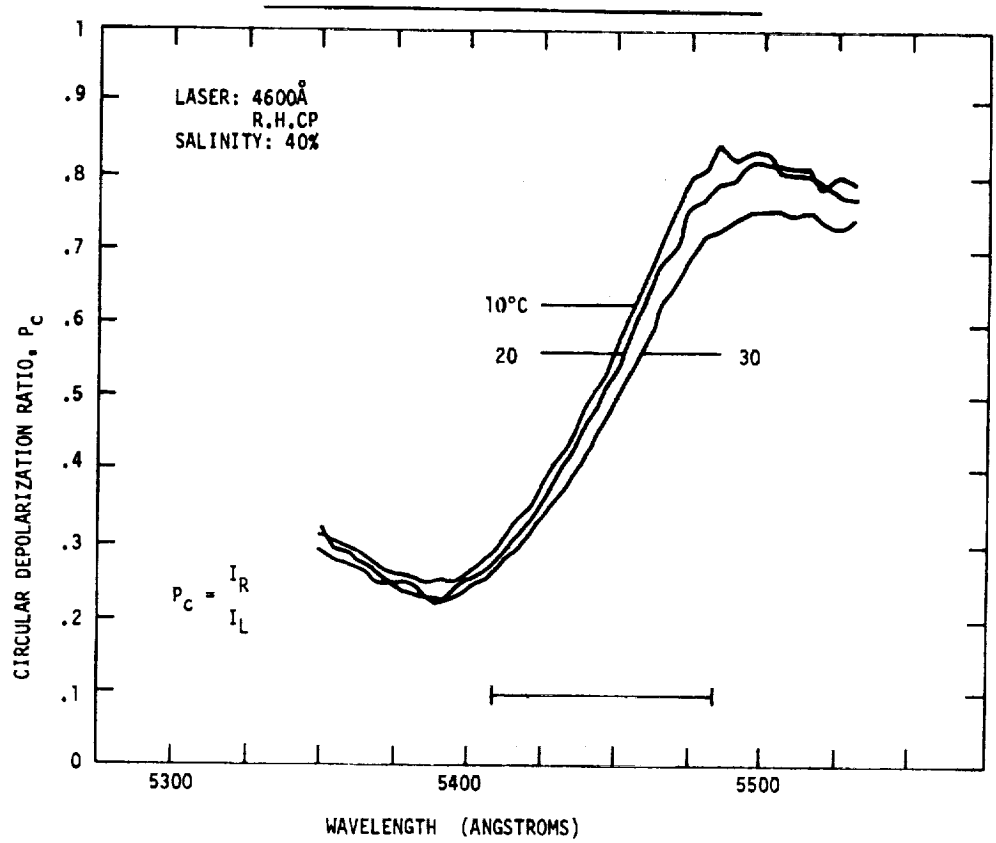

Figure 6. Circular depolarization ratio of 40°/oo aqueous solution of NaCl vs. wavelength

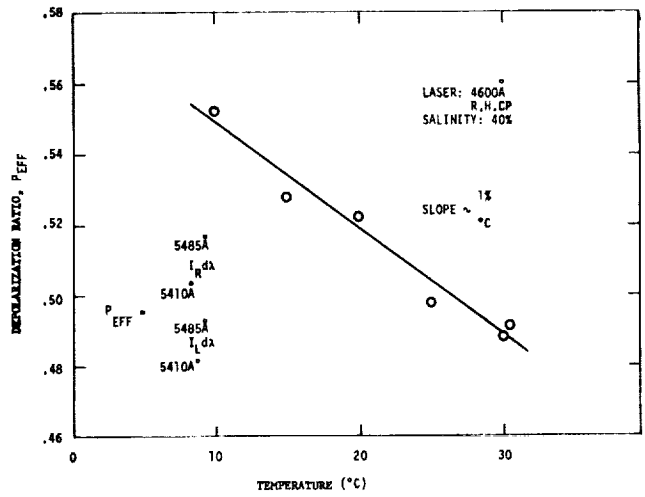

Figure 7. Circular depolarization ratio of 40°/oo aqueous solution of NaCl vs. temperature

RAMAN MEASUREMENT SYSTEM

Figure 8 shows schematically the design of a system for measuring two components of Raman radiation backscattered from the ocean. The laser output passes through an interference filter to block stray radiation at UV and Raman wavelengths, and is then right-hand circularly polarized by a linear polarizer and quarter-wave plate. The left- and right-handed backscattered Raman returns are converted by another quarter-wave plate to two linearly polarized components which are separated by a polarizing beamsplitting cube. A second interference filter blocks stray scattered light of the laser wavelength. Gated integrators are used to select the portion of the outputs of the photomultiplier tubes corresponding to a given depth interval.

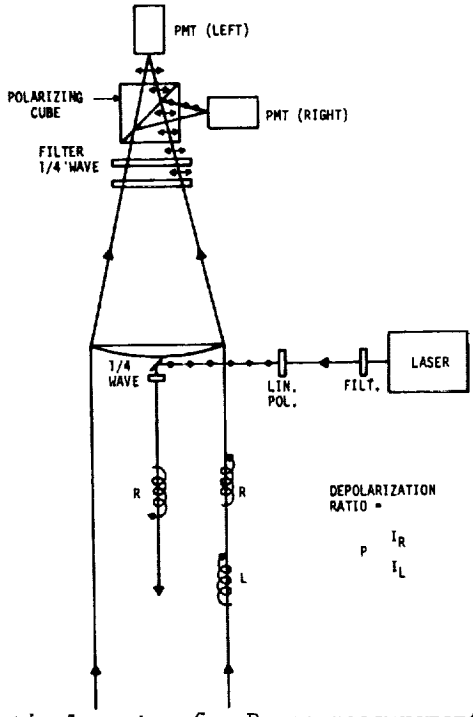

Figure 8. Optical system for Raman measurements in the field

Typical parameters of the Raman system are listed in TABLE 1. The average and peak power values listed represent reasonable design objectives for flashlamp-pumped dye lasers. The 10-nsec pulse duration, needed to permit range gating with a depth resolution of one meter, would be achieved using an output coupling device. The field of view of the receiver is chosen fairly small to reduce the amount of ambient daylight detected.

Table I. Raman System Parameters - Coastal Use

Laser	
Type:	Flashlamp pumped dye with output coupler.
Pulse length:	10 ns
Wavelength:	4600 Å
Average power:	~ 10 watts
Peak power:	~ 10^6 watts
Receiver	
Aperture diameter:	0.3 m
Field of view:	± 10 mrad
Altitude	
	100 m

TABLE 1.-RAMAN SYSTEM PARAMETERS - COASTAL USE

FIELD PERFORMANCE OF RAMAN SYSTEM

For temperature precision of one degree centigrade, we require Raman ratio measurement statistical precision of one percent and thus 10^4 photoelectrons in the weaker (depolarized) Raman component. The yield depends upon the total laser energy utilized in a given measurement. In Figure 9 we show the photoelectron return in the weaker component for the Raman system described in TABLE 1 at an altitude of 100 meters. The attenuation length of the seawater has been chosen as two meters, which is typical of coastal waters in which the Raman technique appears to have the greatest utility. A one-watt laser could give a statistical temperature precision of 0.5°C at a depth of eight meters (four attenuation lengths) in one second.

It is desirable to be able to make Raman measurements during daylight hours for convenience of aircraft operation and correlation with other remote sensing and sea truth observations. Daylight radiance is compared with the peak Raman signal received in Figure 10. The significant parameter here is the peak laser power transmitted. With 10^6 watts peak power, a signal/background ratio of unity could be achieved at a depth of about 5 meters. Precise measurements can still be made with signal/background = 1 provided that (1) the statistical fluctuations of the signal and background are averaged for a period three times longer than that required without background, and (2) the ambient background intensity does not vary significantly from pulse to laser pulse. Evidently a higher peak laser power - say, 3×10^6 watts - would be highly desirable for daylight use, together with an average power of the order of 1 watt.

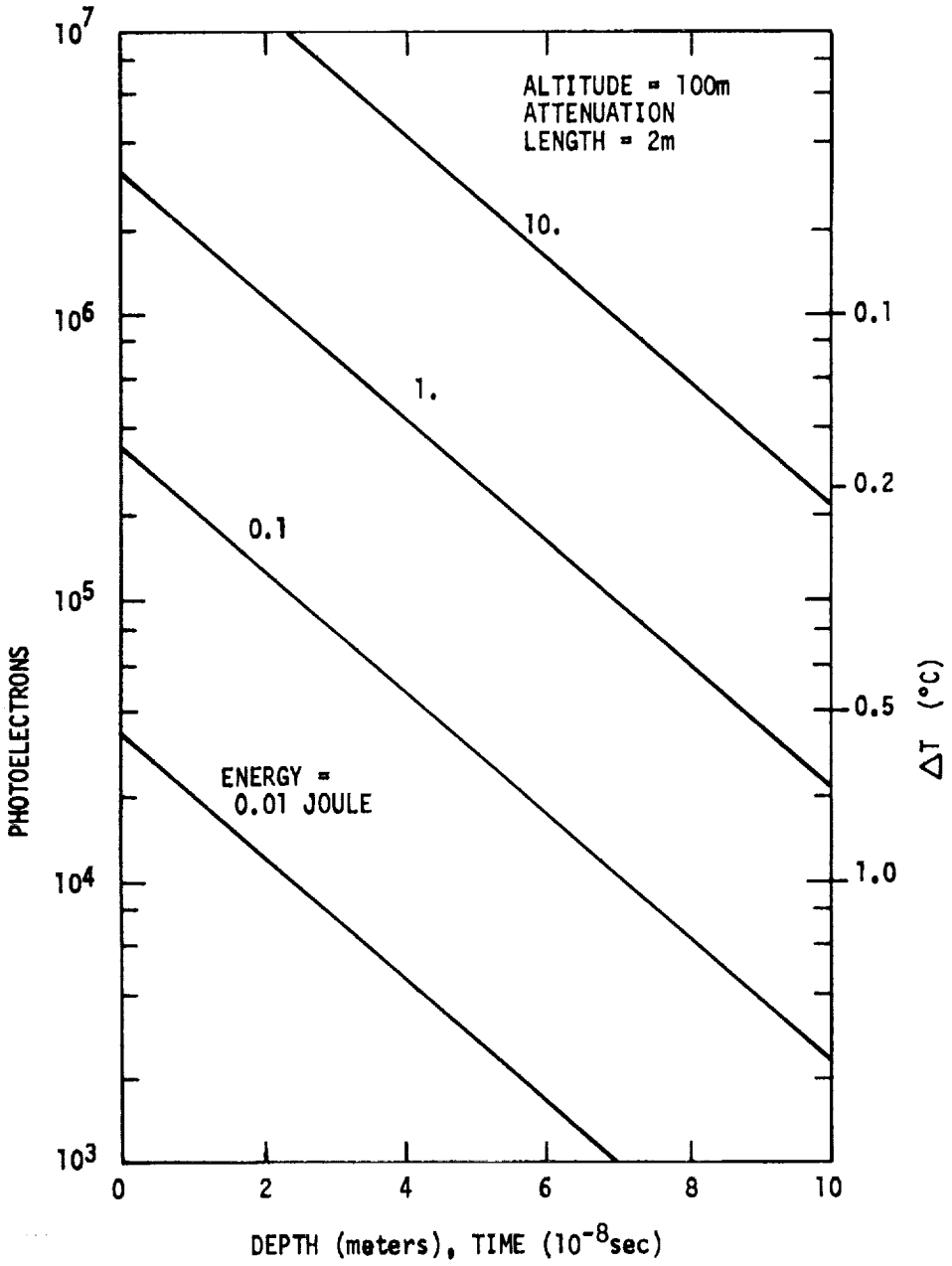

Figure 9. Total Raman return vs. depth as a function of laser energy

REFERENCES

1. Chang, C. H. and Young, L. A., "Seawater Temperature Measurement from Raman Spectra", AERL Research Note 920 (July 1972).

2. Chang, C. H. and Young, L. A., Final Technical Report, Contract N62269-73-C-0073 (to be published.)

MEASUREMENT OF RAMAN SPECTRA OF H_2O AND $SO_4^=$ IN SEAWATER

William M. Houghton
NASA-Langley Research Center

ABSTRACT

A study of applying laser Raman spectroscopy to remote sensing of the sulfate ion ($SO_4^=$) in seawater is in the progress at NASA-Langley. The $SO_4^=$ Raman spectrum has been obtained from true seawater samples in the laboratory using a CW laser Raman Spectrometric System. Radiometric calculations indicate the feasibility of obtaining usable $SO_4^=$ Raman signals in a field experiment. One of serious difficulties expected in the field experiment would be from fluorescence of phytoplankton and organics.

This paper describes an on-going research program at the Langley Research Center (LRC) which has as its ultimate goal the remote sensing of salinity. It is a cooperative effort between LRC and Old Dominion University (ODU). Dr. Allen Bandy of ODU has been, through a NASA Grant, conducting a laboratory investigation of the Raman spectroscopy of seawater.

Certain polyatomic ions, such as $SO_4^{=}$, NO_3^{-}, $PO_4^{\equiv}$, and HCO_3^{-}, exhibit Raman spectra but, at seawater concentrations, only that of $SO_4^{=}$ is feasible to detect. Although the capability of remotely sensing $SO_4^{=}$ would be of general interest in chemical and biological oceanography, the most exciting pay-off would be for remote determination of salinity. The well tested principle of constancy of composition says that the ratio of $SO_4^{=}$ to chlorine is a constant regardless of salinity. This holds well in the open ocean where good mixing occurs, but must be used with caution in nearshore environments where effects of land may add or subtract $SO_4^{=}$. A graduate student of Dr. Bandy, A. V. Zimmermann, has conducted a study of the $SO_4^{=}$ chemistry in the lower Chesapeake Bay and has observed the principle to be generally valid.

Radiometric calculations were performed by Stewart Ocheltree at LRC which show the amount of signal to be expected for the Raman line of $SO_4^{=}$. Figure 1 shows a typical LIDAR system and the "radar equation" which describes the returned Raman signal. The symbols not defined by the figure are: N, the $SO_4^{=}$ concentration; σ, the $SO_4^{=}$ Raman cross section; A, the area of the collecting lens; α, the total absorption coefficient; and n, the index of refraction of seawater. Figure 2 shows the results obtained from this equation for the LIDAR system parameters listed. The distance, D, is the position of the leading edge of the pulse (assumed rectangular). The absorption coefficients correspond to clear ocean water (.05 M^{-1}) and Murky Bay water (1.0 M^{-1}) (note the receiver heights are small, indicating we plan to be working relatively near the water surface). The return signals are encouraging--the 10^{-7} watt level corresponds to about 5000 photons during a counting time of 20 nanoseconds. Figure 3 shows the Raman spectrum for distilled water. The features due to translation, libration, bending, and stretching are indicated by ν_r, ν_l, ν_B, and ν_s, respectively. $SO_4^{=}$ indicates the position of its Raman line with respect to the other features. Roughly speaking, the peak intensity of the $SO_4^{=}$ line is about the same as that of the ν_s water line.

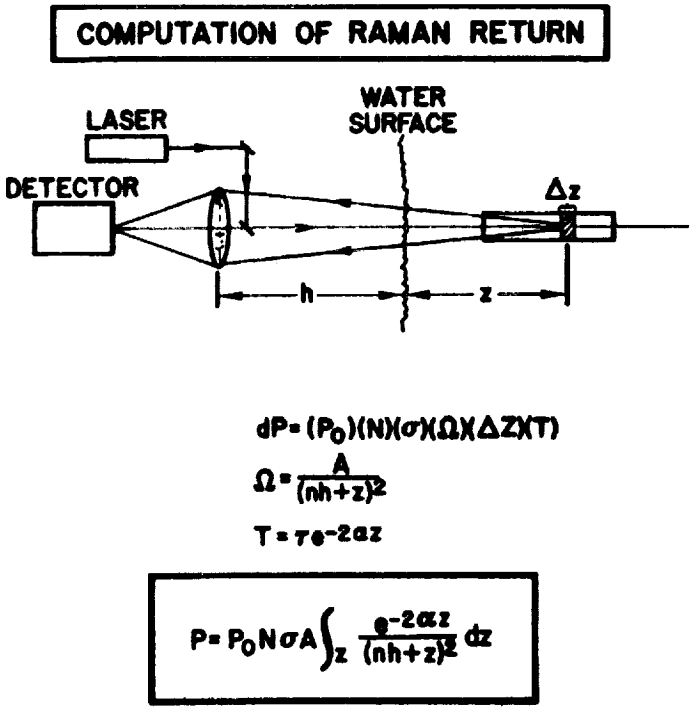

Figure 1. Computation of Raman return

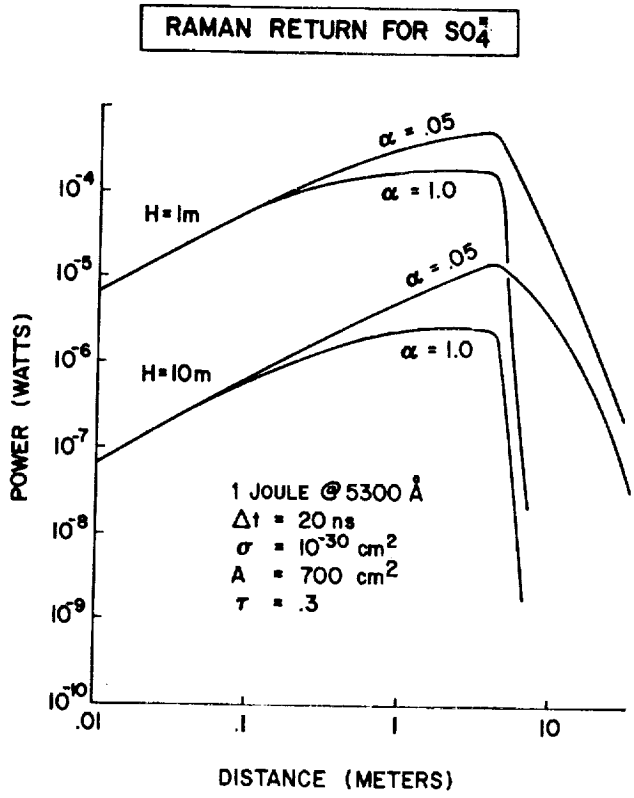

Figure 2. Raman return for $SO_4^=$

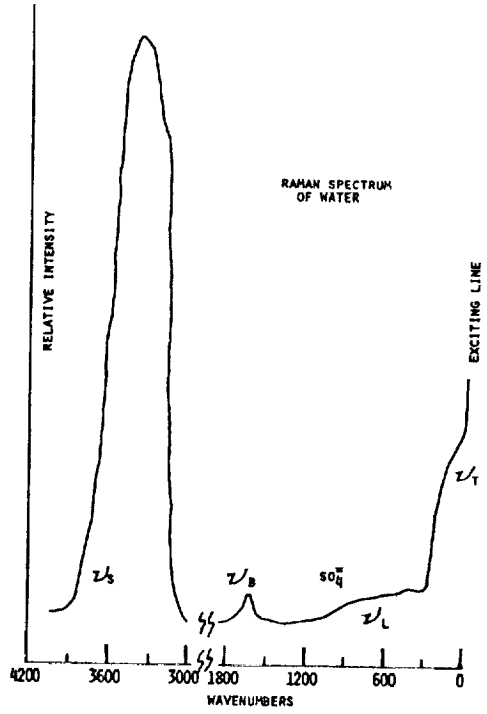

Figure 3. Raman spectrum of water

Figures 4 and 5 are Raman spectra of real seawater made in Dr. Bandy's laboratory at ODU. The excitation source was a one-watt Argon ion laser and the detector a one-meter double monochromator. (Note how well the $SO_4^=$ line stands out, even with a high background level.) Figure 4 was for an untreated water sample; whereas that of Figure 5 was filtered with charcoal. The background has been tacitly assumed due to fluorescence from organic material in the sample.

The scheme for standardizing the $SO_4^=$ signal is to record the water Raman signal also and thus use water as an internal standard of the two water lines, ν_B and ν_S, the ν_S may be the more desirable for several reasons; i.e., it is nearer in strength and wavelength than the ν_B and chlorophyll fluorescence is more likely to interfere with ν_S than ν_B.

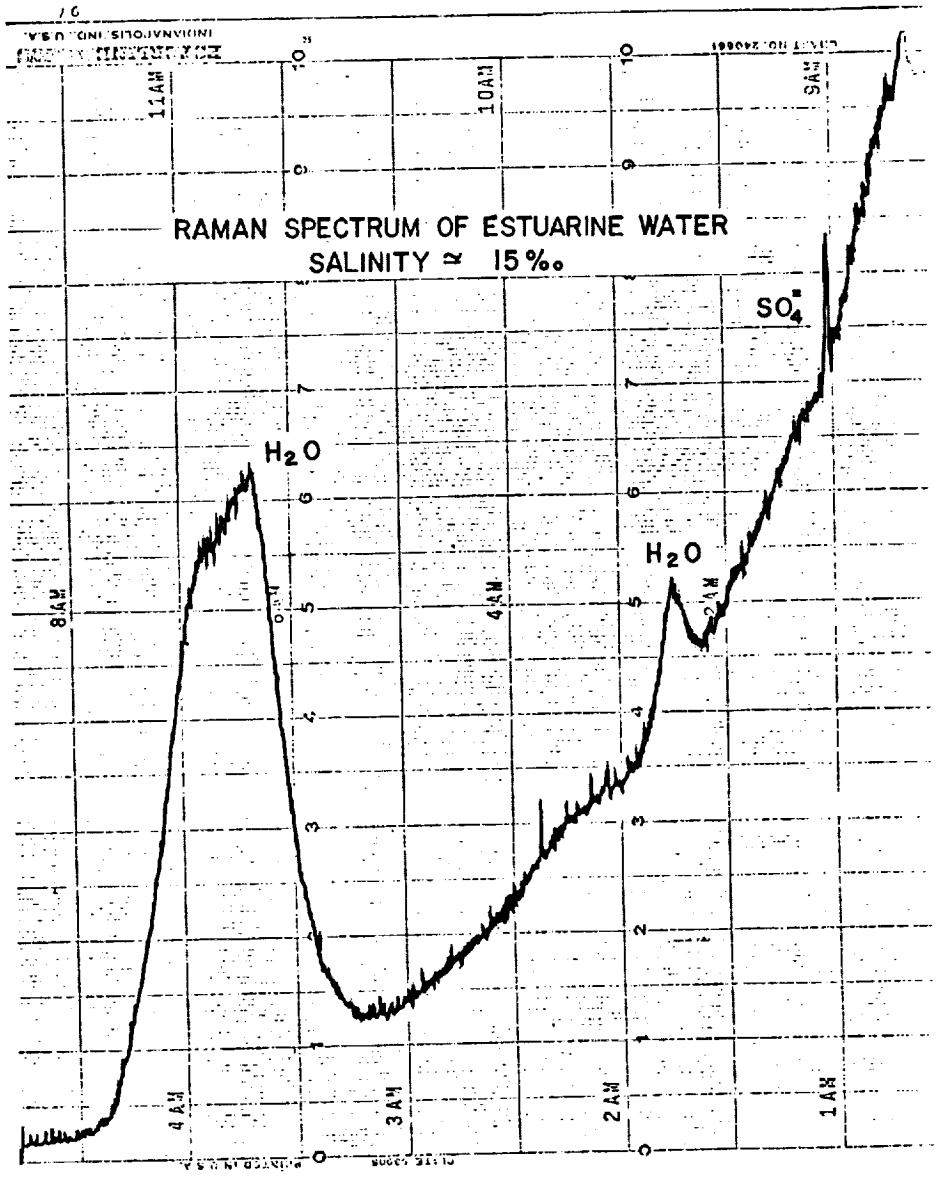

Figure 4. Raman spectrum of estuarine water salinity ≈ 15°/øo

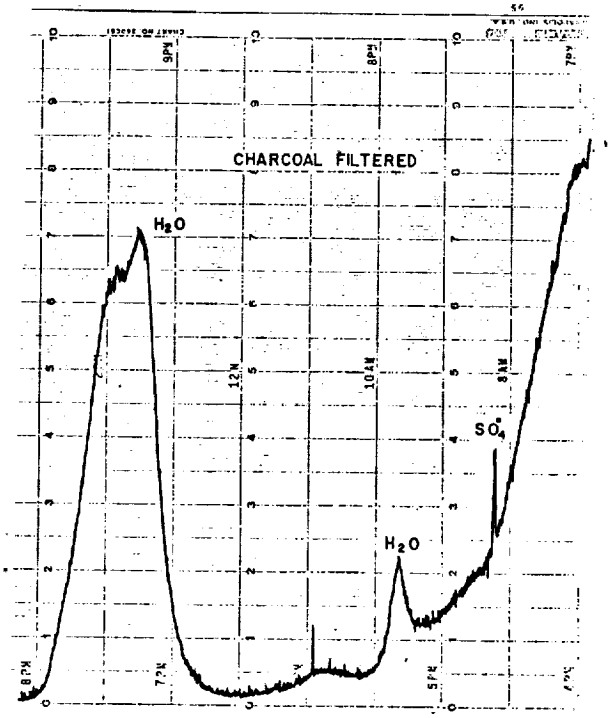

Figure 5. Charcoal filtered

Figure 6 shows how well the $SO_4^=$ can be detected after bucking out the background and increasing the amplification. This spectrum is for the charcoal filtered sample to which a nitrate solution was added for standardization.

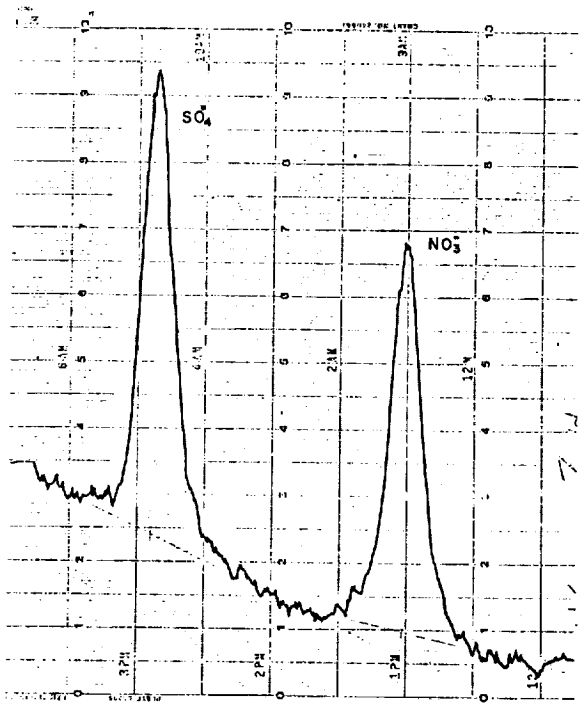

Figure 6. Tabulation of charcoal filtered spectrum with nitrate solution addition

From these laboratory spectra, two points should be noted. The $SO_4^=$ Raman line is fairly narrow, cm^{-1}, or about 12 Å for 500 Å excitation. This implies that the laser line must be narrow, with a width less than 1 Å. Secondly, fluorescence can be strong, and, with the wide range of emission spectra from photoplankton and assorted organics, poses a serious drawback to $SO_4^=$ detection. It would be desirable for the detector to display a spectrogram to evaluate the background.

For field measurements a pulsed laser is desired to allow depth resolution. Figure 7 is a diagram of the equipment being assembled and tested in the laboratory and which will be used in preliminary field studies. Since a laser with the performance parameters required for $SO_4^=$ detection is not available to us at present and will represent a considerable expense, the Figure 7 equipment will be used to obtain the strong water line, ν_s, and to study fluorescence and environmental problems which may interfere or prohibit $SO_4^=$ detection. Figure 8 shows a Raman spectrum obtained in the laboratory with this system. A 1/4-meter monochromator with a laser line rejection filter was used as the detector in the preliminary laboratory studies. Interference filter detectors are also being evaluated for detection.

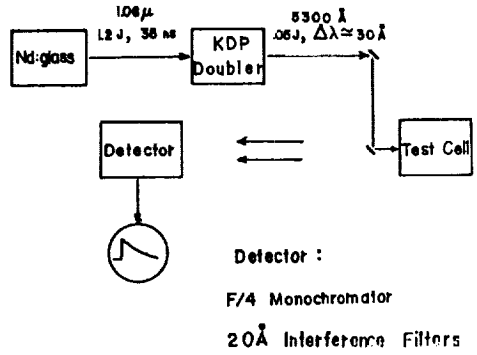

Figure 7. The equipment undergoing testing for use in field studies

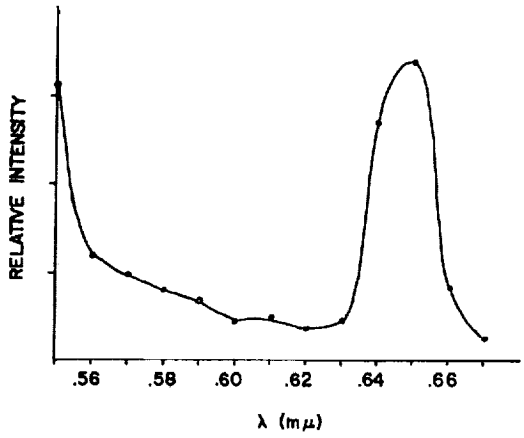

Figure 8. H_2O Raman with pulsed Nd:glass

SUMMARY

The $SO_4^=$ Raman spectrum has been obtained from true seawater samples in the laboratory using a CW laser Raman spectrometric system. Radiometric calculations indicate the feasibility of obtaining usable $SO_4^=$ Raman signals in a field experiment. The most serious difficulty expected is from fluorescence of phytoplankton and other organics.

DEVELOPMENT OF A LASER FLUOROSENSOR FOR AIRBORNE SURVEYING OF THE AQUATIC ENVIRONMENT

Michael P. F. Bristow
Canada Centre for Remote Sensing

Wayne R. Houston and Raymond M. Measures
University of Toronto

ABSTRACT

A field based laser fluorosensor, employing a pulsed nitrogen laser and telescope-photomultiplier detector system, has been successfully tested at night from a cliff top site overlooking Lake Ontario providing target ranges greater than 274 meters (900 feet). Remotely sensed spectra and amplitude changes in the fluorescence emission of natural waters have shown potential as a water quality indicator. In this connection, a convenient internal reference standard with which to gauge the amplitude of the fluorescence signal is realized in the form of the concurrent water Raman emission. Remote measurements of oil fluorescence emission spectra suggest that airborne laser fluorosensors are capable of detecting and characterizing the oil in a given slick and that environmental aging of these slicks does not significantly alter their fluorescence emission signature. This system has now been modified for airborne operations with a view to the eventual development of a compact lightweight emission scanning laser fluorosensor.

INTRODUCTION

Feasibility studies (refs. 1, 2, 3) have demonstrated the ability of laser fluorosensors to remotely monitor the environment. Potential applications of this technique are oil spill detection and characterization, water pollution monitoring, algae distribution surveying and water movement studies. The present work, conducted at the University of Toronto's Institute for Aerospace Studies, has been directed principally at developing a system capable of remotely detecting and monitoring the signatures of environmental pollutants. Fluorescence excitation and emission spectra can be characterized by a number of parameters, viz. band centre and peak wavelengths, bandwidth, shape, structure and amplitude (in relation to some reference level). In addition, a pulsed laser excitation source provides a means for obtaining fluorescence lifetime values. Utilization of these properties thereby allows for detecting and monitoring the concentration of a specific pollutant or for characterizing the unknown pollutant in an unambiguous manner. In the latter case, the remotely sensed fluorescence data would be compared to laboratory measurements made on material obtained from the suspected source with the purpose of providing evidence suitable for use in prosecution proceedings.

An ideal fluorescence excitation source might be a continuously and dynamically tunable (dye) laser capable of being programmed to generate both excitation and emission spectra in conjunction with a real time spectrally scanned receiver system. However, as an interim step in the development of such a device, a field laser fluorosensor has been constructed using a fixed ultraviolet wavelength laser source cojoined to a single fluorescence receiver capable of being spectrally scanned by sequential use of a series of interference filters. The latter expedient is acceptable in the static target situations encountered in ground-based field operations but is not suitable for airborne operations where ground resolution requirements, in relation to the aircraft ground speed, dictate the need for a real time spectral scanning capability.

FIELD LASER FLUOROSENSOR

The field unit shown schematically in Figure 1 consists of a commercially available pulsed ultraviolet laser as the excitation source joined to a telescope-detector with the telescope field of view adjusted so as to overlap the laser excitation field of view for any desired range down to 24 meters (80 feet). The non-coaxial configuration was chosen because of the large diameter and divergence of the laser beam (see TABLE 1). The AVCO C950 laser whose characteristics are given in TABLE 1, provides pulses of relatively high peak power but of low brightness due to the high beam divergence inherent in the superadiant nature of the lasing process. A doubling of beam brightness was achieved using a sphero-cylindrical spectacle lens but at the expense of enhancing the far field mode structure shown in Figure 2. This improvement in brightness was not sufficient to provide for adequate signal discrimination against the solar background shot noise for all but the most efficient fluorescent targets such as low viscosity crude oils. By careful spatial filtering of the returned fluorescence image corresponding to the laser beam modes shown in Figure 2, a 10X reduction in background signal could be achieved with a resultant signal to background noise ratio improvement of $10^{1/2}$. However, as this was found to be insufficient to facilitate daytime fluorescence measurements, the present experiments were conducted under dusk or nighttime conditions. In order to monitor the laser output power, a quartz beam splitter was arranged to deflect a small percentage of the laser output beam onto a PIN photodiode whose peak output had been calibrated to give a direct measure of the peak laser power. This power monitor unit is located over the output aperture of the laser unit as shown in Figure 1. The receiver-detector system consists of a Criterion CD-8, 20 cm diameter, f/8 Newtonian telescope with a two-channel photomultiplier detector package in place of the usual eyepiece (see Figure 1). The principal detector monitors the fluorescence return signal via a series of interference filters in conjunction with an ultraviolet blocking filter; this series of sixteen 100 Å wide filters ranging from 4000 Å to 7000 Å are placed sequentially in front of the detector via a side access port so as to

build up a fluorescence emission spectrum of the target. The peak amplitude of the returned fluorescence pulse as recorded on an oscilloscope is then corrected for detector and filter spectral effects and plotted as a function of emission wavelength to provide a fluorescence emission spectrum of the target under investigation. The second photomultiplier monitors the backscattered laser pulse via a quartz beamsplitter and an interference filter centered at 3371 Å. The backscattered laser pulse, when displayed on the other time base of a two-channel oscilloscope, together with the laser output pulse from the PIN photodiode, provides information regarding the laser output power and the target range. A typical oscillogram is shown in Figure 7. The upper trace shows the laser power output pulse at zero time on the left-hand side, together with the backscattered pulse indicating a target range of approximately 121.9 meters (400 feet). The intervening noise signal is due to the atmospheric aerosol which in this case is a barely visible evening mist. Arriving in coincidence with the laser backscatter, the fluorescence emission from an oil covered target, is shown on the lower trace. For operation in the field, the laser fluorosensor was supported in the universal mount shown in Figures 3 and 4. This mount is readily panned and tilted allowing the laser and telescope to be pointed at any desired target. The two axes of rotation are then locked by means of pneumatically operated clamps. Control and operation of the laser and receiver unit together with the electronic monitoring function were conducted from the field van shown in Figure 3. Power for the experiment was supplied by a 5 kw generator carried in a two-wheel trailer together with the laser gas supplies and cooling and vacuum pumps.

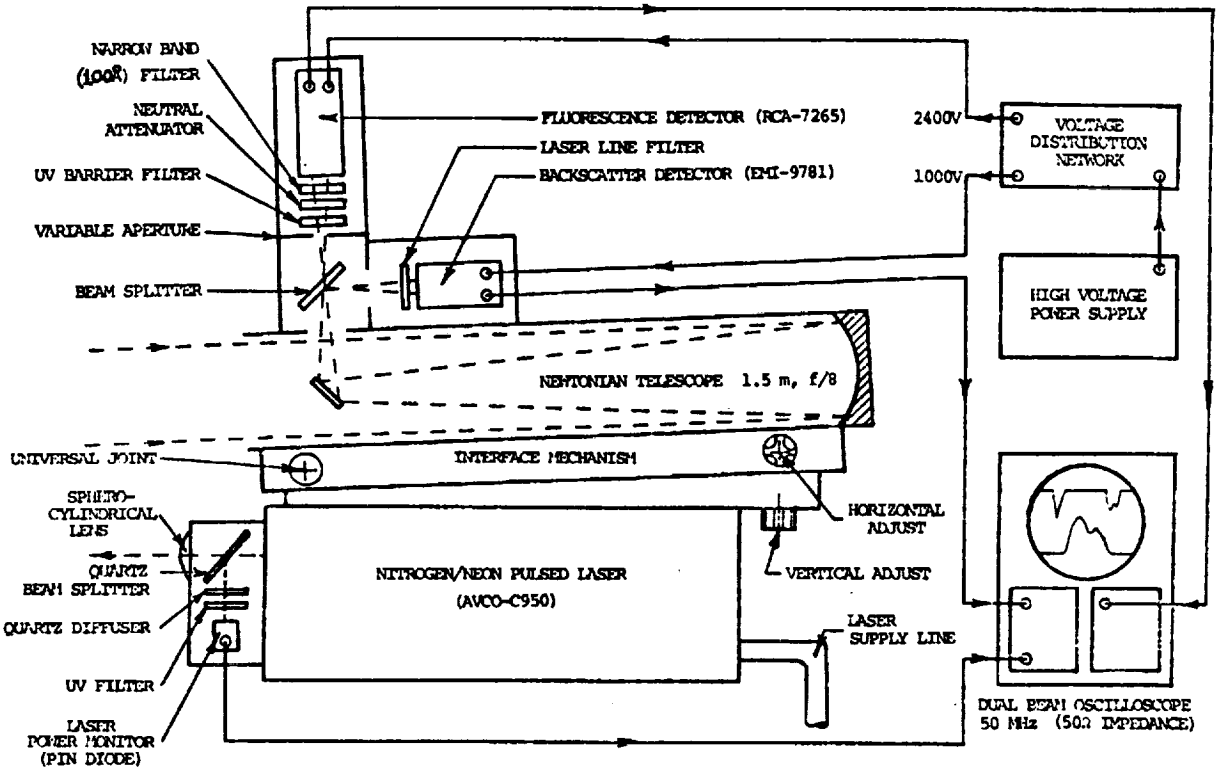

Figure 1. Schematic diagram of laser fluorosensor system

TABLE 1.-CHARACTERISTICS OF THE AVCO C-950 NITROGEN/NEON LASER

	NITROGEN LASER	NEON LASER
Centre Wavelength	3371.1 Å	5400.56 Å
Bandwidth	1 Å	10^{-2} Å
Pulse Width (FWHM)	9 nsec	3 nsec
Maximum Pulse Peak Power	140 kw	20 kw
Pulse Repetition Rate	1 to 100 pps (continuously variable) or single shot.	
Polarization	Unpolarized	
Output Beam Dimensions	5 cm x .3 cm	
Full Angle Far Field Beam Divergence (unmodified)	26.2 mrad x 4.5 mrad	
Full Angle Far Field Beam Divergence with Sphero-cylindrical lens	13.5 mrad x 3.6 mrad	

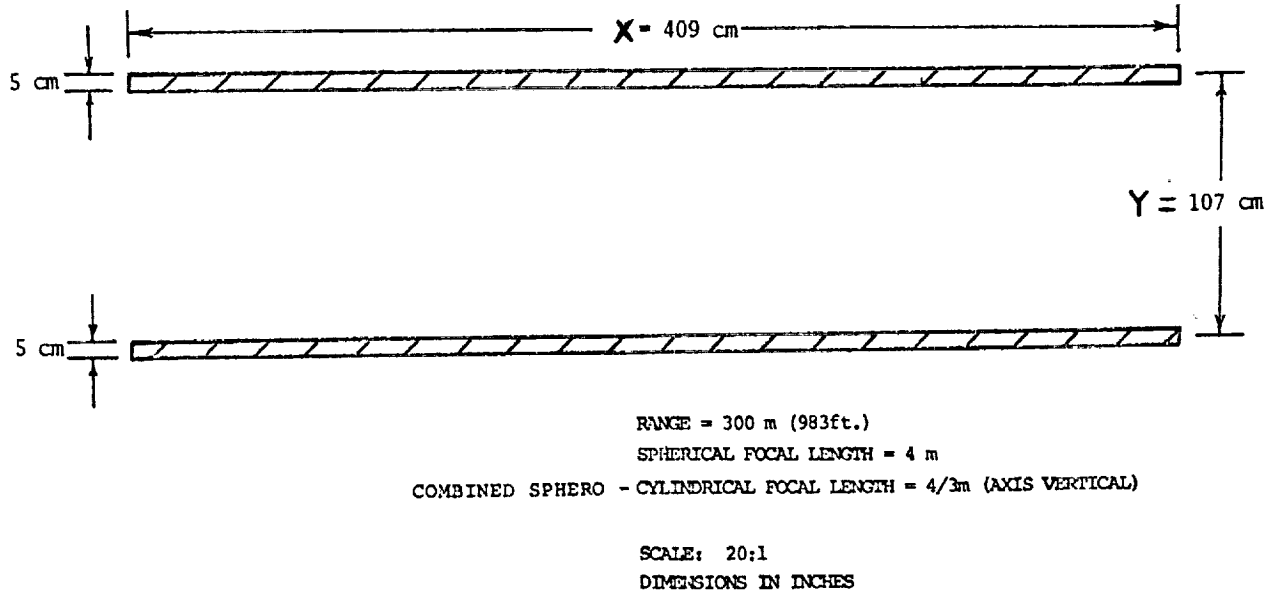

Figure 2. Far field spatial mode structure of nitrogen/neon laser as modified by sphero-cylindrical spectacle lens

Figure 3. Mobile laser fluorosensor system at field site overlooking Lake Ontario near Toronto

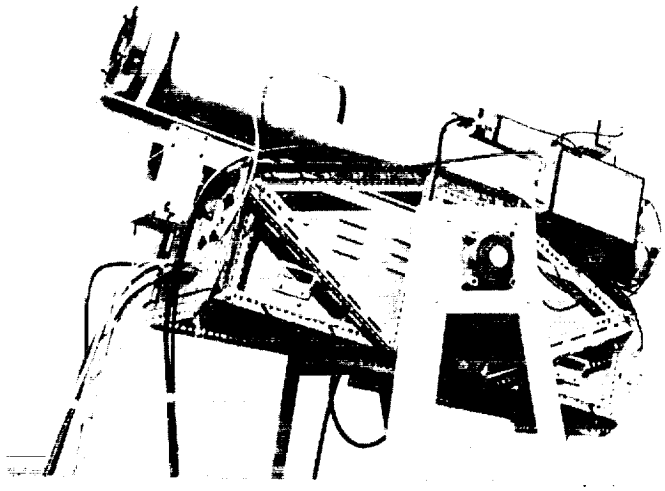

Figure 4. Field laser fluorosensor unit

FIELD SITE

The clifftop field site overlooking Lake Ontario, is located on the Scarborough Bluffs, east of Toronto. The geometry of the location, shown in Figure 5, provides a minimum laser-to-water surface range of about 274.3 meters (900 feet) at an angle of incidence of 73 degrees. When corrections are made for surface and Lambert cosine law effects, this range becomes equivalent to a normal incidence flying altitude of 487.7 meters (1600 feet).

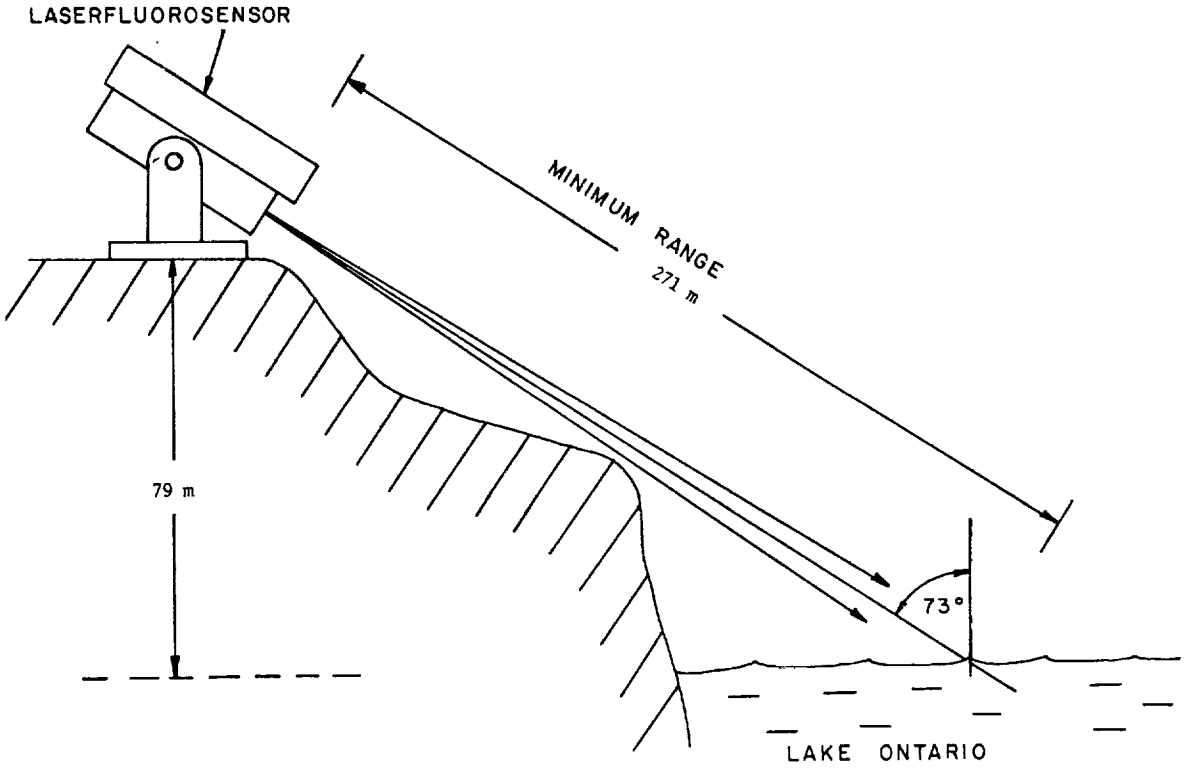

Figure 5. Schematic showing geometry of field test site

As a check on the operation of the laser fluorosensor, a series of water fluorescence emission measurements were made for different ranges and corresponding angles of incidence. The experimental measurements are shown in Figure 6, with the data point for the minimum range of 271.9 meters (892 feet) normalized to unity. The intensity of the water fluorescence signal is seen to fall off with increasing range in accordance with the theoretical relationship

$$I\ (r,\emptyset) \propto \frac{\cos \emptyset\ (1 - R(\emptyset))}{r^2}$$

where $\emptyset$ is the angle of incidence, r is the target range and $R(\emptyset)$ is the specular reflectance for the water surface at angle $\emptyset$. Cos $\emptyset$ represents the Lambert cosine law dependence of I, $1/r^2$ represents the inverse square law variation of I with range and $(1 - R(\emptyset)$ predicts the reduction in the fluorescence emission due to surface reflection losses of the incident laser beam. The fall in amplitude in the fluorescence return at ranges beyond 323.1 meters (1060 feet) was observed to coincide with a marked reduction in water turbidity suggesting that the suspended material responsible for the turbidity is in some way related to or responsible for the increased water fluorescence.

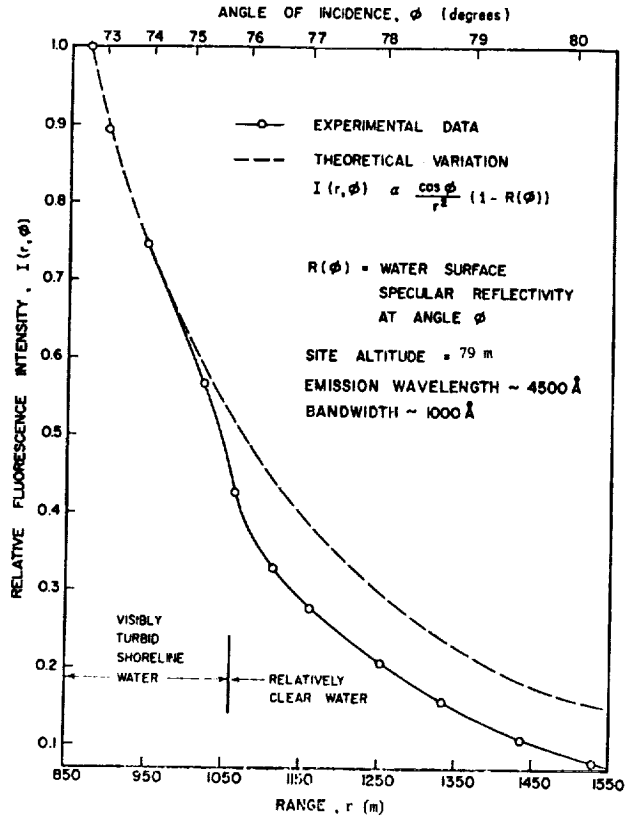

Figure 6. Variation of water fluorescence with range

OIL FLUORESCENCE MEASUREMENTS

With the purpose of remotely sensing fluorescence emission spectra of oil spills, a 6.1 m x 4.6 m (20 ft. x 15 ft.) oil containment boom was constructed and anchored in a spot directly under the cliff top location of the laser fluorosensor. Unfortunately, under the action of even light winds or water currents, the typically 37.9 leter (10 gallon) quantities of crude oil placed within the boom, were rapidly swept under the boom sides and lost from the target area. Apparently oil boom technology requires that the boom skirts be several meters deep in order to prevent loss of oil in this manner. Tracking the movement of an oil slick even during dusk conditions proved to be difficult in spite of the increased surface reflectivity of the oil in relation to the water background, although this problem could have been avoided by use of a low light level TV camera. In addition, recording of meaningful fluorescence spectra requires that a uniformly thick oil slick be presented to the laser beam. This unfortunately was not possible due to the rapid and irregular manner in which oil slicks tend to disperse. The oscillogram shown in Figure 7 was obtained during one of these attempted experiments. The lower trace shows the fluorescence emission from the oil slick at 4600 Å together with the corresponding background water fluorescence signal. The water fluorescence was obtained by panning the laser fluorosensor unit off the oil slick onto a region of uncontaminated water having the same range as the oil target. The oil fluorescence signal, originally about 20X larger than that of the water background, has a value about 6X larger after a 30-minute dispersal. The double pulse shape of the return signal is due to the difference in the return path lengths of the upper and lower far field laser beam modes striking the lake surface at 73° angle of incidence. The backscattered laser pulse seen on the right-hand side of the upper trace is somewhat smaller than that normally seen from lake water, as most of the laser radiation is either absorbed in the oil slick or lost to specular reflection. In fact, a backscat-

tered laser signal was not observed for the initially opaque oil slick. As a result of the above mentioned oil slick problems, a field experiment was performed in which the oil slick was simulated by smearing a thin film of crude oil onto a 1.2 m x 2.4 m (4 ft. x 8 ft.) steel sheet. This target was situated at a range of about 121.9 meters (400 ft.) from the laser fluorosensor with the sheet oriented for normal incidence of the laser beam. A typical result for this target is shown in the oscillogram of Figure 8. The resultant emission spectra obtained from these measurements is shown in Figure 9, together with a laboratory spectrofluorometer emission scan on a sample of the same crude oil. The instrument used was an AMINCO SPF 125-S Scanning Spectrofluorometer employing a xenon lamp/grating monochromator excitation source in conjunction with a grating emission monochromator with a Hamamatsu R446S photomultiplier having a modified S-20 spectral response. The oil fluorescence emission measurements were facilitated using an opaque sample accessory. For purposes of comparison, the field results shown in Figure 9, obtained with a photomultiplier having an S-20 spectral response, have been normalized to the modified response of the R446S detector. The two spectra appear to be in agreement on the short wavelength side of the peak but the bandwidth of the spectrofluorometer curve is somewhat narrower than that for the laser fluorosensor data. An explanation for this discrepancy has not

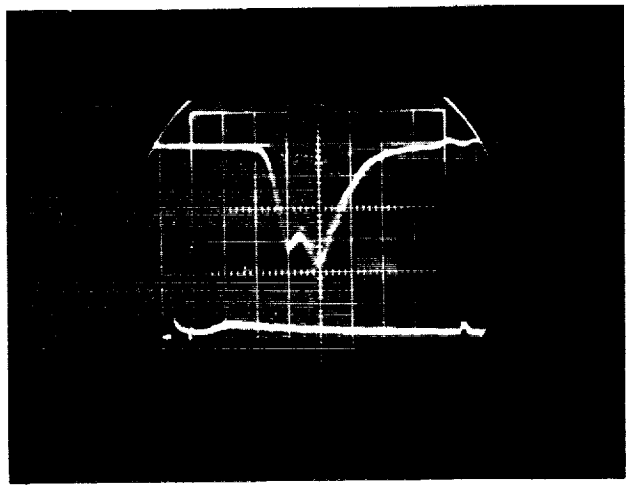

Range:	272 meters
Angle of Incidence:	73°
Oil Sample:	Leduc Crude, API, 39.8°
Exposure:	20 pulses
Upper Trace:	Horizontal scale: 200 nsec/cm Vertical scale: 200 mV/cm
Lower Trace:	Horizontal scale: 20 nsec/cm Vertical scale: 100 mV/cm

Time increasing to the right.

Figure 7. Lower trace shows fluorescence emission (4600 Å) from oil slick (large pulse) and water background (small pulse) on Lake Ontario off Scarborough Bluffs. Upper trace shows laser output and backscattered pulses.

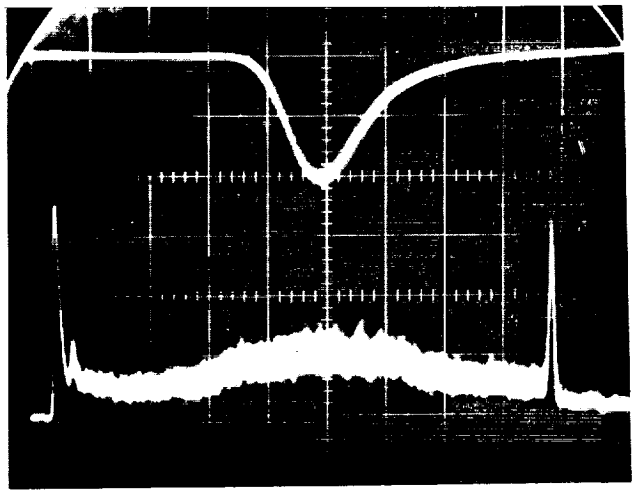

Range:	120 meters
Angle of Incidence	0°
Oil Sample:	Leduc Crude, API, 39.8°
Exposure:	20 pulses
Upper Trace:	Horizontal Scale: 100 nsec/cm Vertical Scale: 100 mV/cm
Lower Trace:	Horizontal Scale: 10 nsec/cm Vertical Scale: 500 mV/cm

Time increasing to the right.

Figure 8. Lower trace shows fluorescence emission (4400 Å) from an oil film on a steel sheet. Upper trace shows laser output and backscattered pulses.

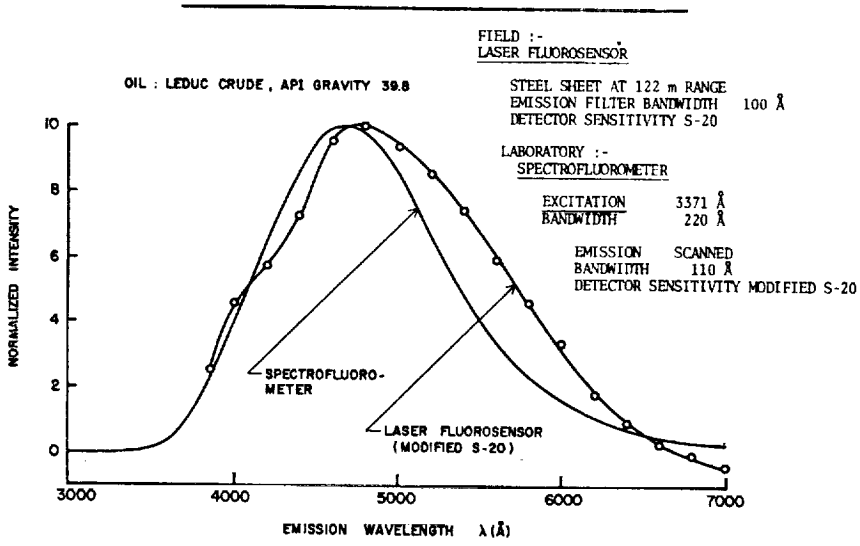

Figure 9. Fluorescence emission of crude oil film using laser fluorosensor compared to laboratory measurement.

been found but several possibilities exist. First, it is possible that certain volatile fluorescent hydrocarbons have evaporated from the sample on the steel sheet thereby broadening and displacing the emission spectra to longer wavelengths. However, it cannot be ruled out that the spectrofluorometer contributes its own artefact to the data. The emission monochromator uses a grating blazed for peak efficiency at 5000 Å but typical efficiency curves for a 5000 Å blaze grating supplied by Bausch and Lomb, do not significantly change the spectrofluorometer curve. This discrepancy was also encountered in the water fluorescence measurements and is further discussed later. Ultimately, good agreement between laboratory and remotely sensed data must be obtained, particularly in the case of oil pollution, where close correlation between airborne and laboratory measurements is essential if this type of data is to be used as evidence in the prosecution of those responsible for the pollution.

A question frequently asked is: "What effect does prolonged environmental exposure have on the fluorescence spectra of crude oil and refined oil products?" Again, in the absence of a controlled oil spill, a thin layer of crude oil was applied to a steel sheet target and exposed to the effects of sun, wind, rain, and atmospheric oxidation. Field measured spectra obtained immediately after application of the oil film and also after a 48-hour exposure period are shown in Figure 10. Aging reduces the fluorescence signal to about half that of its initial value but does not induce any significant change in shape or position of the spectral curve. No explanation is yet available for the reduction in the amplitude of the fluorescence signal with time or atmospheric exposure. It is possible that some of the more highly fluorescent aromatic hydrocarbons located in the surface layers of the oil film are lost to the atmosphere leaving an asphaltic matrix layer which acts as an optical barrier. Clearly this type of situation is less likely to occur in the non-static situation encountered in a real oil spill. Laboratory fluorescence studies performed by Parker at the Admiralty Materials Laboratory in the UK (ref. 4) confirm the general conclusion of the present aging measurements. In addition, the effects of prolonged exposure of crude oil to a marine environment has been studied by a group at the Woods Hole Oceanographic Institution (ref. 5) who have shown that crude oils stranded at sea can maintain their compositional integrity for periods of many months.

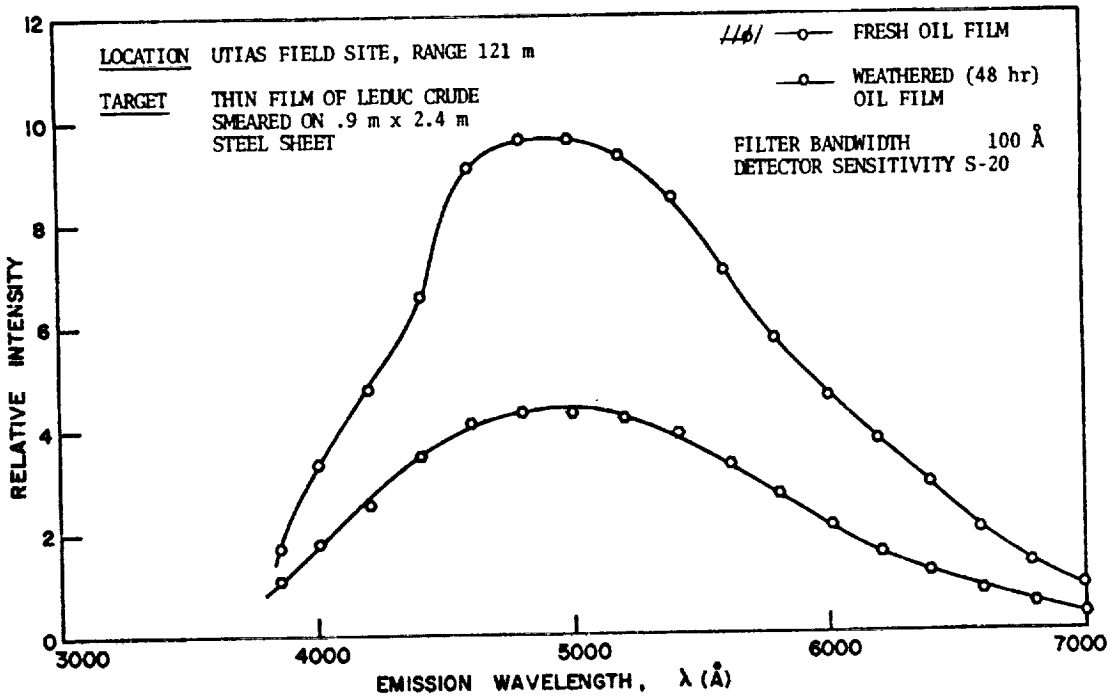

Figure 10. Effect of environmental exposure on fluorescence emission of crude oil film using laser fluorosensor.

WATER FLUORESCENCE MEASUREMENTS

Water fluorescence, or more specifically the fluorescence of the dissolved material in natural waters, is generally regarded as an annoying background signal level against which either laboratory or field fluorescence measurements are made. However, preliminary measurements have shown that this water fluorescence, although small in relation to typical oil, dye or chlorophyll signals, is also amenable to spectral analysis particularly when using a high power ultraviolet laser as the excitation source. Unpublished results obtained at the University of Toronto's Institute for Aerospace Studies (ref. 6) have demonstrated a number of interesting trends. Laboratory spectrofluorometer measurements on a wide range of river and lake water samples have indicated excitation spectra peaking between 3400 Å and 3500 Å for the majority of samples. The emission fluorescence spectra, however, could be differentiated according to whether the sample location was considered polluted or relatively clean. Samples obtained from relatively unpolluted northern rivers and lakes had emission spectra peaking between 4100 Å and 4325 Å whereas samples obtained from sites close to dense population centers tended to have emission peaks between 3900 Å and 4150 Å. Unexpectedly, the samples from the uninhabited regions tended to exhibit stronger fluorescence signals than those from the unpopulated regions although a coarse correlation between pollution level and fluorescence signal was observed for the latter group of samples.

The nature of this blue water fluorescence is not well understood, but is thought to be due to the aqueous solutions of large complex organic molecules, particularly of the aromatic type. For natural unpolluted waters, some of the materials thought to contribute to this fluorescence signal are:

a. Airborne dust, pollens and bacteria,

b. aqueous extracts and decay products of wood and vegetation,

c. aqueous extracts of soil material, and

d. algae, bacteria, molds and fungi.

In addition to the material described above, polluted river and lake waters will contain dissolved organic material from a number of possible sources; viz.

a. pulp and paper mill effluents,

b. sewer effluents,

c. industrial effluents other than those in group (a) and

d. leaked crude and refined mineral oil constituents from watercraft, shipping and industrial sources.

It has been suggested that this characteristic blue water fluorescence might be used as a water quality indicator possibly as a measure of total organic carbon. However, in view of the relatively low intensity of this water fluorescence being close to the shot noise limit of the fluorescence detector, a series of experiments was conducted at the field site to determine the ability of the laser fluorosensor to produce water fluorescence spectra. Figure 7 indicates the amplitude relationship between the fluorescence of a slick of crude oil and, in this case, the background water fluorescence at 4600 Å. This measurement was made approximately 30 minutes after the formation of the slick at which point the oil fluorescence signal had fallen to one-third of its original value under the dispersive action of wind and wave action. Figure 11 shows the fluorescence emission spectra for Lake Ontario water obtained at the Scarborough Bluffs field site on three different occasions but for otherwise similar conditions. A number of interesting features are apparent from these three spectra. The day-to-day variation in overall amplitude of the fluorescence signal

indicates a significant change in the concentration of the substances responsible for this fluorescence. The center wavelength for the fluorescence band lies at about 4350 Å which is more consistent with the fluorescence of unpolluted lake water than that of the relatively polluted water to be expected close to a population center such as Toronto (ref. 6). In addition to the principal fluorescence band, there appears to be a secondary peak in the region of 5100 Å. The band located at 6850 Å is due to chlorophyll a, probably in the form of algae. The reason for the inverse relationship between the chlorophyll a peak at 6850 Å and the blue water fluorescence band is not clear. Possibly the presence of a specific pollutant responsible for the blue water fluorescence has an adverse effect on the surface algae population or, alternatively, the substances causing or associated with the water fluorescence are blocking the chlorophyll excitation or emission radiation. The final feature of interest in these spectra concerns the apparent rise in the fluorescence signal below 4000 Å. In the absence of an interference filter for this region, a sample of the same lake water was obtained and a simulated field measurement conducted in the laboratory. The water fluorescence spectra of Figure 12 was obtained by using the pulsed nitrogen laser as the excitation source together with a scanning type monochromator (Heath EU-700/E) operated in a 90° configuration with the sample cell located immediately adjacent to the monochromator entrance slit. The photomultiplier detector was of the side-on type (EMI 9781B) with a modified S-5 spectral response. The spectral feature at 3810 Å in Figure 12 is clearly identified as the Raman band for the OH vibrational stretching mode of water. The large amplitude of this 60 Å wide Raman band in relation to the water fluorescence signal was a little surprising. This arises because the Raman emission is characterized by a given vibrational frequency shift in relation to the exciting frequency whereas the fluorescence emission is characterized by a fixed electronic transition which is independent of the exciting frequency. Consequently the ratio of the peak amplitude of the Raman emission band to that of the corresponding fluorescence emission will bear an inverse relationship to the bandwidth of the exciting laser radiation. Laboratory spectro-fluorometers employ excitation bandwidths of the order of 100 Å whereas the nitrogen laser has a bandwidth of 1 Å resulting in a corresponding enhancement of the water Raman band in relation to the water fluorescence emission. However, the ratio of the peaks of the Raman band to that of the fluorescence band was initially somewhat smaller, having a value of 7 rather than the value of 17 for the spectra in Figure 12. This is due to the effect of the intense ultraviolet laser radiation in producing photolytic decomposition of the large complex organic molecules responsible for the water fluorescence which are probably present in concentrations below the parts per billion range. The principal reason for interest in this water Raman band lies in its possible use as a built-in standard with which to compare the water fluorescence signal in much the same manner as the molecular nitrogen Raman band is used in atmospheric Raman LIDAR pollution studies. However, in contrast to the atmospheric case, careful consideration must be given to differential absorption and scattering effects on the fluorescence and Raman emissions particularly with regard to operation over polluted or turbid waters.

It is the essence of remote sensing that the monitoring device be able to record the experimental data without having recourse to direct immersion sensing or laboratory analysis to provide a complete and detailed picture of the substances being observed. Clearly any laser-fluorosensor must faithfully reproduce the required fluorescence spectra without incurring any unknown environmental or instrumental effects. In Figure 13, the water fluorescence emission spectra obtained using the laser fluorosensor, is compared to that obtained using the spectrofluorometer for the same water samples. As in the case of the oil fluorescence comparison, the spectral profile obtained on the spectrofluorometer is narrower and located at shorter wavelengths than that obtained using the laser fluorosensor. As a check on the validity of these two measurements, the water fluorescence spectra of Figure 12, also for the same sample, is displayed in Figure 13. The agreement between the field measurements and those from the laser-monochromator appears to confirm the earlier suggestion that the spectrofluorometer data contains some instrumental artefact. This suggests that care must be exercised when comparing fluorescence spectra obtained using different instrumental methods.

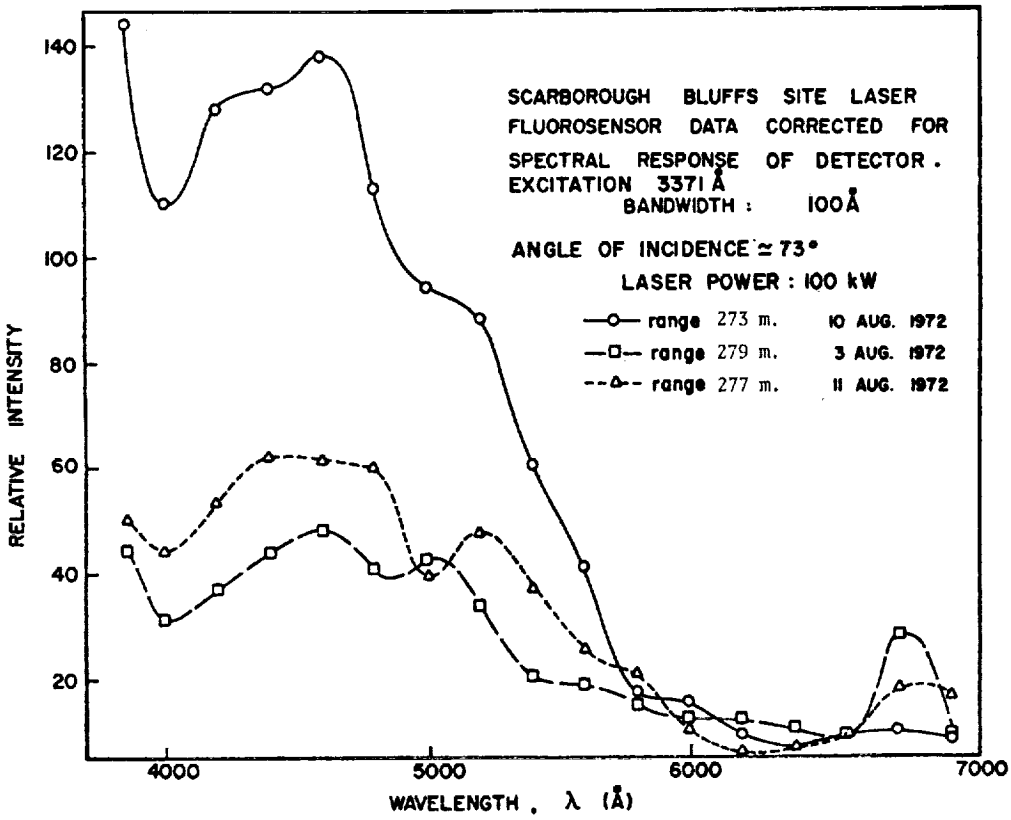

Figure 11. Lake Ontario water fluorescence emission

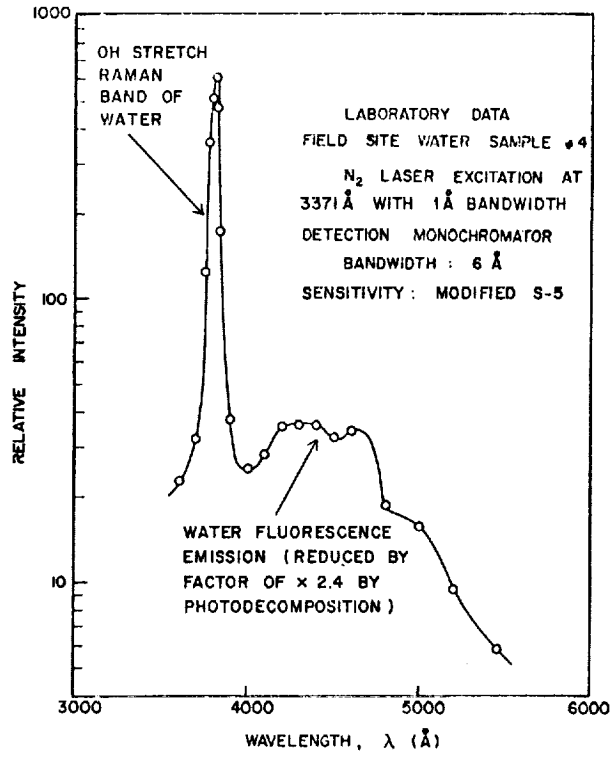

Figure 12. Lake Ontario water fluorescence emission

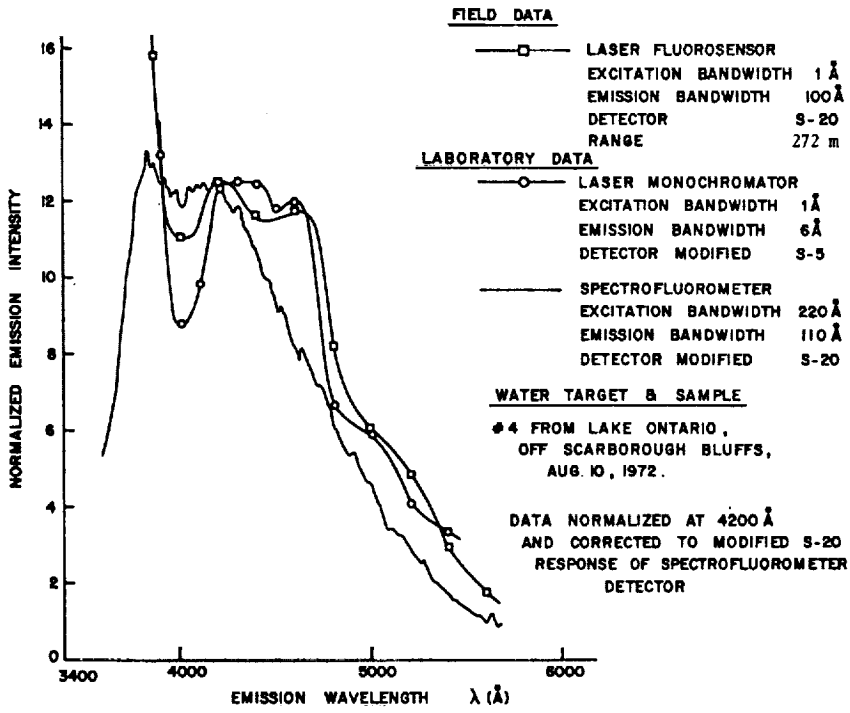

Figure 13. Water fluorescence emission excited at 3371 Å using laser fluorosensor compared to laboratory measurements

A complete understanding of this water fluorescence phenomenom will only come when it is possible to unravel the chemistry of the specific substances involved. However, the possibility that the fluorescence of natural waters might be used as a water quality or pollution indicator would seem to demand further investigation.

AIRBORNE LASER FLUOROSENSOR

As the logical development in the evolution of this sensing device, the laser fluorosensor is now being prepared for airborne testing and operations in a DC3 aircraft at the Canada Centre for Remote Sensing in Ottawa. A schematic of the modified field laser fluorosensor unit is shown in Figure 14. Rather than aim the system directly downward or use individual output and return beam folding mirrors, a single high quality UV reflecting mirror was used to fold both beams. Apart from this mirror and the antivibration shock mounts, the system is identical to that employed in the field trials as described above. However, the electronic monitoring and recording system has been improved with a view to recording the continuously changing fluorescence target information on a real time basis (see Figure 15). A waveform digitizer (Lecroy WD2000) provides for real time analog-to-digital conversion of the individual returned fluorescence pulses which are then processed by an airborne data acquisition system (ADAS) and stored on magnetic tape. Real time capability is also provided by the two channel sampling oscilloscope (Philips PM3400) which outputs DC voltages to an oscillographic chart recorder (Honeywell 1858) corresponding to the peak laser and fluorescence return pulses. A nanosecond resolution time interval counter (Hewlett-Packard 5360) which is gated by the laser output and returned pulses, provides a value for the target range. Photographs of the airborne laser fluorosensor and the complete airborne system including the laser support package and electronics are shown in Figures 16 and 17, respectively. As an assistance to both nighttime aircraft navigation and target location, the laser fluorosensor is used in conjunction with a wide angle low light level TV camera (Cohu 2856). Crude and refined oils have optical refractive indices in the region of 3/2 whereas that for water is closer to 4/3 so that the normal incidence reflection from an oil slick will be approximately 4% as against 2% for water. The higher visible region reflectivity of the

oil slick in effect contrasts the oil slick against the water background thereby facilitating nighttime observation of oil spills with the low light level TV camera.

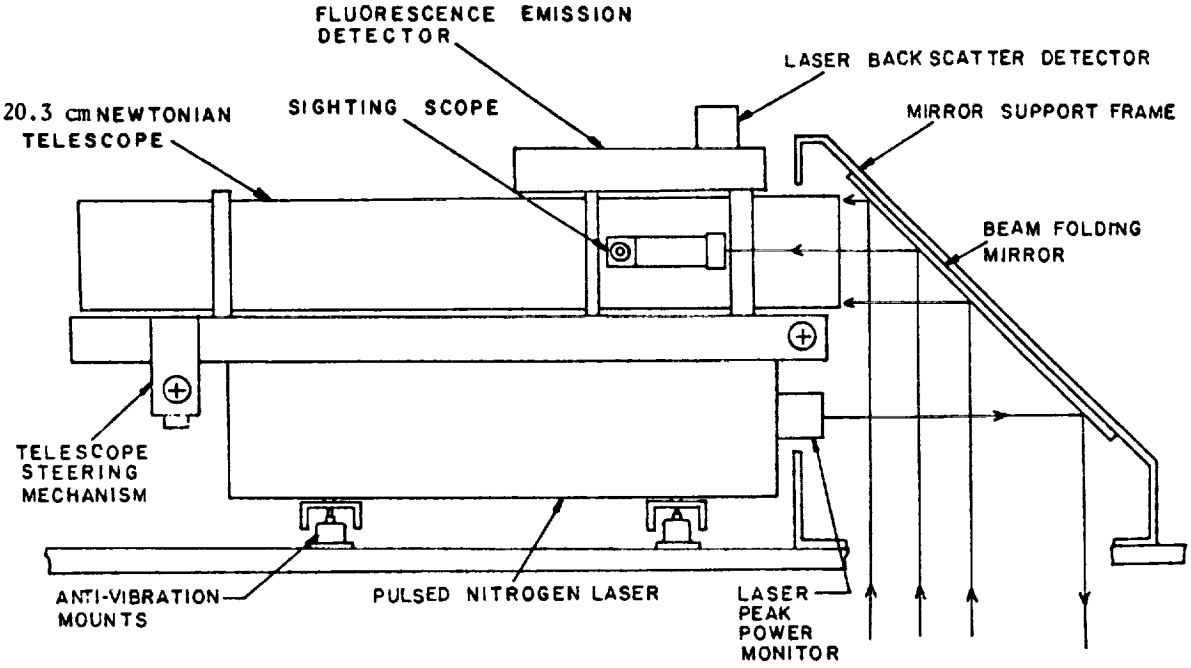

Figure 14. Schematic of field laser fluorosensor as modified for airborne operations

DISCUSSION

Testing of the laser fluorosensor device in a fixed field site location has provided much experience and information ultimately needed in the design of a light and compact production type airborne laser fluorosensor.

Promising results have been obtained, suggesting that the laser fluorosensor has the ability to remotely detect and record the spectral fluorescence characteristics of natural and polluted waters. However, much analytical work must be done if the laser fluorosensor is to become a useful airborne water quality monitor.

To date, the laser fluorosensor is the only remote sensing device which has demonstrated an ability to detect and characterize an oil spill. This ability becomes all the more important when it is realized that there exists no easy method for taking samples from an oil slick after the slick has been located by an aircraft whether it be a spotter plane or a sophisticated sensing platform.

a. Direct sampling of the spill from the aircraft is hazardous to both aircraft and shipping alike.

b. Hovercraft and helicopters produce strong side and down-drafts which tend to disperse the oil slick.

c. Patrol boats generally arrive 1 to 2 hours after the first sighting of the spill by which time the slick has either dispersed or drifted to another location.

d. It is almost impossible to sight an oil slick from the bridge or deck of a ship until the vessel is directly over the slick due to the poor oil-water contrast encountered when the slick is viewed in near grazing incidence illumination.

e. Seaplanes encounter the same difficulties as given in sub-paragraphs b. and d., above.

It is essential that an oil spill be characterized in such a manner that its identity can be directly related to that of a sample removed from the suspect ship. This information would then be used as evidence in legal proceedings against those responsible for the slick. Remotely sensed fluorescence excitation or emission spectra appear to provide the information needed to constitute a characteristic signature suitable for use as prosecution evidence.

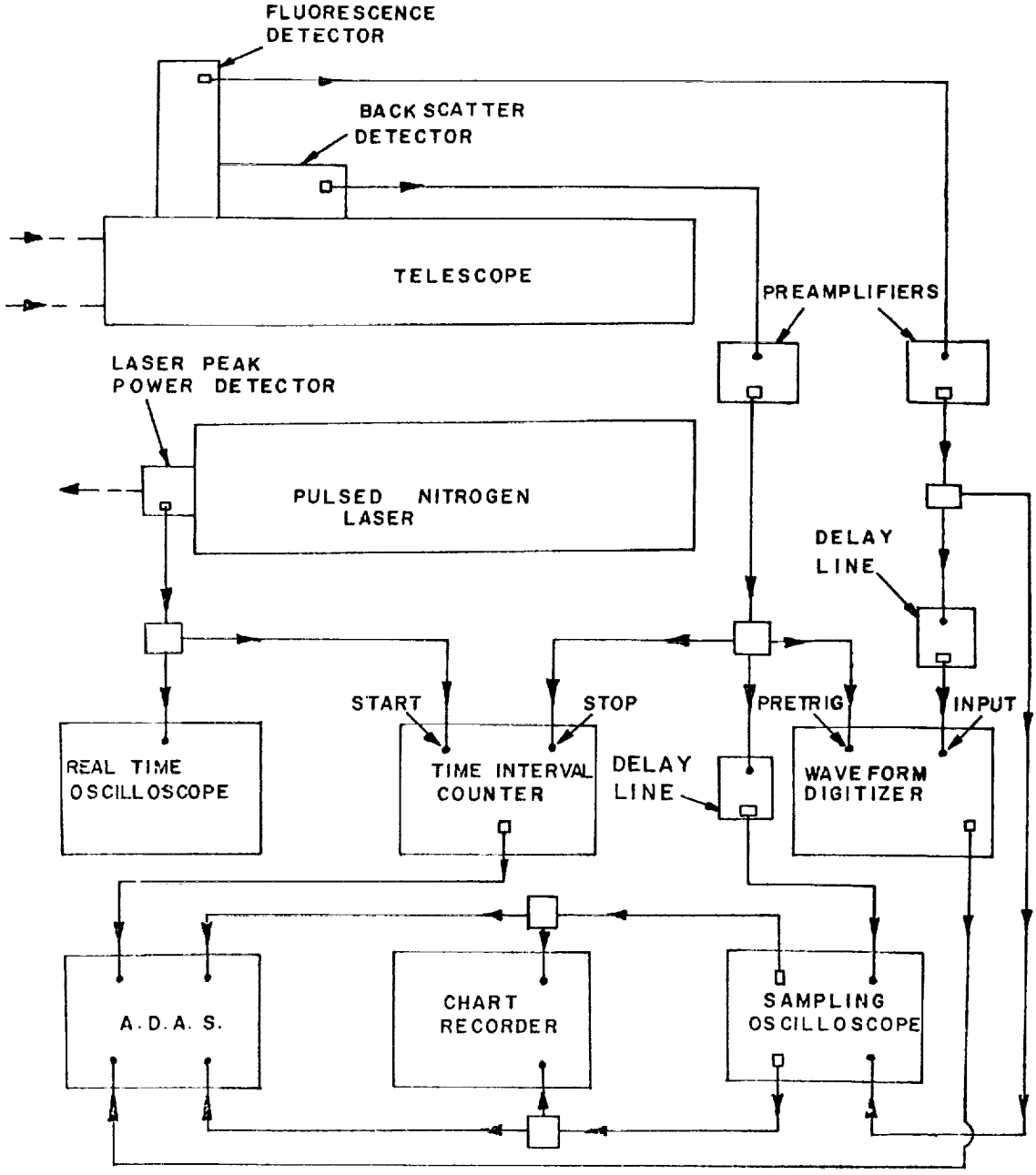

Figure 15. Schematic of airborne laser fluorosensor monitoring and recording system

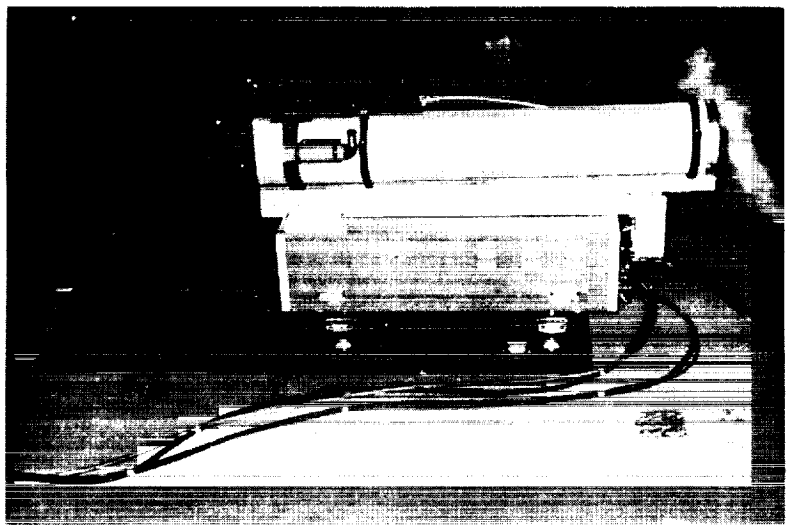

Figure 16. Airborne laser fluorosensor unit

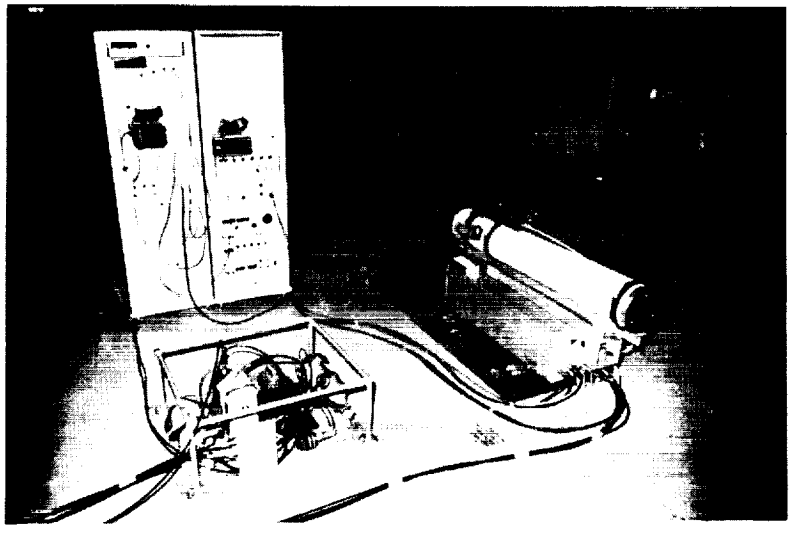

Figure 17. View of complete airborne system including laser support package and electronics

REFERENCES

1. Measures, R. M. and Bristow, M., "The Development of a Laser Fluorosensor for Remote Environmental Probing," AIAA Paper 71-1121. Joint Conference on Sensing of Environmental Pollutants, Palo Alto, California, Nov. 8-10, 1971.

2. Measures, R. M. and Bristow, M., Can. Aeron. Space J. 17, 421, 1971.

3. Fantasia, J. F.; Hard, T. M. and Ingrao, H. C., "An Investigation of Oil Fluorescence as a Technique for Remote Sensing of Oil Spills", Report #DOT-TSC-USCG-71-7, June 1971. Transportation Systems Centre, Dept. of Transport, Cambridge, Mass.

4. Anon., Water and Pollution Control, p. 31, Sept. 1972.

5. Blumer, M.; Ehrhardt, M.; and Jones, J. H. Deep Sea Research 20, 239, 1973.

6. Drewes, P. L., Fluorescence Characteristics of the Water Environment, M.A.Sc. Thesis, Dec. 1971. Institute for Aerospace Studies, University of Toronto.

MULTIWAVELENGTH LIDAR FOR REMOTE SENSING OF CHLOROPHYLL a IN ALGAE AND PHYTOPLANKTON

Peter B. Mumola, Olin Jarrett, Jr., & Clarence A. Brown, Jr.
NASA, Langley Research Center

ABSTRACT

A theoretical and experimental analysis of laser induced fluorescence for remote detection of chlorophyll a in living algae and phytoplankton is presented. The fluorescent properties of various species of algae representative of the different color groups are described. Laboratory measurements of fluorescent scattering cross sections is discussed and quantitative data presented. A "scattering matrix" model is developed to demonstrate the essential requirement of multiwavelength laser excitation in order to make accurate quantitative measurements of chlorophyll a concentration when more than one color group of algae is present in the water (the typical case). A practical airborne laser fluorosensor design is considered and analysis of field data discussed. Successful operation of the Langley ALOPE (Airborne LIDAR Oceanographic Probing Experiment) system is described and field measurements presented. Accurate knowledge of α, the optical attenuation coefficient of the water, is shown to be essential for quantitative analysis of chlorophyll a concentration. The feasibility of remotely measuring α by laser radar is discussed.

INTRODUCTION

The application of laser radar (LIDAR) technology to the remote detection of fluorescent materials, notably oil and chlorophyll a, in natural waters has been actively pursued by several groups in the United States and Canada. Thus, a common appreciation for the value of remote sensing to the oceanographic community and to those responsible for water quality management is assumed. NASA Langley Research Center (LaRC) has initiated a program to develop an airborne fluorosensor with a multiwavelength laser for detection of chlorophyll a in living algae where more than one color group may be present.

LABORATORY SPECTRAL STUDIES

Since chlorophyll a is insoluble in water, this molecule is found in a host material, namely, algae and phytoplankton. The optical properties of the host material alter the fluorescence excitation and emission spectra of the chlorophyll a molecule. Therefore, knowledge of the optical properties of the algae as it is found in nature, rather than in acetone extract solution, is required for remote detection application.

During the past year, LaRC personnel have measured the fluorescence excitation and emission spectra of over 45 different species of algae representative of the four major color groups (blue-green, green, golden-brown, and red). Using Rhodamine B as the fluorescence standard, the effective fluorescence cross section has been computed as a function of excitation wavelength for each species. The apparatus used in these studies is shown in Figure 1. A fluorescence spectrophotometer, Hitachi Perkin-Elmer Model MPF-2A, was modified to improve its red sensitivity. The spectra were recorded on both a strip chart and magnetic tape, the latter being used for input to computer programs for cross-section computation. Excitation spectra were measured by setting the emission monochromator to 685 nm, the chlorophyll a fluorescence peak, and scanning the excitation wavelength from 360 nm upward through the visible spectrum. Both monochromators were set to 5 nm slit widths to obtain usable signal levels without destroying the spectral resolution. Emission spectra were then recorded by setting the excitation monochromator to the optimum excitation wavelength (determined above) and scanning the emission monochromator from that wavelength upward to 800 n. Similar spectra were measured using a 10^{-7} molar solution of Rhodamine B in ethanol. Cross sections were then computed using these spectra and accounting for instrumental effects such as monochromator transmittance and lamp spectral intensity. Figure 2 shows typical results for algae of each color group. Note in the emission spectra that each color group emits strongly at 685 nm due to the presence of chlorophyll a, though other fluorescent components may also be present. The excitation spectra differ from one color group to another, each having a unique region for optimum excitation. Spectra within any given color group are, however, remarkably similar as shown in Figure 3 for golden-brown algae. Therefore, one can characterize the fluorescent excitation properties of any algae by the color group to which it belongs. Note that these cross sections were computed for single molecules of chlorophyll a and a spectral resolution of 5 nm. This will be important in the analysis which follows.

It should be noted that no single excitation wavelength can be chosen to uniformly stimulate chlorophyll a fluorescence in all algae. Spectral overlap also precludes selective excitation of any one color group of algae. One method of measuring the concentration of chlorophyll a can be shown in the LIDAR equation:

$$P_{rec} = \begin{cases} \dfrac{\xi A}{2R^2} \dfrac{\Delta\lambda_D}{\Delta\lambda_f} \dfrac{\theta_r^2}{\theta_l} \dfrac{\sigma_f(\lambda_l) n \, P_o(\lambda_l)}{(\alpha_f + \alpha_l)} & \text{For single fluorescent scatterer} \\ \text{or} & \\ \dfrac{\xi A}{2R^2} \dfrac{\Delta\lambda_D}{\Delta\lambda_f} \dfrac{\theta_r^2}{\theta_l^2} \sum_{j=1}^{4} \dfrac{\sigma_{fj}(\lambda_l) n_j \, P_o(\lambda_l)}{\alpha_f + \alpha_l} & \text{For four different fluorescent scatters} \end{cases}$$

where

ξ = optical efficiency of receiver

A = effective area of telescope primary mirror (m^2)

$\Delta\lambda_D$ = detector bandwidth (nm)

$\Delta\lambda_f$ = fluorescence bandwidth (20 nm)

θ_r = receiver field of view (rad)

θ_l = laser beam divergence (rad)

n = density of chlorophyll _a_ (molecules/m^3)

σ_f = effective fluorescence cross section (m^2)

P_o = laser output power (W)

λ_l = laser wavelength (nm)

α = attenuation coefficient of water (m^{-1})

P_{rec} = fluorescent power received (W)

and subscripts f and ℓ refer to fluorescence and laser wavelengths, respectively. If all algae were equally excited at a given wavelength, then the upper form of the equation (for single σ f) would be appropriate. As previously shown, algae of each color group possess different cross sections and therefore the bottom form of the LIDAR equation is required. Since the algae color groups have different fluorescence excitation spectra, the use of four wavelengths yields four equations. These equations can thus be solved simultaneously to yield the unknown chlorophyll _a_ concentration contained in each color algae. In matrix form this can be expressed as

$$\begin{bmatrix} P_{rec}(\lambda_1) \\ \cdot \\ \cdot \\ \cdot \\ P_{rec}(\lambda_4) \end{bmatrix} = C_1 \begin{bmatrix} \frac{P_o(\lambda_1)}{\alpha_f + \alpha_1} & 0 & \cdots & 0 \\ 0 & \frac{P_o(\lambda_2)}{\alpha_f + \alpha_2} & \cdots & 0 \\ 0 & 0 & \cdots & \frac{P_o(\lambda_4)}{\alpha_f + \alpha_4} \end{bmatrix} \begin{bmatrix} \sigma_{f1}(\lambda_1) & \cdots & \sigma_{f4}(\lambda_1) \\ \cdot & & \cdot \\ \cdot & & \cdot \\ \cdot & & \cdot \\ \sigma_{f1}(\lambda_4) & \cdots & \sigma_{f4}(\lambda_4) \end{bmatrix} \begin{bmatrix} n_1 \\ \cdot \\ \cdot \\ \cdot \\ n_4 \end{bmatrix}$$

or

$$\begin{bmatrix} P_{rec}(\lambda_1) \\ \cdot \\ \cdot \\ \cdot \\ P_{rec}(\lambda_4) \end{bmatrix} = C_1 \pi\chi \begin{bmatrix} n_1 \\ \cdot \\ \cdot \\ \cdot \\ n_4 \end{bmatrix}$$

Therefore

$$\begin{bmatrix} n_1 \\ \cdot \\ \cdot \\ \cdot \\ n_4 \end{bmatrix} = C_1^{-1}\, \chi^{-1}\, \pi^{-1} \begin{Bmatrix} P_{rec}(\lambda_1) \\ \cdot \\ \cdot \\ \cdot \\ P_{rec}(\lambda_4) \end{Bmatrix}$$

The elements contained in the χ matrix are obtained from the cross-section measurements previously described. The laser power at each wavelength can be measured and controlled. Accurate knowledge of α at all the appropriate wavelengths is essential for quantitative determination of chlorophyll a concentration. Since $\alpha_f > \alpha_e$ for all laser wavelengths under consideration (450 nm-650nm), and the optical window of water decreases with increased wavelength, at least α_f must be known to yield quantitative measurements. In open waters, data are available indicating that α does not vary rapidly in time or space. In estuarine and coastal waters, changes are more rapid and frequent measurements of α must be obtained.

Assuming α is known or measurable, the above matrix technique can be used to determine the concentration of chlorophyll a in the algae present in a body of water and the distribution of chlorophyll a in different color groups.

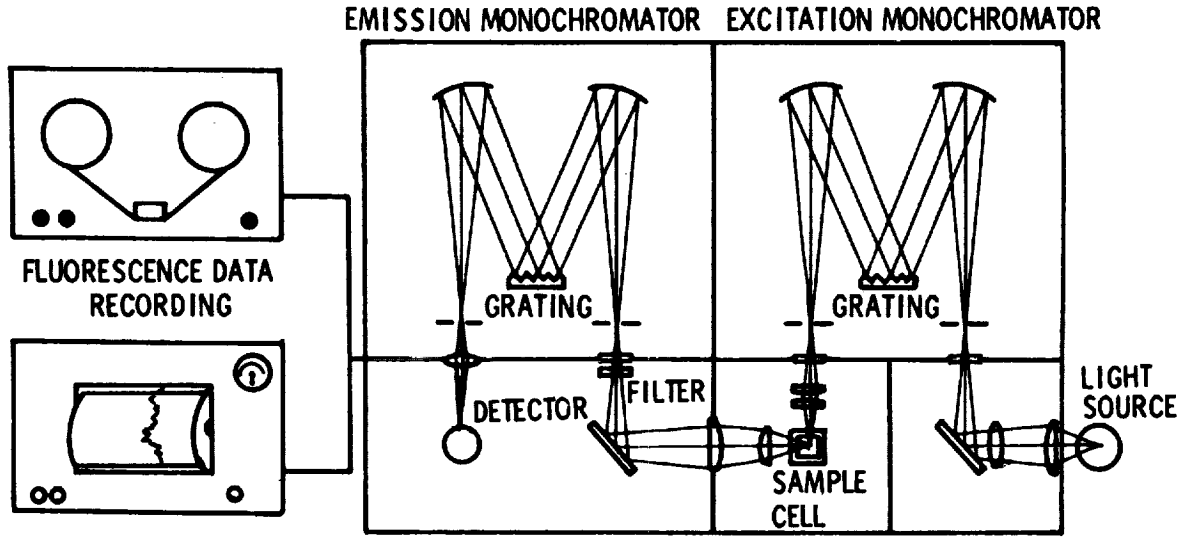

Figure 1. Laboratory apparatus used in fluorescence and emission studies

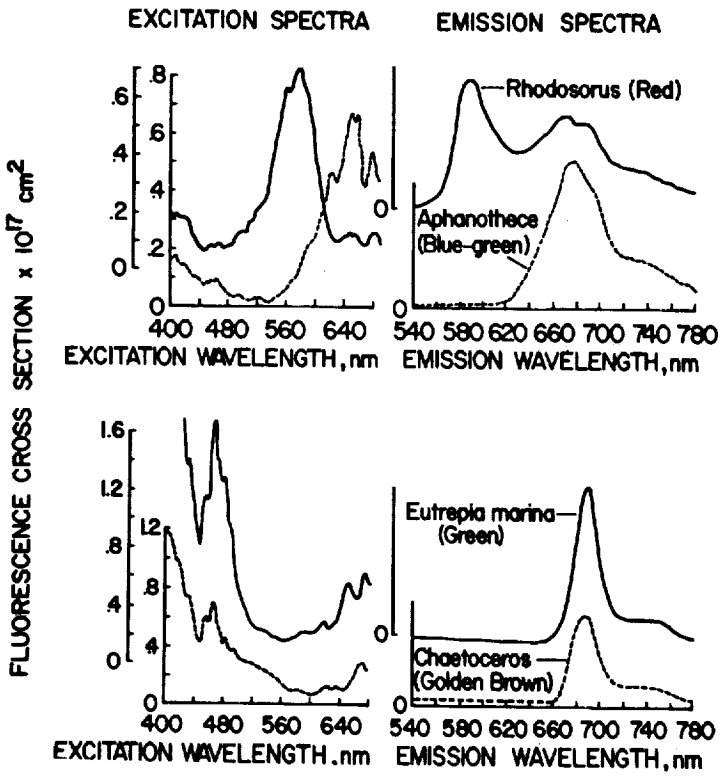

Figure 2. Typical fluorescence cross-sections and emission spectra of red, blue-green, green, and golden brown algae samples

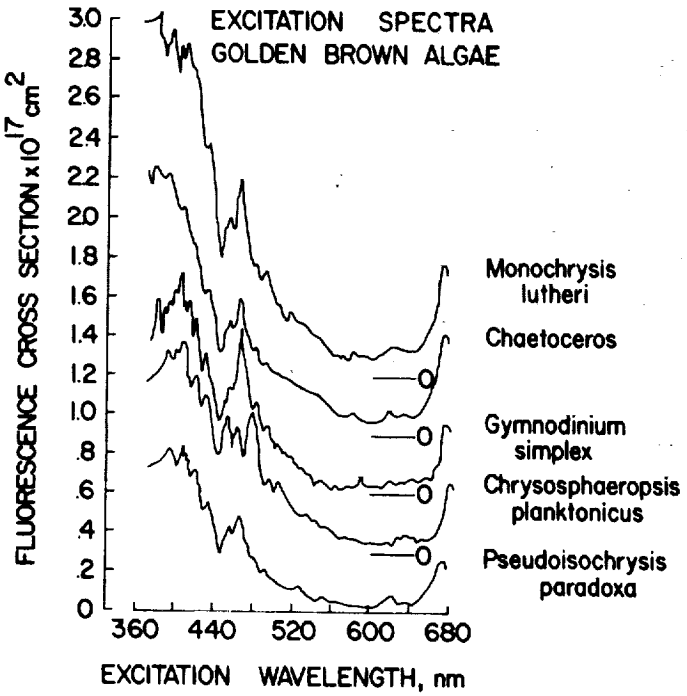

Figure 3. Effective fluorescence cross-sections of chlorophyll a in golden brown algae. Data shown are normalized to single molecule values with a 5 nm resolution.

MULTIWAVELENGTH LIDAR INSTRUMENT

Figure 4 shows a schematic of the airborne LIDAR system which has been designed and fabricated at Langley Research Center to demonstrate the multiwavelength concept of chlorophyll a detection. The laser used in the system is a unique four-color dye laser pumped by a single linear xenon flashlamp. Figure 5 shows a cross-sectional view of the laser head. The head consists of four elliptical cylinders spaced 90° apart with a common focal axis. The linear flashlamp is placed along this axis and its radiant emission is equally divided and focused into the dye cuvettes located on the surrounding focal axes. Fluorescent dyes form the active medium for the four separate dye lasers. A rotating intracavity shutter permits only one color at a time to be transmitted downward to the water.

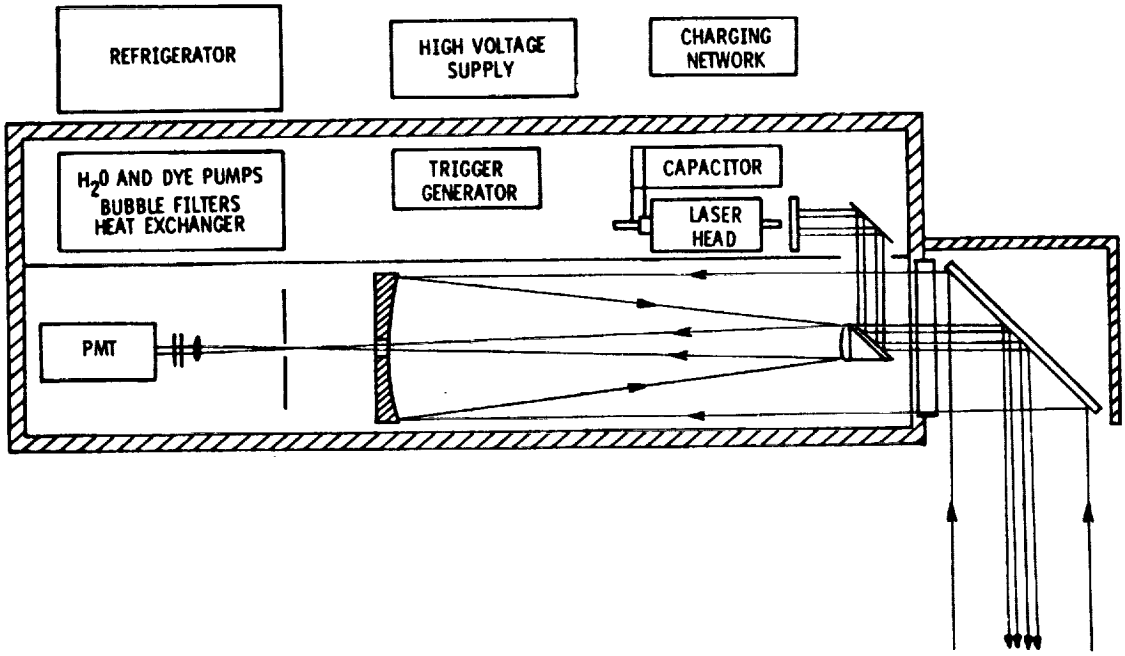

Figure 4. Schematic of the airborne multi-wavelength LIDAR system

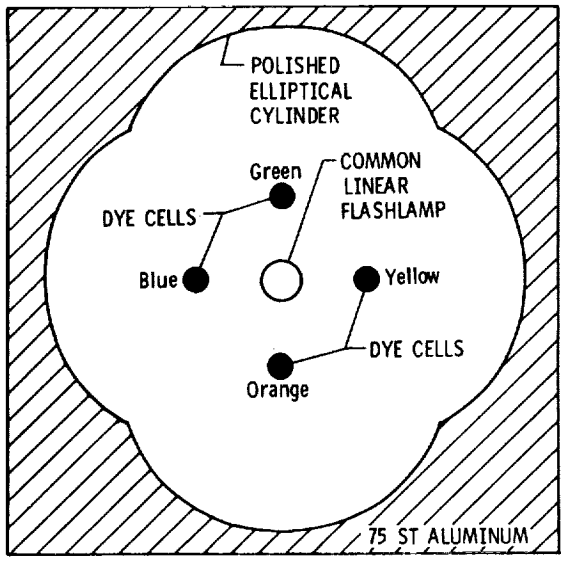

Figure 5. Cross-sectional view of the four-color dye laser used for fluorescence excitation

The resulting fluorescence from the chlorophyll a is collected by a 25.4-cm diameter Dall-Kirkham type telescope. The signal is then passed through a narrow bandpass filter centered at 685 nm and on to the photomultiplier (PMT) tube. The PMT signal is digitized by a waveform digitizer and stored on magnetic tape for later analysis. The dyes and the water for the flashlamp are kept at a uniformly cool temperature by the refrigerator. The high voltage supply, charging network, coaxial capacitor, trigger generator, and a spark gap along with a central control system complete the package. Figure 6 shows the completed system prior to installation in a helicopter for flight evaluation.

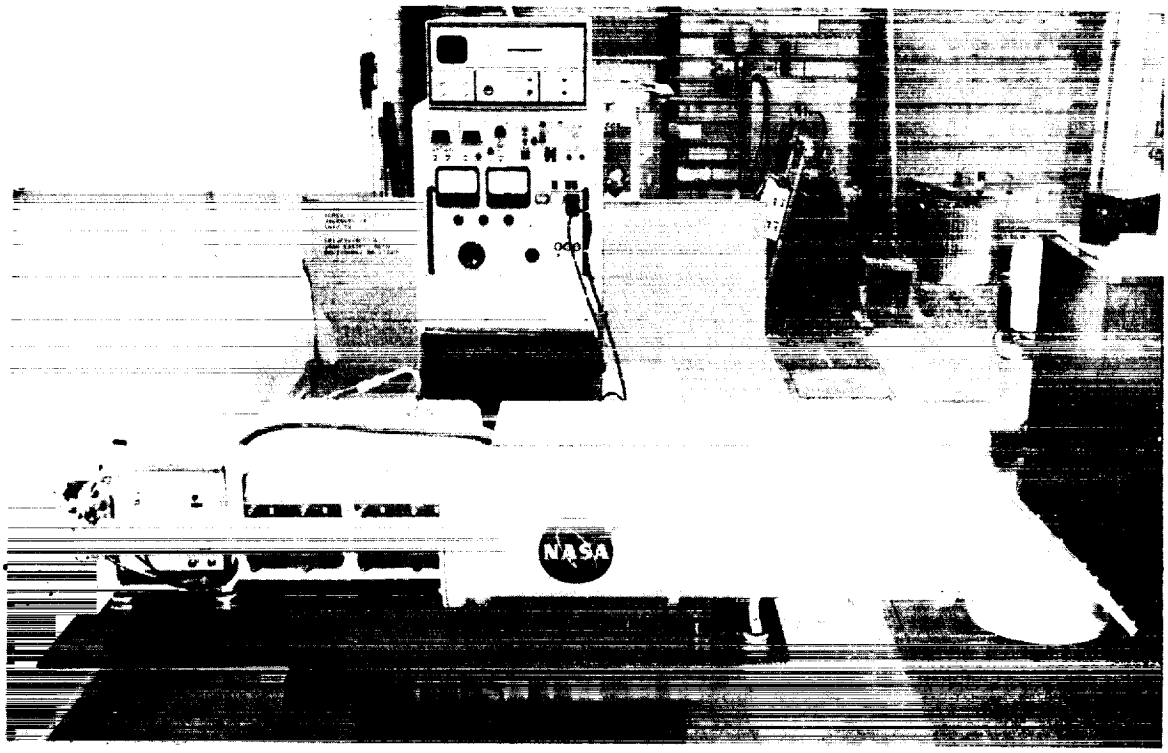

Figure 6. Complete LIDAR package prior to helicopter installation

Field tests have been performed to demonstrate the capabilities of this new technique. Experiments have been conducted from a fixed height platform (George P. Coleman Bridge, Yorktown, Virginia) 30 meters over the York River. This site was selected because it was convenient to both Langley Research Center and the Virginia Institute of Marine Science (VIMS). Ground truth data (chlorophyll a concentration, salinity, and algae species identification) were supplied by VIMS using standard water sampling techniques. The attenuation coefficient (at 632.8 nm) and temperature of the water were measured on site by Langley personnel.

Measurements were made every half-hour on the evening of July 9, 1973, and data are shown in Figure 7 along with ground truth data supplied by VIMS. Chlorophyll a concentrations shown represent the total chlorophyll contribution of all color groups. A bioassay performed by VIMS indicated a dominance of golden-brown (dinoflagellates) and green algae. The ratio of golden-brown to green algae varied over the course of these measurements and was in general agreement with observations obtained with the LIDAR system.

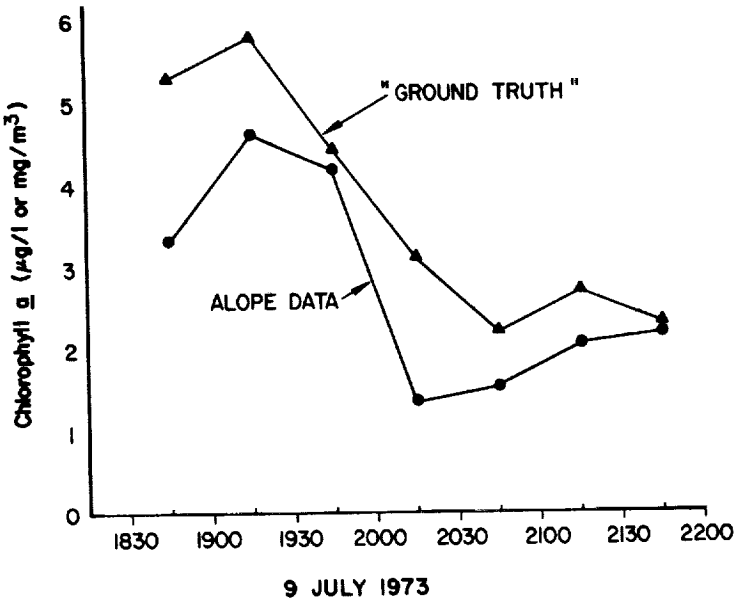

Figure 7. Field data acquired from a fixed height platform over the York River near Yorktown, Virginia

On July 25, 1973, the LIDAR system was successfully flight-tested over the James River between Hampton Roads and the Chickahominy River. Flight altitude was 100 meters and the speed was 120 km/hr. The flight path is shown in Figure 8 along with the chlorophyll a concentration measured over the 138-kilometer roundtrip flight. During each flight leg, the laser was fired at a rate of 0.5 pps. The data plotted in Figure 8 represent average chlorophyll a concentration over each leg. For example, leg No. 16 data represent an average of 63 laser firings of each color or 252 shots total. There is sufficient data, however, from each four-color cycle to determine chlorophyll a content without averaging. In fact, the data collected over the entire flight (approximately 75 minutes long) represent nearly 500 separate chlorophyll a measurements.

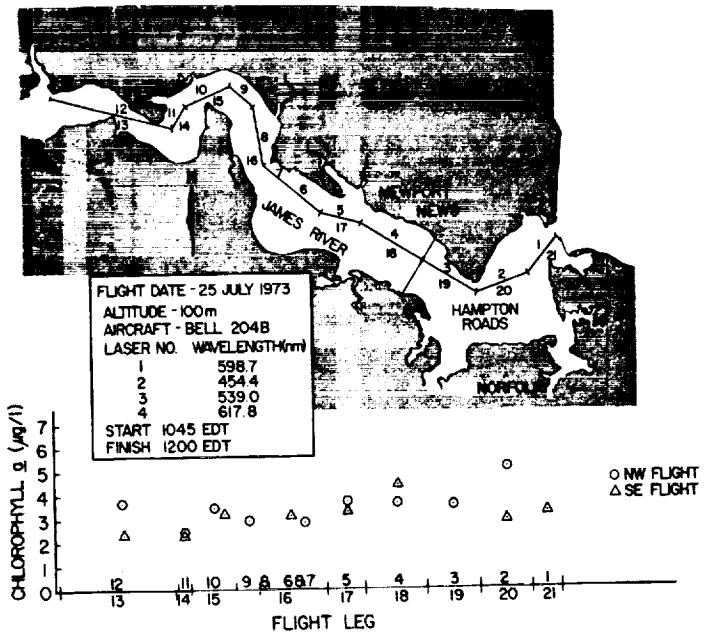

Figure 8. Flight data acquired over the lower James River

SUMMARY AND CONCLUSIONS

A multiwavelength laser fluorosensor has been developed to remotely measure chlorophyll a concentration in living algae in natural waters. Preliminary field operation of the instrument and technique has been demonstrated from both fixed height and airborne platforms. The maximum operational altitude of the present system is approximately 300 meters (estimate based on data acquired at 100 meters). Laser energies varied with color from 0.6 mJ (454.4 nm) to 7.15 mJ (598.7 nm). These values are well within the eye safe limits at the operational altitude of 100 meters. Greater energies could be employed to accommodate higher altitude operation. System stability appears to be excellent as evidenced by the fact that laser alignment has remained constant for over six months.

The major disadvantage of all optical remote sensors of water constituents is their dependence on foreknowledge of α (or its components "a" and "s" due to absorption and scattering, respectively) to make quantitative measurements. This is true for the multiwavelength LIDAR technique as well. Data can only be analyzed quantitatively when α is known. Studies are now underway to determine the feasibility of remote α measurements by LIDAR techniques. It may be possible, with slight instrument modifications, to monitor α simultaneously with the chlorophyll a concentration.

ACKNOWLEDGMENTS

The authors are grateful for the cooperation of Drs. Franklin Ott and Robert Jordan of the Virginia Institute of Marine Science for obtaining laboratory algae sample and ground truth data and to Messrs. L. G. Burney, C. S. Gilliland, and B. T. McAlexander of NASA Langley Research Center for their assistance in the design, fabrication, and testing of the LIDAR flight instrument.

THE FLUORESCENCE OF CHLOROPHYLL AND YELLOW SUBSTANCES IN NATURAL WATERS: A NOTE ON THE PROBLEMS OF MEASUREMENT AND THE IMPORTANCE OF THEIR REMOTE SENSING

Charles S. Yentsch
University of Massachusetts

In other publications, I have emphasized that there are two chromophylls which, if sensed remotely from high altitude, would revolutionize our ability to survey large areas of the world's oceans. The chromophylls of importance are: the photosynthetic pigments of plankton algae and a group of organic materials frequently termed "dissolved yellow substances". These are derived from plants and carried into the ocean by fresh water inflow.

Using water color as an index when attempting to estimate the concentration of these chromophylls, an immediate problem is that the attenuation characteristics of each overlap (Figure 1). The attenuation of light by phytoplankton (P) is characterized by two distinctive bands (450, 675 nm) which represent absorption by chloroplastic pigments. Yellow substances (Y) are characterized by a strong ultraviolet absorption which "tails" over into the visible region. In combination with the chromatic characteristics of pure water, these two chromophylls characterize the color of natural waters. The problem is that the specific influence by either substances is not easily distinguished. Because of this "competitive absorption" one might suggest that chlorophyll should be remotely sensed at long wavelengths (i.e.,675 nm) - where yellow substance absorption is minimal. The difficulty with this approach is that a very weak backscattered signal occurs at these wavelengths, primarily because of intense absorption of light at long wavelengths by water alone.

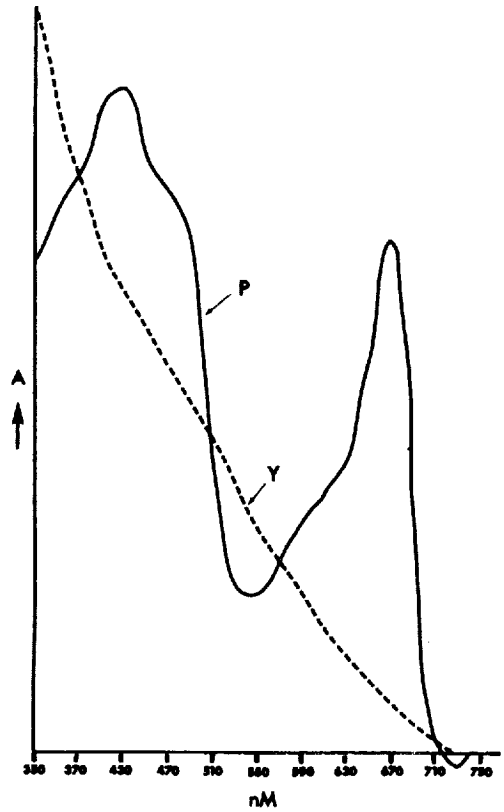

Figure 1. The attentuation of light by phytoplankton (P) and dissolved yellow substances (Y).

One might also think that competitive absorption would not be much of a problem in the open ocean. Here waters of high salinity would be relatively free of yellow substance; hence, chlorophyll detection (via color change) would not be complicated by the presence of yellow substance. Unfortunately, this is not the case. The attenuation characteristics of particulate matter from the open ocean show that in addition to phytoplankton (Figure 2, note peak at 675 nm), there are particles which strongly attenuate at short wavelengths which is again the characteristic of yellow substances.

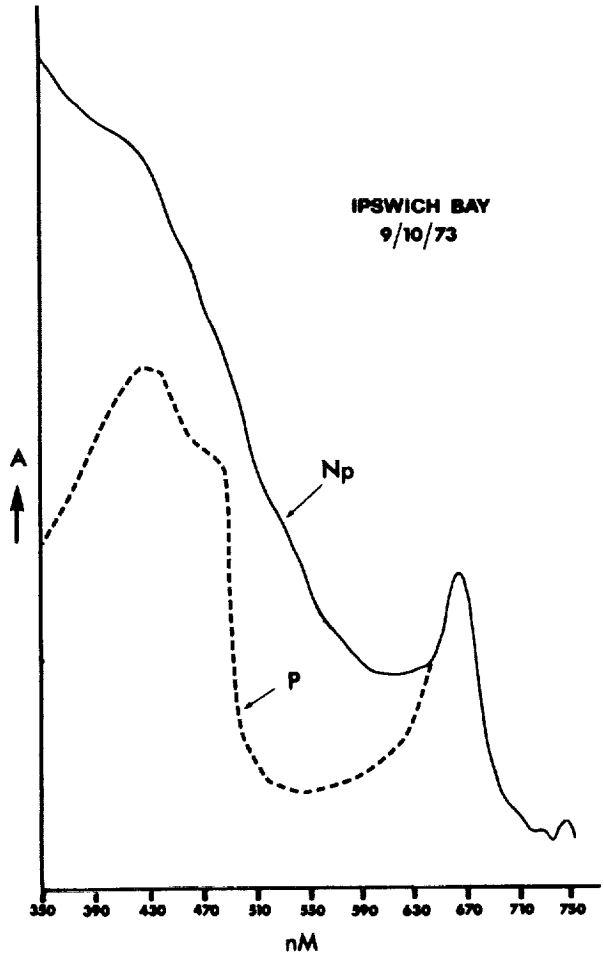

Figure 2. The attenuation of light by particulate matter (NP) from coastal water, and phytoplankton (P). (In the former, note the high attenuation at short wave length).

A means of minimizing competitive absorption is by the use of fluorescence. Fortunately, the chloroplastic pigments and yellow substances are fluorophores, and their excitation and emission characteristics are different. For example, the fluorescence characteristics for naturally occurring particulate matter is shown in Figure 3. It should be noted that this is the same sample whose attenuation characteristics are shown in Figure 2. The fluorescence analysis (excitation spectra) resolves the difference between light absorption by phytoplankton as opposed to the other particulate organics. Furthermore, Figure 4 shows excitation and emission characteristics of dissolved yellow substances are different from chloroplastic fluorescence. One can distinguish between the two chromophylls by exciting at 350 nm and measuring fluorescence at 500 nm, to measure yellow substance, and by exciting at 450 nm and measuring fluorescence at 675 nm, to measure chlorophyll.

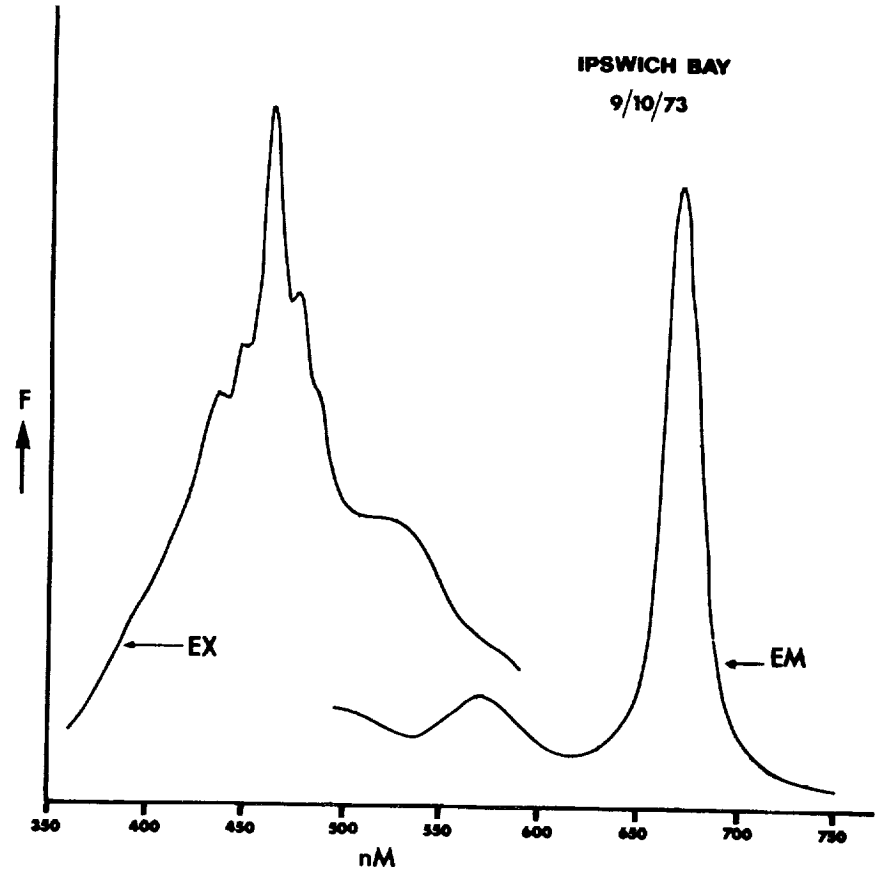

Figure 3. Fluorescence excitation and emission characteristics of particulate matter from coastal water. (Curves are uncorrected for phototube response.)

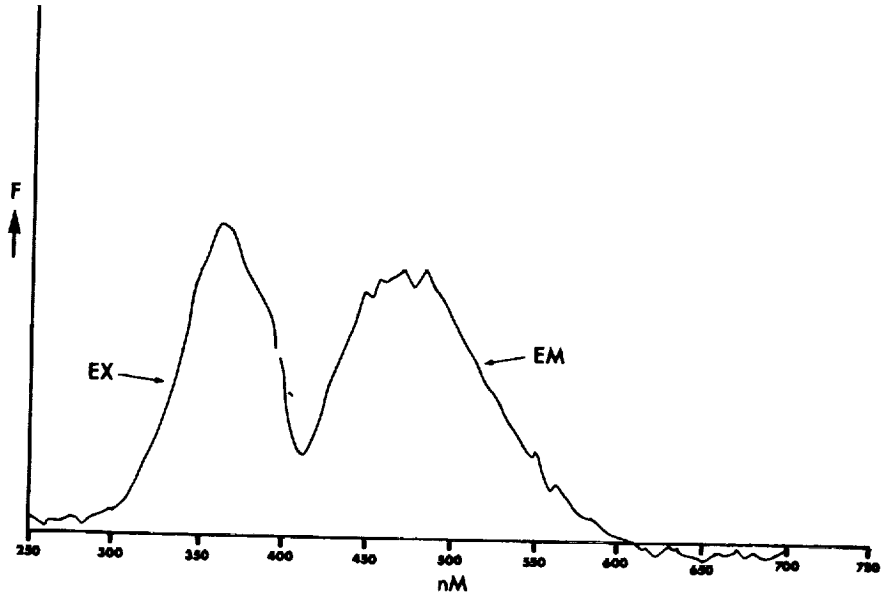

Figure 4. Fluorescence excitation ane emission characteristics dissolved yellow substances from coastal waters.

Many of you sitting in the audience are probably thinking: OK, we can distinguish between the two. Of what use is this? The answer can only be completed by emphasizing the importance of each measurement. The relationship between ocean productivity (chlorophyll) and the distribution of pelagic fishes has been emphasized as a means of scouting fields for commercial catch. In coastal water, it has also been emphasized that chlorophyll determination (via water color) would be a unique technique for the estimation of the extent of eutrophication. I should like to emphasize the importance of the latter, which when armed with the ability to sense the amount of fresh water in the coastal zone, offers the means of assessment of the source of the problem. This is where sensing yellow substance becomes of importance. In a sense, one can think of the amounts of yellow substances as a colorimetric or fluorometric indicator* of fresh water...or to put it simply, the source of the organics is largely through fresh water run-off situations. Figure 5 is an example of how chlorophyll and yellow substances are used as environmental indicators. The section of stations runs from the mouth of the Merrimack River out some 35 miles to sea. The influence of the river in coastal waters is shown by low salinities and high yellow substances near the coast. The reasons for the high productivity (high chlorophyll) is that the river is heavily polluted. Thus, the source of eutrophication of the coastal waters is traced either by salinity or yellow substance to the Merrimack River.

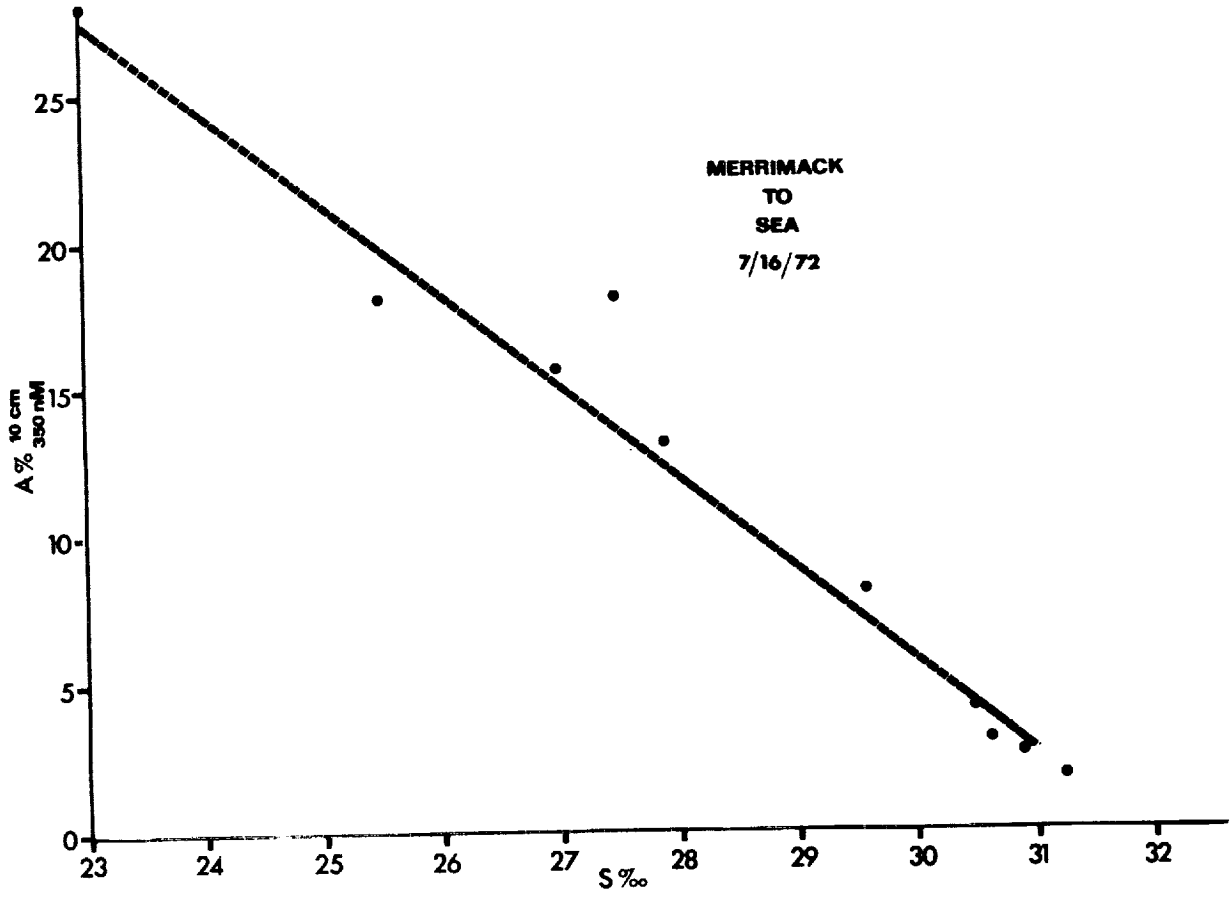

Figure 5. A section of observations of chlorophyll and yellow substance extending from the mouth of the Merrimack River into the Gulf of Maine.

*Light absorption at 350 nm and fluorescence at 500 nm are directly related.

You might ask, can organic compounds such as yellow substances truly serve as a conservative indicator of salinity? To put it another way, why is it not decomposed? The answer to this lies in the unknown organic structure of these compounds and their biochemical relationships. However, for the sake of this discussion, a comparison between yellow substances and salinity shows a surprisingly close correlation (Figure 6), one which could be used to estimate the percentage of fresh water (Merrimack) throughout this section.

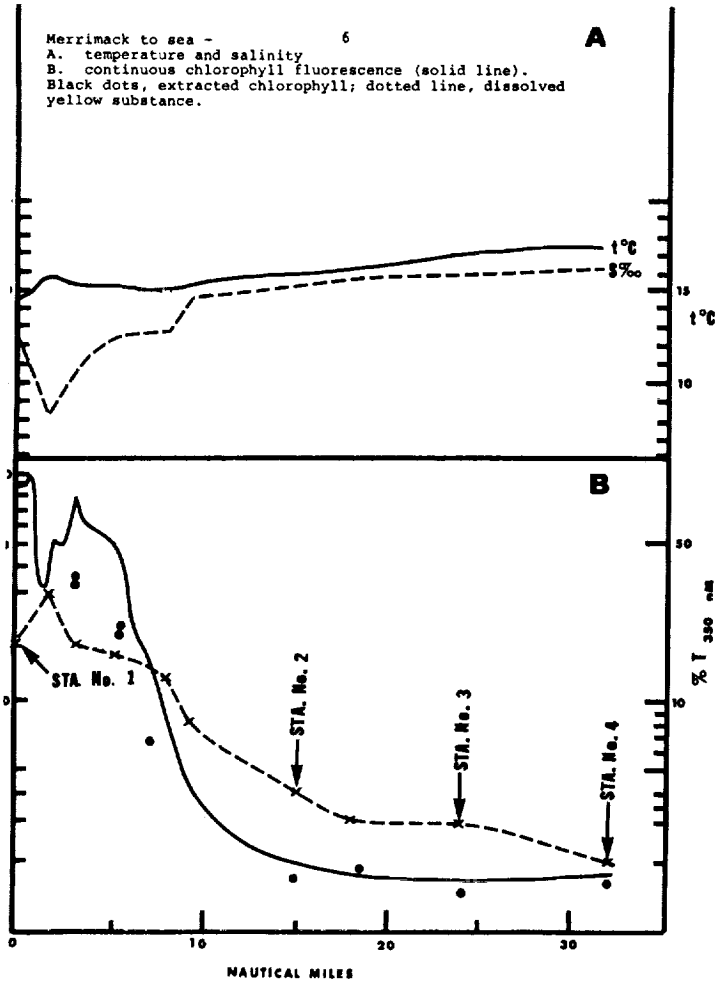

Figure 6. Comparison of salinity and dissolved yellow substance.

In conclusion, the high altitude observer equipped with temperature, chlorophyll and yellow substance sensors has the possibility of detecting the magnitude of eutrophication and its sources in coastal waters. The laser induced fluorescent devices are likely the technical means, and as they become available, I predict they will become a major tool in coastal zone management.

LIFES: LASER INDUCED FLUORESCENCE AND ENVIRONMENTAL SENSING

Wayne R. Houston, D. G. Stephenson, and Raymond M. Measures
University of Toronto - Institute for Aerospace Studies

ABSTRACT

A laboratory investigation has been conducted to evaluate the detection and identification capabilities of "laser induced fluorescence" as a remote sensing technique for the marine environment. The relative merits of fluorescence parameters including emission and excitation profiles, intensity and lifetime measurements are discussed in relation to the identification of specific targets of the marine environment including crude oils, refined petroleum products, fish oils and algae. Temporal profiles displaying the variation of lifetime with emission wavelength have proven to add a new dimension of specificity and simplicity to the technique.

INTRODUCTION

Laser induced fluorescence represents a powerful new tool for investigating the environment. A number of groups in the last year or so have indicated that this technique may be employed for the remote detection of several broad classes of targets (Ref. 1, 2, 3, 4). In an earlier paper at this meeting, Dr. Bristow described the field results obtained with the prototype laser fluorosensor developed at the University of Toronto Institute for Aerospace Studies (UTIAS). Our recent activity has concentrated upon exploring the identification potential of this new kind of remote sensor. We have been able to demonstrate that a tunable laser fluorosensor may enable the API gravity of a sample of crude oil to be determined fairly directly. A study of the variation in the fluorescence lifetime with emission wavelength has revealed a new kind of spectral signature that could have significant ramifications in the field of remote sensing.

LASER INDUCED FLUORESCENCE PARAMETERS

Several features of laser induced fluorescence possess potential information relating to the target under excitation. However, in order that a measured parameter be specific to a constituent of interest, the fluorescence observed must be either solely from that constituent, or easily discriminated from background fluorescence. This condition can be satisfied in any one of the four sets of circumstances described below.

(1) The target has no background medium (e.g. an optically thick oil spill on water).

(2) The quantum yield of the background medium is extremely small compared to the component of interest.

(3) The laser wavelength, λ^{ℓ}, is tuned so as to only excite the constituent under observation.

(4) The fluorescence wavelength, λ, is selected so as to arise only from the component of interest.

The amplitude of the fluorescence within a given spectral interval is the simplest parameter to monitor; however, its usefulness is very limited since its interpretation is both complex (requiring a thorough knowledge of the instrumental calibration, geometrical situation and the medium under investigation) and in many instances ambiguous. The emission spectrum represents some improvement, for although the spectral response function of the photodetection system has to be known, it is possible with this approach to detect the presence of broad classes of targets under limited conditions. A further improvement in specificity can be attained from a study of the excitation profiles. These spectral signatures can be generated using a tunable dye laser to sweep the exciting frequency through the absorption band of the target under consideration.*

In many ways measurement of the fluorescence lifetime of the medium under study represents both a simple and informative parameter. Such an approach can only be used when the optical depth of the medium is small enough that the lifetime is much larger than the double transit time through the medium. In order to be able to ascertain the lifetime associated with the returned radiation, allowance has to be made for the finite response time of the system.

*If the target is optically thick to the laser radiation and the attenuation is absorption dominated (as opposed to scatter dominated), saturation prevents the emission amplitude from reflecting the true excitation profile (see Ref. 3, p.5 and Ref. 5, p. 226).

The laser backscattered radiation as observed through the photodetection system was used to evaluate the instrumental response function. A best fit to this curve was then obtained and a series of profiles generated to simulate the convolution of this response function with a number of exponential decay curves of the form:

$$f(t) = \frac{1}{\tau} e^{-t/r}$$

where τ is the fluorescence lifetime of the constituent of interest. The full width at half maximum, t_w, for this set of synthesized waveforms was then plotted against τ to yield the simple relation

$$\tau \approx 1.26\ t_w - 6.75\ (\text{nsec}).$$

Figure 1 illustrates the experimental fit to both the synthesized response function and a fluorescence decay curve with a lifetime of 6.5 nsec.

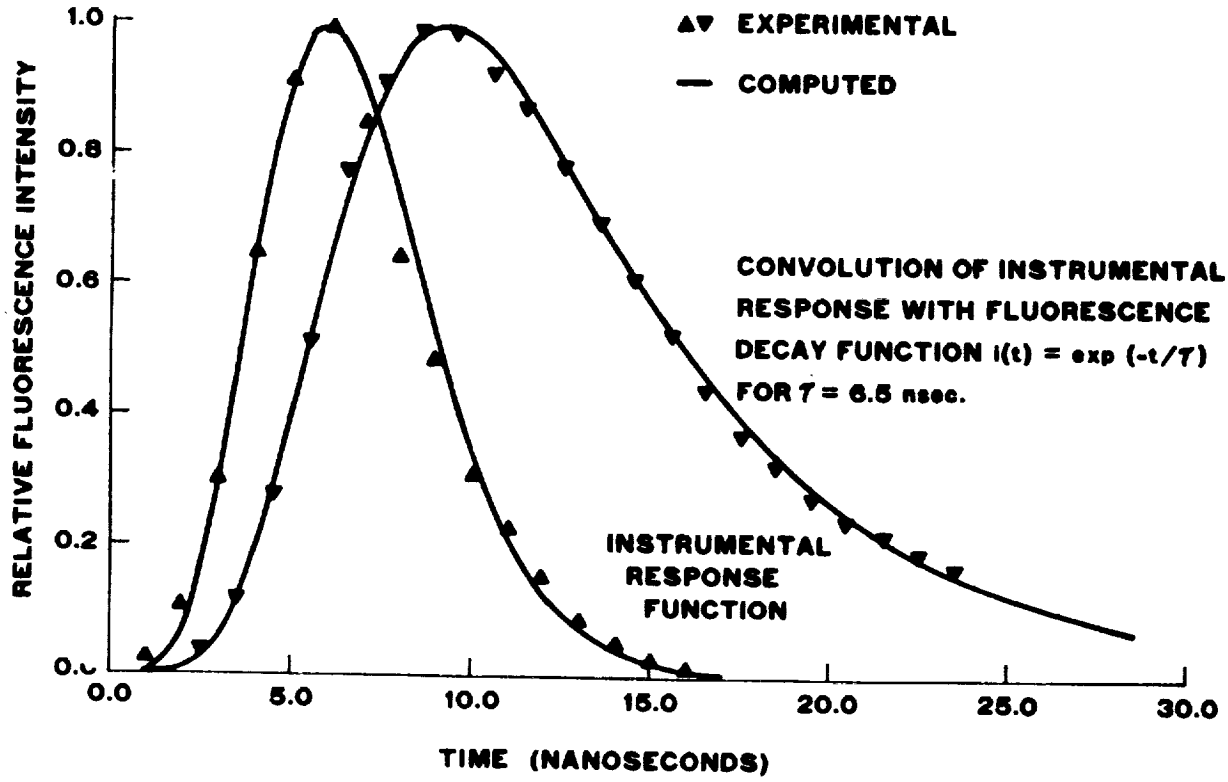

Figure 1. Instrumental response and typical convoluted fluorescence signal shape

INSTRUMENTATION

Spectrofluorometer.-- Profiles of fluorescence emission were recorded using an Aminco SPF-125S spectrofluorometer. This instrument utilized a 150 W xenon high pressure DC arc lamp as the source of excitation. For analysis of optically thick samples, a modified sample compartment provided for normal incidence of the excitation beam and near normal angle of view of the fluorescence emission. The excitation and emission monochromator gratings were blazed at 300 nm and 500 nm respectively, and the photomultiplier was a Hamamatsu (HTV) R446S having modified S-20 response.

Tunable Laser Fluorosensor.-- The tunable laser fluorosensor is illustrated in Figure 2. The main distinguishing feature of this fluorosensor was that it provided a selection of two wavelengths of excitation, 347 nm and 460 nm. These particular wavelengths were chosen in order to accommodate that range of crude oil absorption wavelengths expected. The 347 nm excitation was provided by a TRG-104A second harmonic ruby laser. Typical output pulses had peak powers from 150 to 450 kw and full width at half maximum of 17 nsec. Approximately 8% of the above power was actually used for fluorescence excitation, while the main portion was used to optically pump an organic dye laser, which in turn, furnished the 460 nm radiation. The dye laser, shown in the schematic of Figure 2, had an approximate conversion efficiency of 6%, a range of tunability from 440 nm to 480 nm, and spectral bandwidth of about 1.5 nm. The detection of fluorescence was accomplished using an optical glass objective lens (14.5 cm DIA., 33 cm F.L.), and an EMI-9781B photomultiplier, together with appropriate filters. The ruby laser power was monitored by an E.G. & G. SD-100 photodiode. The photomultiplier and photodiode signals were displayed on the upper and lower beams, respectively, of a Tektronix Type 556 oscilloscope.

The targets studied using this instrumentation included several types of crude oil spills on a 91.5 cm depth of water, located 1.5 metre from the fluorosensor. The water tank used a 50 cm DIA. stainless steel lining for low fluorescence yield, and was outfitted with an overhead mirror placed at 45° to the horizontal plane.

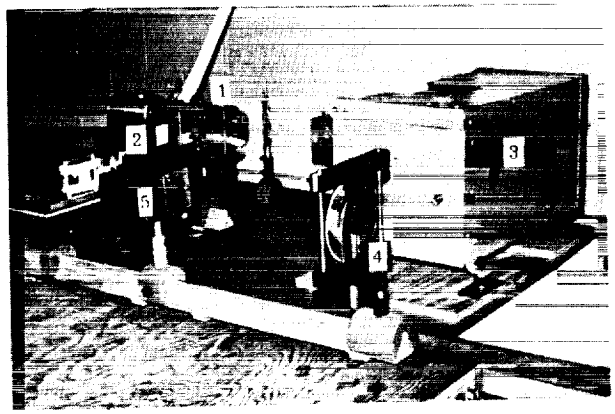

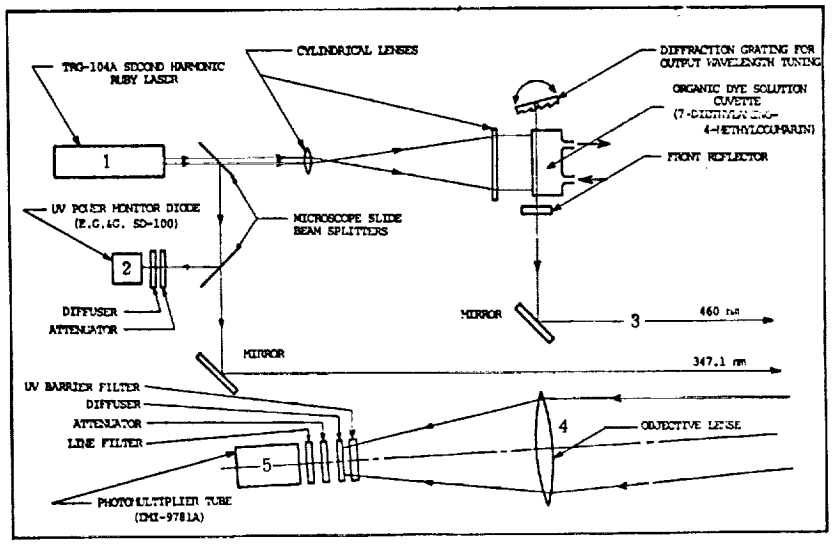

Figure 2. Photograph and schematic of the tunable laser fluorosensor

Short Pulse Laser Fluorosensor.-- The short pulse laser fluorosensor, which was used in fluorescence lifetime determinations, is illustrated in Figure 3. The source of excitation was a modified Phase-R model N250 nitrogen laser having 337.1 nm output pulses of 1 kw peak power, 4.0 nsec full width at half maximum, and repetition rate up to 20 pps, shown in Figure 4. The fluorescence from the target was collected by a quartz lens and focused on the entrance slit of a Spex 1700 II monochromator. A Schott KV-370 filter was used to block stray scattered laser radiation. The monochromator bandwidth was about 3.0 nm. The monochromated light was then detected using an EMI-9781B photomultiplier, and the resultant pulse was displayed on a Tektronix 7704 oscilloscope having 150 MHz bandwidth. The angle of 35° between the laser beam direction and the detector line of sight was chosen in such a

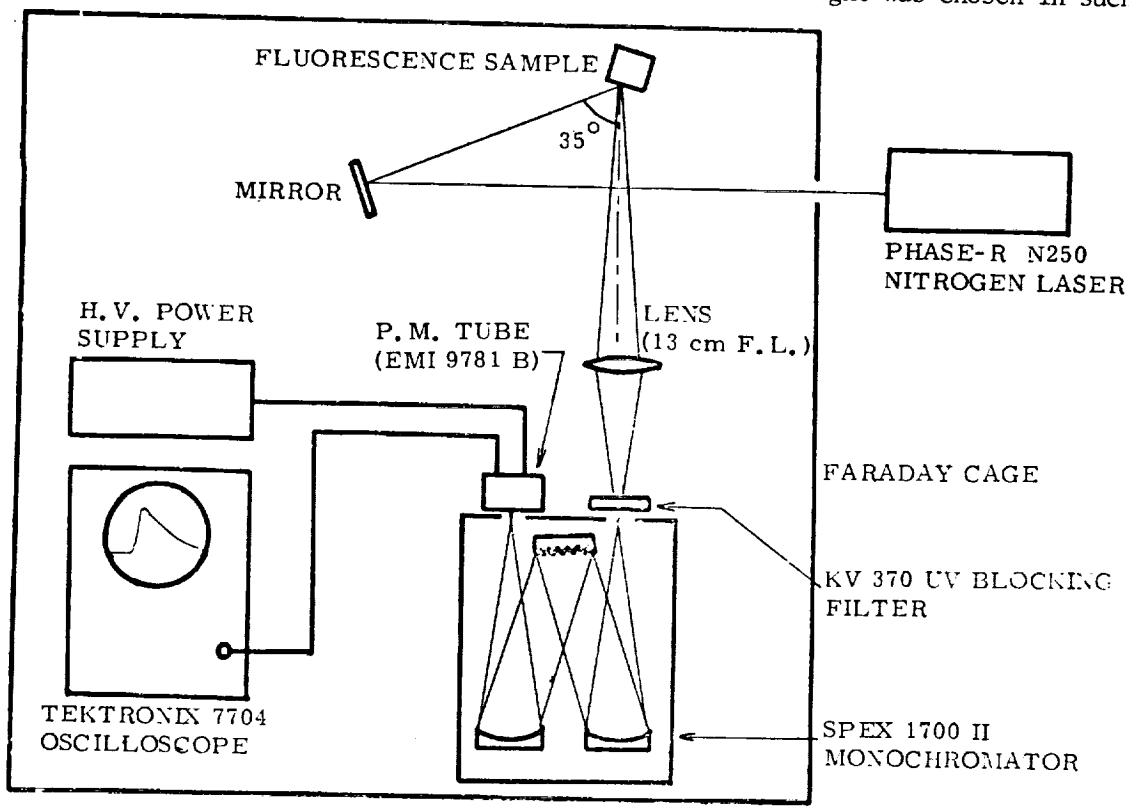

Figure 3. Schematic of fluorescence lifetime measurement apparatus

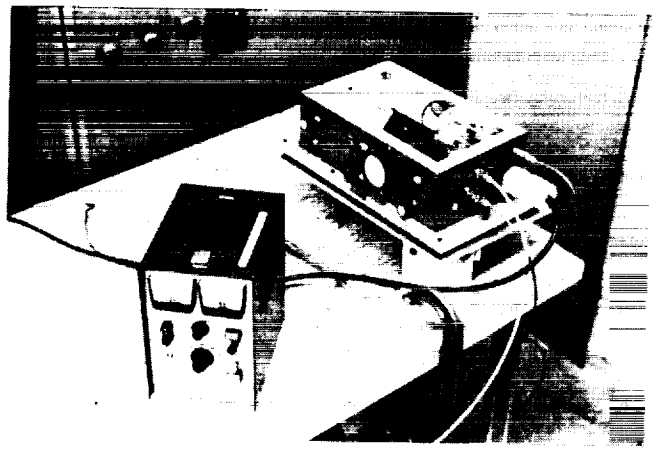

Figure 4. The Phase-R N250 nitrogen laser and associated equipment

way as to abolish polarization effects which distort the exponential nature of the fluorescence decay being detected. (The nitrogen laser output was polarized parallel to the plane containing the laser beam and the detector line of sight.)

EXPERIMENTAL RESULTS AND DISCUSSION

Crude Petroleum Oils

Sample Description.-- A list of the crude oil samples studied, together with their API gravities, peak emission wavelengths and fluorescence lifetimes is presented in TABLE 1.

TABLE 1.-PETROLEUM CRUDE OIL SAMPLE DESCRIPTION

SAMPLE NUMBER	OIL TYPE	ORIGIN	SUPPLIER	GRAVITY (°API)	PEAK EMISSION WAVELENGTH, λ_p (nm)	FLUORESCENCE LIFETIME AT λ_p (nsec)
6	BUNKER C		IMP. OIL	16.7±.2	525 ± 2	2.4 ± .2
14	CHAUVIN CRUDE		B.P.	26.0	477	2.1
1	MED. CRUDE	ANGOLA	GULF	26.4	456	2.9
9	MIDALE CRUDE	SASK.	TEXACO	30.1	460	2.0
13	CABINDA CRUDE	ANGOLA	GULF	30.2	470	3.8
15i	MIDALE CRUDE	SASK.	SHELL	30.3	458	2.4
3	MED. CRUDE	SASK.	SHELL	31.0	454	2.4
10	NSO	ALBERTA	B.P.	36.0	454	3.9
15iv	IP CRUDE	ALBERTA	SHELL	37.3	465	3.9
12	SPECIAL BLEND	ALBERTA	TEXACO	38.0	468	5.5
4	SOUR CRUDE	ALBERTA	SHELL	38.9	440	4.1
11	LEDUC CRUDE	WEST.CAN.	IMP. OIL	39.8	465	6.5

Excitation wavelength was 337.1 nm in all cases.

Emission Profiles and Relative Intensity.-- Emission profiles for the crude oil samples were generated by the spectrofluorometer, using an excitation wavelength of 337.1 nm. This wavelength was chosen to simulate nitrogen laser excitation. Five examples of the crude oil emission profiles are presented in Figure 5. Excitation and emission monochromator bandwidths are indicated on the figure. The Schott UG-11 filter was placed at the output of the excitation monochromator in order to block the low level broad band unmonochromated leakage emitted from the excitation side of the instrument. The Schott KV-370 "cut-on" filter was placed at the input to the emission side in order to block scattered ultraviolet radiation. Note that the emission profiles peak in the range from 450 to 550 nm and have bandwidths (FWHM) of about 150 nm. The variation in peak emission wavelength among different samples is sufficient to permit a small degree of identification potential. When peak emission wavelength is plotted against the oil API gravity, a rough trend first reported by Fantasia et al (Ref. 4) becomes apparent: lighter oils fluorescence at shorter wavelengths. However, the trend is not pronounced enough to be used for remote determination of oil API gravity. Clearly, other parameters would be required to remotely identify a specific oil type.

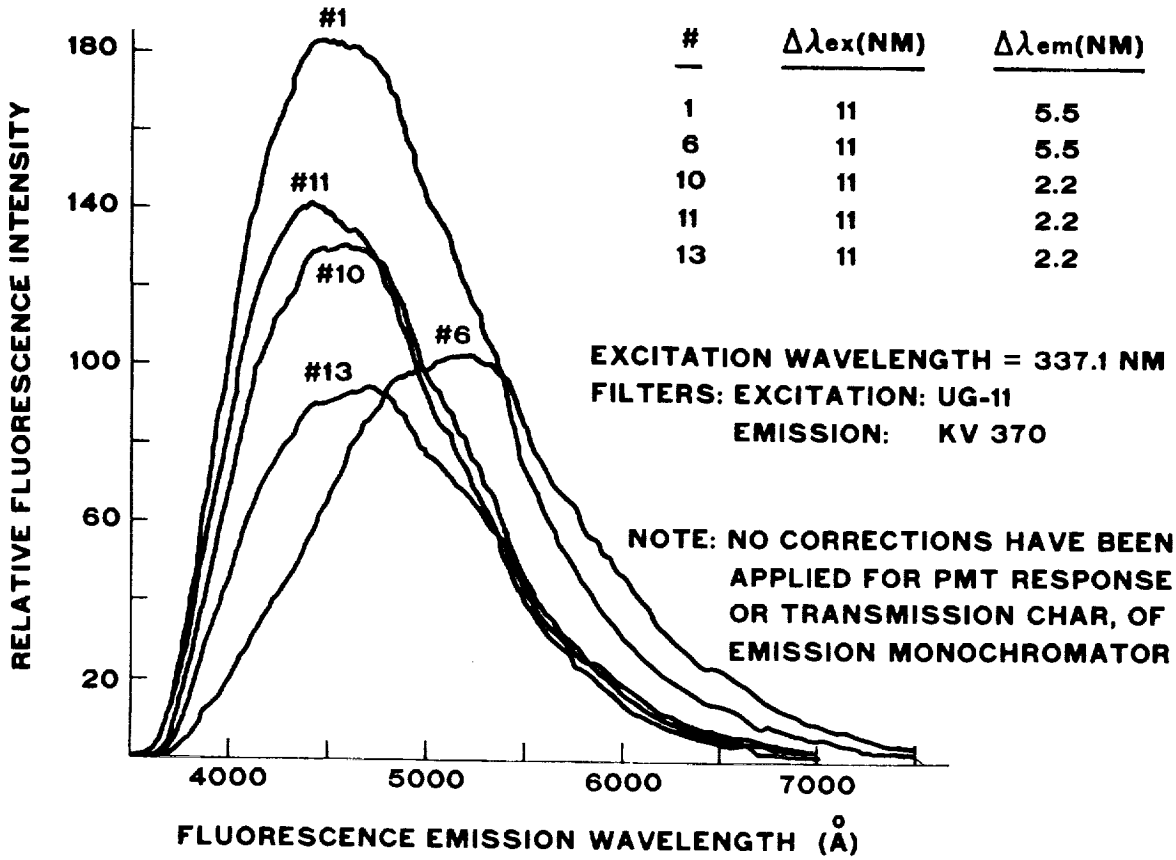

Figure 5. Fluorescence spectra of crude oils

If the relative intensity, measured at the peak emission wavelength, is plotted against API gravity, another rough trend develops; as pointed out by Fantasia et al (Ref. 4), the intensity increases as the API number increases. Once again, this trend is not predictable enough to be used by itself to identify the oil type. Furthermore, the inherent difficulty in remotely measuring the relative intensity makes this parameter unattractive for identification purposes. Nevertheless, intensity can be used as a non-specific detection parameter.

Excitation Profiles.-- According to the work of Fantasia et al (Ref. 4), peak excitation wavelengths for crude oils vary from 350 to 450 nm. In addition, a rough trend was observed in that lighter oils had progressively shorter peak excitation wavelengths. With a view to checking these results, and to assessing the remote sensing potential of this phenomenon, the "tunable laser fluorosensor" (see paragraph two under Instrumentation) was employed. For each of four crude oil samples, two measurements of the fluorescence intensity were made at a fixed emission wavelength of 567 nm; the first measurement $F(\lambda_1, \lambda_F)$ resulted from 347.1 nm excitation (second harmonic of ruby laser) while the second measurement $F(\lambda_2, \lambda_F)$ resulted from 460 nm dye laser excitation. Since the relative intensities are proportional to the corresponding excitation coefficients (Ref. 3), the ratio $F(\lambda_1, \lambda_F)/F(\lambda_2, \lambda_F)$ will reflect the shape of the excitation profile for each of the samples investigated. Since the wavelengths, λ_1 and λ_2, were chosen to encompass the range of excitation profiles likely to be encountered, one would expect, in the light of the results of Ref. 4, that $F(\lambda_1, \lambda_F)/F(\lambda_2, \lambda_F)$ should increase as the API gravity number increases. The results obtained, as shown in Figure 6, verify this expected trend.

It is reasonable to expect that use of a dye laser having a large range of tunability (e.g. coumarin dyes with exciplex operation (Ref. 5)), should enable one to locate the peak excitation wavelengths rapidly and accurately in order to extend the identification potential of the technique.

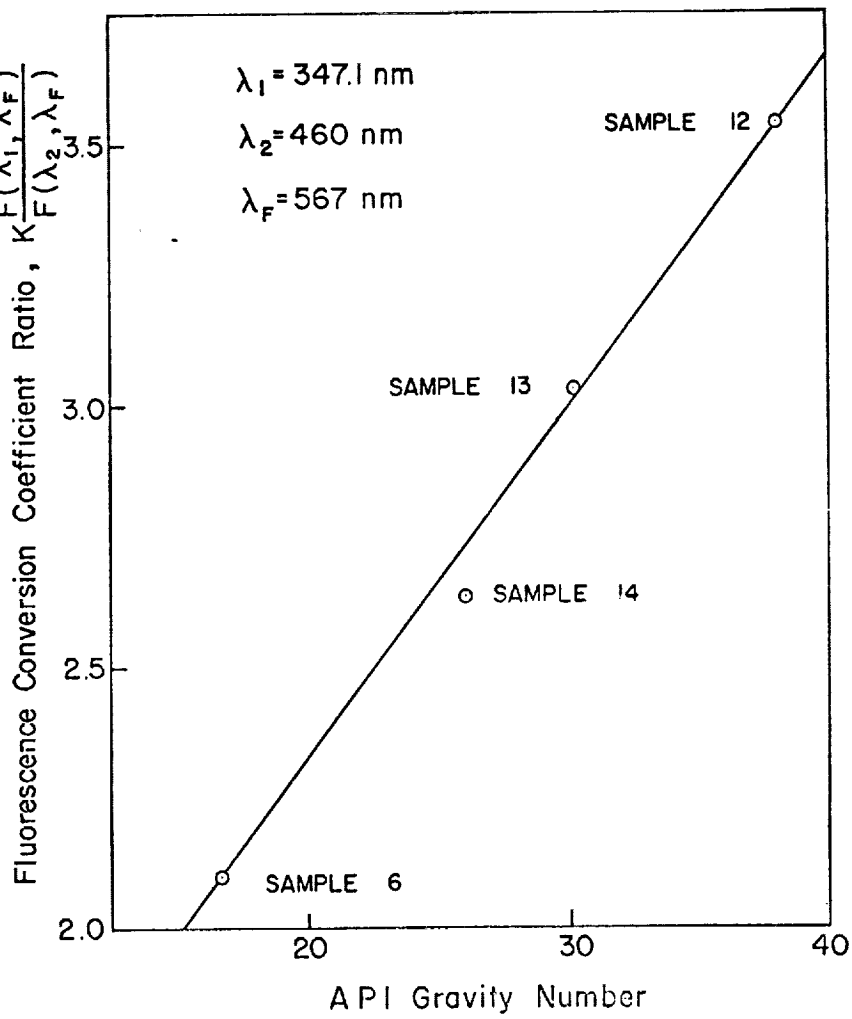

Figure 6. Fluorescence ratios vs. oil sample API gravity indicating the identification potential of the alternating excitation wavelength technique

Lifetimes.-- Using the short pulse laser fluorosensor, the fluorescence lifetime was measured at emission wavelength intervals throughout the emission profiles of each crude oil sample. In Figure 7, temporal decay spectra are presented for five representative crude oils. Note that for each sample, the lifetime increases monotonically with emission wavelength. Note also that from sample to sample, the lifetime increases with increasing API number. This lifetime variation with API is in agreement with the preliminary investigation of Fantasia et al (Ref. 4); however, their lifetime measurements are suspected to include large experimental errors as a result of an incorrect deconvolution procedure (Ref. 6).

A comparison of Figures 5 and 7 leads one to immediately appreciate the higher quality of information available from the lifetime-spectral signatures. It is obvious from Figure 5, that it would be very difficult to distinguish between four of the oil samples on the basis of their emission profiles; on the other hand, Figure 7 shows that these samples could readily be distinguished from a study of their decay characteristics as a function of wavelength. It should be noted that in a practical airborne system, the exact measurement of a lifetime is not necessary, owing to the virtually linear relationship between pulse width and lifetime. Consequently, any laser fluorosensor having appropriate temporal resolution should detect the above trends without need for extensive instrument calibration.

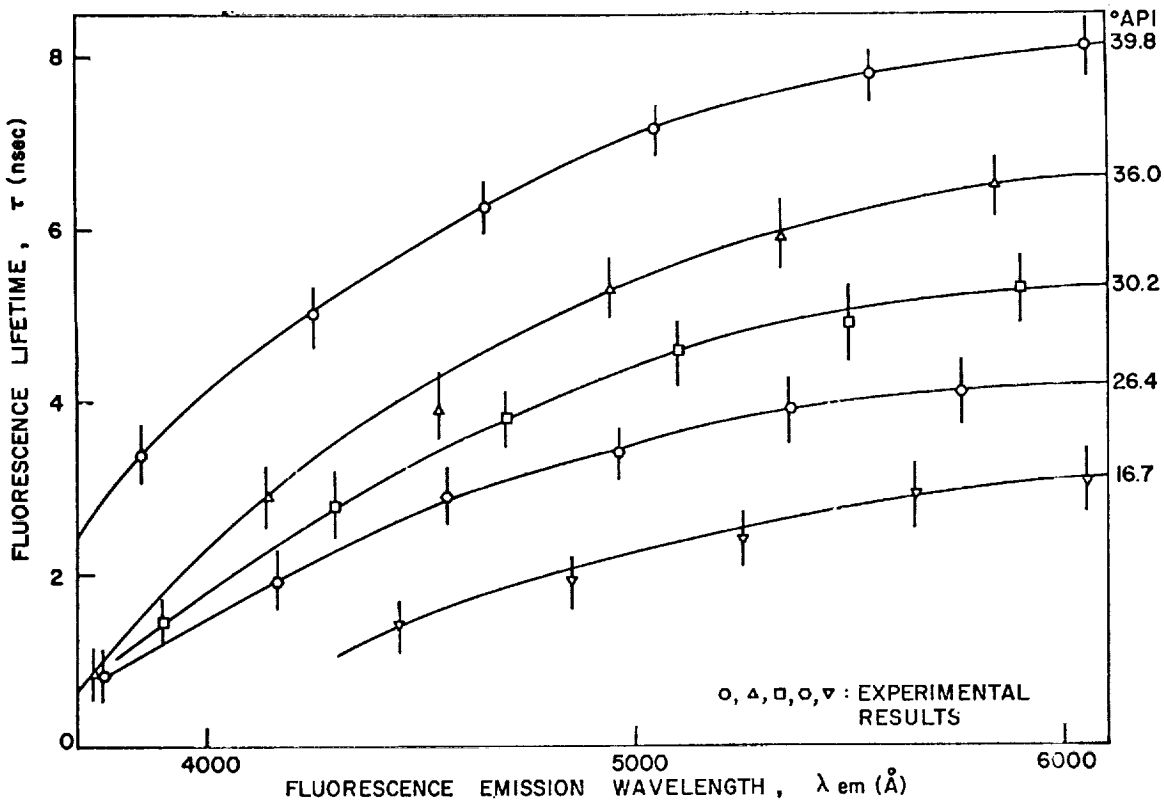

Figure 7. Variation of fluorescence lifetime with emission wavelength for crude oils

Mixing Effects.-- With a view to investigating the effect of mixing crude oils, samples 10 and 6 were mixed in a 1:1 ratio and in a 2:1 ratio. It was found that the resultant emission and lifetime profiles for these mixtures were identical to those profiles computed on a weighted average basis. Similarly, the resultant API numbers were identical to the weighted average of the parent crude oil API numbers. These results are not surprising in view of the fact that crude oils are mechanical mixtures of many components. However, thee results confirm that discrimination of different oil types comprising a well-mixed oil slick would be impossible.

Aging Effects.-- With regard to the effects of aging on fluorescence parameters, we have found that exposure of a crude oil spill to air results in no detectable alteration in the emission profile. However, both relative intensity and temporal profile are subject to changes. Five representative crude oil samples were poured into aluminum weighing dishes and their relative intensities at peak emission wavelength, and temporal profiles, were measured after zero, 24, 48, 72 and 96 hours of air exposure. In parallel, the same tests were duplicated for 1 mm thick oil slicks on a 1 cm depth of tap water.

The intensity variations observed are summarized in Figure 8. Notice that all samples displayed a decrease in intensity, approaching some limiting value after 96 hours of exposure. In each case, the limiting value was approximately 70% of the initial intensity.

The changes in temporal profile observed for sample 11 are presented in Figure 9. Note that the lifetime decreased by about 1.5 nsec across the spectrum, reaching a steady value after about 72 hours. In addition, the temporal profile developed a dip about 505 nm, after 48 hours of aging. Samples 1 and 6 developed similar dips in the temporal profile, at 455 and 485 nm respectively. On the other hand, samples 10 and 13 developed no temporal profile dips, but decreased in lifetime by 2.0 and 1.0 nsec, respectively, across the spectrum.

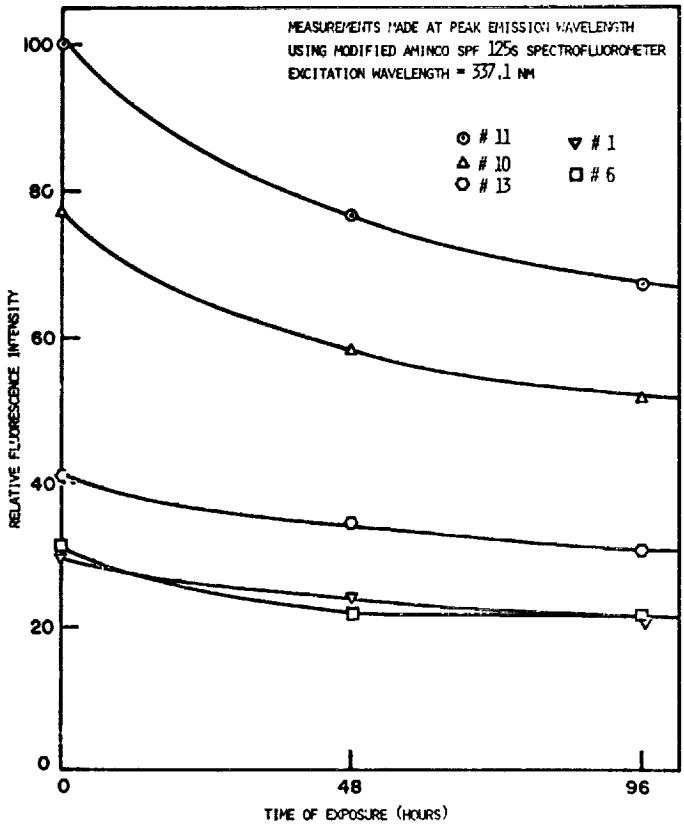

Figure 8. Variation of fluorescence intensity with time of exposure for petroleum crude oils

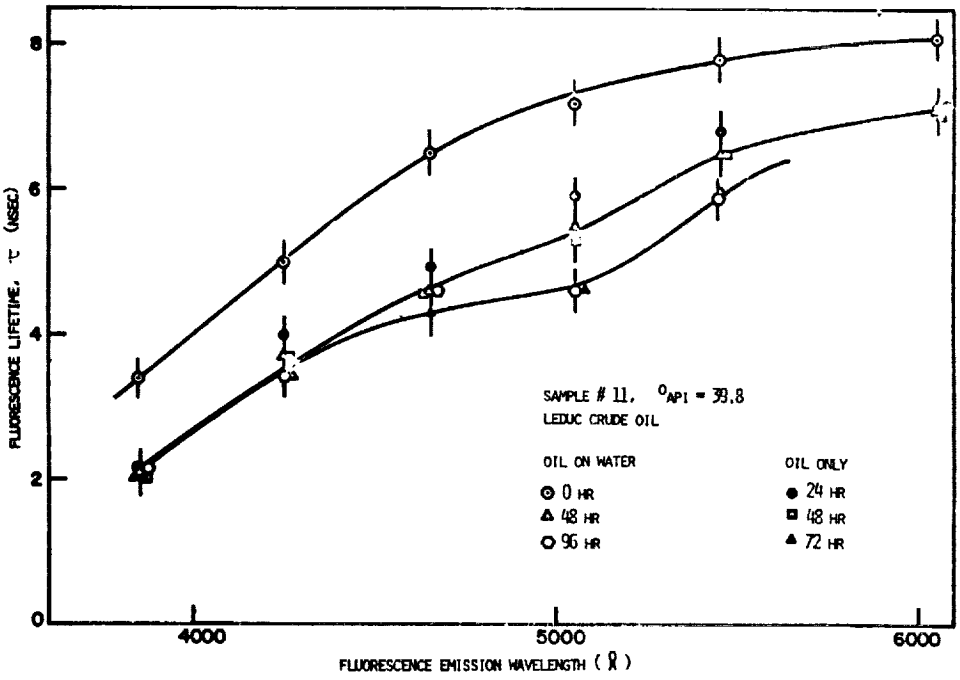

Figure 9. Effect of exposure on fluorescence lifetimes of a crude oil

It was found that the crude oil spills on water displayed the same aging behavior as the pure oil samples. Hence, no special effects due to dissolution were noted for the 1 nm oil slicks considered.

Clearly, the effects of aging can complicate the problem of identification of crude oil types. However, these effects may be useful if identification has already been accomplished, since the aging effects can be used to estimate the time of occurrence of a spill. Of course, this potential is all but completely lost after 96 hours.

Refined Petroleum Products.-- The fluorescence parameters for five refined products, supplied by Imperial Oil Ltd., were determined. Measurements of emission profile and relative intensity were carried out using the spectrofluorometer. The emission profiles obtained are presented in Figure 10. Lifetime measurements at 400 nm were made using the short pulse laser fluorosensor. The lifetimes, relative intensities, and relevant emission profile parameters are summarized in TABLE 2.
The peak emission wavelengths for all five samples were quite near 400 nm being, in general, much shorter than for crude oils. The bandwidths, all approximately 60 nm, are about one-half the corresponding values for crude oils. The values of relative intensity were of the same order of magnitude as the crude oils, but did not differ greatly from sample to sample. The fluorescence lifetimes were generally much longer than for crude oils, and displayed a marked variation from sample to sample, as shown in TABLE 2.

It is evident from the results for the limited number of samples studied, that refined products can be differentiated from crude oils using emission profile and lifetime measurements, and that they can be identified more specifically by fluorescence lifetimes measured at 400 nm.

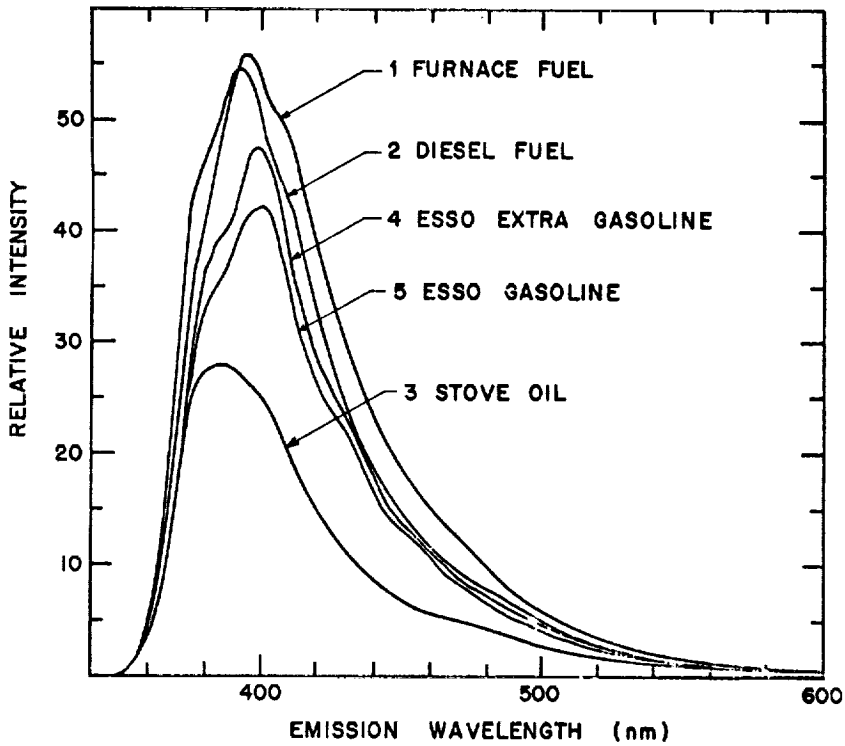

Figure 10. Fluorescence emission profiles for refined petroleum products

TABLE 2.-FLUORESCENCE CHARACTERISTICS OF REFINED PETROLEUM PRODUCTS

SAMPLE	GRAVITY (°API)	PEAK EMISSION WAVELENGTH, λ_p (nm)	PROFILE FWHM (nm)	LIFETIME AT λ_p (nsec)
1. FURNACE FUEL	37.0	395	60	19.8
2. DIESEL FUEL	37.0	393	55	14.1
3. STOVE OIL	42.3	382	56	9.4
4. ESSO EXTRA GASOLINE	55.6	400	57	7.5
5. ESSO GASOLINE	60.8	400	58	7.7

SUPPLIER: Imperial Oil Limited

EXCITATION WAVELENGTH: 337.1 nm

Fish Oils.-- The fish oil samples are described in TABLE 3. Emission profiles generated using the spectrofluorometer are presented in Figure 11. These profiles look very much like those obtained for the crude oils (see Figure 5) having peak emission wavelengths in the 400 to 470 nm range and bandwidths (FWHM) from 120 to 150 nm, with the exception of Flounder and Redfish, where multiple peaks were observed. The relative intensities were also of the same order of magnitude as for crude oils.

TABLE 3.-FISH OIL SAMPLE DESCRIPTION

OIL TYPE	SOURCE	SUPPLIER	GRAVITY (°API)	PEAK EMISSION WAVELENGTH, λ_p (nm)	LIFETIME AT λ_p (nsec)
COD LIVER	NEWFOUNDLAND	FRB	21.15	420 $\pm$ 2	3.7 $\pm$ .3
FLOUNDER BODY	NOVA SCOTIA	NSP	21.55	407 462	5.5 5.5
REDFISH BODY	NOVA SCOTIA	NSP	21.85	388 407	5.9 6.9
HERRING BODY	NOVA SCOTIA	NSP	22.35	470	4.9
HERRING BODY	CHEDABUCTO BAY	FRB	22.4	460	6.5

SUPPLIERS: FRB - Fisheries Research Board, Halifax, Nova Scotia
NSP - National Sea Products Limited, Halifax, Nova Scotia

EXCITATION WAVELENGTH: 337.1 nm

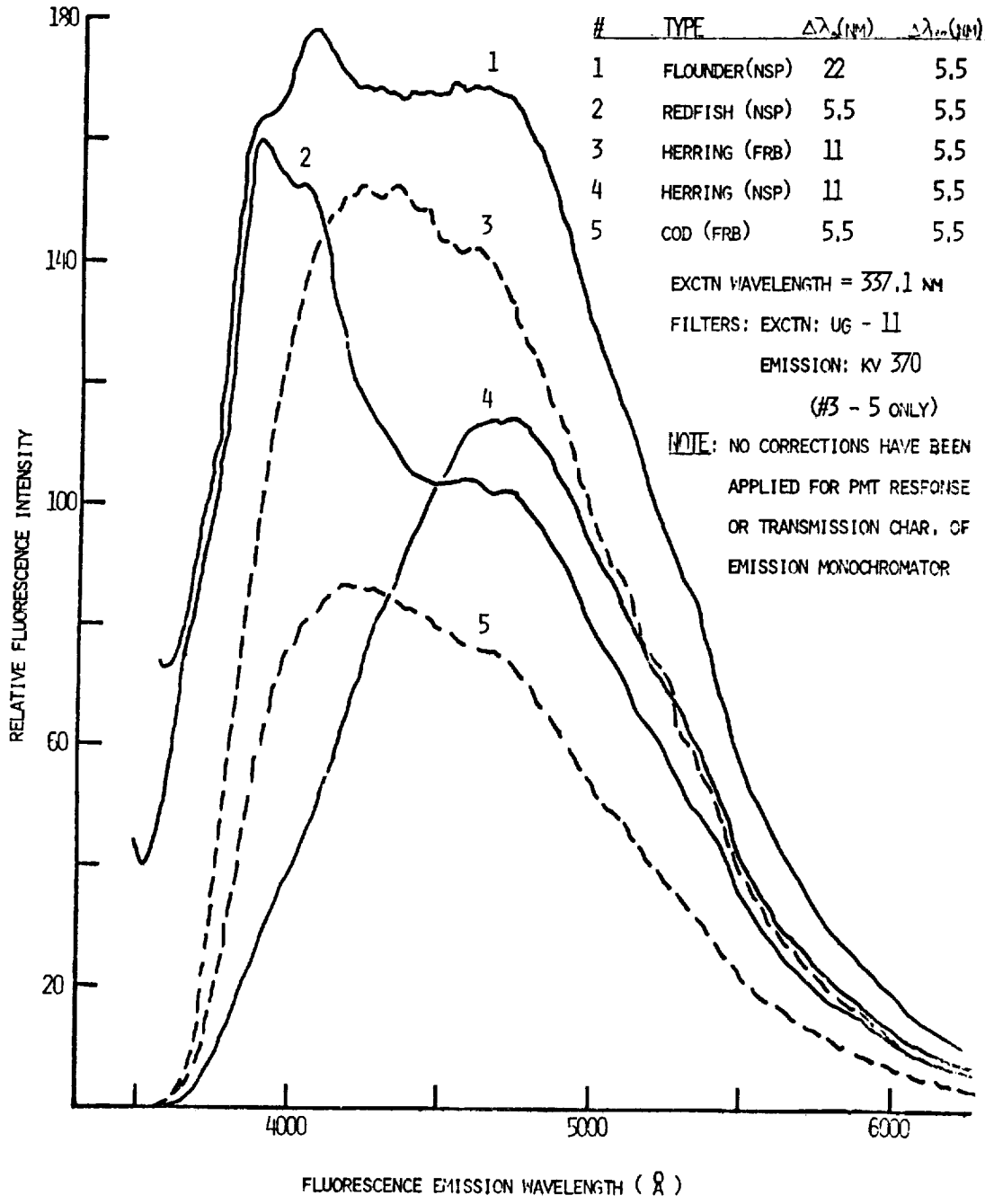

Figure 11. Fluorescence spectra of fish oils

Lifetime profiles were generated for each sample using the short pulse laser fluorosensor. From these results, summarized in Figures 12a and 12b, we can see that although the lifetime values fall into the same range as for crude oils (from 2 to 7 nsec), the shapes of the temporal profiles differ considerably. Where the crude oil temporal profiles increase monotonically (see Figure 7), the fish oil profiles display maxima, minima, and points of inflection.

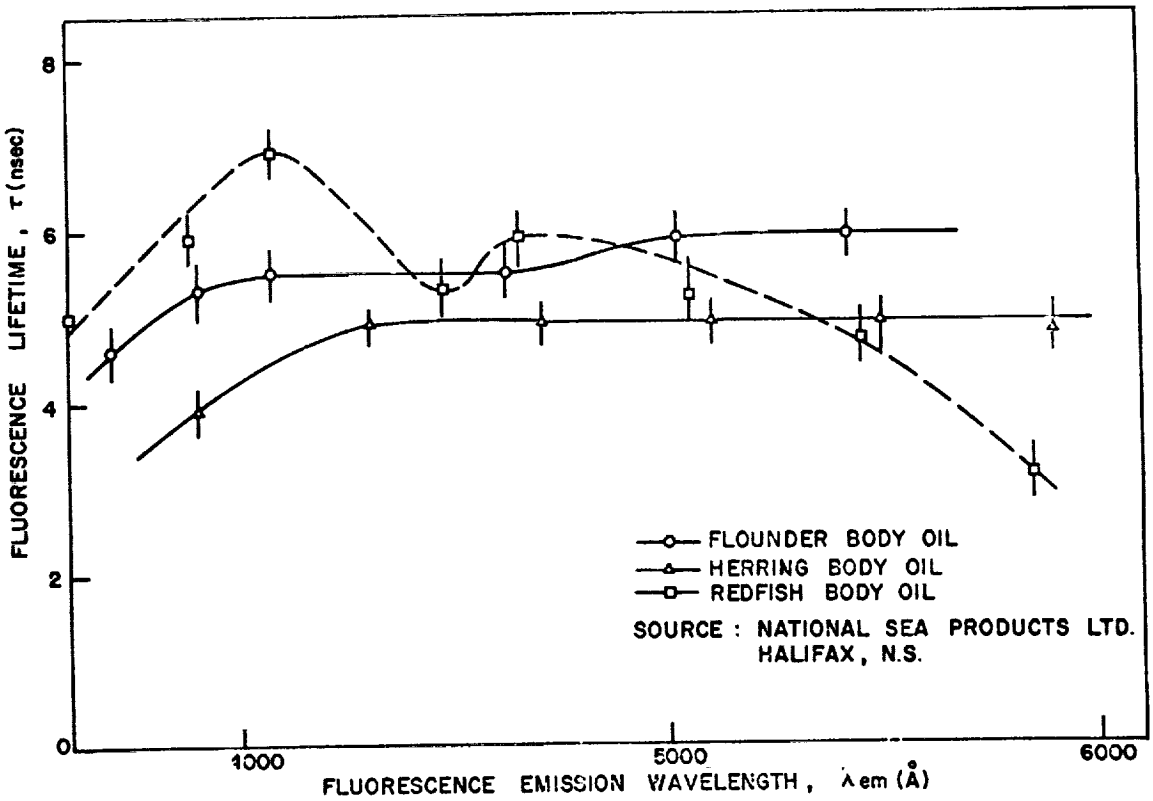

Figure 12a. Variation of fluorescence lifetime with emission wavelength for fish oils

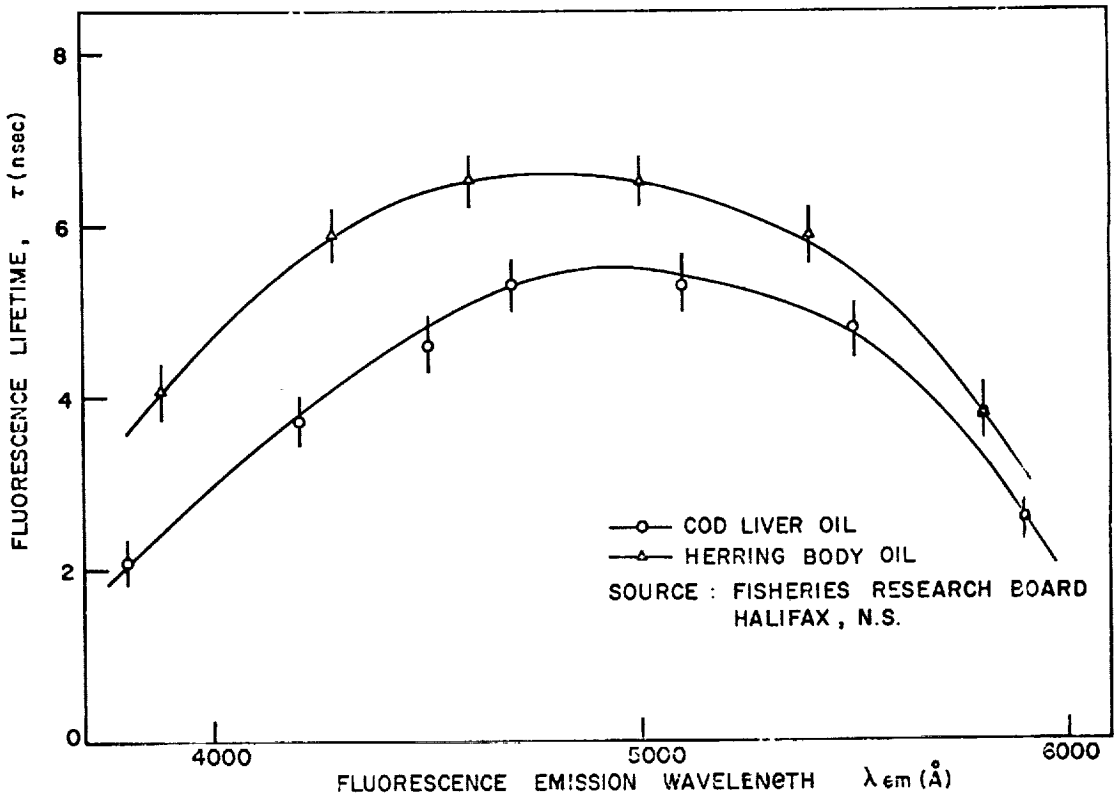

Figure 12b. Variation of fluorescence lifetime with emission wavelength for fish oils

In the light of the above results, it is conceivable for an airborne fluorosensor, equipped only with the emission profile scanning capability, to detect a fluorescent target on the sea, and to identify it as a crude oil, although in reality, a fish oil slick may have been responsible for the signal. Even a lifetime measurement at one emission wavelength may not be sufficient to discount a false alarm. However, a complete lifetime against wavelength profile would ensure positive identification. If a target is identified as a fish oil, the range of variation in emission and temporal profiles studied seems to afford potential for identification of the type of fish oil. However, the task is complicated by other factors, since two similar fish oil types from two different locations may display different spectral and temporal characteristics, as our results have shown for the two Herring oil samples studied.

An aging experiment for fish oil slicks was carried out simultaneously with the crude oil aging experiment, following the same procedure as outlined in "Aging Effects". It was found that the emission profiles, relative intensity, and temporal profiles did not change significantly throughout the 96 hours of exposure to air, although the characteristic fish odors did decrease in strength.

Algae. -- Four algae samples were supplied by the University of Toronto Department of Botany. The two green algae, Chlorella and Tribonema, and the blue-green algae, Phormidium, were prepared in Bold's Basal Medium (BBM) and the brown algae, Nitzchia sp., was prepared in a modified Chu 10 medium. A summary of the analysis for these samples is presented in TABLE 4. The peak excitation and emission wavelengths were determined using the spectrofluorometer, and the fluorescence lifetime for Chlorella was determined using the short pulse laser fluorosensor. The measured lifetime of 1.5 + 0.2 nsec for Chlorella was in agreement with values reported in the literature (Ref. 7). The lifetimes for the other algae were so short that they could not be resolved with our instrumentation. Notice that the peak emission wavelengths of three of the four samples are contained in a 5 nm interval, but that the peak excitation wavelengths are sufficiently different to permit identification. Jarrett et al (Ref. 8) have taken advantage of this fact in designing an algae identification fluorosensor incorporating a four wavelength dye laser as the excitation source.

A preliminary investigation was conducted to assess the potential of LIF for algae quantification. The relative fluorescence intensities of six different concentrations of each algae sample were measured using the spectrofluorometer. This procedure could not be applied to Tribonema since its filamentary growth could not be accurately diluted. The sample pathlength was 1.001 cm in each case;since the attenuation length of the aqueous medium at 337 nm was of the order of 50 cm, as estimated by a transmission experiment, the samples were considered to be optically thin. However, intensity I and concentration C were not found to follow a linear relationship, but rather, a power function of the form:

$$I = m\, C^{x}$$

where m and x are constants. The value of x for each sample is given in TABLE 4. Strickland (Ref. 9) has attributed this power function behavior to the scattering properties of the cellular algae structures.

In relating these results to the remote sensing regime, we must realize that in most cases, the water depth will be much greater than one attenuation length; hence, optically thick analysis must be used. Consequently, if attenuation is absorption dominated, quantification is impossible (Ref. 3). However, if attenuation is scattering dominated, quantification may be possible if the extinction coefficient associated with the scattering process, s_3, is shown. The situation is further complicated by diurnal variations in the algae fluorescence characteristics (Ref. 10) caused by changes in cell chlorophyll content under dark and light conditions.

TABLE 4.-FLUORESCENCE CHARACTERISTICS OF ALGAE

ALGAE TYPE[a]	PEAK EXCITATION WAVELENGTH[b] (nm)	PEAK EMISSION WAVELENGTH[b,c] (nm)	LIFETIME[d] (nsec)	EXPONENT[e] x
CHLORELLA (Chlorophyceae)	436 ± 2 470	683 ± 2	1.5 ± .2	.83 ± .04
TRIBONEMA (Xanthophyceae)	428	680	d	e
PHORMIDIUM (Cyonophyceae)	376	660	d	.77 ± .03
NITZCHIA SP.	460	685	d	.88 ± .04

NOTES:
[a] Samples supplied by University of Toronto Dept. of Botany
[b] Excitation and Emission Bandwidths were 22 nm
[c] Excitation Wavelength was 337.1 nm
[d] Lifetimes too short to be resolved
[e] Dilutions could not be performed on this sample.

CONCLUSIONS

If a laser induces fluorescence in a remote target of the marine environment, the process of identification of the target must progress through two phases. The first phase is the target family identification. In most cases we have studied, a measurement of the peak emission wavelength and emission profile bandwidth is sufficient; however, the differentiation of crude oils and fish oils may require knowledge of the complete temporal-wavelength profile.

The second phase is species identification within the family. Crude oil types may be classified by a matrix of fluorescence parameters including peak emission wavelength, relative intensity, peak excitation wavelength and lifetime at the peak emission wavelength. The ground truth parameter of API gravity may be added to the matrix.

The problem has been found to be complicated by aging effects; however, if crude oil species identification is accomplished, then the aging effects may be used to determine spill occurrence time. For the small number of refined petroleum products studied, species identification seemed most promising using fluorescence lifetime measurements at 400 nm. The possibility of fish oil species identification using both the emission and temporal spectral signatures, allows the application of fish school tracking to enter the realm of feasibility. Finally, algae species may be identified by their characteristic peak excitation wavelengths. Quantification of algae, although possible, is complicated first by the necessity for complete knowledge of the water extinction coefficient and second, by diurnal variations in cell chlorophyll content.

REFERENCES

1. Kim, H. H., Applied Optics, Vol. 12, 7, 1454 (1973).

2. Measures, R. M.; Houston, W. R.; Bristow, M., Casi Journal, Dec. 1973 issue.

3. Measures, R. M.; Bristow, M.; University of Toronto Institute for Aerospace Studies, Report No. 175, Dec. 1971.

4. Fantasia, J. F.; Hard, T. M.; Ingrao, H. C.; Report No. DOT-TSC-USCG-71-7, Transportation Systems Centre, Cambridge, Mass., June 1971.

5. Parker, C. A. Photoluminescence of Solutions, Elsevier, New York, 1968.

6. Dienes, A.; Shank, C. V.; and Kohn, R. L., IEEE J. of Quantum Electronics, QE-9, 833, August 1973.

7. Munro, I. H. and Ramsey, I. G., J. Sci.Instr., 1,147 (1968).

8. Murty, N. R. and Rabinowitch, E., Biophys. J., 5, 655 (1965).

9. Jarrett, O.; Mumola, P. B.; Brown, A., Proc. of the Int'l. Symposium on Remote Sensing and Water Resources Management, Canada Centre for Inland Waters, Burlington, Ontario, June 1973.

10. Strickland, J. D. H., Deep Sea Res., 225 (1968).

11. Glooschenko, W. A.; Nicholson, H. F.; Moore, J. E., Abstracts of the 3rd Canadian Oceanographic Symposium, CCIW, Burlington, Ontario, May 1973.

HIGHER SPECIFICITY HYDROSPHERIC IDENTIFICATION AND QUANTIFICATION WITH REMOTE LASER INDUCED LUMINESCENCE

H. Gerald Gross
McDonnell Douglas Astronautics Co.

(Paper not available at time of publication)

A REMOTE SENSING LASER FLUOROMETER

R. A. O'Neill, Anthony R. Davis, Harry G. Gross, J. Kruus
Environment Canada

ABSTRACT

The Water Science Subdivision has built a sensor which is able to identify certain specific substances in water by means of their fluorescence spectra. In particular, we have used the sensor to detect oil, lignin suphonates and chlorophyll. A sample does not have to be placed inside our sensor, making it different from a conventional laboratory instrument. We have been able to measure the fluorescence spectra of water at ranges up to 75 m and to detect oil spills on water at altitudes up to 300 m.

Blue light from a laser is used to excite the fluorescence of the target. Any light from the ambient background illumination, from the reflected laser light or from the induced fluorescence is gathered by a small telescope focused on the target. Optical filters are used to block the reflected laser light and to select the wavelengths of interest in the fluorescence spectrum of the target. The remaining light is detected with a photomultiplier tube. The background illumination is suppressed by making the detection system sensitive only to signals which are modulated with the same frequency and phase as the incident laser beam. The amplitude of the laser induced fluorescence in the wavelength interval selected by the optical filters is displayed on a meter or strip chart recorder.

The apparatus can be mounted in an aircraft and has been flown with the cooperation of the Canada Centre for Remote Sensing. We have been able to detect fluorescence of the water's surface in flights over a controlled oil spill, oil refineries, pulp plants and a controlled dye spill. It has also been possible to make a tentative interpretation of a number of features observed during these flights.

On the ground, the system has been used to examine river water, and experiments are being planned to monitor the chlorophyll concentrations in Lake Erie from on board the M. S. Martin Karlsen, a ship from the Canada Centre for Inland Waters.

INTRODUCTION

In today's context of environmental management, it is often desirable to have an instrument capable of detecting certain specific substances at a distance. The utility of such an instrument is greatly increased if it is able to operate at night, to perform well under adverse conditions, to monitor large areas from a variety of land, ship and airborne platforms or to run unattended for long periods.

Fluorescence spectra of some interesting substances dissolved in water are unique. The fluorescence spectrum of chlorophyll in water shows a strong peak in the red whereas oil in water fluoresces with a blue-green light. In addition to this uniqueness, the integration of the intensity of the fluorescence radiation in particular wavelength intervals can yield quantitative information on the concentrations. The present work describes a remote sensing laser fluorometer constructed to observe organic and biological materials in water.

FLUORESCENCE

Fluorescence occurs when a molecule absorbs a photon and subsequently emits another photon of less energy. The longer wavelength light (lower energy photon) is known as the fluorescence radiation. The optimum wavelength for absorption of light by the molecule and the wavelengths of subsequent emissions are determined by the molecular structure.

The spectra obtained by observing the fluorescence of different solutions are quite different. Figure 1 shows the fluorescence spectrum of chlorophyll in natural river water. (The spectrum was taken using a filter and a red sensitive photomultiplier tube. This spectrum is not corrected for photomultiplier or filter response functions. The chlorophyll peak at 680 nm is quite prominent as is the very broad peak near 520 nm. The latter spectral feature is probably due to the fluorescence of organic material carried by the river water. A blocking filter, made of 2 layers of Wratten #8 gelatin material and used to attenuate the laser line, tends to cut out all the light below about 510 nm altering shape of the peaks in the vicinity of 520 nm.) This may be compared to Figure 2 which shows a spectrum obtained from an oil-water system. (This spectrum was taken with the land-based fluorosensor using a variable filter and blue-green sensitive photomultiplier. Laboratory experiments on this oil showed the fluorescence spectrum to peak near 480 nm; however, the blocking filter used to attenuate the reflected laser light also attenuates the peak of the oil fluorescence. Thus, this spectrum and the one shown in Figure 1 do not appear to differ significantly in the region from 520-600 nm.) Both spectra were obtained by exciting the target with a beam of blue light having a wavelength of 442 nm. The spectrum of chlorophyll in water has a peak in the deep red at 680 nm whereas the oil dispersed in water shows a peak in the blue-green at 520 nm. These spectra were taken with the remote sensing laser fluorometer which contains filters (see The Laser Fluorosensor) to render the instrument insensitive to wavelengths less than 510 nm. Thus, the maximum of the oil fluorescence (below 500 nm) is not observed. Pure water does not fluoresce.

A general feature of fluorescence spectra of solutions is the presence of very broad peaks. The width of these peaks is a handicap in the identification of specific types of mineral oils. It has been shown (Fantasia et al. 1971) that the fluorescence peaks in the spectrum often shift to the larger wavelengths the greater the API density. Even over wide variations of the API gravity (5°-40°) the peak emission wavelength does not vary more than 50 nm. In laboratory measurements, the fluorescence spectrum has some importance as a method of distinguishing oil types. With the device described in present work, however, only gross features in the fluorescence spectrum are used to distinguish oil or chlorophyll from the background of other fluorescing organic materials in the water.

Another property of fluorescence radiation is a detectable time delay between the excitation of the molecule and the fluorescence emission. Many substances have different characteristic decay times; for mineral oils, however, they are all virtually the same. Fantasia et al, (1971) found the lifetime to lie between 9 and 21 ns with most at 10 ± 1 ns. The spread in the fluorescence lifetimes is insufficient to make use of this property for identifying different types of oils. The system described in this work is unable to take advantage of any information about the nature of the target molecules which could be derived from the fluorescence lifetimes.

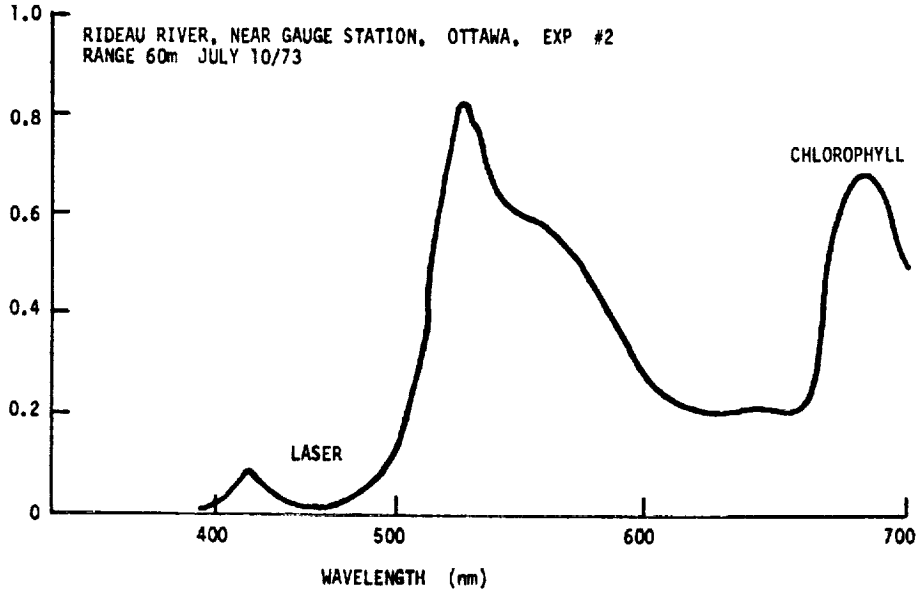

Figure 1. Fluorescence spectrum of chlorophyll in natural river water.

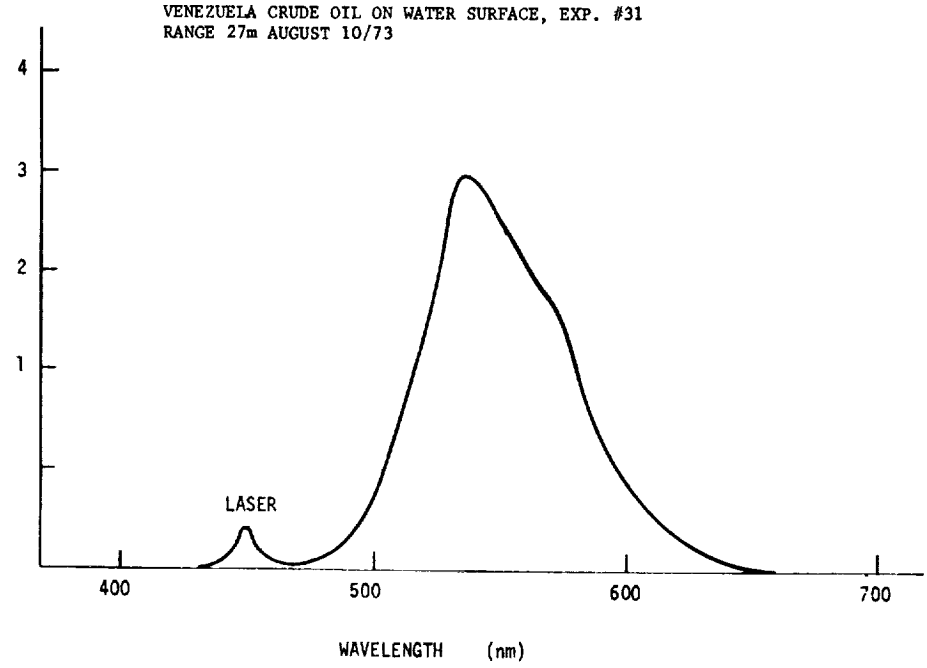

Figure 2. Fluorescence spectrum of chlorophyll in an oil-water system.

REMOTE SENSING

There are numerous reasons for choosing a remote sensing instrument over a conventional laboratory instrument when monitoring the general state of the environment. Perhaps the most obvious is that larger areas may be observed than by point sampling techniques. This gross overview sometimes enables one to see the forest in spite of the trees. Another advantage is that by using non-contacting techniques there are fewer problems in the construction of instruments and data acquisition systems to operate in severe environments or to operate unattended for long periods of time. No sample cells are used so that no special techniques are needed to keep them clean. Difficulties associated with operating sensors underwater do not exist with this device.

In the experimental stages of a project there is a great need to make careful laboratory measurements of selected targets using the remote sensing instrument. This yields valuable information which can be used later in the interpretation of field measurements. In the initial stages of development, too, samples must be taken at the same time as field measurements are made to establish the "ground truth".

There are two philosophies which may be followed in the interpretation of remote sensing data. The first (and the ideal) is to expect the sensor to establish unambiguously the nature of the targets. This involves very sophisticated equipment, a great deal of work and a vast amount of data. The device described in the present work has not progressed to this stage but is, in some respects, more specific than the approach frequently used by exploration geophysicists, by whom the sensor is used to detect anomalies which merit further investigations.

The Department of the Environment decided to develop an airborne fluorosensor. Initially it was to be used as a detector of oil spills. Now, however, there are other potential uses for which the instrument is as well suited as for its original policing role. The present system is the result of the part time activities of two men over a period of two years.

THE LASER FLUOROSENSOR

The present fluorosensor uses a Helium-Cadmium laser. This is a CW* laser with two lines which are useful for exciting fluorescence. A blue line at 442 nm has provided the excitation for all the field trials of the fluorosensor. The laser can produce about 25 mw of light in the blue line whereas an ultraviolet line at 325 nm is about five times less intense. The ultraviolet line could be useful for exciting the fluorescence of light oils which do not fluoresce when excited with the blue line. The laser may be converted to ultraviolet operation by changing the laser cavity reflectors and beam director which steers the beam onto the target.

As an aid in the detection of the fluorescent signal, the beam is modulated using a tuning fork chopper. This operates a frequency of 550 Hz.

The receiver consists of an eight-inch Schmitt Cassegrain telescope which is focused onto the laser spot on the surface of the water. This gathers the ambient background light, the reflected laser light and the fluorescent light. The light is then focused onto a series of filters. The divergence of the telescope is approximately the same as the 1 mr divergence of the laser beam.

*CW stands for Continuous Wave. The laser itself is producing light continuously. This is to be contrasted with a pulsed laser which emits light in short bursts. The laser light in our system is modulated externally to the laser using a tuning fork chopper.

Two sets of filters are used. The first is a high pass filter used to prevent reflected laser light from reaching the detector. The second is a narrow band filter which operates in the pass band of the blocking filter. By changing the narrow band filters, a spectrum of the fluorescence radiation may be taken. In the aircraft, a single filter is chosen which admits only light which could come from the fluorescence of the target of interest. In the ground based system, a variable thickness dielectric interference filter is used which enables spectra to be taken without the bulk, weight or resolution of a dispersion type component.

The filtered beam may be expanded with an eyepiece so that it fills the photocathode of a photomultiplier tube. In some cases, the beam is merely passed through a field stop to limit the field of view of the photomultiplier. The particular photomultiplier selected depends on the expected fluorescence of the target. For examining oil spills, a blue-green sensitive one is chosen whereas a red sensitive photocathode is necessary for chlorophyll work.

The signal from the photomultiplier tube is fed into a lock-in amplifier which also has a reference input from the laser chopper. Provided the photomultiplier is not saturated, the lock-in amplifier detects the portion of the returning signal which is in phase with the chopper. In so doing, the signal due to the constant ambient background illumination is rejected. The output of the lock-in amplifier, then, is a measure of the fluorescence signal which has been excited by the modulated laser beam.

The overall systems weigh 100 kg including all power supplies and electronics. About 600 watts of 60 Hz 120 VAC are required. The lock-in amplifier and displays require approximately 0.8 m of rack space. Floor space required in the present aircraft configuration is a rectangle 1.3 by 0.3 m with at least 0.6 m vertical clearance. The laser can be oriented differently to provide a differently shaped package if necessary. Finally, and perhaps the most important, the complete package costs less than $10,000.

Figure 3 shows a schematic diagram of the airborne laser fluorosensor. (In this system the fluorescence is excited by using a chopped laser beam. A small mirror is used to direct the beam downward onto the ground. The reflex sight consists of a 45° mirror which may be swung into the light path so that visual observations may be made. An eyepiece expands the beam of light collected by the telescope onto the interference filter and photocathode of the photomultiplier tube. The wavelength interval detected by the photomultiplier is determined by the particular interference filter selected on the filter wheel. A lock-in amplifier detects only the signals from the photomultiplier.) Lasers have several distinct advantages over conventional light sources. The beam has a very high intensity and a divergence of 1 mr in the present instrument. Such fine collimation aids in steering the beam and obtaining a small bright spot on the target. The fluorescent efficiency of most substances is quite low, being between 10^{-4} and 10^{-6} fluorescent photons per incident photon; hence a high incident flux is needed at the target. To keep integration times in the receiver short enough that fairly small fluorescent features can be detected from the aircraft, a large returning signal is necessary.

A land based version has also been built. Figure 4 is a schematic diagram of the system. (Only small changes have been made from the airborne system. There is no beam directing mirror. A variable thickness dielectric interference filter is used to select the wavelength interval so that a spectrum may be taken. Only the light arriving from the target and its immediate surroundings is seen by the photomultiplier due to a field stop.)

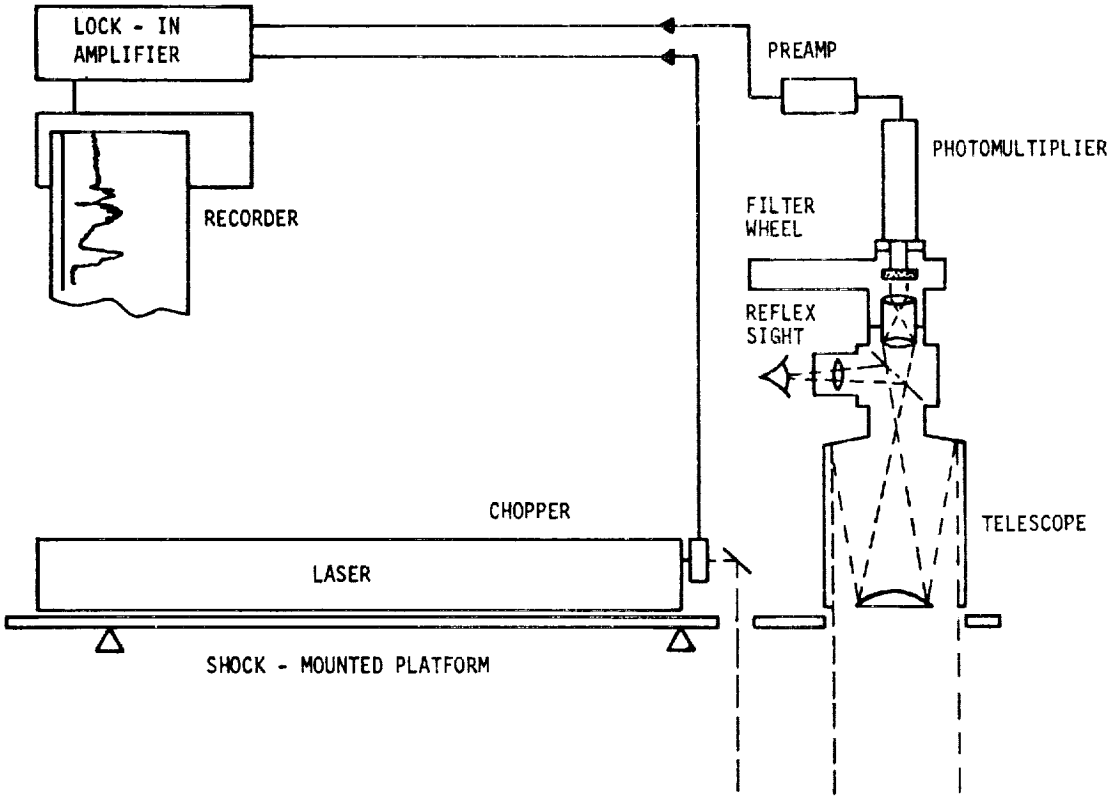

Figure 3. A schematic diagram of the laser fluorosensor in the airborne configuration.

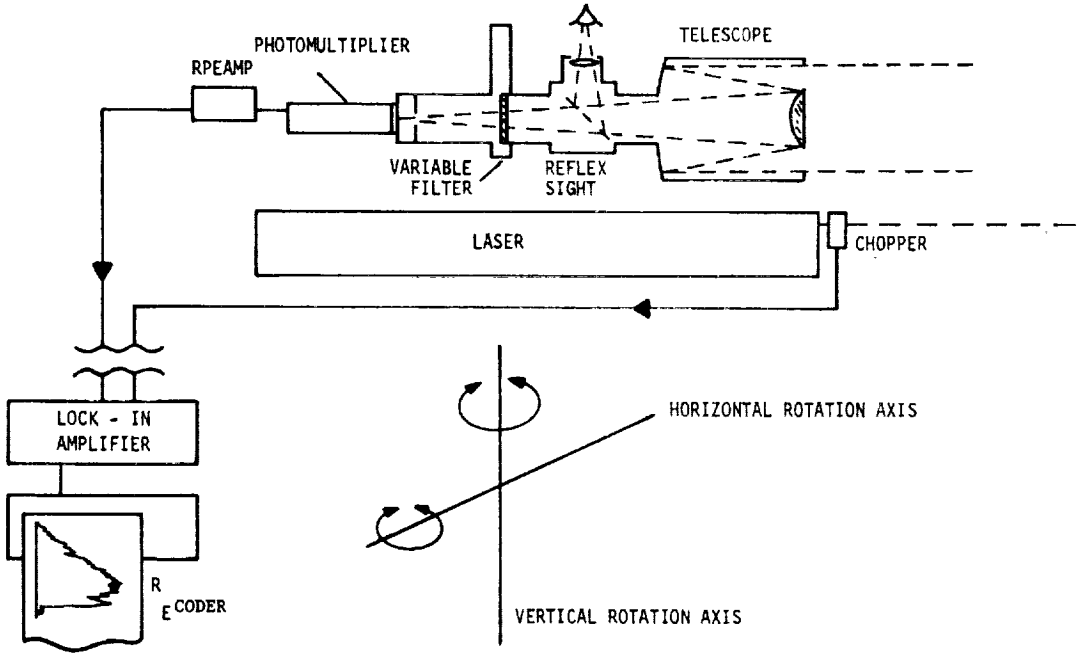

Figure 4. A schematic diagram of the remote sensing laser fluorometer as it is assembled in its land based configuration.

FIELD TRIALS

The airborne system has undergone a series of field trials using a DC-3 as a platform.

The first successful airborne test was over a controlled oil spill in the Bahamas. Figures 5a, b, and c show a portion of a record obtained while flying over the land, the water and the oil spill itself. The wave action tended to pile the oil up into long thick strips or "ropes". What may be seen in this diagram is a series of sharp spikes as the laser spot passes over these thicker sections of the spill. A degree of background fluorescence from the thinner portions of the oil may be seen between the spikes. The passage of the laser spot over the oil patches was confirmed by observation of reflected laser light with a low light level television system on board the aircraft. Bright flashes were seen to arise from the thick ropes of the slick and these may have been correlated with spikes on the record. The interpretation of the remainder of the record is highly speculative. It is worth noting the step in intensity observed in the fluorescence as the exciting laser spot moved from the land to the ocean. The high background fluorescence in the water is probably caused by chlorophyll and other dissolved organic materials. The sharp spike dividing the land record from the ocean record could be due to oil on the beach, but it might result from reflection of the beam by the wet sand on the foreshore. The intensity of such a reflection could be so high as to be seen by the photomultiplier tube even through the blocking filters. One other possible explanation might be fluorescence due to the small organisms living on the wet beach.

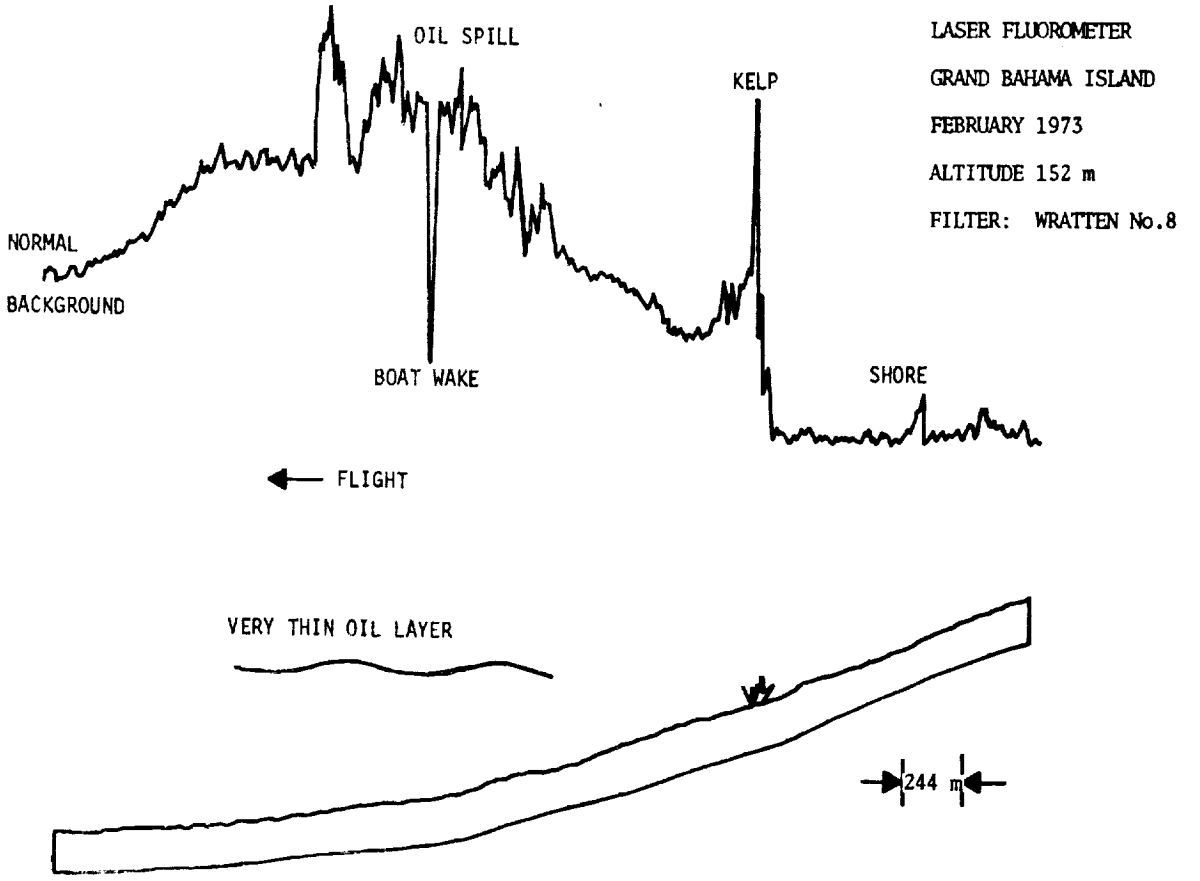

Figure 5a. Data and interpretation from flight of laser fluorosensor over controlled oil spill.

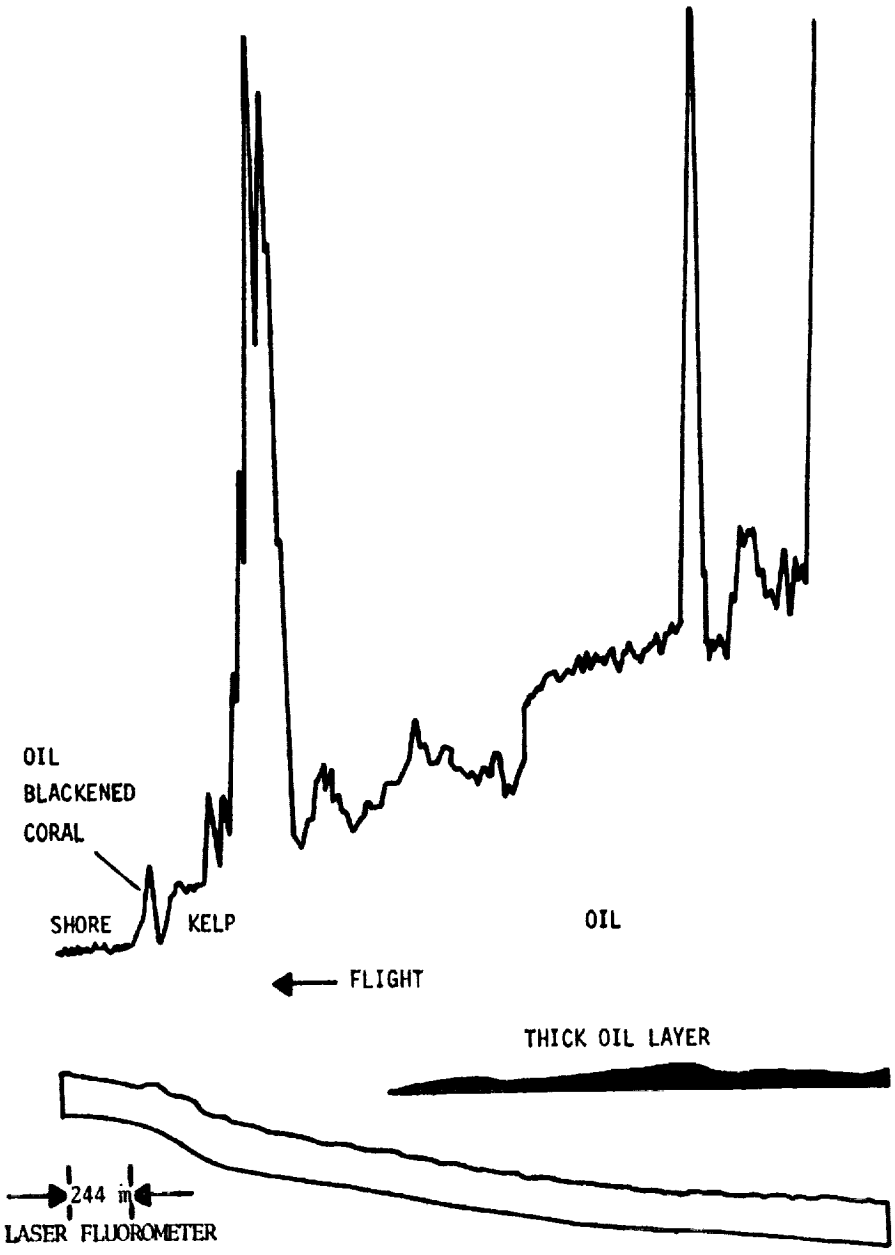

Figure 5b. Continuation of 5a.

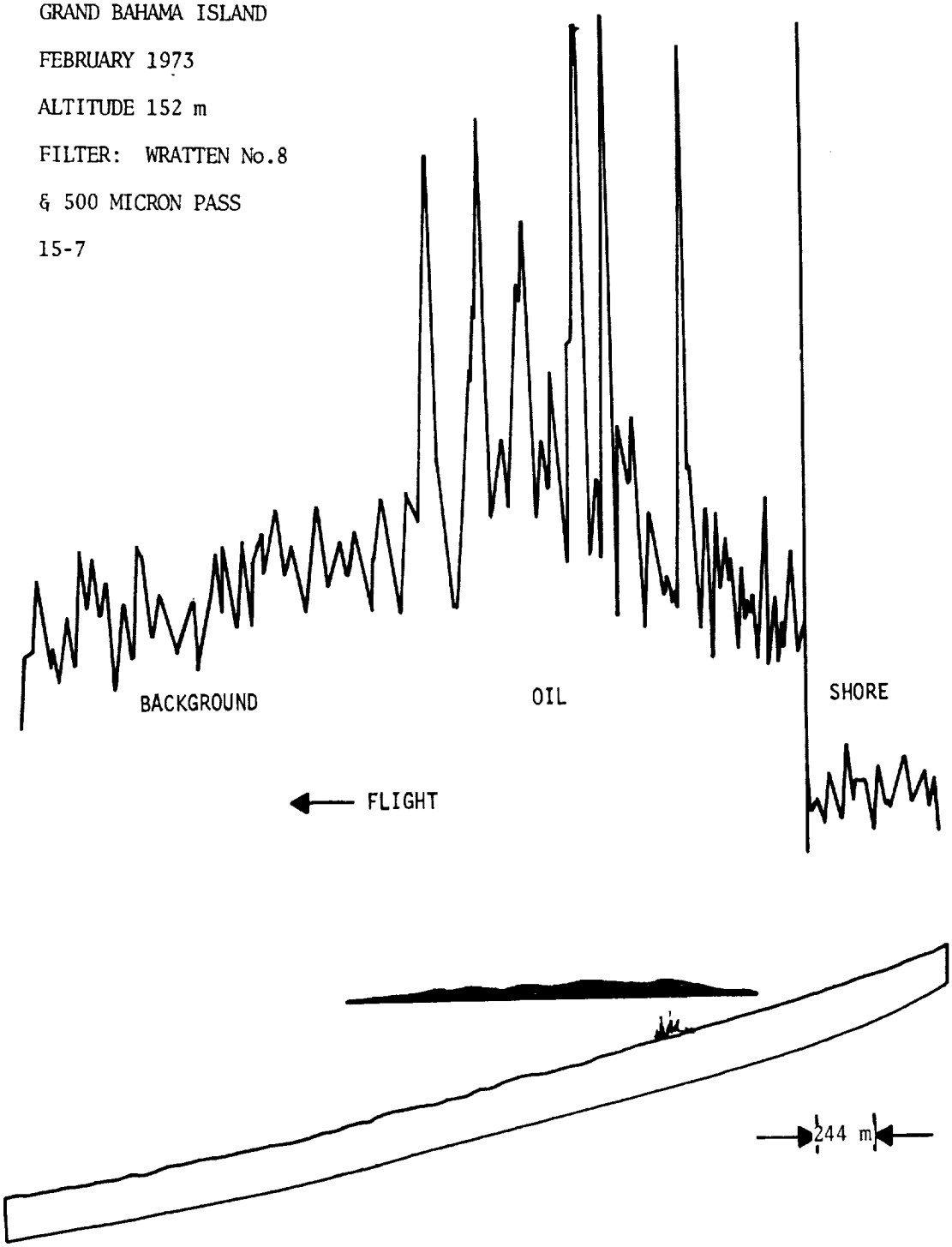

Figure 5c. Another pass over same oil spill shown in Figures 5a & 5b using a filter with a 10 nm band pass centered at 500 nm.

Figure 6 shows the record obtained in a flight over the St. Lawrence River at Montreal near some oil refineries. It was known that oil spills were often seen on the river in this area and that the oil seemed to gather near the shore, the actual shipping channel being swept clean by boats moving in the river. The record shows less fluorescence in the centre of the river than near the edges. The fluorosensor, during these flights, was flown with only the blocking filter and a blue-green sensitive photomultiplier thus the record shows the sum of all the fluorescence. Again there is an increase in the fluorescence signal as the aircraft passes from land to water.

The system has also been flown over rhodamine dye spills in Lake Ontario. In this case the spill was so small that the spot was only over the spill for a second time. This caused a single sharp spike on the record.

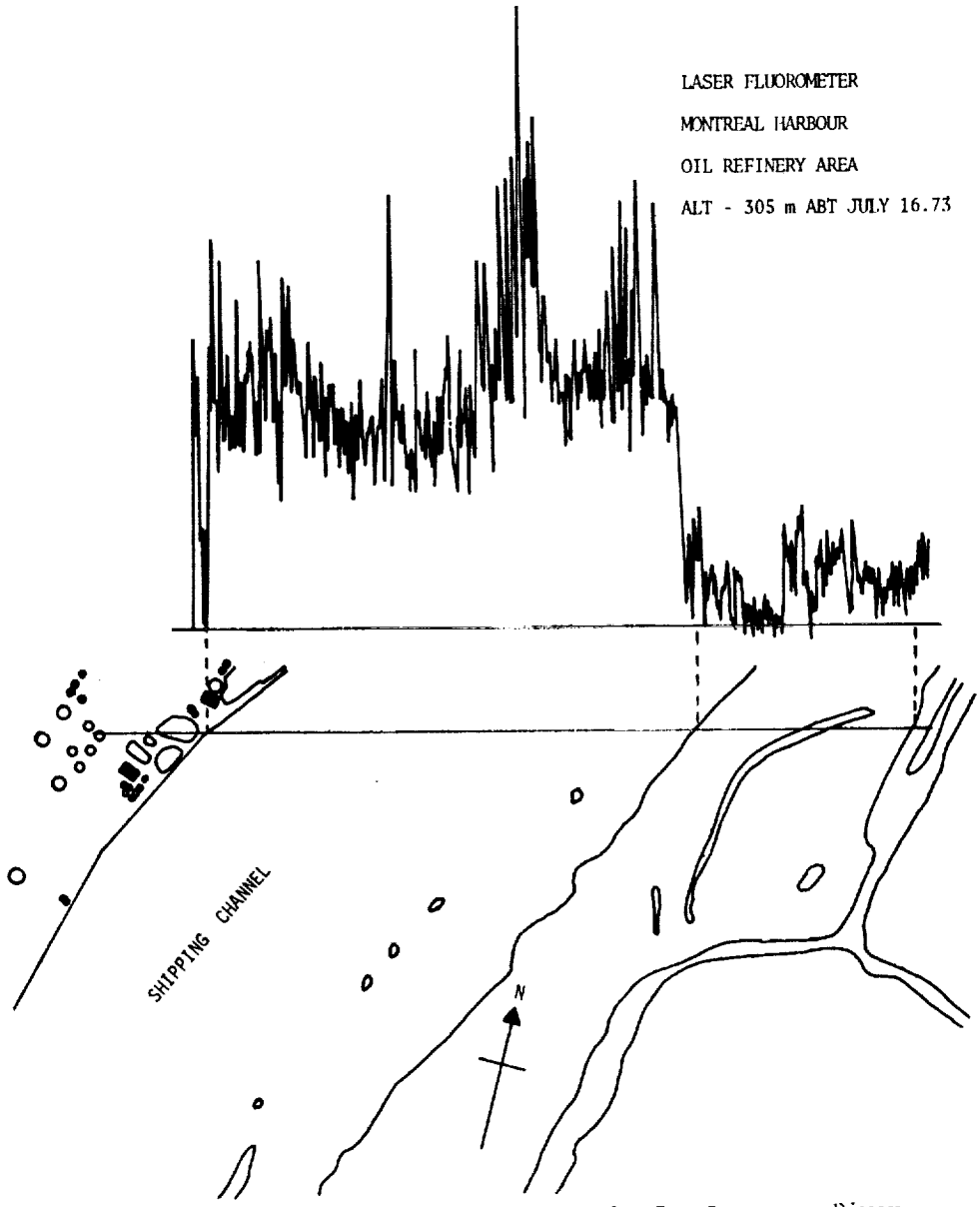

Figure 6. Record of a flight over the St. Lawrence River in the Montreal oil refinery area.

Pulp plant effluents have also been overflown. Figure 7 shows the record of a recent flight over the holding ponds of a sulphite process paper mill. The water in the pond is a deep tea colour and has quite high concentrations of lignin sulphonates. The lignin sulphonates result from the breaking down of the woody cells in the tree. In addition to this, the pond contains a number of wetting agents. In the laboratory, these substances do not cause the water from the ponds to fluoresce much differently from samples of ordinary river water. In pulp plant effluents, the peak at 520 nm in Figure 1 is much more intense than in river water. Also, the chlorophyll peak was not observed in the spectrum of the pulp plant effluent.

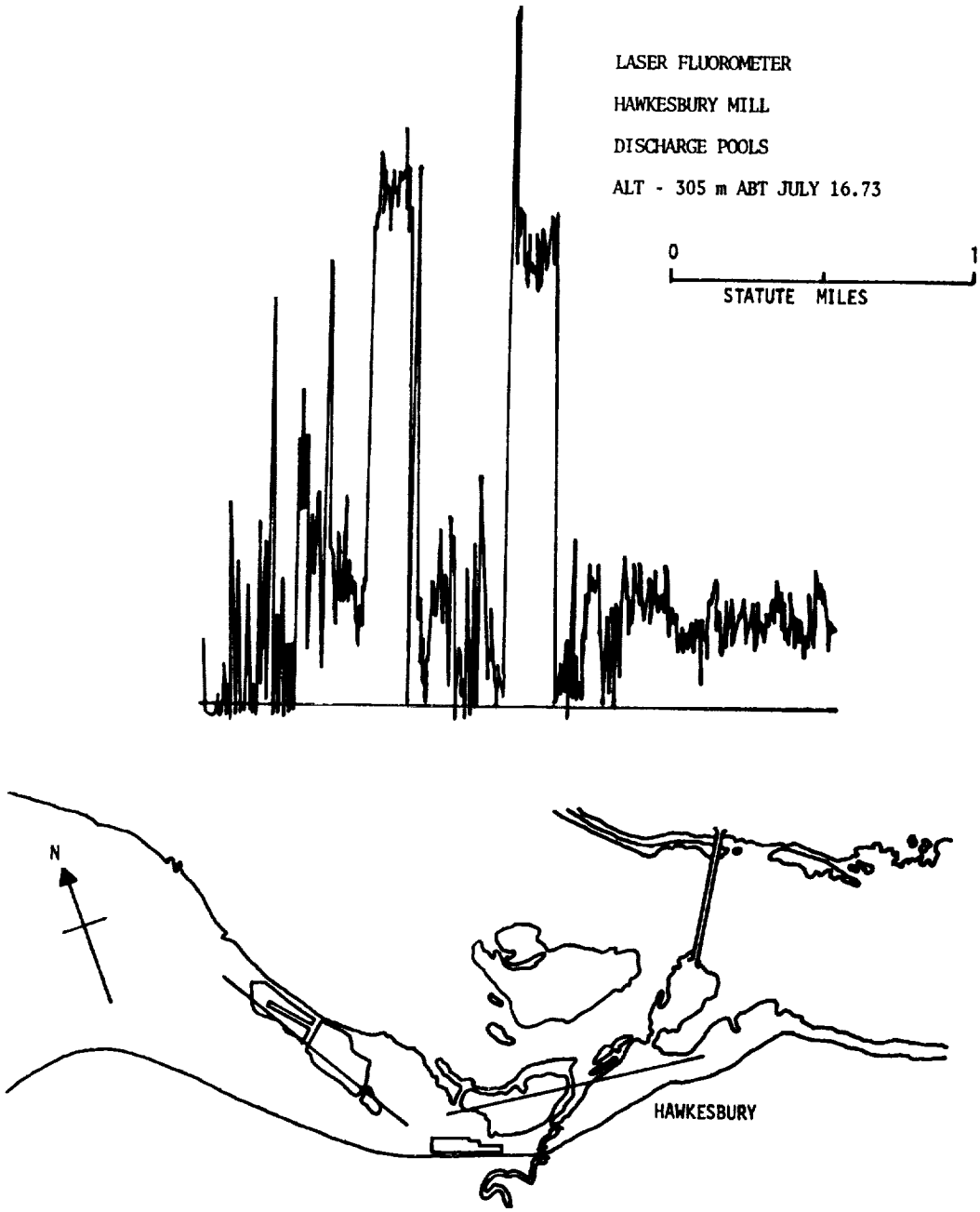

Figure 7. Fluorescence record from a flight over a sulphite process paper mill.

Pilots find it very difficult to fly precisely over small areas or in particular directions. The fluorosensor yields superior results if flown at low altitudes, slowly, and at night--all of which make it difficult for the pilot. In the airborne tests, the fluorosensor has been operated successfully at altitudes between 150 and 300 m and at speeds of up to 53 m/s (120 mph).

Figure 1 shows a spectrum obtained by the land based fluorosensor. Even though a blocking filter is in the optical train, some of the laser light still appears in the spectrum. In our limited sampling to date, the broad peak at 520 nm is a common feature in naturally occurring waters of the Ottawa area. It is probably due to suspended and dissolved organic material which is carried by the river. The fluorescence peak of lignin sulphonate appears at 520 nm. A water Raman line occurs at 520 nm but is extremely weak and makes no effective contribution to the size of the peak. The chlorophyll peak at 680 nm in the deep red is quite important. Chlorophyll is the most common substance in water to fluoresce in the red portion of the spectrum when excited with blue light.

At one time, chlorophyll fluorescence was used as a measure of the biological activity in the water. Such data were acquired with very simple laboratory fluorometers. This technique is now rarely used, though it is able to give the concentration of chlorophyll in the sampled volume. Chlorophyll is incorporated into plant cells in many ways. Some forms are active biologically whereas others merely store the chlorophyll. It is the way in which the chlorophyll is being used, as well as the amount, which determines the biological activity of water. Thus, the only knowledge that chlorophyll exists in a water sample is insufficient to draw conclusions concerning the condition of the water.

Plans have been made to mount the fluorosensor on a ship from Canada Centre for Inland Waters in order to monitor the chlorophyll levels in the waters of Lake Erie. Canadian waters are murky enough that the laser fluorosensor is only able to analyze the fluorescence in the top few centimeters of the lake. This is due to both the high extinction coefficient of the water which varies from 0.3 to 2.0 m^{-1} (Jerome 1973) and to the very low fluorescent conversion efficiencies. The latter are of the order, typically of 10^{-5} fluorescence photons per incident photon striking the molecule (Fantasia et al, 1971).

Another possible use, which has yet to be tested, is the detection of phenolic residues from petrochemical plants.

Though the present programme has emphasized measurements relating to water quality, the same systems could be used on land. Some suggested uses have been: looking for oil pipeline leaks and performing airborne forest health surveys. In such measurements it would be crucial and quite difficult to develop a reliable method of interpretation. Were the system to have an automatic scanning capability so that the fluorosensor could display a scene, both interpretation and the navigation would be simplified.

OTHER LASER FLUOROSENSORS

Other groups have been working on airborne laser fluorosensors. The Water Science device differs markedly from the other systems because it uses a CW laser. This particular approach may not be as versatile as a system using a pulsed laser system. The main advantage of using a CW laser may be found in the simplicity of the signal handling electronics. The compactness of the fluorosensor package and the low power consumption of the system have enabled the Water Science device to be flown before some of the larger pulsed laser fluorosensors.

Measures and Bristow (1971) have built quite a successful system at the University of Toronto. Their device is now continuing development at the Canada Centre for Remote Sensing under the direction of Dr. Bristow. It has undergone extensive land based field trials but has yet to be mounted in an aircraft. This instrument uses a pulsed ultraviolet laser and uses pulse detection techniques to observe the fluorescence signal in the light gathered by a telescope. This approach has several advantages. The first is that almost all organic materials fluoresce when excited by ultraviolet radiation; thus, many potential targets are available. The second advantage is that a pulsed system enables one to select the range at which it is desired to measure the fluorescence. This would be useful in clear water where the fluorescence could be measured remotely as a function of depth. Range gating could make this device potentially useful for observing fluorescence and Raman effects in the atmosphere as well. The laser is powerful enough that daylight operation is possible. The system is handicapped by its large physical dimensions and power requirements.

Fantasia et al (1971) working under contract to the U.S. Coast Guard have constructed a similar system to the Measures and Bristow device. Fantasia has done a very careful analysis of the optical parameters of the system and had a great deal of the optics custom built. This approach has led to a very exotic system capable of measuring fluorescence spectra; however, the cost is of the order of one hundred thousand dollars. The weight, physical dimensions and power requirements have prevented the device from flying yet.

Gross and Hyatt (1971) of MacDonnell Douglas have made a study of many fluorescent materials in order to find possible targets for a remote sensing laser fluorometer. A sensor has not actually been built.

Kim (1973) and Jarrett et al, (1973) of NASA have constructed a four colour laser which has been used to excite the fluorescence of algae. It has been observed that different types of algae fluoresce with different intensities when exposed to light. The fluorescent intensity as a function of the exciting wavelength is a characteristic of the target algae. By measuring the intensity of the fluorescence spectrum at four wavelengths when excited by four other wavelengths, one should be able to determine the concentration of up to four species of algae in the water. Kim (1973) has been able to fly a system operating on this principle over Lake Ontario to obtain surface algae concentrations. The algae were found to be more prevalent on the Rochester, N.Y. side of the lake than on the Toronto shore or in the middle.

Carswell et al. (1971) at York University in Toronto have built a LIDAR system. In this particular device, the back scattered light rather than the fluorescence radiation is observed. By measurements of the back scattered intensity and depolarization as a function of distance, certain atmospheric effects can be detected. A marine system will enable the depth of the thermocline and the turbidity of the water to be measured.

CONCLUSION

The present system using a CW laser may be used in applications where fluorescence is already an established analytical tool but where remote sensing of the target is desirable.

The remote sensing laser fluorometer is able to detect chlorophyll and oil. It seems unlikely that a fluorometric device will be able to make unambiguous identifications of oil types. The chlorophyll concentration may be related to the chemical oxygen demand or some other gross indication of water quality. Lignin sulphonates have been shown to fluoresce in much the same way as naturally occurring waters in the Ottawa area. This could be used by pulp plants to monitor the contents of holding ponds before their contents are discharged into the rivers. Investigations employing the fluorescence of naturally occurring water are likely to make great use of a remote sensing instrument of the type described in the present work. If used in conjunction with stream gauging stations, or controlling automatic sampling units, a remote sensing laser fluorometer would provide useful information on the temporal rather than the spacial characteristics of the water flowing past the sensor.

The fluorosensor may also be employed to make remote reflectance measurements. In this mode though, it is limited to a single wavelength. Such measurements would be more useful if additional exciting wavelengths were available.

POSSIBLE FUTURE DEVELOPMENT

The laser fluorosensor was designed to determine whether it was possible to make fluorometric measurements remotely. Hence, the instrument has only the basic components necessary to test the idea. For detailed or comprehensive surveys, the system may need many additions. The more obvious improvements, such as increasing the laser power or the diameter of the telescope to improve the sensitivity of the instrument, are quite straightforward. The present system is only able to operate in twilight or darkness because the photomultiplier tends to saturate before the fluorescence signal is detected. Further study is warranted in this area so that the fluorosensor's operation may be extended into bright daylight*. Most of the other improvements are concerned with methods of acquiring the data and the enhancement of its display to facilitate more certain interpretation.

A low light level television system has been found to be extremely useful during airborne operations. Primarily, it has shown where the laser spot is striking the ground. At present, the system has no automatic way of recording both the fluorescence signal and a view of the target. This recording may be done by superposing a measure of the fluorescence signal on a television display of the laser spot as it moves over the water's surface. The entire display then could be recorded on videotape. While interpretative techniques are being developed with a simple fluorosensor, such a videotape recording would be most useful.

A significant step in the fluorosensor's development would be to incorporate a beam scanning system so that a scene could be swept out. This would yield a map of the fluorescence similar to a false colour photograph or to a television display of the target with which it could be compared directly. The scanning display could be checked for fluorescent anomalies. In an aircraft, a one dimensional scanning system could be used so that a swath was swept out as the laser passed over the targets. An image could be formed of the fluorescent target features as well as making the navigation easier. The development of a scanning system could be quite expensive.

A third improvement could be made by exciting the targets simultaneously with more than one colour of light. The fluorosensor than could be quite useful for making measurements of reflected light at several different wavelengths. The additional exciting wavelengths would yield additional data on the fluorescence which would aid in the interpretation of returning signals.

The addition of more excitation wavelengths could be usefully combined with a fourth improvement: a rapid scanning spectrometer. This would enable the fluorescence spectrum to be taken very rapidly. The process now is quite time consuming with the circular variable filter and is too slow to be used in the airborne configuration. Details such as relative peak heights and peak shapes in the fluorescence spectrum could be quite important in the identification of returning fluorescence signals from some targets. Many rapid scanning spectrometers have been developed, some of which could be used almost without modification on the present laser fluorosensor.

*Daylight operation is possible with pulsed lasers with high peak pulse powers.

REFERENCES

1. Carswell, A. I.; McQuillan, A. K.; and McNeil, W. R. (1971). Canadian Aeronautics and Space J. 17 419.

2. Fantasia, J. F.; Hard, T. M.; and Ingrao, H. C. (1971). Report DOT-TSC-USCG-71-7. National Technical Information Service, Springfield, Virginia 22151.

3. Gross, H. G. and Hyatt (1971). Proceedings of the 7th International Symposium on Remote Sensing of Environment. Page 869. Willow Run Laboratories, Institute of Science & Technology, The University of Michigan, Ann Arbor, Michigan.

4. Jarrett, Jr., O.; Mumola, P. B.; and Brown, Jr., C. A. (1973) Paper presented at Remote Sensing of Water Resources, International Symposium, Canada Centre for Inland Waters, Burlington, Ontario, Canada.

5. Jerome, J. (1973). Private communication concerning extinction coefficients observed in the Great Lakes.

6. Kim, H. H. (1973). Reported in Electro Optical Systems Design, July 1973 and Mumola, P. B. and Kim, H. H. (1972). 1972 IEEE Conference on Engineering in the Ocean Environment, Newport, Rhode Island.

7. Measures, R. M. and Bristow, M. (1971). Canadian Aeronautics and Space J. 17.

SUPPLEMENT

A set of diagrams (Figures A-1 through A-7) relating to the remote sensing laser fluorometer.

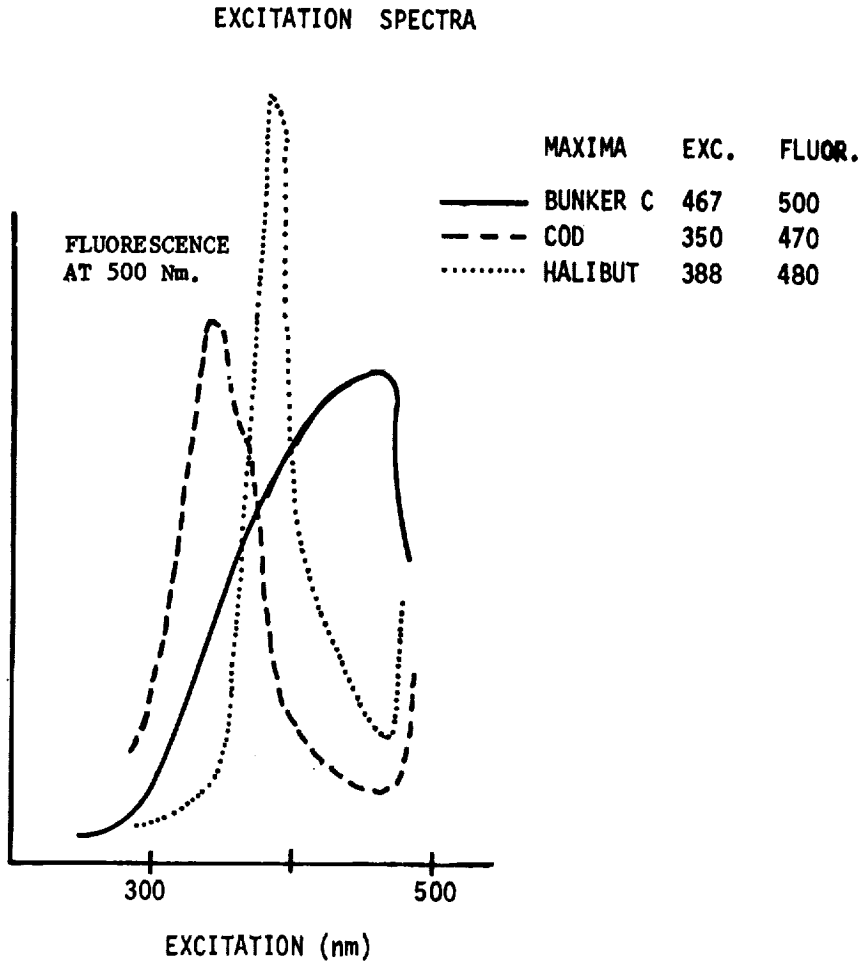

Figure A-1. Excitation spectra.

(A plot of the intensity of fluorescence at 500 nm as a function of the exciting wavelength for two fish oils and one mineral oil. It may be seen that the optimum excitation wavelengths for fish oils lie in the ultraviolet whereas optimum excitation wavelength for Bunker C oil occurs at 467 nm. The remote sensing laser fluorometer has an exciting line at 442 nm which causes very little fluorescence in fish oil. The fluorosensor can be expected to excite the fluorescence of Bunker C oil quite well. The He-Cd laser also has a line at 325 nm in the ultraviolet which could be used to detect fish oils.)

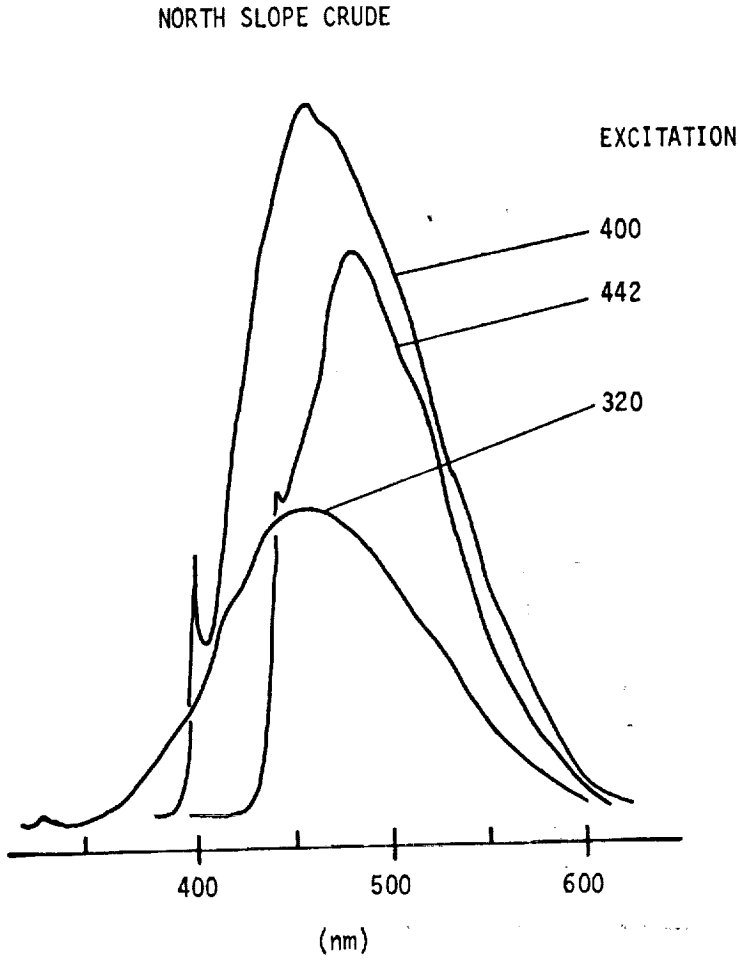

Figure A-2. Fluorescence spectra of north slope crude oil for several different exciting wavelengths.

(The laser fluorosensor uses an excitation line at 442 nm for which the fluorescence is about 80% of what could be obtained if the oil were excited by radiation with a wavelength of 400 nm. The fluorosensor may also use an ultraviolet excitation line at 325 nm which would not induce strong fluorescence in North Slope crude oil.

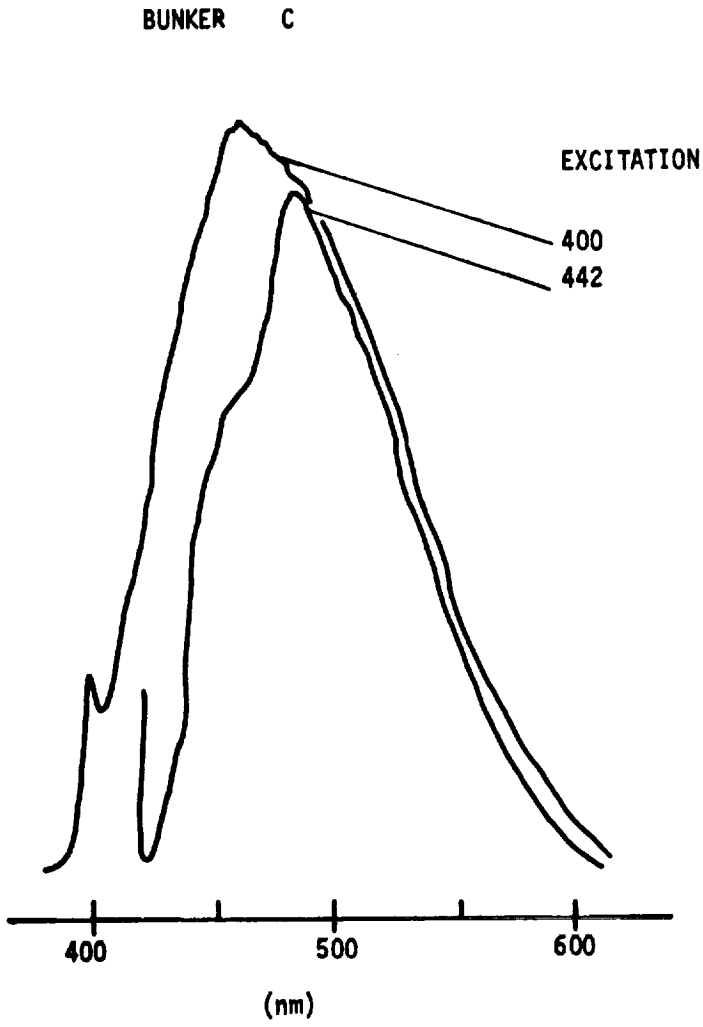

Figure A-3. Fluorescence spectra for Bunker C fuel oil at two wavelengths.

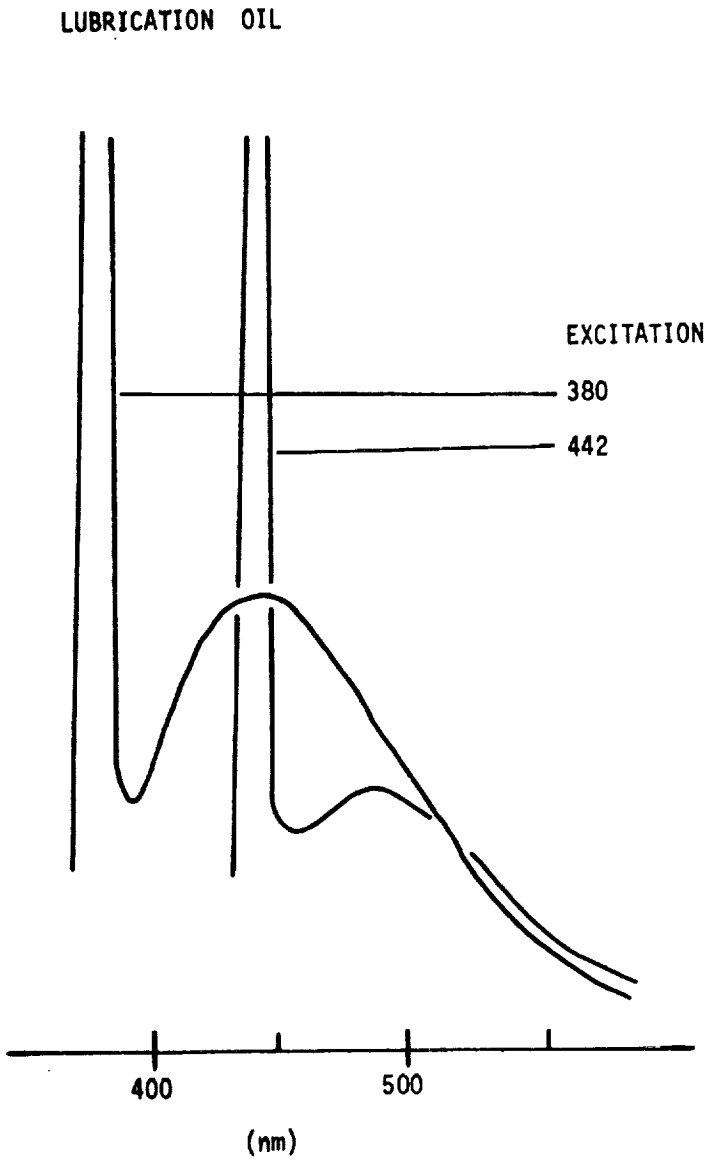

Figure A-4. Fluorescence spectra from lubricating oil at two excitation wavelengths.

(Detection of lubricating oil would be improved if the remote sensing laser fluorosensor were to use ultraviolet excitation.)

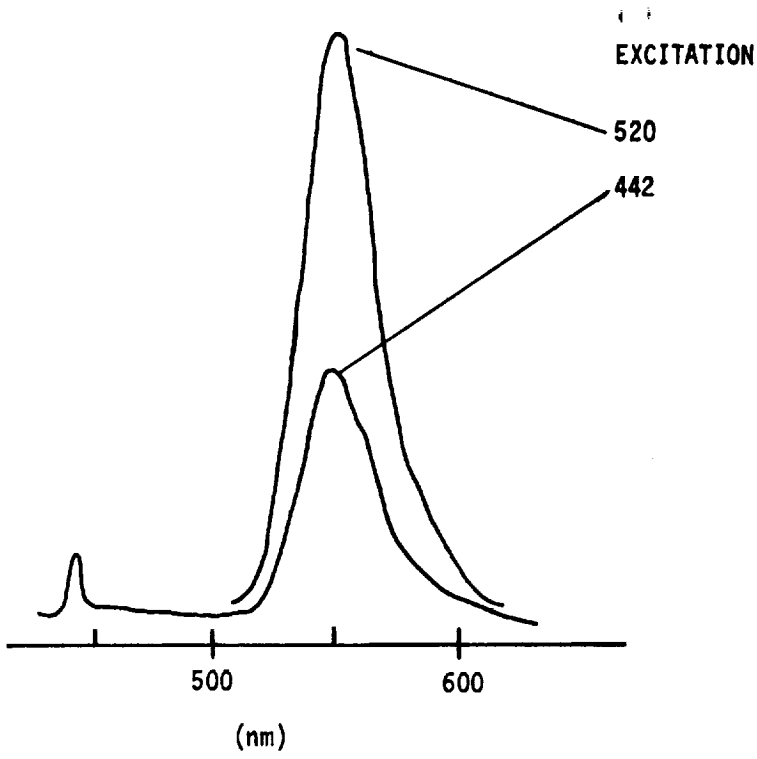

Figure A-5. Fluorescence spectra of Rhodamine 6G dye for two wavelengths.

(The fluorosensor is able to excite fluorescence using a wavelength of 442 nm. This spectrum was taken with a conventional laboratory instrument and may be compared to Figure A-6.)

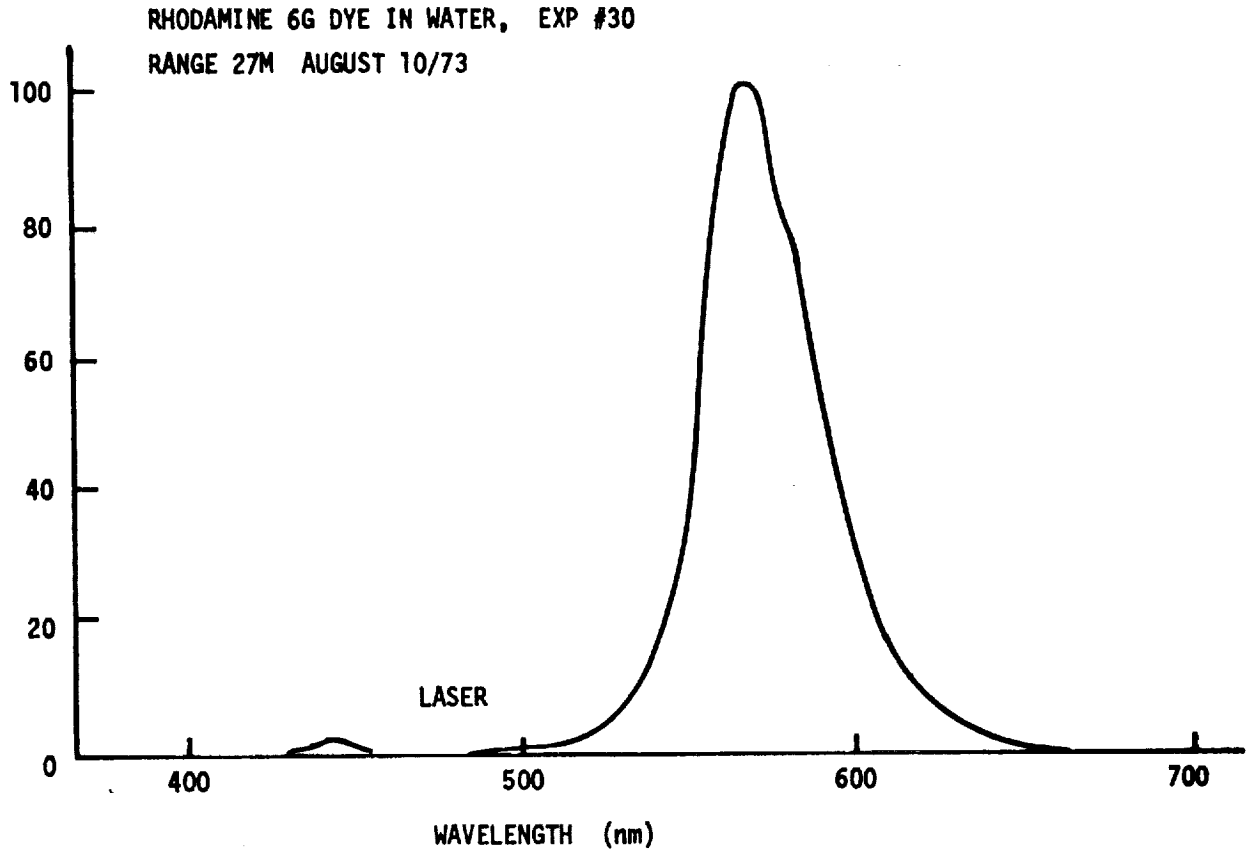

Figure A-6. Spectrum of Rhodamine 6G dye obtained with the land based version of the remote sensing laser fluorosensor at a range of 27 m.

(A variable thickness dielectric interference filter was used to select the wavelengths for the spectrum. This spectrum should be compared to Figure A-5 which is a fluorescence spectrum taken of the same material on a conventional grating type laboratory instrument.)

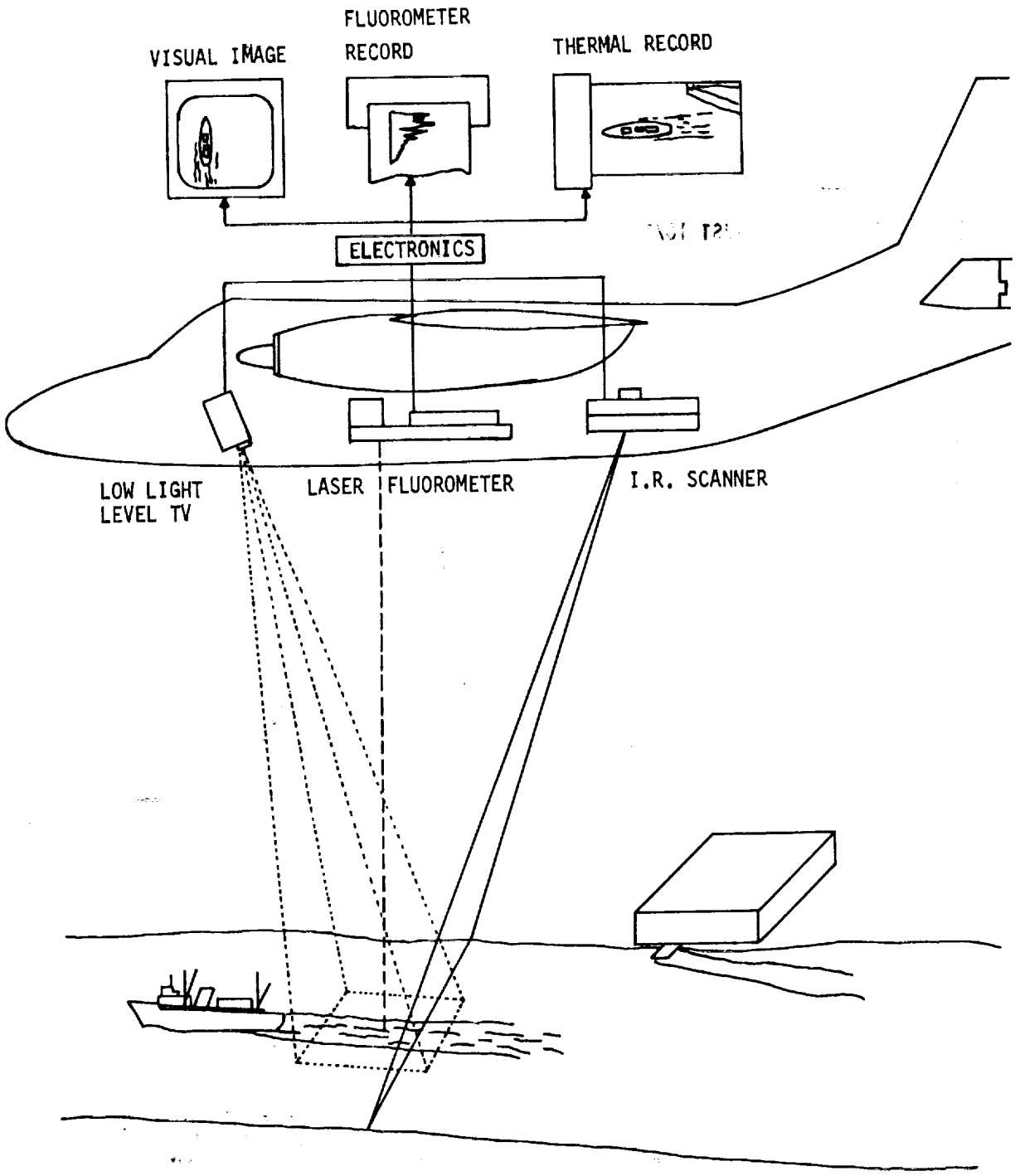

Figure A-7. A diagram emphasizing that the laser fluorosensor should be operated at the same time as other sensors

(One sensor alone is seldom able to provide complete identification of an anomaly; hence, information from other sensors working in different portions of the electromagnetic spectrum must also be used. Though, in this diagram, only passive sensors are shown operating with the laser fluorometer, other active sensors could also be used.)

AN AIRBORNE LASER FLUOROSENSOR FOR THE DETECTION OF OIL ON WATER

Hongsuk H. Kim
NASA-Wallops Station

and

George D. Hickman
Sparcom, Inc.

ABSTRACT

An airborne laser fluorosensor for the detection of oil derivatives on water has been tested. The system transmits 337 nm u.v. radiation at the rate of 100 pulses per second and monitors fluorescent emission at 540 nm. Daylight flight tests were made over the areas of controlled oil spills and additional reconnaissance flights were made over a 50 km stretch of the Delaware River to establish ambient oil baseline in the river. The results show that the device is capable of monitoring and mapping out extremely low level oil on water which cannot be identified by ordinary photographic method.

A remote active sensor system designed to detect laser induced fluorescence from organic and biological materials in water has been suggested by a number of investigators (Refs. 1, 2). Several different laser airborne systems are in the process of being developed in both the U.S. and Canada (Refs. 3, 4).

In this presentation, we would like to report our successful operation of an airborne laser fluorosensor system which is designed to detect and map surface oil, either natural seepage or spills, in large bodies of water. The test flights were conducted in daylight; preliminary results indicate that the sensitivity of the instrument exceeds that of conventional passive remote sensors which are available for the detection of an oil spill today.

The package was jointly developed by NASA Wallops Station and Sparcom, Inc. of Alexandria, Va. The salient features of the system consist of a pulsed nitrogen laser, a f/1 28 cm diameter Cassegranian telescope and a high gain photomultiplier tube (RCA 8575) filtered by a U.V. blocking filter (0.01% and 0.3% transmission at 337 nm and 390 nm, respectively). The laser produces a nominal 1 m joule pulse of 10 nsec duration at 337 nm contained in a rectangular beam having a half angle divergence of approximately 30 by 2 mradians. The repetition rate 100 pulses per second affords one good spatial resolution when operated from an aircraft flying at 300 km/hr. Figure 1a is a photograph showing the laser equipment installed in NASA DC-4 aircraft. Figure 1b is an illustration of Figure 1a.

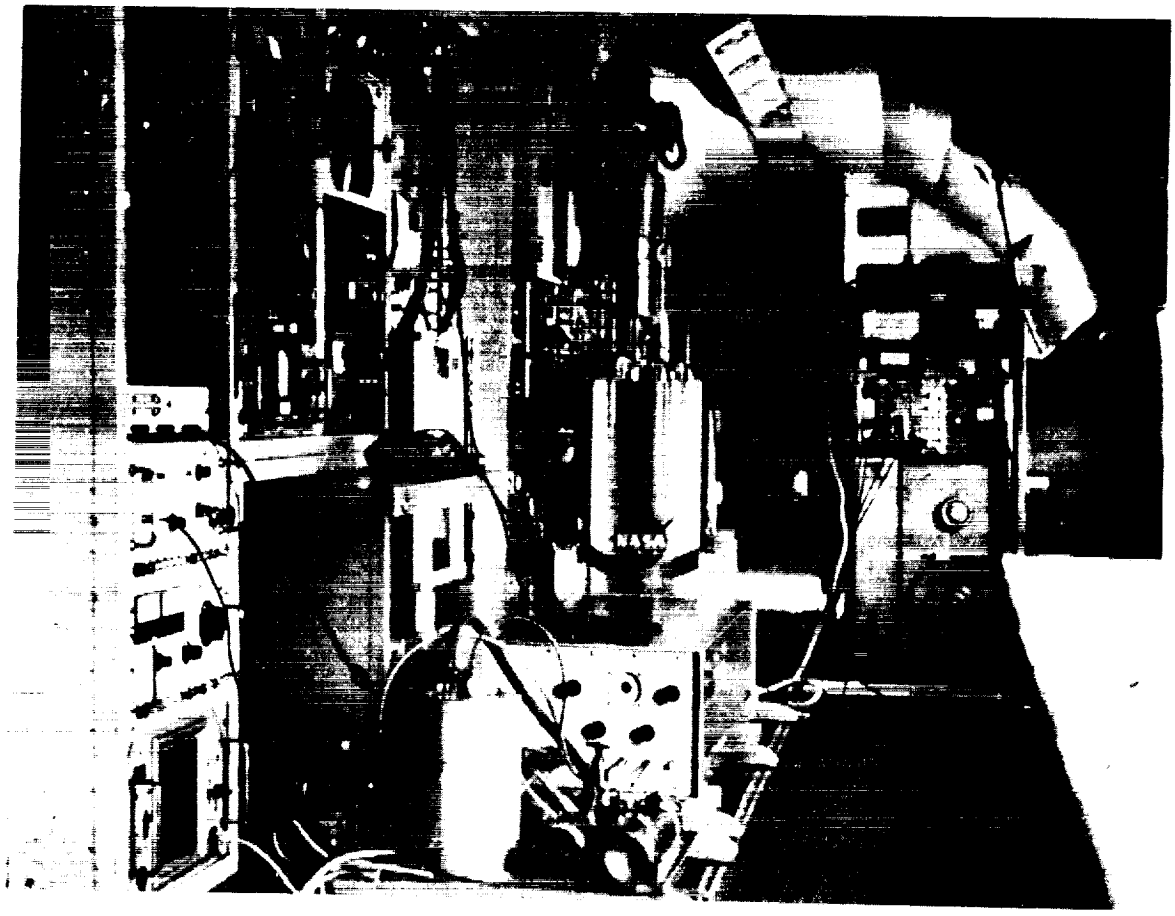

Figure 1a. Laser fluorosensor installed in NASA's DC-4 aircraft

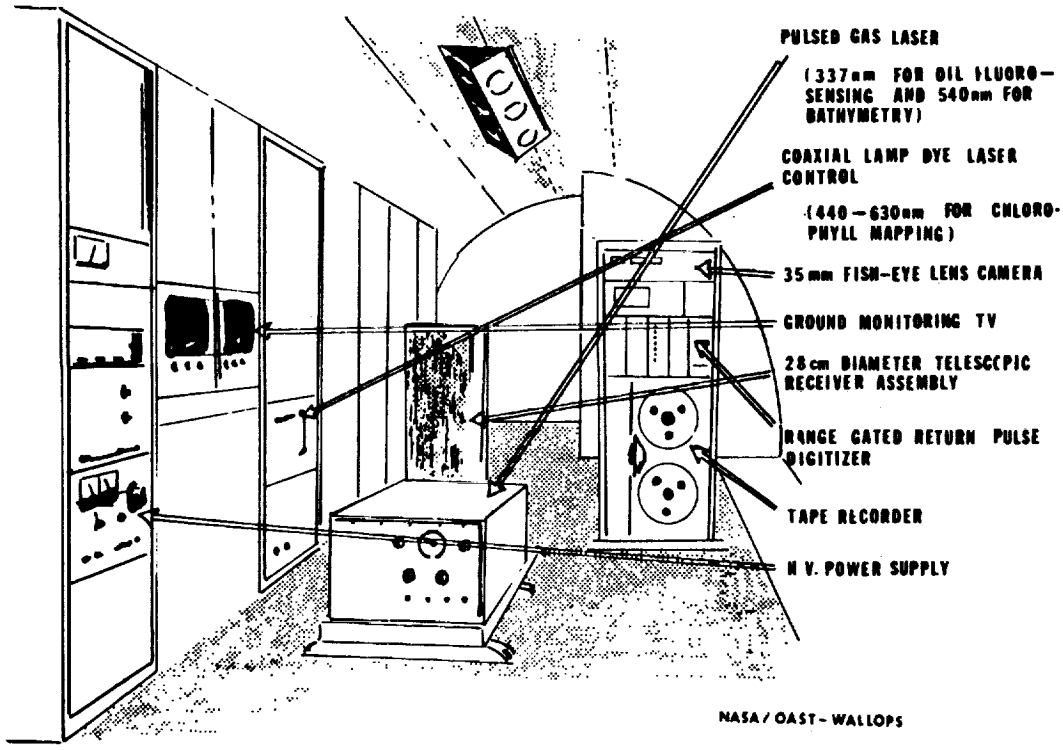

Figure 1b. An illustration of Figure 1a

The laser induced fluorescence of the oil in the 450 - 500 nm spectral region was monitored. Each return pulse (Figure 2) was fed into a range gated multimode analog-to-digital (A/D) conversion unit which recorded the peak amplitude of fluorescence. Even though the pulse width of the return fluorescence did not exceed 10 nsec, the width of the input gate to the ADC was considerably wider. This was to insure signal detection as fluctuations occurred in the laser/oil distance which were produced by aircraft motion: roll, pitch and changes in altitude.

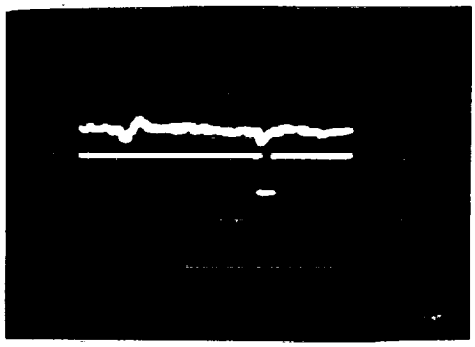

UPPER TRACE: FLUORESCENCE SIGNAL DETECTED

LOWER TRACE: 50ns WIDE RANGE GATING

TARGET : AMBIENT OIL AND RIVER-WATER BACK-GROUND, CLEAR SKY, 10:30 a.m.

Figure 2. Delaware River overflight. 24 Aug. 73

A 35 mm frame aerial camera equipped with a wide angle lens viewed the same area on the water surface as seen by the fluorosensor. Our experiences gained through previous NASA aircraft photo surveillance missions have shown us that the color photographic image technique is still one of consistently reliable positive indicators of the presence, position, and extent of the oil slicks (Ref. 5).

The first series of flight tests were conducted in conjunction with a controlled oil spill off Norfolk, Virginia in May 1973. This spill consisted of 1514 liters (400 gallons) of No. 4 grade heating oil. The field experiments were managed by the U.S. Coast Guard. The NASA aircraft, containing both the oil fluorosensor and a dual channel microwave radiometer (Ref. 6), flew over the spill site at altitudes ranging from 30.48 - 304.8 meters (100 - 1000 ft). Figure 3 illustrates typical return signals which were obtained at the airborne receiver from the surface oil as the plane passed over the slick. The data shown in this figure was obtained from an aircraft altitude of 121.9 meters (400 ft.). This figure shows a large but fairly constant background previous to ($\leq$ .41 seconds) and after ($\geq$ .48 seconds) the plane's passage over the spill. There is a marked increase in the amplitude of the detected signal during the period of time that the aircraft was over the oil slick. Detection of the oil was recorded by the dual channel microwave radiometer during the time period of .43-.45 seconds, which is close to the center of the spill. In all probability this represented the thickest layer of oil. This single qualitative experiment dramatically showed that while the microwave radiometer was able to detect the central portion of the spill, the increased sensitivity of the laser fluorosensor permitted detection of approximately the entire visual extent of the slick. Although thickness of the oil changes as the oil spreads on the surface of the water, the amplitude of the fluorescent signal remained essentially constant (Figure 3). Since oil exhibits extreme absorption in the UV region of the spectrum, one would expect the amplitude of the fluorescence to be relatively independent of thickness. This is in agreement with the flight test results. Confirmation of the dependence of oil thickness on fluorescence has been made in the laboratory.

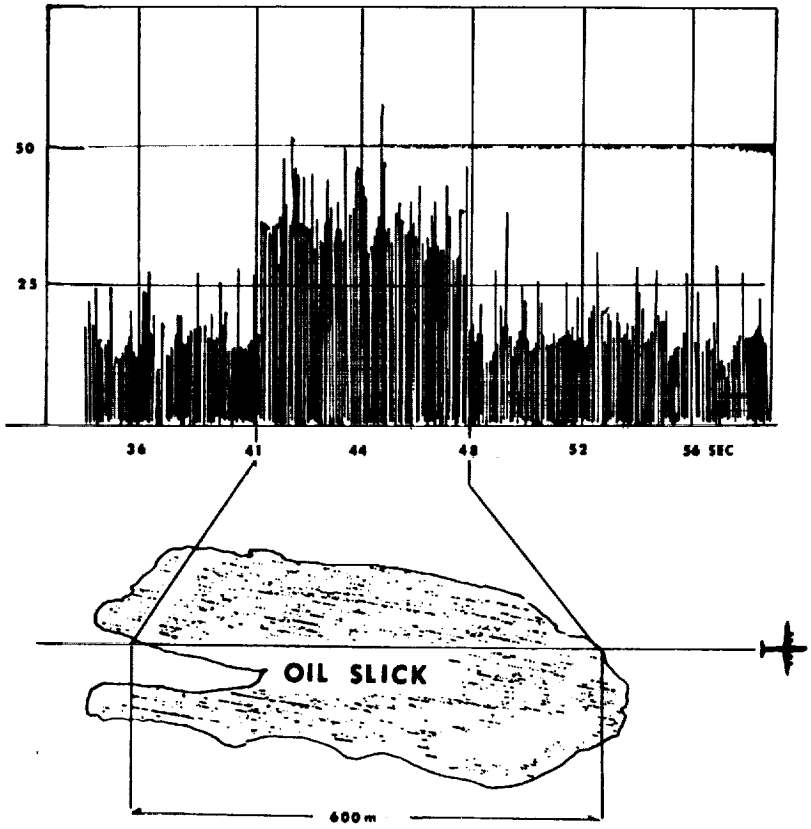

Figure 3. Typical fluorescent signals observed with laser fluorosensor-aircraft altitude 121.9 meters (400 ft.)

A second set of flight tests consisting of six separate flights was made in August 1973 to detect ambient oil on the Delaware River. Figure 4 shows the results of one of these flights from a 48 km section of the river between the Chesapeake and Delaware Bay Canal to the Delaware - Pennsylvania state line. The observed fluorescent intensity was approximately five times higher in the upper section of the Delaware River as in the lower section of the river. The background noise was substantially reduced over that recorded in the initial flight test. This was accomplished by narrowing the gate width of the digitizer input from 250 to 50 nsecs. The system was calibrated to register a value of 50 on the ADC unit against a thin oil film target in full view of the receiver at an altitude of 152.4 meters (500 ft.) and a value of zero against ambient noise in the open sea. This was accomplished by adjusting the gains of the phototube and the threshold levels of the input discriminator to the digitizer. Therefore, our calibration procedure assured us that the signal observed in the lower section of the river was a real fluorescence and not background noise.

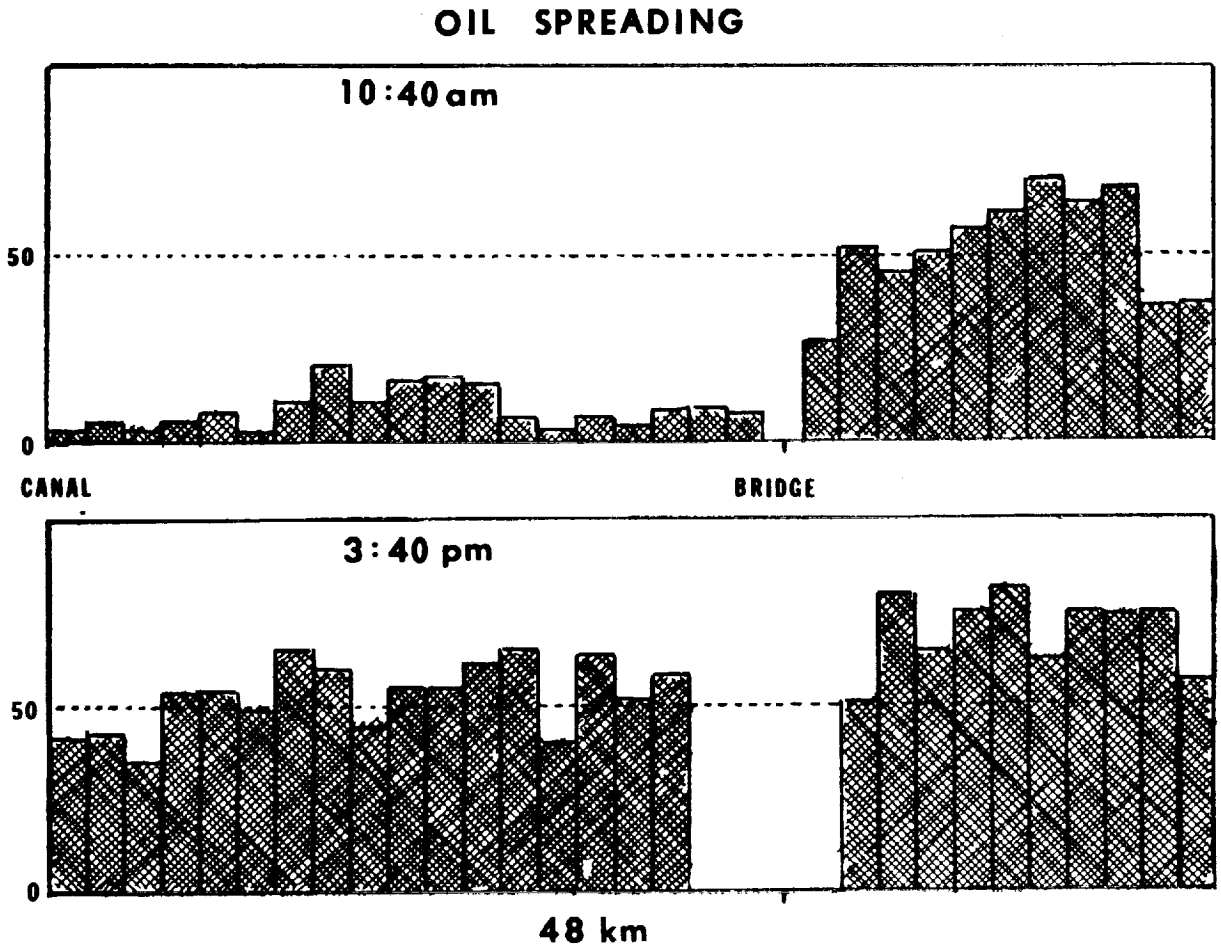

Figure 4. Oil spreading in Delaware River observed with an airborne laser fluorosensor

Figure 5 shows a bar chart of the morning flight results, previously shown in Figure 4, along with the return afternoon flight made the same day. Each block in the figure represents an average value of 3000 return pulses. This figure shows dramatically the change in the intensity of the oil in the lower section of the river in a fairly short time.

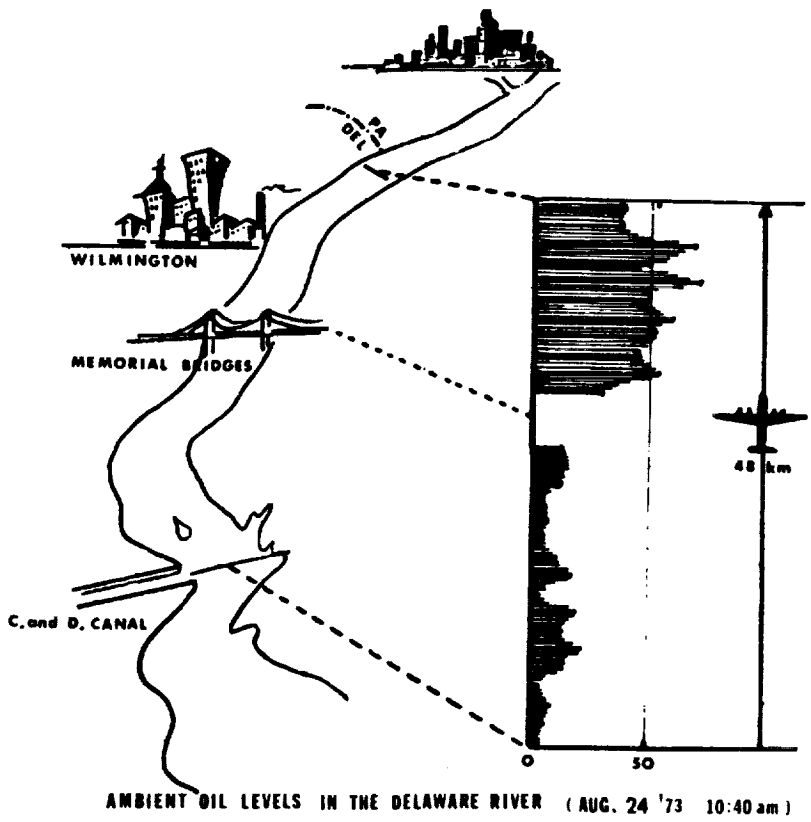

Figure 5. Ambient oil levels in the Delaware River measured with the airborne laser fluorosensor (Aug. 24, 1973 10:40 a.m.)

Images from the aerial photography showed the presence of oil when a scale reading of 50 or greater was reached on the ADC output. Therefore, photography did not show the presence of oil in the lower section of the river during the morning flight, although detection of the oil was made with the laser fluorosensor. This is significant, in that it shows the tremendous sensitivity of the laser fluorosensor in detecting traces of oil that can not be detected by other remote sensors.

REFERENCES

1. Hickman, G. D. and Morre, R. B., "Laser Induced Fluoresin Rhodamine B and Algae", Proc. 13th Conf., Great Lakes Res. 1970.

2. Fantasia, J. F.; Hard, T.M.; Ingrao, H. C., "An Investigation of Oil Fluorescence as a Technique for the Remote Sensing of Oil Spills", DOT-TSC Report 71-7.

3. Kim, H. H., "New Algae Mapping Technique by the Use of an Airborne Laser Fluorosensor", Applied Optics, Vol. 12, p. 454-62, July 1973.

4. Munday, J. C. Jr.; McIntyre, W. G.; Penney, M. E.; Oberholtzer, J. D. "Oil Slick Studies Using Photographic and Multi-Scanner DATA", Proc. of the 7th National Symposium of Remote Sensing of the Environment. Willow Run Lab, University of Michigan, Ann Arbor, 1971. p. 1027.

5. Hollinger, J. P. and Mennella, R. A. "Oil Spills: Measurements of their Distribution and Volumes by Multifrequency Microwave Radiometry", Science, Vol. 191, p. 54, July 1973.

APPENDIX

ROSTER OF PARTICIPANTS

James S. Bailey
Department of the Navy
Office of Naval Research
Arlington, VA 22217

Jacob Bechner
Old Dominion University
Department of Physics
Norfolk, VA 23508

David E. Bowker
National Aeronautics and Space Administration
Langley Research Center
Mail Stop 214
Hampton, VA 23665

Richard M. Boykin, Jr.
National Aeronautics and Space Administration
Langley Research Center
Hampton, VA 23665

Duane Bright
Naval Oceanographic Office
Washington, DC 20373

Michael Bristow
Canada Centre for REmote Sensing
Department of EMR
Ottawa, Ontario, Canada K1A 0E4

Philip Brockman
National Aeronautics and Space Administration
Langley Research Center
Hampton, VA 23665

Clarence A. Brown, Jr.
National Aeronautics and Space Administration
Langley Research Center
Mail Stop 214
Hampton, VA 23665

Lewis G. Burney
National Aeronautics and Space Administration
Langley Research Center
Hampton, VA 23665

Michael A. Calabrese
National Aeronautics and Space Administration
Washington, DC 20546

A. I. Carswell
York University
Department of Physics
Toronto, Canada M3J 1P3

Theodore Chamberlain
Chesapeake Research Consortium
The Johns Hopkins University
Baltimore, MD 21218

Richard F. Chaney
Computer Sciences Corporation
Wallops Station
Wallops Island, VA 23337

Davidson T. Chen
National Aeronautics and Space Administration
Wallops Station
Wallops Island, VA 23337

Clifford Crandall
Director, Hydrographic Development Division
Naval Oceanographic Office
Washington, DC 20373

Thomas H. Curry
National Research Council
National Academy of Science
2101 Constitution Avenue, NW
Washington, DC 20418

Anthony Davis
Department of Environment
562 Booth Street
Ottawa, Ontario, Canada

Donald D. Davis, Jr.
National Aeronautics and Space Administration
Langley Research Center
Hampton, VA 23665

John S. Derr, Jr.
Physical Research Division
Chemical Laboratory
Edgewood Arsenal, MD 21010

Dick S. Diller
National Aeronautics and Space Administration
Washington, DC 20546

J. Dixon
Perkin-Elmer Corporation
Main Avenue (Mail Station 274)
Norwalk, CT 06897

Bennie W. Dodke
National Aeronautics and Space Administration
Langley Research Center
Hampton, VA 23665

H. Dolezalek
Office of Naval Research
800 North Quincy Street
Arlington, VA 22217

Leslie Dunn
Environmental Protection Agency
P.O. Box 15027
Las Vegas, NV 89114

Charles Eastwood
National Aeronautics and Space Administration
1600 S. Joyce Street
Arlington, VA 22202

Herman G. Eldering
BAIRO-ATOMIC
125 Middlesex Trp.
Bedford, MA 01730

Frank Eliot
Earth Satellite Corporation
1747 Pennsylvania Avenue, NW
Washington, DC 20006

Reginald J. Exton
National Aeronautics and Space Administration
Mail Stop 234
Langley Research Center
Hampton, VA 23665

Murray Felsher
Environmental Protection Agency
Office of Technical Analysis
401 M. St., SW, Room 3211-J
Washington, DC 20460

William H. Fuller, Jr.
National Aeronautics and Space Administration
Mail Stop 492
Langley Research Center
Hampton, VA 23665

Charles S. Gilliland
National Aeronautics and Space Administration
Mail Stop 492
Langley Research Center
Hampton, VA 23665

Lowell R. Goodman
National Oceanic and Atmospherics Administration
Wallops Station
Wallops Island, VA 23337

Harry G. Gross
Environment Canada
Inland Waters
Ottawa,Ontario, Canada K1A 0E7

Shashi K. Gupta
Virginia Associated Research Center
Newport News, VA 23606

Charles A. Gurtler
National Aeronautics and Space Administration
Mail Stop 159
Langley Research Center
Hampton, VA 23665

Joseph M. Hallissy
National Aeronautics and Space Administration
Langley Research Center
Hampton, VA 23665

Herbert B. Hallock
Grumman Aerospace Corporation
56 Brookhill Lane
Huntington, NY 11743

David W. Hancock
National Aeronautics and Space Administration
Wallops Station
Wallops Island, VA 23337

Robert V. Hess
National Aeronautics and Space Administration
Mail Stop 160
Langley Research Center
Hampton, VA 23665

George D. Hickman
Sparcom, Inc.
4660 Kenmore Avenue
Alexandria, VA 22304

Frank Hoge
National Aeronautics and Space Administration
Wallops Station
Wallops Island, VA 23337

Donald C. Holmes
Environmental Protection Agency
Office of Monitoring System
635 Maryland Avenue, NE
Washington, DC 20002

William M. Houghton
National Aeronautics and Space Administration
Mail Stop 234
Langley Research Center
Hampton, VA 23665

Wayne R. Houston
Institute for Aerospace Studies
University of Toronto
Downview, Ontario, Canada M3H 5T6

Warren A. Hovis
National Aeronautics and Space Administration
Goddard Space Flight Center
Greenbelt, MD 20771

Norden E. Huang
North Carolina State University
Department of Geosciences
Raleigh, NC 27609

Don Hutcheson
10224 Falls Road
Potomac, MC 20854

Olin Jarrett, Jr.
National Aeronautics and Space Administration
Langley Research Center
Hampton, VA 23665

Hongsuk H. Kim
National Aeronautics and Space Administration
Wallops Station
Wallops Island, VA 23337

Roland W. Kinney
National Research Council
National Academy of Science
2101 Constitution Avenue
Washington, DC 20418

V. Klemas
University of Delaware
College of Marine Studies
Newark, DE 19711

John D. Koutsandreas
Environmental Protection Agency
Office of Monitoring
Waterside Mall
Washington, DC 20560

A. Kuo
Virginia Institute of Marine Science
Gloucester Point, CA 23062

Donald W. Lear
Environmental Protection Agency
Annapolis, MD 21404

Robert S. Levine
National Aeronautics and Space Administration
Langley Research Center
Hampton, VA 23665

Curt A. Levis
Ohio State University
Columbus, OH 43212

Lt. Allen T. Maurer
U.S. Coast Guard GDET-1
400 7th Street, SW
WAshington, DC 20590

Harold E. Maurer
National Aeronautics and Space Administration
Wallops Station
Wallops Island, VA 23337

William T. Mayo, Jr.
Texas A&M University
Remote Sensing Center
College Station, TX 77840

Nelson McAvoy
National Aeronautics and Space Administration
Goddard Space Flight Center
Greenbelt, MD 20771

W. R. McCluney
National Aeronautics and Space Administration
Code 652
Goddard Space Flight Center
Greenbelt, MD 20771

Cdr. G. R. McFadden, USN
Defense Mapping Agency
Building 56, Naval Observatory
Washington, DC 20305

Raymond Measures
Institute for Aerospace
University of Toronto
4925 Dufferin Street
Downview, Ontario, Canada M3H 5T6

S.H. Melfi
Environmental Protection Agency
NERC-LV
P.O. Box 15027
Las Vegas, NV 89114

William H. Michael, Jr.
National Aeronautics and Space Administration
Langley Research Center
Hampton, VA 23665

Peter B. Mumola
National Aeronautics and Space Administration
Mail Stop 401
Langley Research Center
Hampton, VA 23665

Roger N. Neece
General Land Office
200 E. 12th Street
Austin, TX 78701

G. Burton Northam
National Aeronautics and Space Administration
Mail Stop 401A
Langley Research Center
Hampton, VA 23665

John David Oberholtzer
National Aeronautics and Space Administration
Wallops Station
Wallops Island, VA 23337

Stewart L. Ocheltree
National Aeronautics and Space Administration
Mail Stop 234
Langley Research Center
Hampton, VA 23665

Kenneth J. Petri
U.S. Naval Air Development Center
Warminister, PA 18974

J. Plascyk
Perkin-Elmer Corporation
Main Avenue (Mail Station 274)
Norwalk, CT 06897

S. K. Poultney
Quantimum Electronics Group
Department of Physics
University of Maryland
College Park, MD 20742

R. G. Quiney
Spar Aerospace Products Ltd.
825 Caledonia Road
Toronto, Ontario, Canada M6B 3X8

Charles A. Requet
National Aeronautics and Space Administration
Lewis Research Center
Cleveland, OH 44135

Maurice Ringenbach
NOAA-National Ocean Survey
6015 Executive Blvd.
Rockville, MD 20852

Rose Ann Rowlett
General Land Office
120 E. 12th
Austin, TX 78701

Bernard Rubin
National Aeronautics and Space Administration
Mail Code REF
Washington, DC 20546

Shardanand
National Aeronautics and Space Administration
Wallops Station
Wallops Island, VA 23337

Sebastian Sizgoric
York University
2480 Shepard Avenue
Mississauge, Ontario, Canada

Abraham D. Spinak
National Aeronautics and Space Administration
Wallops Station
Wallops Island, VA 23337

D. G. Stephenson
University of Toronto
Institute for Aerospace Studies
4925 Dufferin St.
Downview, Ontario, Canada M3H 5T6

Robert L. Swain
National Aeronautics and Space Administration
Mail Stop 401
Langley Research Center
Hampton, VA 23665

Steve R. Twidwell
Texas WAter Quality Board
P.O. Box 13246 Captional Station
Austin, TX 78711

C.S. Welch
Virginia Institute of Marine Science
Gloucester Point, VA 23062

Andrew R. Wineman
National Aeronautics and Space Administration
Mail Stop 214
Langley Research Center
Hampton, VA 23665

Charles S. Yentsch
University of Massachusetts
Marine Station
Box 128 Lanesville Station
Gloucester, MA 01930

Lee A. Young
Avco Everett Research Lab
2385 Revere Beach Parkway
Everett, MA 02149

Albert V. Zimmerman, III
National Aeronautics and Space Administration
Langley Research Center
Hampton, VA 23665

*U.S. GOVERNMENT PRINTING OFFICE: 1975 - 635-053/98